

Elsevier

Radarweg 29, PO Box 211, 1000 AE Amsterdam, The Netherlands
The Boulevard, Langford Lane, Kidlington, Oxford, OX5 1GB, UK
32 Jamestown Road, London NW1 7BY, UK
225 Wyman Street, Waltham, MA 02451, USA
525 B Street, Suite 1800, San Diego, CA 92101-4495, USA

First edition 2014

Copyright © 2014, Elsevier B.V. All rights reserved

No part of this publication may be reproduced, stored in a retrieval system or transmitted in any form or by any means electronic, mechanical, photocopying, recording or otherwise without the prior written permission of the publisher

Permissions may be sought directly from Elsevier's Science & Technology Rights Department in Oxford, UK: phone (+44) (0) 1865 843830; fax (+44) (0) 1865 853333; email: permissions@elsevier.com. Alternatively you can submit your request online by visiting the Elsevier web site at <http://elsevier.com/locate/permissions>, and selecting *Obtaining permission to use Elsevier material*

Notice

No responsibility is assumed by the publisher for any injury and/or damage to persons or property as a matter of products liability, negligence or otherwise, or from any use or operation of any methods, products, instructions or ideas contained in the material herein. Because of rapid advances in the medical sciences, in particular, independent verification of diagnoses and drug dosages should be made

British Library Cataloguing in Publication Data

A catalogue record for this book is available from the British Library

Library of Congress Cataloging-in-Publication Data

A catalog record for this book is available from the Library of Congress

ISBN: 978-0-444-63380-4

ISSN: 0079-6468

For information on all Academic Press publications
visit our website at store.elsevier.com

Printed and bound in United Kingdom

14 15 16 12 11 10 9 8 7 6 5 4 3 2 1



Working together
to grow libraries in
developing countries

www.elsevier.com • www.bookaid.org

PREFACE

This year's volume of *Progress in Medicinal Chemistry* considers a new approach to drug design in what has historically been the most important class of receptor targets. In addition, we examine progress in the design of ligands for three specific proteins providing potential therapies for important disease classes. Our first chapter reviews an entirely new strategy for finding agonists and antagonists of G-protein coupled receptors (GPCRs) made possible by breakthroughs in the understanding of how their structure and function are linked, and in the effective crystallisation of lipid soluble proteins. Two chapters are concerned with ion channel targets in the central nervous system (CNS), one modulating neurotransmitter release and the other nerve signal conduction. They illustrate differing methods of achieving target selectivity. A fourth chapter analyses recent work on a protease long thought to be important in Alzheimer's disease progression.

GPCRs are at the top of the list of historical successes in drug discovery. Recent times have seen the field boosted by breakthroughs in understanding of allosteric modulation and of the regulation of different intracellular signalling processes, but possibly the most significant advance from the medicinal chemistry viewpoint is the increasing availability of crystal structures of stabilised proteins. In [Chapter 1](#), Congreve and colleagues review the information obtained from such GPCR crystal structures which represent forms normally present only transiently in the fluxional native receptor. Their emphasis is on the key interactions within the ligand binding sites, and several examples are given of how this knowledge is starting to be exploited for drug discovery, with crystal structures of key GPCR illustrated. Visualisation of the complex and divergent shapes and physicochemical features of ligand binding sites enables computational and medicinal chemists to carry out virtual screening, and to design optimised small-molecule agonists and antagonists with improved potency, selectivity and ligand efficiency. The authors also briefly outline complementary approaches to structure-based drug discovery including fragment-based screening.

P2X7 is a member of the purinergic family of receptors. It is an adenosine triphosphate (ATP)-gated ion channel thought to contribute to neuro-inflammatory tone involved in neuropsychiatric and neurodegenerative disorders as well as neuropathic pain. [Chapter 2](#) reviews the work of many teams of researchers and illustrates the challenge of designing drug-like

ligands for a rather lipophilic binding site. This work has nevertheless resulted in several distinctive clinical candidates, and the efficacy of these potential drugs in clinical studies of CNS diseases is eagerly awaited.

Alzheimer's disease is acknowledged to be one of the most important challenges for health-care systems today, and this will increase as the average age of the population rises. Much debate is focussed on the role of amyloid peptides and their precursor proteins in the causation of the disease, and a great deal of research effort has been expended in this direction. Secretases are involved in regulation of the amyloid proteins, and Hall and colleagues in [Chapter 3](#) specifically review recent work on gamma secretase. A key problem is finding drugs which modulate enzyme activity only in the disease-causing pathway, and while several compounds have advanced into clinical trials, there is as yet no sign of a successful drug emerging. Work continues on achieving clinical efficacy with an adequate safety profile, and the authors review differing approaches taken to address this challenge.

The importance of voltage-gated calcium channels (VGCCs) in basic physiological processes such as cardiac and neurological function has generated intense interest in these proteins as targets of pharmacological intervention. N-type calcium channels are a subset of VGCCs distinguished by their physiology, pharmacology and significance to the pathology of chronic pain. While as a class calcium channel blockers have provided a significant number of successful medicines for treating cardiovascular disorders, despite decades of investigation, only a single drug targeting the specific N-type channel function has entered the marketplace, and one with severe limitations on mode of delivery. [Chapter 4](#) summarises current understanding of the biology, physiology and pharmacology of N-type calcium channels and the implication of these features for therapeutic intervention. From this basis of understanding, the authors describe recent efforts to discover and develop peptide-based modulators of N-type calcium channel function, and in particular small-molecule blockers with potential for oral dosing.

GEOFF LAWTON
DAVID WITTY
October 2013

CONTRIBUTORS

Anindya Bhattacharya

Janssen Research and Development, LLC, San Diego, CA, USA

Christa C. Chrovian

Janssen Research and Development, LLC, San Diego, CA, USA

Miles Congreve

Heptares Therapeutics Ltd, BioPark, Welwyn Garden City, Hertfordshire, United Kingdom

João M. Dias

Heptares Therapeutics Ltd, BioPark, Welwyn Garden City, Hertfordshire, United Kingdom

Adrian Hall

Department of Chemistry, Discovery Research, Neuroscience and General Medicine
Product Creation Unit, Eisai Ltd., EMEA Knowledge Centre, Mosquito Way, Hatfield,
United Kingdom

Margaret S. Lee

Research & Translational Medicine, Zalicus Inc., Cambridge MA, USA

Michael A. Letavic

Janssen Research and Development, LLC, San Diego, CA, USA

Fiona H. Marshall

Heptares Therapeutics Ltd, BioPark, Welwyn Garden City, Hertfordshire, United Kingdom

Toshal R. Patel

Department of BioPharmacology, Discovery Research, Neuroscience and General Medicine
Product Creation Unit, Eisai Ltd., EMEA Knowledge Centre, Mosquito Way, Hatfield,
United Kingdom

Jason C. Rech

Janssen Research and Development, LLC, San Diego, CA, USA



Structure-Based Drug Design for G Protein-Coupled Receptors

Miles Congreve, João M. Dias, Fiona H. Marshall

Heptares Therapeutics Ltd, BioPark, Welwyn Garden City, Hertfordshire, United Kingdom

Contents

1. Introduction	1
2. Structural Architecture of GPCRs	3
3. GPCR Protein–Ligand X-Ray Structures	31
4. Mechanisms of Activation: Agonist Bound Structures	35
5. Biased Agonism	39
6. Traditional Approaches to GPCR Drug Discovery and the Need for Change	40
7. Potential of SBDD and FBDD for GPCR Drug Discovery	41
7.1 Beta Adrenergic Receptors	42
7.2 Histamine Receptor	45
7.3 Adenosine Receptors	46
7.4 CXCR4 Receptor	52
7.5 CRF ₁ Receptor	53
8. Conclusions and Outlook	54
Acknowledgments	55
References	55

Keywords: GPCR, Structure-based drug design, SBDD, Fragment-based drug design, FBDD, Fragment, Antagonist, Agonist



1. INTRODUCTION

All cellular surfaces within the human body encompass membrane spanning proteins, which sense the environment and trigger intercellular communication by activating signal transduction pathways. G protein-coupled receptors (GPCRs) are the largest family of membrane-bound receptors and they mediate responses to diverse natural ligands including

hormones, neurotransmitters and metabolites, which can vary in structure from simple ions, through small organic molecules to lipids, peptides and proteins [1–3]. Binding of the ligand to the GPCR protein results in a conformational change. This leads to recruitment of intracellular signalling molecules including G proteins and β -arrestin [4,5]. GPCR activation can lead to rapid cellular responses such as the activation of ion channels, slower responses mediated by cascades of intracellular enzymes or long-term changes in gene expression. Such events can result in various physiological responses including contraction or relaxation of smooth muscle, synaptic transmission in the nervous system, recruitment of immune cells to sites of inflammation or long-term behavioural changes [6].

The prevalence of GPCRs combined with their pivotal role in cell sensing and signalling means that they are one of the richest sources of drug targets for the pharmaceutical industry. Drugs that mimic or block the activity of the natural ligands of GPCRs are used to treat diseases of the central nervous system, such as schizophrenia and Parkinson's disease, diseases of the cardiovascular and respiratory system, such as hypertension and asthma, metabolic diseases including diabetes and obesity, as well as cancer and HIV infection [7–9]. Currently, up to 30% of marketed drugs are directed at GPCR targets [10,11]. Despite this success, a wealth of novel drug targets remains as yet untapped. Fewer than 20% of the 390 non-olfactory GPCRs have been drugged with small molecules and over 100 of these receptors remain 'orphans' whose ligands and biology are as yet uncharacterised [12]. In 2010 there were over 3000 GPCR-targeted drugs in clinical development, although the majority were aimed at the same targets as existing drugs [13].

During the past 5 years there has been a revolution in the industry's approach to GPCR drug discovery, enabled by the ability to obtain purified protein for biophysical and structural studies. The structures of more than 20 GPCRs have been solved in complex with peptides and small molecule ligands and, in some cases, in both active and inactive conformations. This provides an unprecedented wealth of information regarding the molecular interactions of ligands with their receptors, allowing rational structure-based drug design (SBDD) to be employed effectively with GPCRs for the first time. Here we review the information obtained from GPCR crystal structures with an emphasis on the key interactions within the ligand binding sites and some examples of how this knowledge is starting

to be exploited for drug discovery. We also briefly outline complementary approaches to structure-based drug discovery including fragment-based screening. Finally, we discuss future challenges and opportunities in this rapidly moving field.



2. STRUCTURAL ARCHITECTURE OF GPCRS

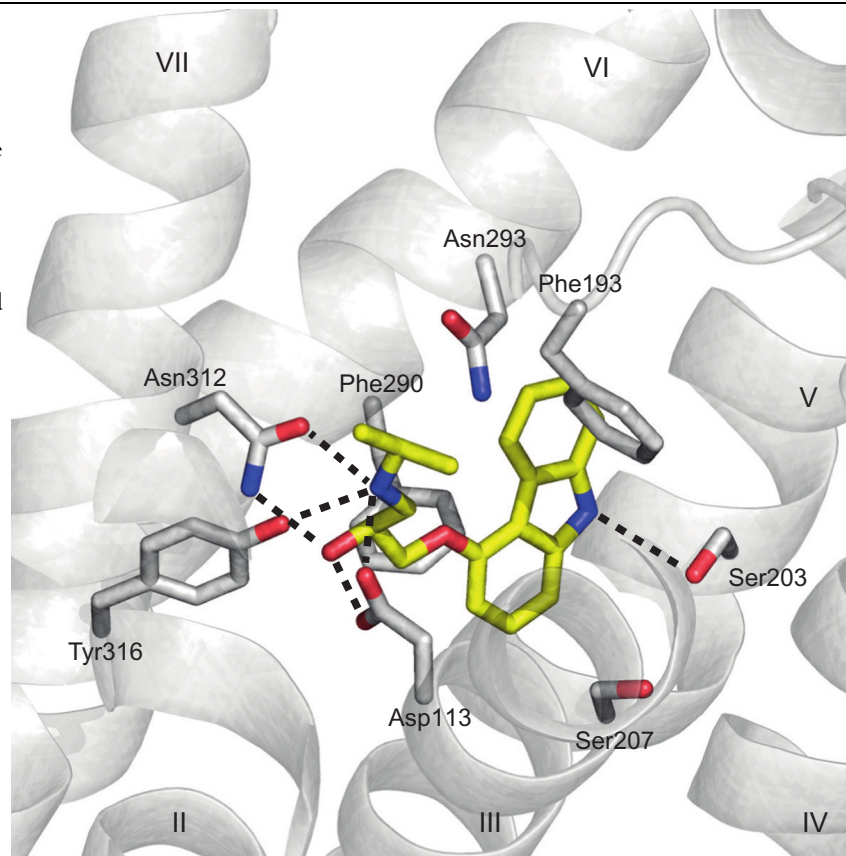
GPCRs feature the common topology of seven membrane spanning α -helices (7TM) with an extracellular N-terminus and intracellular C-terminus. Although all GPCRs are considered to be derived from a common ancestral protein they have diverged into a large family with over 800 members which can be classified into different sub-families [14]. Over 400 of these are olfactory receptors involved in smell and taste. The remaining receptors fall into five main families (Class A, Secretin and Adhesion [together Class B], Class C and Frizzled). Class A or rhodopsin is the largest family with approximately 300 members and includes the aminergic (e.g. dopamine and histamine) receptors, neuropeptide receptors, chemokine receptors, receptors for lipids and eicosanoids and glycoprotein hormone receptors. Despite the great diversity in ligand structure, the mechanisms involved in receptor activation are remarkably well conserved, with almost all drugs for Class A receptors binding to the same region, whatever the nature of the natural endogenous ligand [15].

Class B GPCRs comprise both the Secretin family (15 members) and the Adhesion family (33 members). The Secretin family includes many targets important in disease including the glucagon-like peptide receptor (GLP-1), a target for diabetes, and the parathyroid hormone receptor (PTH1), a target for bone diseases such as osteoporosis. This family has proved extremely difficult to drug with small molecules, although many of the natural peptide ligands serve as therapeutic agents [15,16]. Structures of the first two representatives of Class B receptors, the glucagon receptor and the corticotropin releasing factor (CRF₁) receptor have recently been solved [17,18] (Table 1.1). The Adhesion family members are characterised by a conserved transmembrane domain (TMD) linked to a very large extracellular domain, which comprises adhesion-like subdomains and a domain that undergoes intracellular proteolytic cleavage (known as the GPCR

Table 1.1 List of Published GPCR Crystal Structures
Target GPCR and Description of Binding Pocket **Ligand Binding Site**

β_2 Adrenergic receptor complex with the inverse agonist carazolol (**1**) at 2.4 Å, PDB=2RH1 [19]. Carazolol makes key H-bond interactions with Asp113^{3,32}, Asn312^{7,39} and Tyr316^{7,43} from the basic amine and with Ser203^{5,42} from the carbazole NH.

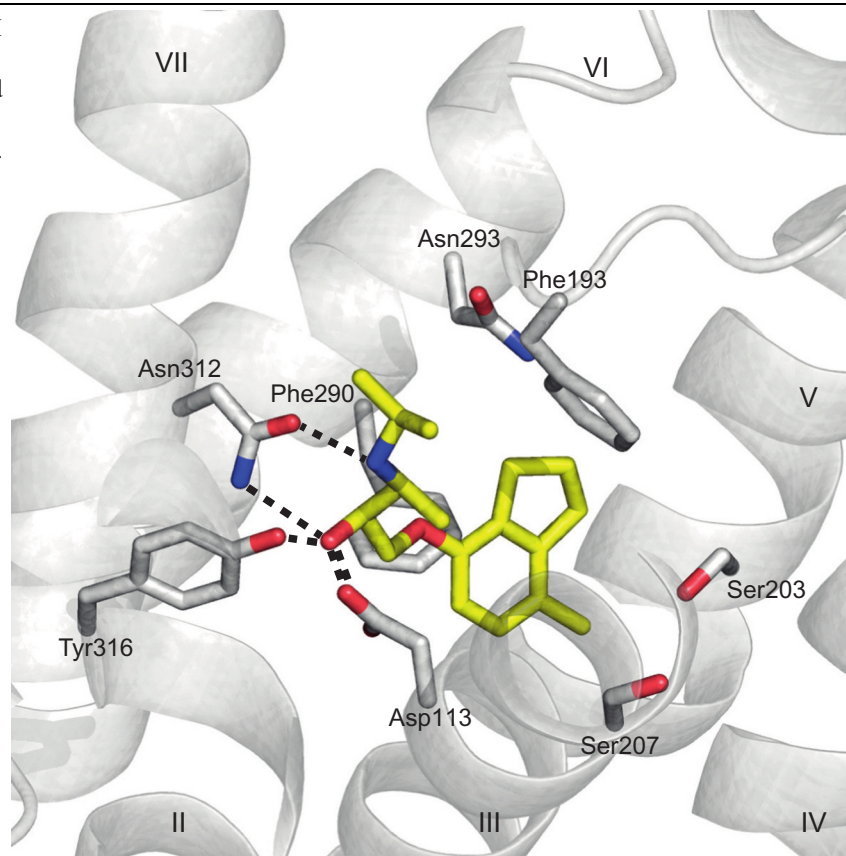
The carbazole ring system is surrounded by hydrophobic interactions within the vicinity of residues Val114^{3,33}, Phe193^{5,32}, Tyr199^{5,38}, Ser207^{5,46}, Phe289^{6,51}, Phe290^{6,52}, Asn293^{6,55} and Tyr308^{7,35}. Other residues in the binding pocket comprise Trp109^{3,28}, Val117^{3,36}, Ser207^{5,46} and Trp286^{6,48}.



β_2 Adrenergic receptor with the inverse agonist ICI 118,551 (**2**) at 2.84 Å, PDB = 3NY8 [20].

The inverse agonist ICI 118551 makes key H-bond interactions with Asp113^{3.32}, Asn312^{7.39} and Tyr316^{7.43}, and a π - π interaction with Phe290^{6.52}.

Other residues in the binding pocket comprise Trp109^{3.28}, Val114^{3.33}, Val117^{3.36}, Thr118^{3.37}, Phe193^{5.32}, Tyr199^{5.38}, Ser203^{5.42}, Ser207^{5.46}, Trp286^{6.48}, Phe289^{6.51}, Asn293^{6.55} and Tyr308^{7.35}.



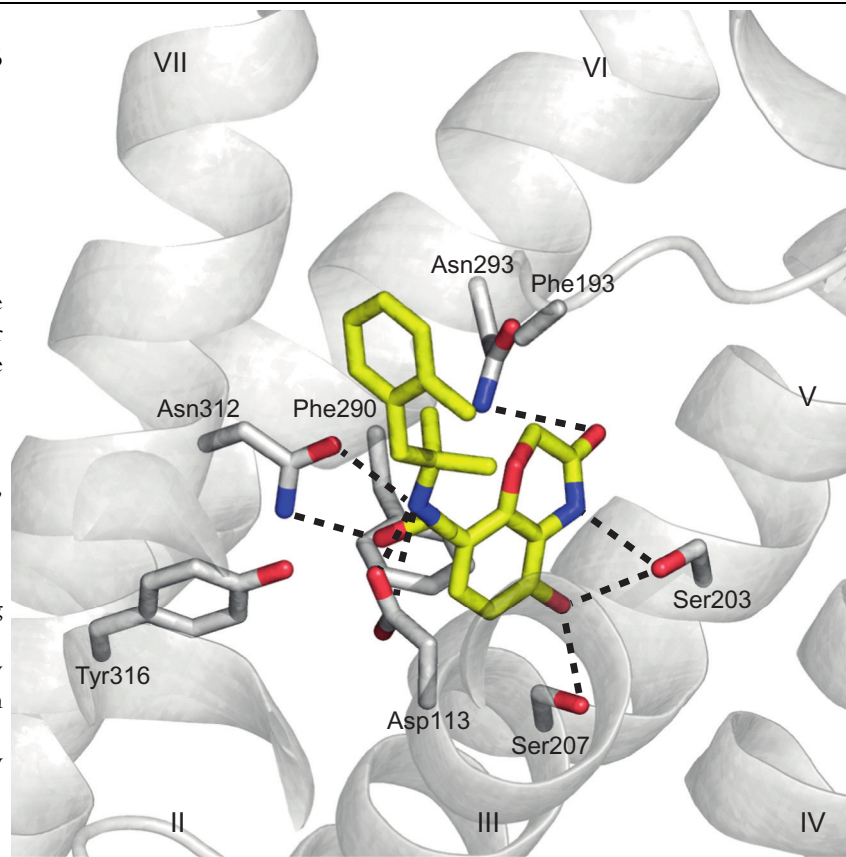
Continued

Table 1.1 List of Published GPCR Crystal Structures—cont'd
Target GPCR and Description of Binding Pocket **Ligand Binding Site**

β_2 Adrenergic receptor-Gs protein complex with the agonist BI-167107 (**3**), at 3.20 Å, PDB = 3SN6 [21].

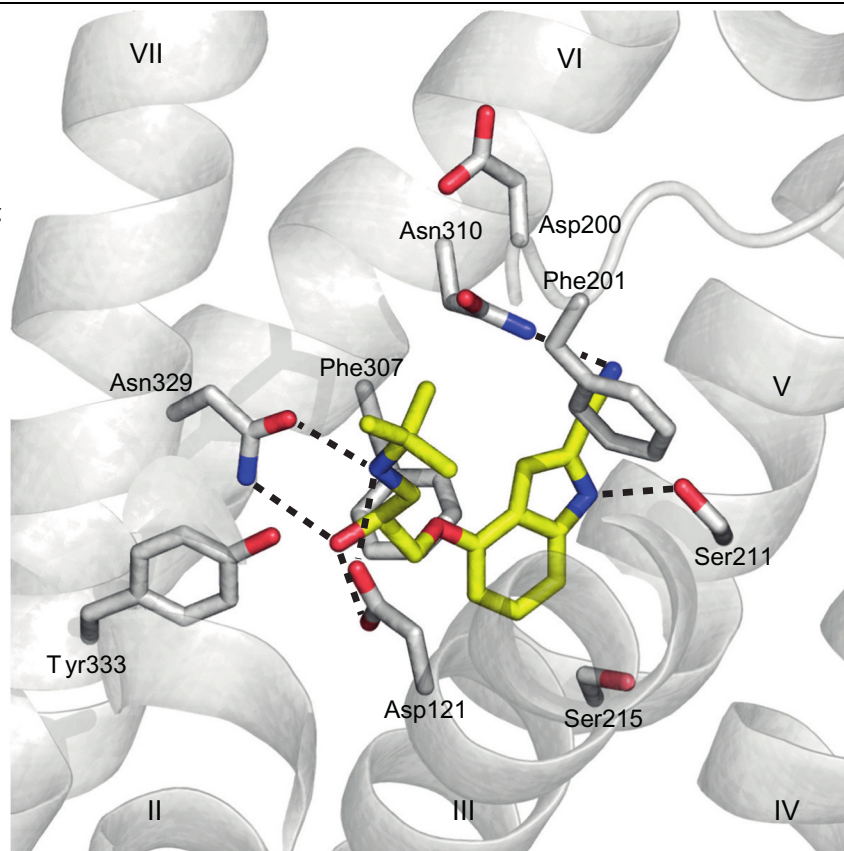
The ligand BI-167107 makes key H-bond interactions with Asp113^{3.32}, Ser 203^{5.42}, Ser207^{5.46}, Asn293^{7.20} and Asn312^{7.39} and a π - π interaction with Phe290^{6.52}. The H-bonding interactions with the two Ser residues on TM5 is typical for an agonist ligand and antagonists or inverse agonists do not interact with either of these residues. Overall the binding site is slightly smaller around the agonist compared with antagonists (see main text).

Other residues in the binding pocket comprise Trp109^{3.28}, Thr110^{3.29}, Val114^{3.33}, Val117^{3.36}, Thr118^{3.37}, Asp192^{ECL2}, Phe193^{ECL2}, Tyr199^{5.38}, Ala200^{5.39}, Ser203^{5.42}, Ser207^{5.46}, Trp286^{6.48}, Phe289^{6.51}, Asn293^{6.55} and Tyr308^{7.35} and Ile309^{7.36}. The residues Asp192^{ECL2} and Phe193^{ECL2} are located in the ECL2 loop, capping the ligand binding site. The side chain of these residues is not clearly visible in the electron density and Phe193^{ECL2} is represented as an alanine stub in the structure coordinates deposited in the PDB, probably due to the loop flexibility corroborated by the high B factors >160.



β_1 Adrenergic receptor complex with the antagonist cyanopindolol (**4**) at 2.7 Å, PDB = 2VT4 [22].

Cyanopindolol makes key H-bond interactions with Asp121^{3.32} and Asn329^{7.39}, from the basic amine and Ser211^{5.42} from the indole NH and Asn310^{6.55} from the cyano group. The indole ring system makes a π - π interaction with Phe307^{6.52}. Other residues in the binding pocket comprise Trp117^{3.28}, Thr118^{3.29}, Val122^{3.33}, Val125^{3.36}, Thr126^{3.37}, Asp200^{ECL2}, Phe201^{ECL2}, Thr203^{ECL2}, Tyr207^{5.38}, Ala208^{5.39}, Ser212^{5.43}, Ser 215^{5.46}, Trp303^{6.48}, Phe306^{6.51}, Phe307^{6.52}, Trp330^{7.40} and Tyr333^{7.43}.

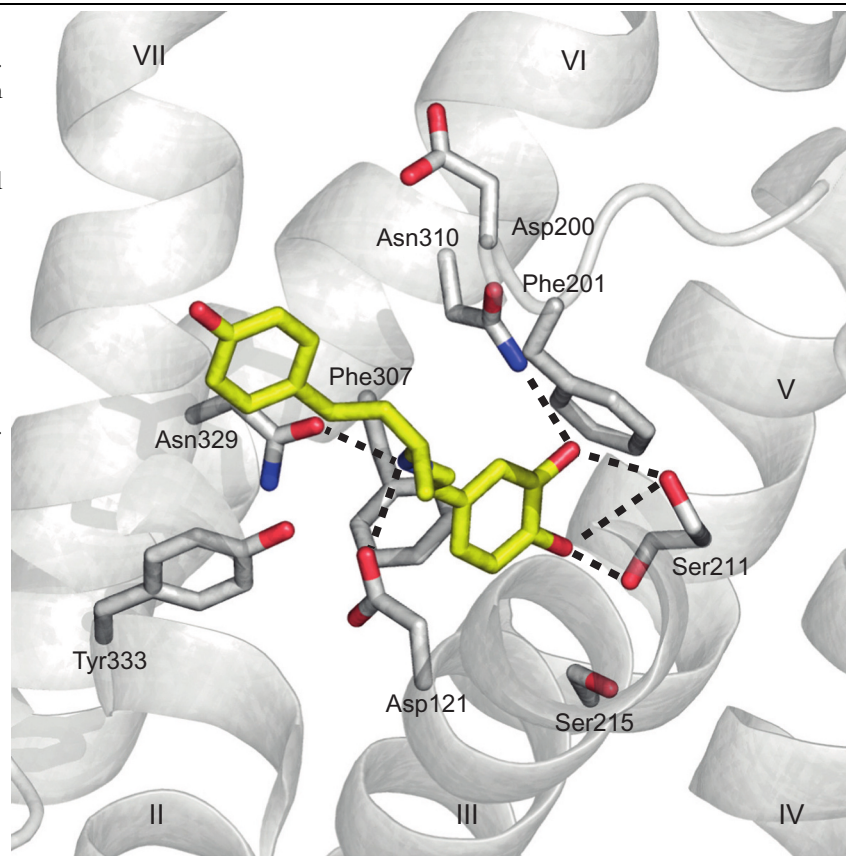


Continued

Table 1.1 List of Published GPCR Crystal Structures—cont'd
Target GPCR and Description of Binding Pocket **Ligand Binding Site**

β_1 Adrenergic receptor complex with the partial agonist dobutamine (**5**) at 2.5 Å, PDB = 2Y00 [23]. Dobutamine makes key H-bond interactions with Asp121^{3,32} and Asn329^{7,39}, from the basic amine and Ser211^{5,42} and Asn310^{6,55} from the catechol. Note that the catechol interacts with the hydroxyl group of Ser211^{5,42} and also its main chain carbonyl.

Other residues in the binding pocket comprise Leu101^{2,64}, Val102^{2,65}, Trp117^{3,28}, Thr118^{3,29}, Val122^{3,33}, Val125^{3,36}, Thr126^{3,37}, Asp200^{ECL2}, Phe201^{ECL2}, Thr203^{ECL2}, Tyr207^{5,38}, Ala208^{5,39}, Ser212^{5,43}, Ser 215^{5,46}, Trp303^{6,48}, Phe306^{6,51}, Phe307^{6,52}, Val326^{7,36}, Trp330^{7,40} and Tyr333^{7,43}.



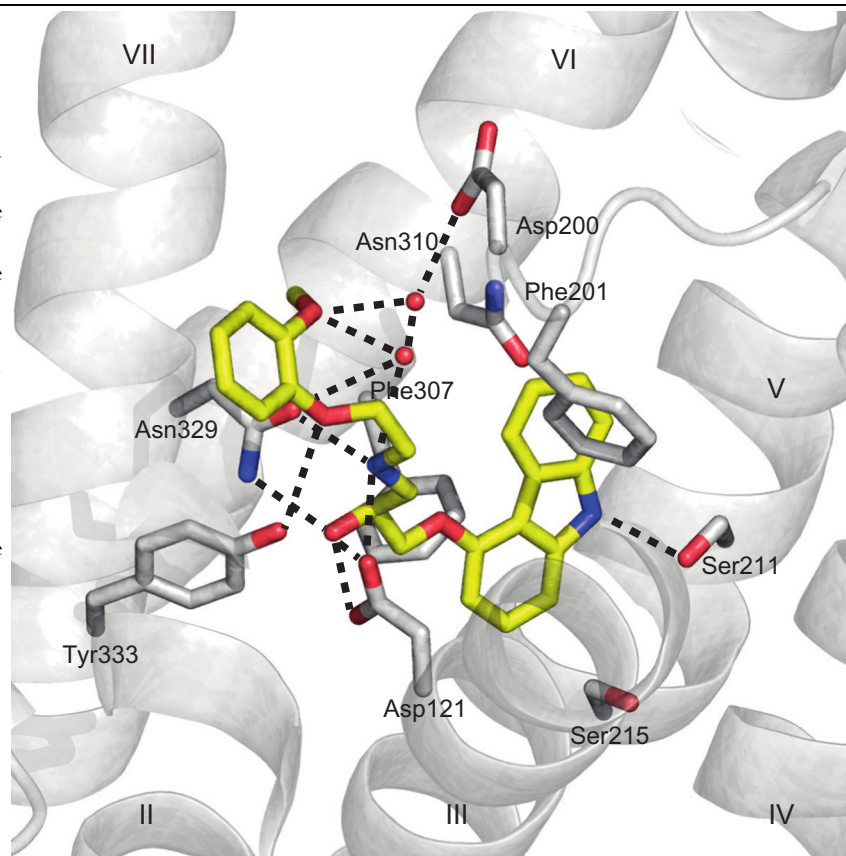
β_1 Adrenergic receptor complex with the biased agonist carvedilol (**6**) at 2.3 Å, PDB = 4AMJ [24]. Carvedilol makes key H-bond interactions with Asp121^{3.32} and Asn329^{7.39}, from the basic amine and the hydroxyl group, and with Asn329^{7.39} and Tyr333^{7.43} with the phenyl ether. The carbazole NH interacts via an H-bond with Ser211^{5.42}. The secondary amine and the phenol of the ligand interact directly with two water molecules from the solvent accessible network H₂O2030 and H₂O2045.

H₂O2030 interacts with the phenol and also with H₂O2045, and also bridges the ligand to Asp200^{ECL2} and Phe201^{ECL2} from ECL2.

H₂O2045 interacts with carvedilol and also H₂O2030 and Asn329^{7.39}.

Overall these new interactions at the top of the binding pocket are proposed to be important in the biased signaling of this molecule.

Other residues in the binding pocket comprise Leu101^{2.64}, Val102^{2.65}, Trp117^{3.28}, Thr118^{3.29}, Val122^{3.33}, Val125^{3.36}, Thr126^{3.37}, Thr203^{5.34}, Tyr207^{5.38}, Ala208^{5.39}, Ser212^{5.43}, Ser215^{5.46}, Trp303^{6.48}, Phe306^{6.51}, Phe307^{6.52}, Asn310^{6.55}, Val326^{7.36}, Trp330^{7.40} and Tyr333^{7.43}.

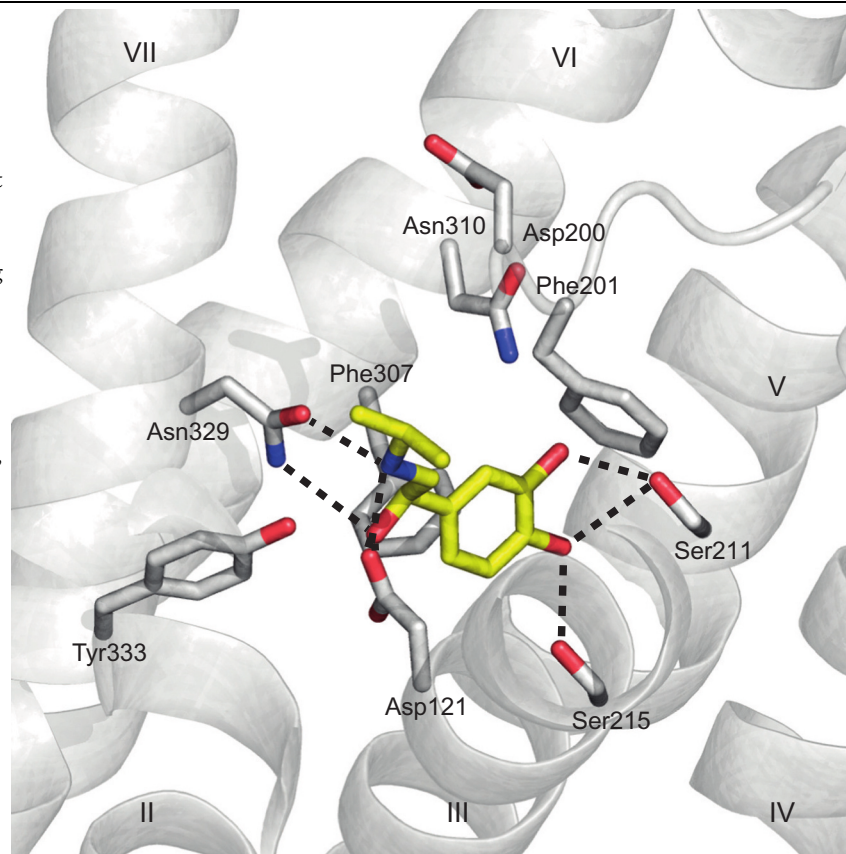


Continued

Table 1.1 List of Published GPCR Crystal Structures—cont'd
Target GPCR and Description of Binding Pocket **Ligand Binding Site**

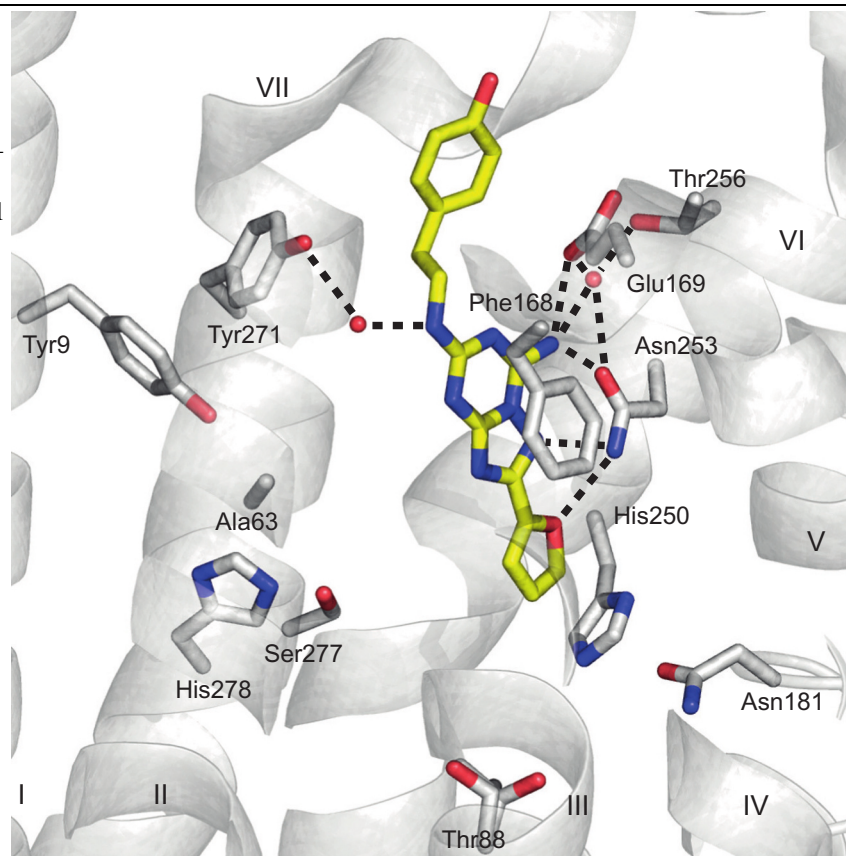
β_1 Adrenergic receptor complex with the agonist isoprenaline (**7**) at 2.85 Å, PDB = 2Y03 [23]. Isoprenaline makes key H-bond interactions with Asp121^{3.32} and Asn329^{7.39}, from the basic amine and the hydroxyl group in the center of the molecule, while Ser211^{5.42} and Ser215^{5.46} interact with the phenol groups from the catechol. The interactions with both these Ser residues on TM5 are important for agonism and overall the binding site is slightly contracted around the agonist compared to antagonist or inverse agonist structures.

Other residues in the binding pocket comprise Trp117^{3.28}, Thr118^{3.29}, Val122^{3.33}, Val125^{3.36}, Thr126^{3.37}, Asp200^{ECL2}, Phe201^{ECL2}, Tyr207^{5.38}, Ser212^{5.43}, Trp303^{6.48}, Phe306^{6.51}, Phe307^{6.52}, Asn310^{6.55} and Trp330^{7.40}.



Adenosine A_{2A} receptor in complex with the inverse agonist ZM241385 (**8**) at 1.8 Å, PDB = 4E1Y [3].

The ligand ZM241385 makes key H-bond interactions with Glu169^{ECL2}, Asn253^{6.55} and a π - π interaction with Phe168^{ECL2}. Several water molecules bridge the ligand to the protein (not all shown). Other residues in the binding pocket comprise Leu85^{3.35}, Thr88^{3.36}, Met177^{5.38}, Asn181^{5.42}, Trp246^{6.48}, Leu249^{6.51}, His250^{6.52}, Thr256^{6.58}, His264^{ECL3}, Leu267^{7.32}, Met270^{7.35}, Tyr271^{7.36}, Ile274^{7.39}, Ser277^{7.42} and His278^{7.43}.



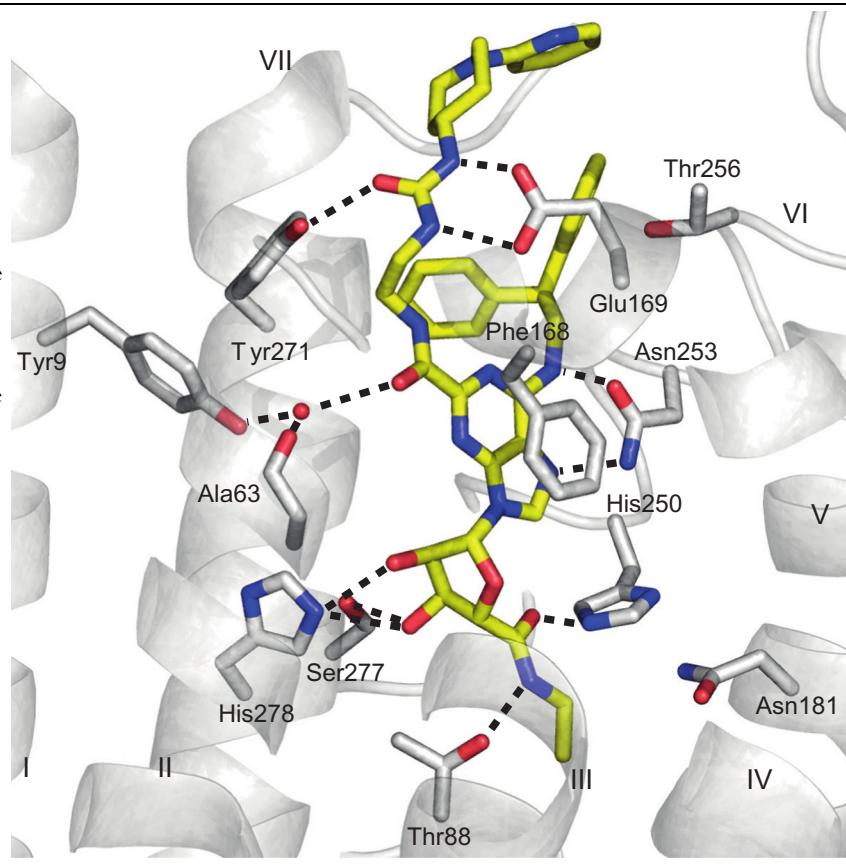
Continued

Table 1.1 List of Published GPCR Crystal Structures—cont'd
Target GPCR and Description of Binding Pocket **Ligand Binding Site**

Adenosine A_{2A} receptor in complex with the agonist UK-432097 (**9**) at 2.7 Å, PDB = 3QAK [25].

The agonist UK-0432097 makes key H-bond interactions with Thr88^{3.36}, Glu169^{ECL2}, His250^{6.52}, Asn253^{6.55}, Tyr271^{7.36}, Ser277^{7.42} and His278^{7.43} and makes a π - π interaction with Phe168^{ECL2}. A water molecule also bridges the ligand to the carbonyl oxygen of Ala63^{2.61} and the hydroxyl group of Tyr9^{1.35}.

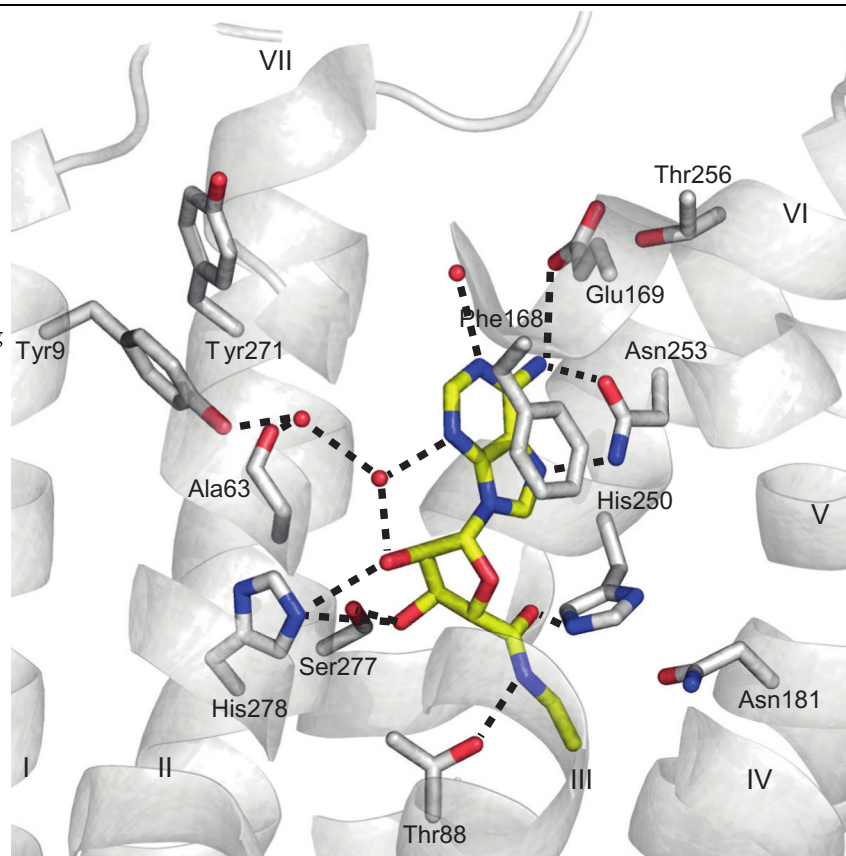
Agonism is linked to the H-bonding interactions with the ribose group and the shape of the binding site in this region changes to accommodate the critical sugar moiety.



Adenosine A_{2A} receptor in complex with the agonist NECA (**10**) at 2.6 Å, PDB=2YDV [26].

The agonist NECA makes key H-bond interactions with Thr88^{3,36}, Glu169^{ECL2}, His250^{6,52}, Asn253^{6,55}, Ser277^{7,42} and His278^{7,43} and makes a π - π interaction with Phe168^{ECL2}. A water molecule bridges the ligand to the carbonyl oxygen of Ala63^{2,61} and the hydroxyl group of Tyr9^{1,35}.

Agonism is linked to the H-bonding interactions with the ribose group and the shape of the binding site in this region changes to accommodate the critical sugar moiety.



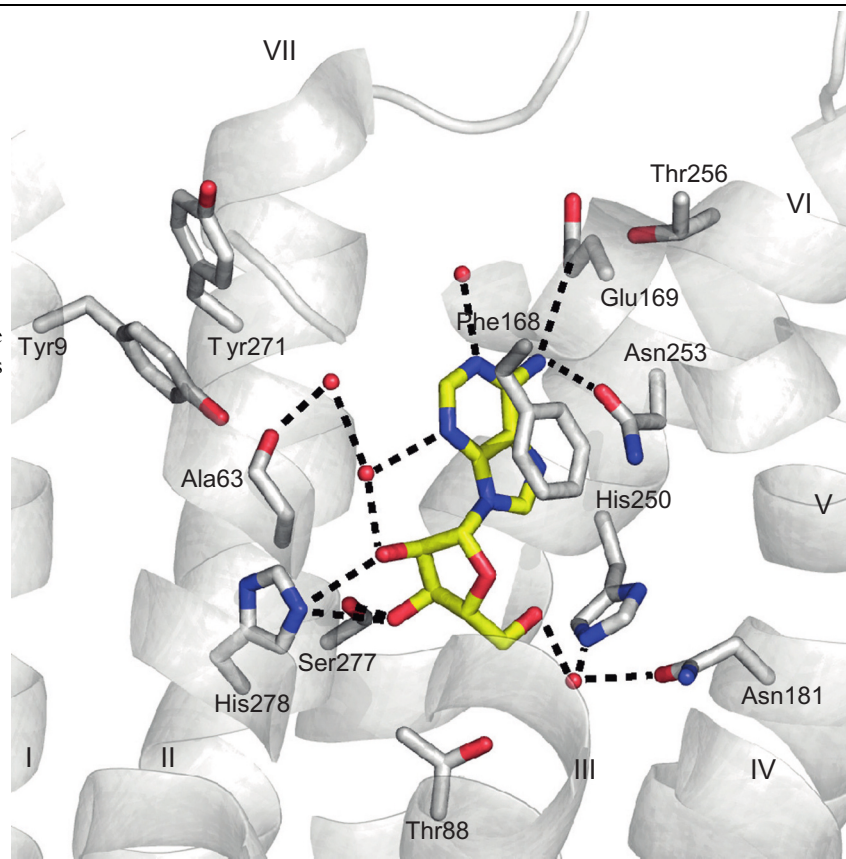
Continued

Table 1.1 List of Published GPCR Crystal Structures—cont'd
Target GPCR and Description of Binding Pocket **Ligand Binding Site**

Adenosine A_{2A} receptor in complex with the physiological ligand adenosine (**11**) at 3.0 Å, PDB = 2YDO [26].

The physiological agonist ligand adenosine makes key H-bond interactions with Glu169^{ECL2}, Asn253^{6.55}, Ser277^{7.42} and His278^{7.43} and makes a π - π interaction with Phe168^{ECL2}. A water molecule network bridges the ligand to the carbonyl oxygen of Ala63^{2.61} and also to Asn181^{5.42} and His250^{6.52}.

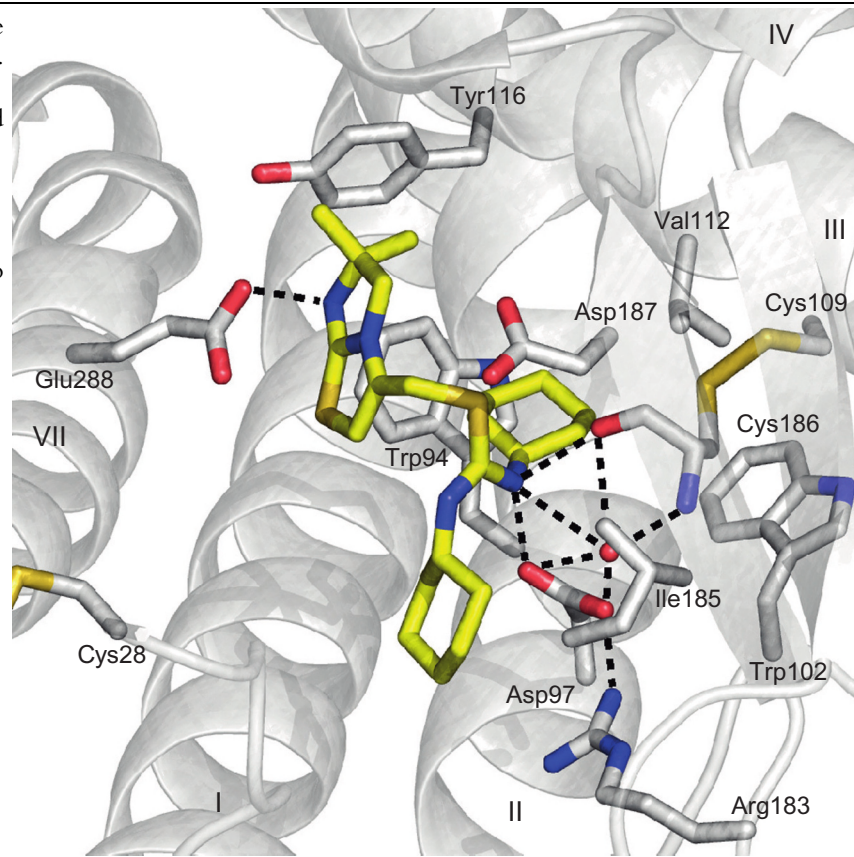
Agonism is linked to the polar interactions with the ribose group and the shape of the binding site in this region changes to accommodate the critical sugar moiety.



CXCR4 chemokine receptor in complex with the antagonist IT1t (**12**) at 2.5 Å, PDB= 3ODU [27]. IT1t makes key H-bond interactions with Asp97^{2,63} and Glu288^{7,39}. The ligand is surrounded by the hydrophobic environment formed by Trp94^{2,60}, Trp102^{ECL1}, Val112^{3,28}, Tyr116^{3,32}, Arg183^{ECL2}, Ile185^{ECL2}, Cys186^{ECL2} and Asp187^{ECL2}.

The ligand sits high in the binding site compared to other Family A ligands. Deeper in the cavity the pocket is polar and unsuitable for the binding of small molecules.

The figure orientation was rotated for clarity, showing helix TM3 on the right.

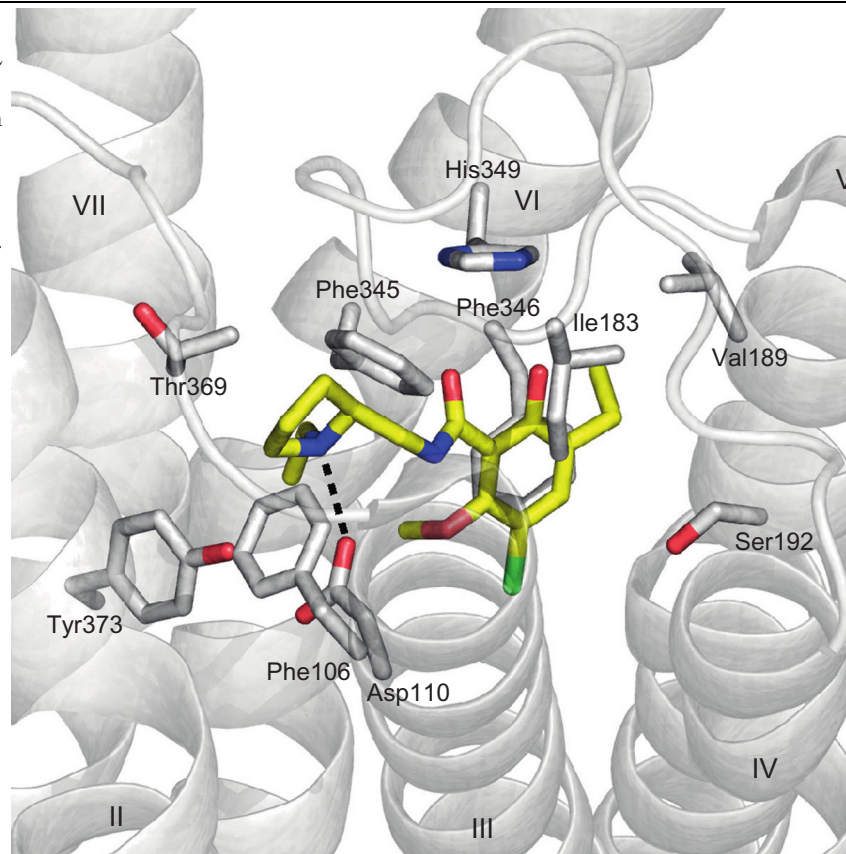


Continued

Table 1.1 List of Published GPCR Crystal Structures—cont'd
Target GPCR and Description of Binding Pocket **Ligand Binding Site**

Dopamine D₃ receptor complex with the antagonist eticlopride (**13**) at 2.89 Å, PDB = 3PBL [28].

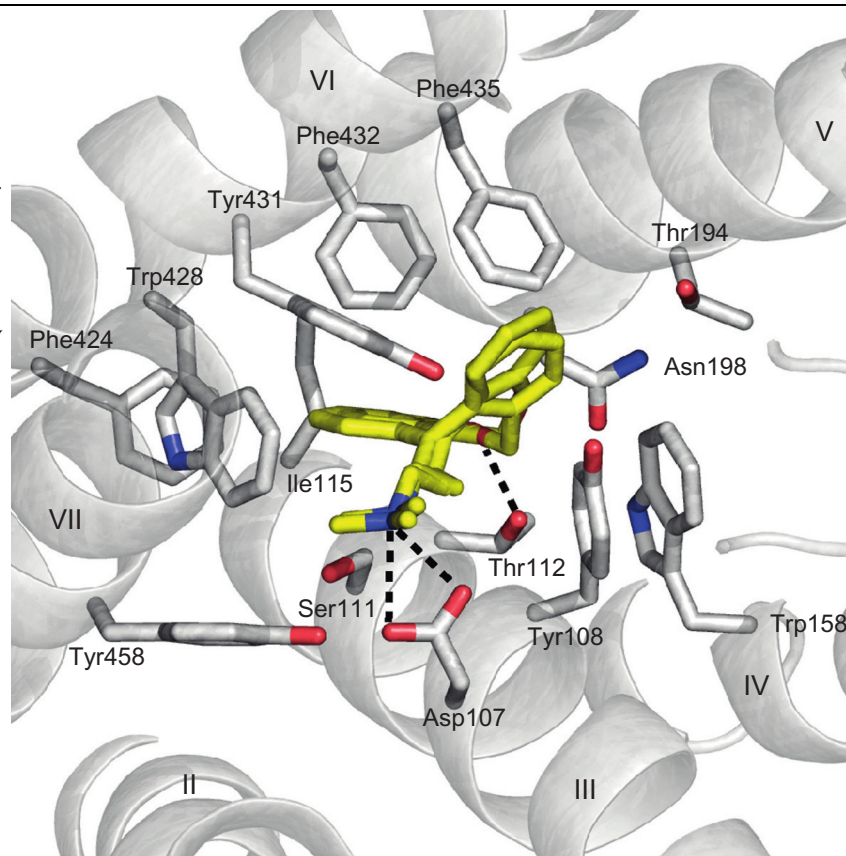
Eticlopride makes a key salt bridge interaction with Asp110^{3,32} and is surrounded by the following, largely hydrophobic, residues Phe106^{3,28}, Ile183^{ECL2}, Val189^{5,39}, Ser192^{5,42}, Phe345^{6,51}, Phe346^{6,52}, His349^{6,55}, Thr369^{7,39} and Tyr373^{7,43}.



Histamine H₁ receptor in complex with the antagonist doxepin (**14**) at 3.10 Å, PDB=3RZE [29].

Doxepin makes key salt bridge interactions with Asp107^{3,32}, and the E isomer (but not Z) of doxepin is within H-bond distance of Thr112^{3,37}. Doxepin makes hydrophobic interactions with Tyr108^{3,33}, Trp428^{6,48} and Phe432^{6,52}. The residues Ser111^{3,36}, Ile115^{3,40}, Trp158^{4,56}, Thr194^{5,43}, Asn198^{5,46}, Phe424^{6,44}, Tyr431^{6,51}, Phe435^{6,55} and Tyr458^{7,43} are also in close vicinity of the ligand.

Note that the doxepin used for crystallisation is a mixture of E and Z isomers. Both forms are represented in the figure and PDB.



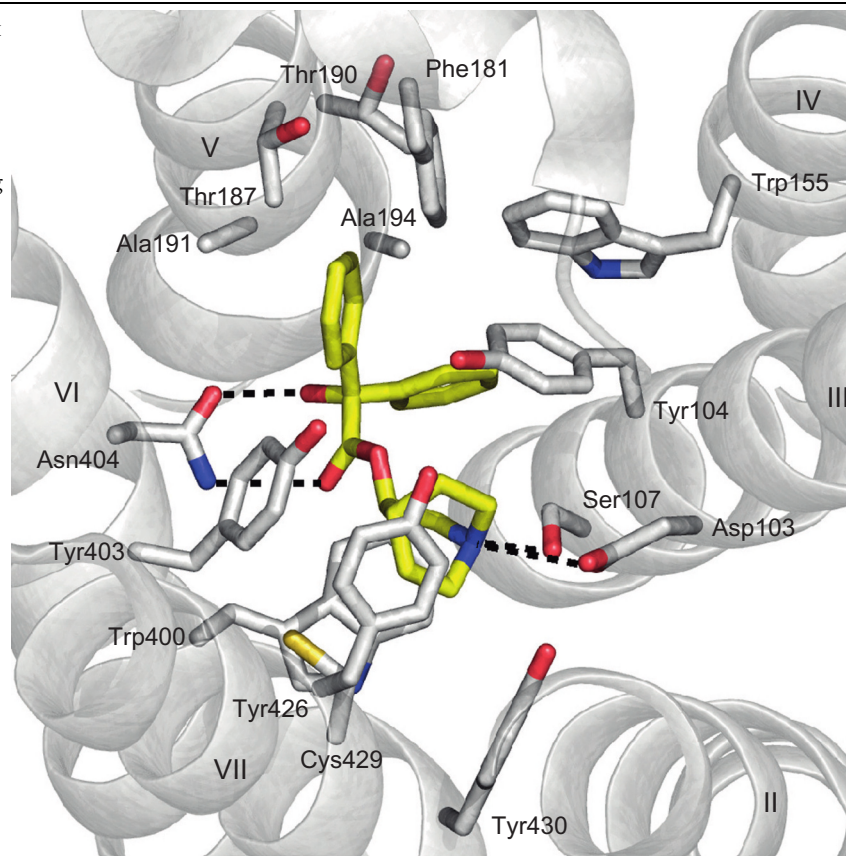
Continued

Table 1.1 List of Published GPCR Crystal Structures—cont'd
Target GPCR and Description of Binding Pocket **Ligand Binding Site**

Muscarinic acetylcholine M₂ receptor in complex with the antagonist QNB (**15**) at 3.00 Å, PDB = 3UON [30].

QNB makes key H-bond interactions with Asp103^{3.32}, Ser107^{3.36} and Asn404^{6.52}. The following residues enclose the ligand in the binding pocket, Tyr104^{3.33}, Val111^{3.40}, Trp155^{4.57}, Phe181^{ECL2}, Thr187^{5.39}, Thr190^{5.42}, Trp400^{6.48}, Tyr403^{6.51}, Tyr426^{7.39}, Cys429^{7.42} and Tyr430^{7.43}.

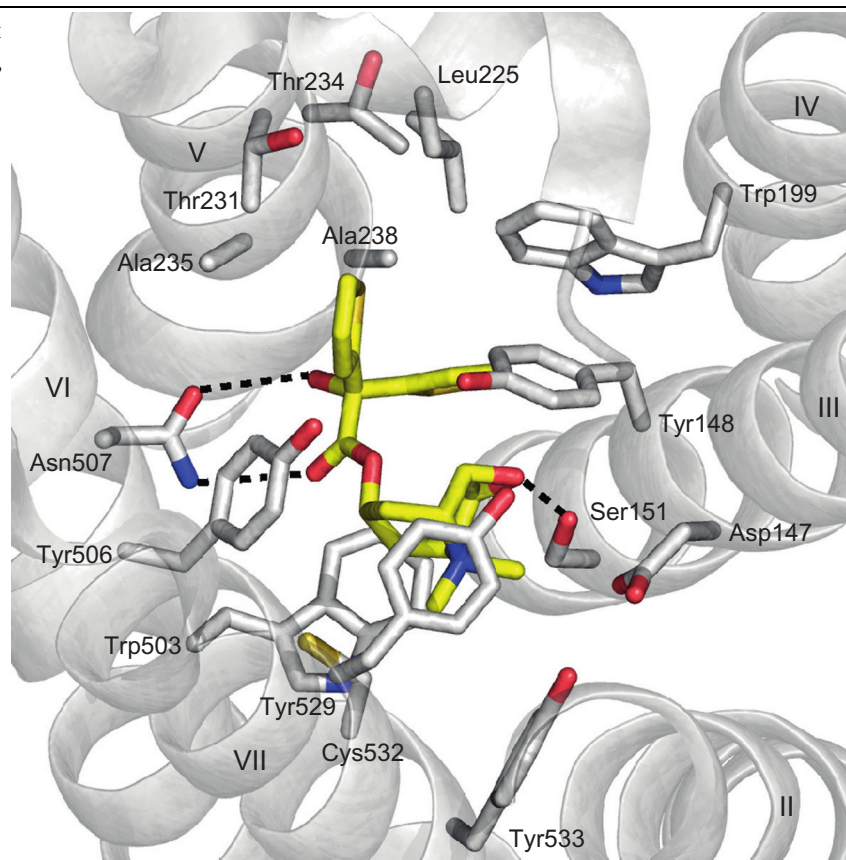
The figure orientation was rotated for clarity, showing helix TM3 on the right.



Muscarinic acetylcholine M₃ receptor in complex with the inverse agonist tiotropium (**16**) at 3.50 Å, PDB = 4DAJ [31].

Tiotropium makes key H-bond interactions with Ser151^{3,36} and Asn507^{6,52} and a π - π interaction with Trp199^{4,57}. The ligand is enclosed by the residues Asp147^{3,32}, Tyr148^{3,33}, Asn152^{3,37}, Leu225^{ECL2}, Thr231^{5,39}, Thr234^{5,42}, Ala235^{5,43}, Ala238^{5,46}, Trp503^{6,48}, Tyr506^{6,51}, Asn507^{6,52}, Tyr529^{7,39}, Cys532^{7,42} and Tyr 533^{7,43}.

The figure orientation was rotated for clarity, showing helix TM3 on the right and keeping the same orientation as M₂.



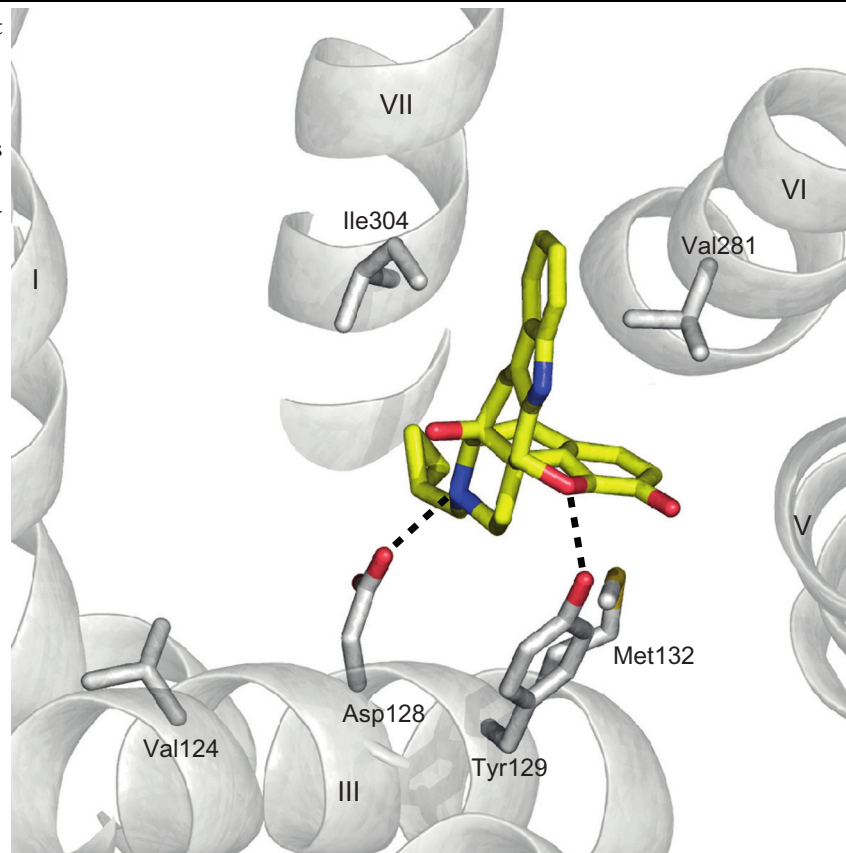
Continued

Table 1.1 List of Published GPCR Crystal Structures—cont'd
Target GPCR and Description of Binding Pocket **Ligand Binding Site**

δ -Opioid receptor in complex with the antagonist naltrindole (**17**) at 3.40 Å, PDB=4EJ4 [32].

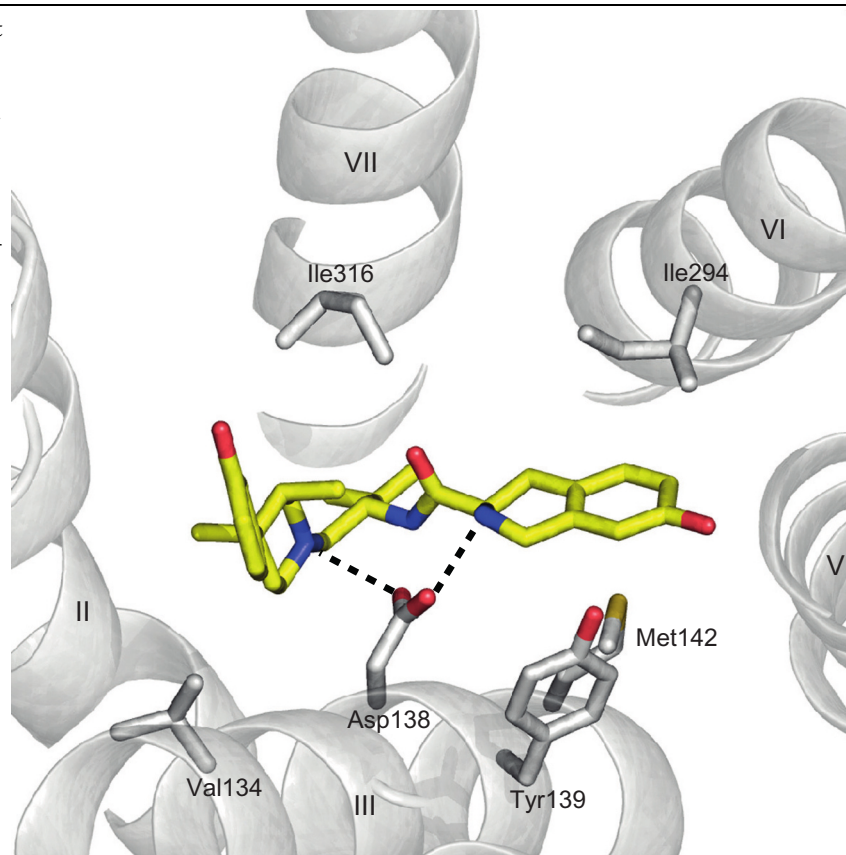
Naltrindole makes key H-bond interactions with Asp128^{3.32} and Tyr129^{3.33} and is enclosed by the hydrophobic environment formed by the residues Met132^{3.36}, Val281^{6.55} and Ile304^{7.39}.

The phenol group on the ligand likely forms water-mediated interactions with residues on TM5 (not shown as water molecules were not visible in the structure).



κ -Opioid receptor in complex with the antagonist JD₁Tic (**18**) at 2.90 Å, PDB = 4DJH [33].

JD₁Tic makes key H-bond interactions with Asp138^{3,32} and, similarly to observed in the other opioid receptors, it is also enclosed in the hydrophobic environment formed by residues Val134^{3,28}, Met142^{3,36}, Ile294^{6,55} and Ile316^{7,39}. The phenol group on the ligand likely forms water-mediated interactions with residues on TM5 (not shown as water molecules were not visible in the structure)

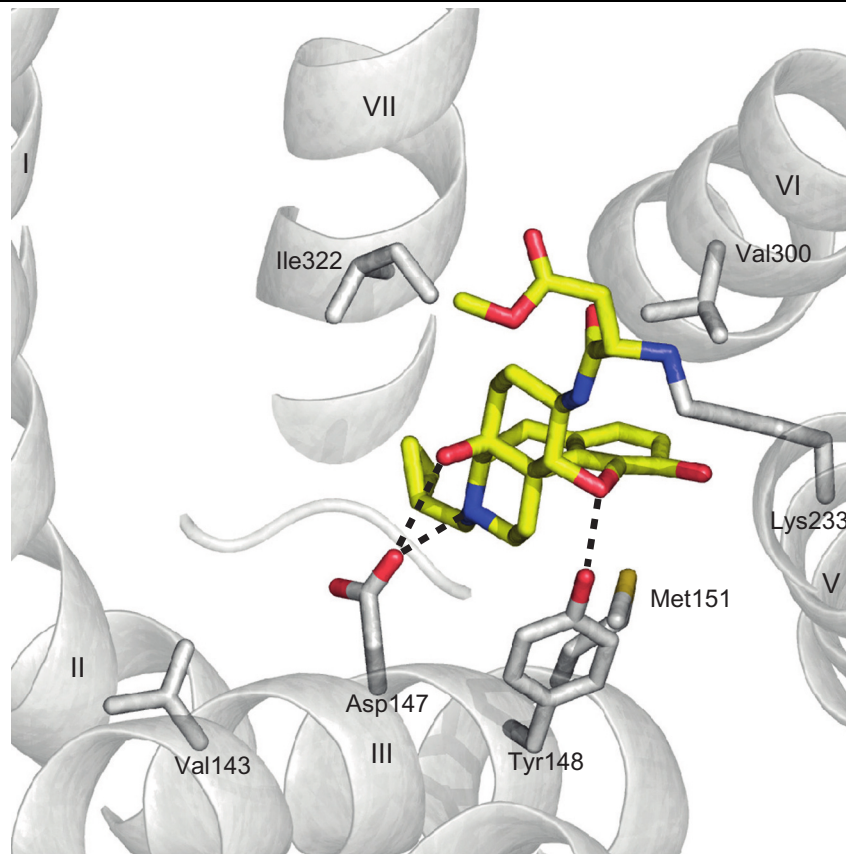


Continued

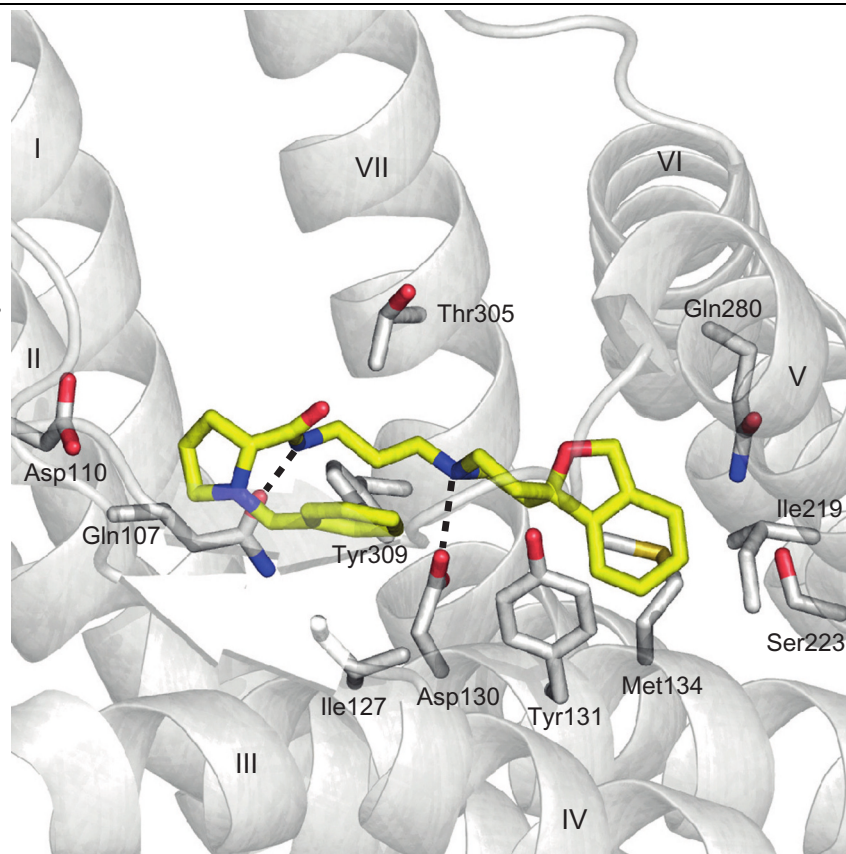
Table 1.1 List of Published GPCR Crystal Structures—cont'd
Target GPCR and Description of Binding Pocket **Ligand Binding Site**

μ -Opioid receptor in complex with beta-funaltrexamine (**19**), a morphinan antagonist at 2.80 Å, PDB = 4DKL [34].

Beta-funaltrexamine makes a covalent bond (via Michael addition) with Lys233^{5,39} and makes key H-bond interactions with Asp147^{3,32} and Tyr148^{3,33}. As observed in the other opioid receptors it is also enclosed in the hydrophobic environment formed by residues Met151^{3,36}, Val300^{6,55} and Ile322^{7,39}.



Nociceptin/orphanin FQ (N/O_{FQ}) receptor in complex with a peptide mimetic antagonist compound-24 (**20**) at 3.01 Å, PDB=4EA3 [35]. Compound-24 makes key H-bond interactions with Gln107^{2,60} and Asp130^{3,32} and a π - π interaction with Tyr131^{3,33}. Tyr309^{7,43} does not interact directly with the ligand but coordinates both Gln107^{2,60} and Asp130^{3,32} bridging the network of interactions. The ligand is also surrounded by the following residues: Asp110^{2,63}, Ile127^{3,29}, Met134^{3,36}, Ile219^{5,42}, Ser223^{5,46}, Gln280^{6,52} and Thr305^{7,39}.

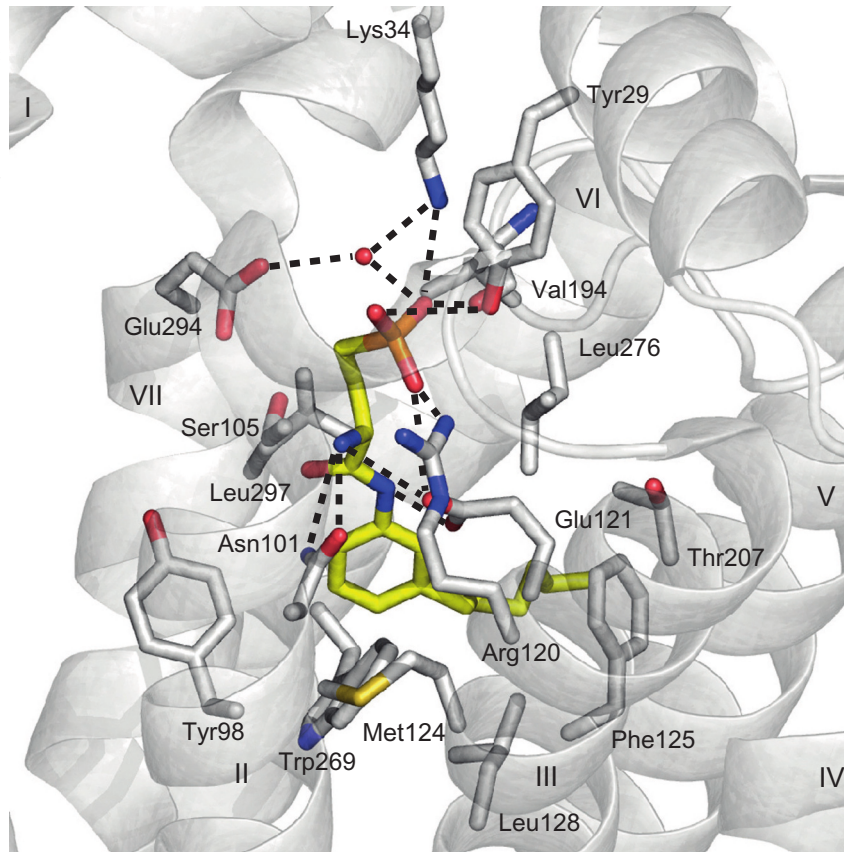


Continued

Table 1.1 List of Published GPCR Crystal Structures—cont'd
Target GPCR and Description of Binding Pocket **Ligand Binding Site**

Sphingosine 1-Phosphate S1P1 receptor in complex with the antagonist sphingolipid mimetic ML056 (**21**) at 2.80 Å, PDB = 3V2Y [36].

The ligand makes key H-bond interactions with Tyr29^{N-term}, Lys34^{N-term}, Asn101^{2.60}, Arg120^{3.28}, Glu121^{3.29} and one water molecule that bridges the ligand to Glu294^{7.37} and also Lys34^{N-term}. The ligand is surrounded by the residues Tyr98^{2.57}, Ser105^{2.64}, Met124^{3.32}, Phe125^{3.33}, Leu128^{3.36}, Val194^{ECL2}, Leu195^{ECL2}, Thr207^{5.44}, Phe210^{5.47}, Trp269^{6.48}, Leu272^{6.51}, Phe273^{6.52}, Leu276^{6.55} and Leu297^{7.40}.

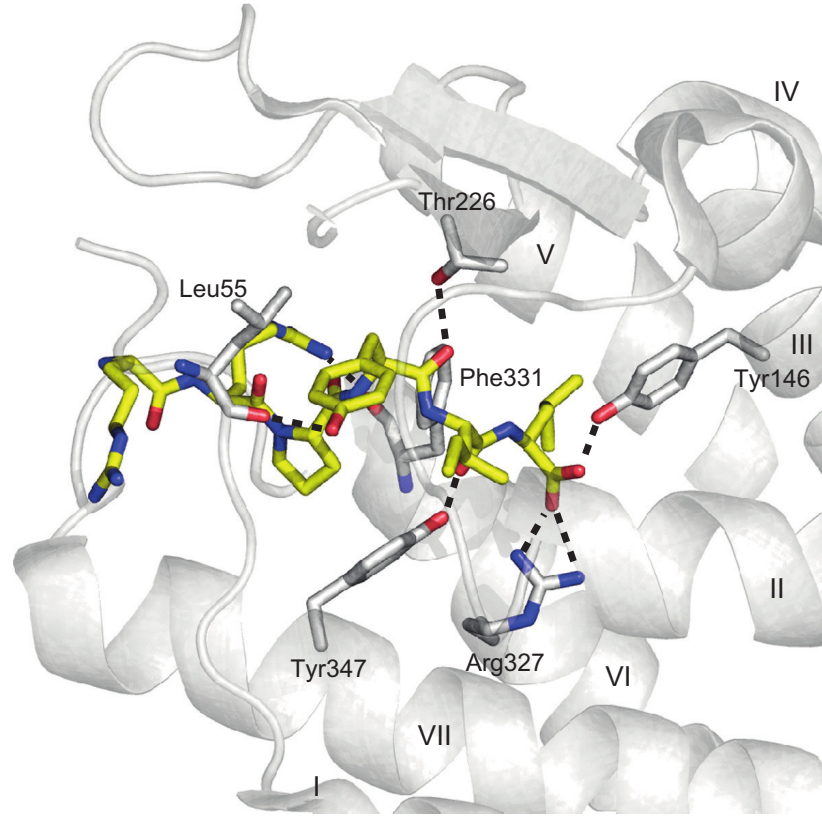


NTS1 neurotensin receptor in complex with the agonist neurotensin peptide fragment NTS₈₋₁₃ (**22**) at 2.80 Å, PDB = 4GRV [37].

The NTS₈₋₁₃ peptide makes key H-bond interactions with the main chain carbonyl of Leu55^{N-term} and Phe331^{6,58}, and with the side chains of Thr226^{ECL2} and Arg327^{6,54}. The C-terminal end of the peptide interacts with Tyr146^{3,29} and Arg327^{6,54}.

This structure is notable as the first Class A agonist peptide receptor structure.

The figure orientation was rotated for clarity, showing helix TM3 on the right.

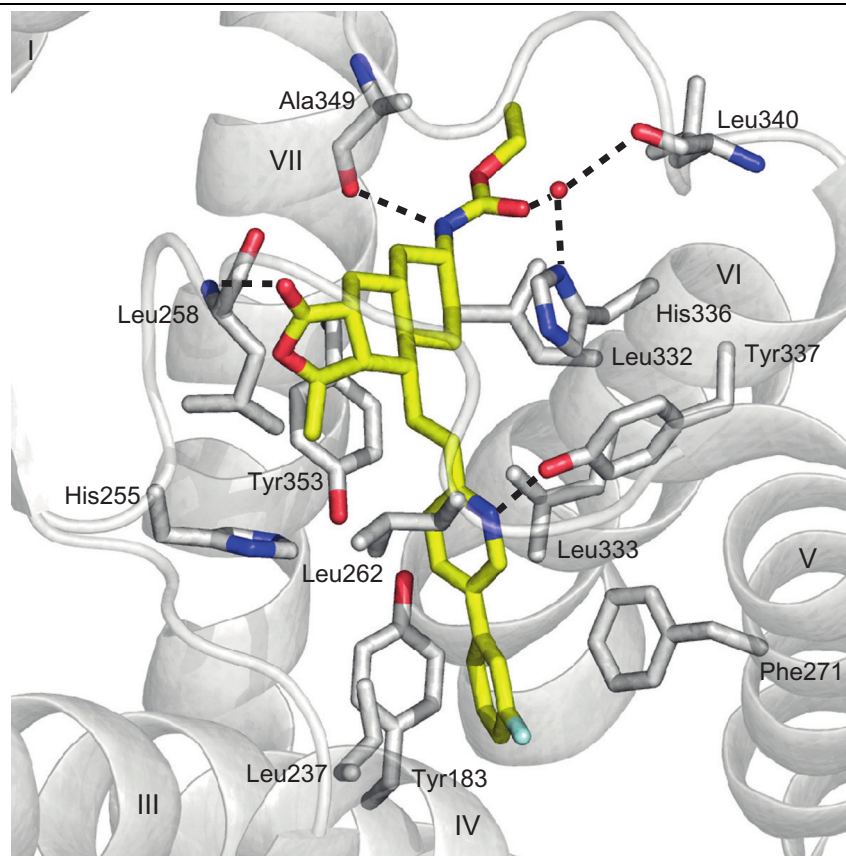


Continued

Table 1.1 List of Published GPCR Crystal Structures—cont'd
Target GPCR and Description of Binding Pocket **Ligand Binding Site**

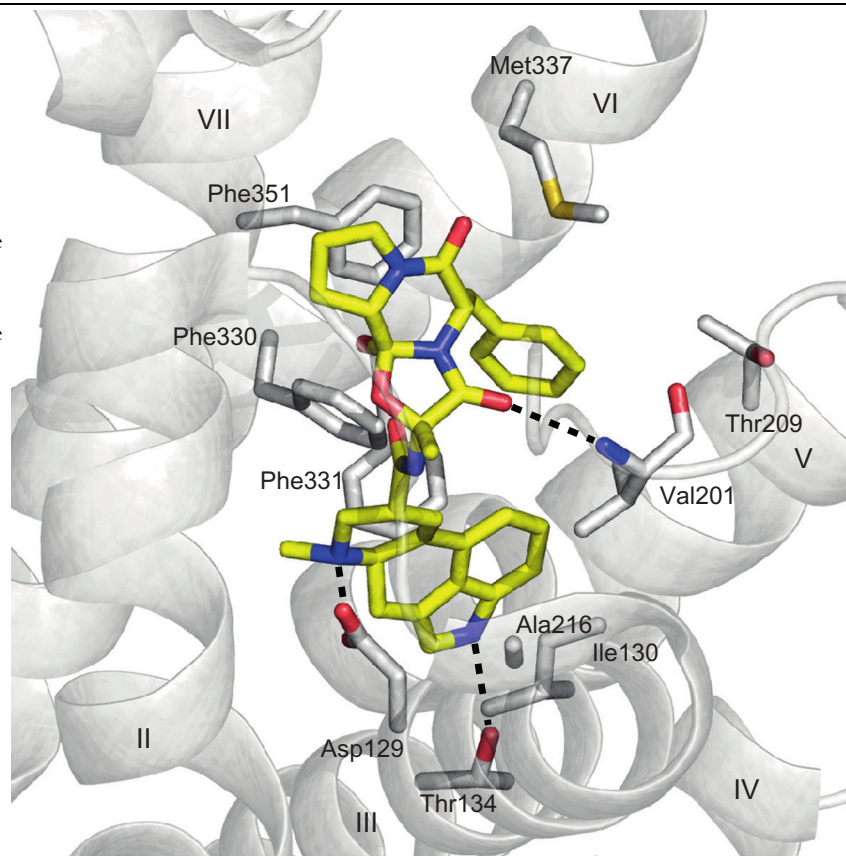
Protease-activated receptor 1 (PAR1) in complex with the antagonist vorapaxar (**23**) at 2.20 Å, PDB = 3VW7 [38].

Vorapaxar makes key H-bond interactions with the main chain nitrogen of Leu258^{ECL2} and the main chain carbonyl of Ala349^{7,31}. The pyridine ring of vorapaxar forms a strong hydrogen bond with the hydroxyl group of Tyr337^{6,59}. The fluoro-phenyl ring makes a π - π interaction with Tyr183^{3,33} and Phe271^{5,39}. One water molecule bridges vorapaxar to His336^{6,58} and Leu340^{ECL3}. The ligand is surrounded by the hydrophobic environment formed by Leu237^{4,60}, His255^{ECL2}, Leu262^{ECL2}, Leu263^{ECL2}, Leu332^{6,54}, Leu333^{6,55} and Tyr353^{7,35}.



5-Hydroxytryptamine receptor 1B (serotonin receptor) in complex with ergotamine (**24**) at 2.70 Å, PDB = 4IAR [39]. A structure with dihydroergotamine (**25**) at 2.80 Å, PDB = 4IAQ was also solved (not shown) [39].

Ergotamine makes key H-bond interactions with the main chain nitrogen of Val201^{ECL2} and with the side chain of Asp129^{3.32} and Thr134^{3.37}. Note the embedded tryptamine fragment within the ligand forms important interactions with the receptor. Other residues in the binding pocket are Trp125^{3.28}, Leu126^{3.29}, Ile130^{3.33}, Cys133^{3.36}, Val200^{ECL2}, Thr203^{ECL2}, Tyr208^{5.38}, Thr209^{5.39}, Ser212^{5.42}, Ala216^{5.46}, Trp327^{6.48}, Phe330^{6.51}, Phe331^{6.52}, Ser334^{6.55}, Met337^{6.58}, Pro338^{6.59}, Phe351^{7.35}, Asp352^{7.36}, Thr355^{7.39} and Tyr359^{7.43}.

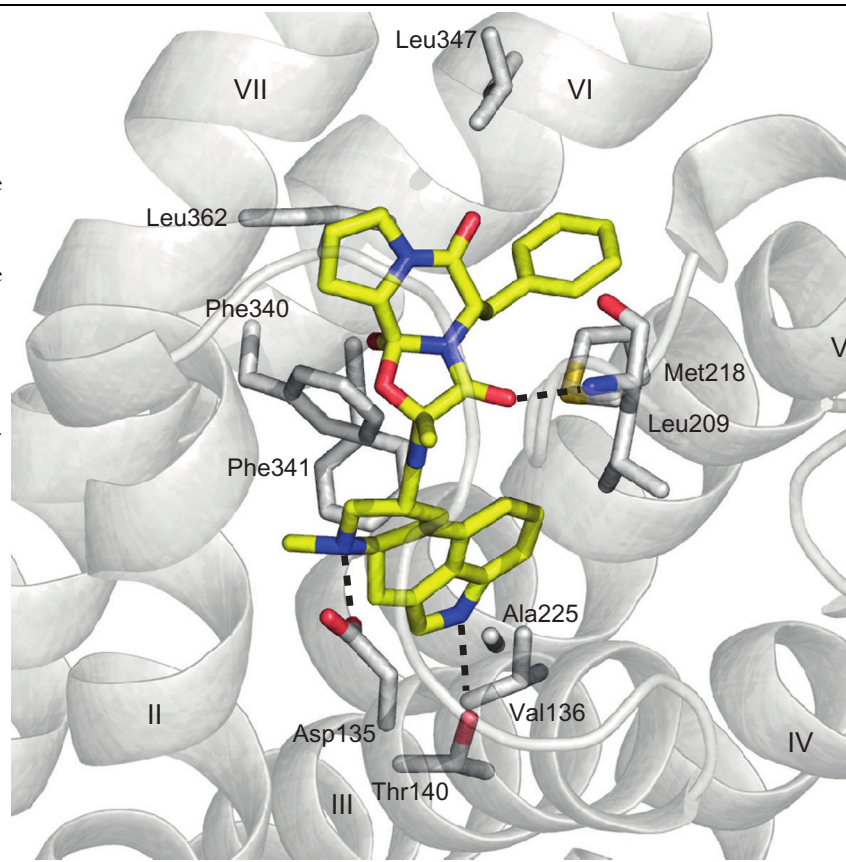


Continued

Table 1.1 List of Published GPCR Crystal Structures—cont'd
Target GPCR and Description of Binding Pocket **Ligand Binding Site**

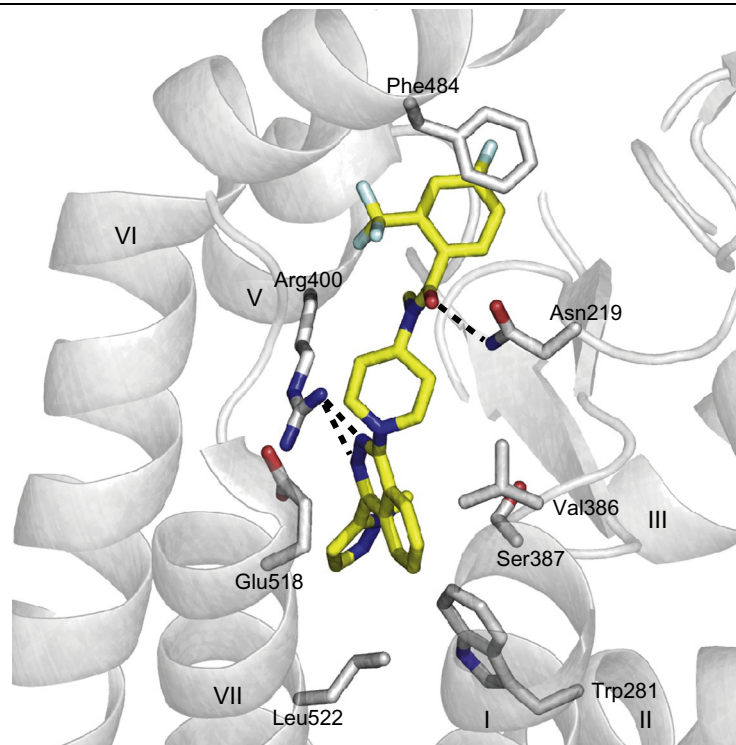
5-Hydroxytryptamine receptor 2B (serotonin receptor) in complex with ergotamine (**24**) at 2.70 Å, PDB = 4IB4 [40].

Ergotamine makes key H-bond interactions with the main chain nitrogen of Leu209^{ECL2} and with the side chain of Asp135^{3.32} and Thr140^{3.37}. Note the embedded tryptamine fragment within the ligand forms important interactions with the receptor. Other residues in the binding pocket are Trp131^{3.28}, Leu132^{3.29}, Val136^{3.33}, Ser139^{3.36}, Val208^{ECL2}, Lys211^{ECL2}, Phe217^{5.38}, Met218^{5.39}, Gly221^{5.42}, Ala225^{5.46}, Trp337^{6.48}, Phe340^{6.51}, Phe341^{6.52}, Asn344^{6.55}, Leu347^{6.58}, Val348^{6.59}, Leu362^{7.35}, Glu363^{7.36}, Val366^{7.39} and Tyr370^{7.43}.



Smoothened SMO receptor in complex with the antagonist LY2940680 (**26**) at 2.45 Å, PDB = 4JKV [41].

This is the first structure in the Class F receptor family. The ligand makes key H-bond interactions with Asn219^{ECDlinker} and Arg400^{5.39}. The fluorophenyl group makes a π - π interaction with Phe484^{ECL3}. The ligand is surrounded by Leu221^{ECDlinker}, Met230^{1.35}, Trp281^{2.57}, Asp384^{ECL2}, Val386^{ECL2}, Ser387^{ECL2}, Ile389^{ECL2}, Tyr394^{ECL2}, Lys395^{ECL2}, Gln477^{ECL3}, Trp480^{ECL3}, Glu481^{ECL3}, Pro513^{ECL3}, Glu518^{7.38}, Asn521^{7.41} and Leu522^{7.42}. The figure orientation was rotated for clarity, showing helix TM3 on the right.



Continued

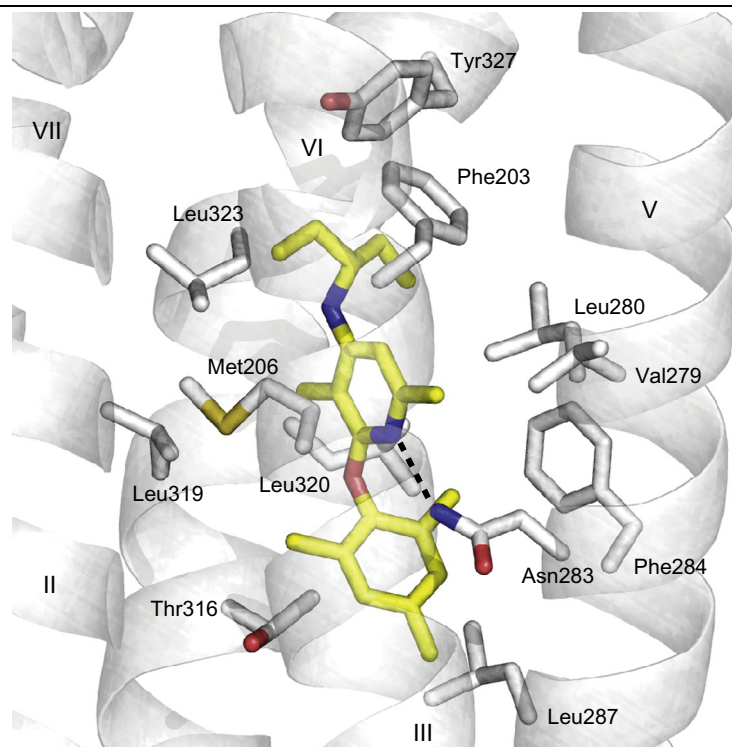
Table 1.1 List of Published GPCR Crystal Structures—cont'd
Target GPCR and Description of Binding Pocket **Ligand Binding Site**

CRF₁ receptor in complex with antagonist CP-376395 (**27**) at 3.0 Å, PDB = 4K5Y [18].

The structure of CRF₁ represents the first family B GPCR to be determined.

The antagonist CP-376395 is much more deeply buried in the binding pocket, when compared to all published class A structures [18].

The ligand makes a key H-bond interaction with Asn283^{5.50} from helix 5, and is surrounded by neighbouring hydrophobic residues Phe203^{3.44}, Met206^{3.47}, Val279^{5.46}, Leu280^{5.47}, Phe284^{5.51}, Leu287^{5.54}, Ile290^{5.57}, Thr316^{6.42}, Leu319^{6.45}, Leu320^{6.46}, Leu323^{6.49}, Gly324^{6.50} and Tyr327^{6.53}.



The figures in this table were prepared with the software Pymol [42].

proteolytic site or GPS domain) to yield two non-covalently attached subunits [43]. Currently, most Adhesion receptors are orphans and their biology and signalling are not well understood. Several have been reported to be activated by interactions with extracellular matrix proteins.

Class C GPCRs, which include the glutamate receptor family, also have a large N-terminus with a bi-lobed amino acid binding domain known as the ‘Venus fly trap’. The receptors function as dimers and bind simple amino acids such as glutamate and γ -aminobutyric acid (GABA) as well as ions [44]. Three taste receptors also fall into this family, including those for sucrose, aspartame and umami. Only two members of Class C are the target of marketed drugs (the GABA_B receptor and calcium sensing receptor), however there are many drugs directed at glutamate receptors currently in development [45–47]. Drugs for this family of GPCRs can bind either within the extracellular amino acid binding domain or within the TMD, where they act as allosteric modulators of the endogenous ligands.

Lastly, the Frizzled Class of GPCRs includes 10 Frizzled (FZD) receptors and the smoothened receptor (SMO). FZD receptors bind Wnt glycoproteins whereas SMO is activated by formation of a complex with another membrane protein called patched [48]. The TMD of this family is linked to a large extracellular domain containing a cysteine rich region that binds the Wnt ligands. In 2012 the first small molecule drug targeting this family was approved for the treatment of cancer, vismodegib. This compound binds within the TMD of SMO [49]. Recently, the structure of the SMO receptor in complex with a small molecule ligand has been solved (see Table 1.1) [41].



3. GPCR PROTEIN-LIGAND X-RAY STRUCTURES

The difficulty in obtaining diffracting crystals for GPCRs is due to the inherent flexibility of these receptors, for they exist in multiple conformational states. Crystallisation requires that the protein be in a single, homogeneous conformation, which can be obtained at least to some extent by the addition of a ligand that preferentially binds to a single conformation (e.g. antagonist or agonist). Crystallisation of membrane-associated proteins is conducted in a detergent medium. During crystallisation, crystal contacts are formed between hydrophilic regions of the protein that protrude from the detergent micelles. So as well as their flexibility, an additional challenge to crystallising GPCRs is that they contain relatively small hydrophilic domains, which are unable to serve as useful crystallisation contacts, and flexible loop regions that often need to be truncated.

Three approaches have proved successful in facilitating GPCR crystallisation. The first is formation of a fusion protein by introducing a well-folded soluble protein such as T4 lysozyme (T4L) into the third intracellular loop (ICL3) of the crystallisation construct. This fusion serves both to reduce the flexibility of the ICL3 region and to increase the surface available for crystal lattice contacts. The T4L fusion approach was first applied successfully to the crystallisation of the β_2 -adrenergic receptor (β_2 AR) [19] and a number of additional GPCR structures have been resolved using this approach (see Table 1.1). Fusion proteins have also been inserted in the second intracellular loop and at the N-terminus of the receptor. The second approach is to generate a complex of the GPCR with antibody fragments; this approach has been used to obtain antagonist and agonist conformations of the β_2 AR. A monoclonal antibody that bound and stabilised intracellular loop 3 (ICL3) of β_2 AR was generated by immunising mice with the receptor reconstituted into proteoliposomes [50]. A Fab (Fragment antigen binding) fragment of this antibody enabled the first crystal structure of β_2 AR to be solved [51], although at considerably lower resolution than the subsequent T4 fusion structure [19]. Remarkably, a nanobody that bound selectively to the active conformation of the β_2 AR receptor was identified by immunising llamas with purified agonist-bound β_2 AR. The nanobody appeared to mimic part of the G alpha subunit in its ability to promote the active conformational state of the receptor, facilitating the co-crystal structure of the receptor and nanobody in a conformation that showed similar conformational changes to those seen in the active opsin structure [21]. The differences in conformation between agonist bound as compared to ground state conformations (inverse agonist or antagonist form) are discussed below.

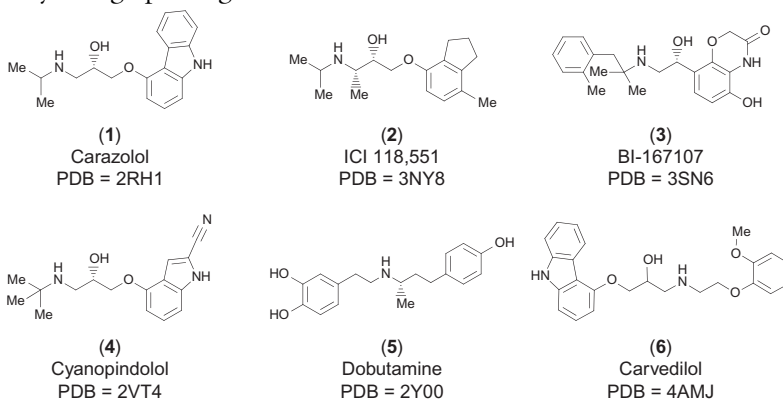
The third approach to facilitating crystallisation is to engineer the GPCR to exhibit higher stability, such that when solubilised from the cell membrane it behaves more like a soluble protein. This conformational thermostabilisation has been employed for several GPCRs including the β -adrenoceptors [52], the neurotensin receptor [53] and the adenosine A_{2A} receptor [54]. These engineered receptors are called stabilised receptors [55] or StaR proteins, and generally contain four to ten point mutations. Thermostabilisation has proved a generally applicable approach that greatly assists in crystallisation of GPCRs using conventional crystallisation methods. Furthermore, thermostabilisation allows structure determination with relatively weak ligands, which is critical to its use in drug discovery.

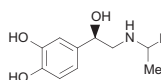
Despite the advances described earlier, the detergent environment required to crystallise GPCRs can still be unfavourable. In order to overcome this problem, crystallisation in a more lipidic environment, that perhaps serves to mimic

the environment of the cell membrane and give further stability to the receptor, is often required to obtain GPCR crystals. One particular method of choice is that of lipidic cubic phase (LCP) crystallisation or *in meso* crystallisation [56]. To date all of the GPCR structures obtained using the T4 fusion approach have also required LCP crystallisation [57]. However, use of the thermostabilisation methodology has allowed the structures of a number of GPCRs with a variety of ligands to be solved in normal vapour diffusion conditions.

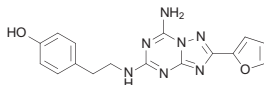
In Table 1.1, each GPCR that has been resolved in complex with a ligand is illustrated and the details of the protein–ligand interactions are described briefly. Where more than one ligand has been solved in complex with its receptor, generally only one example is given, unless the ligands bind to a different conformation of the receptor (e.g. inverse agonist/antagonist, partial agonist/agonist). The chemical structure of each ligand is given, along with its Protein Database code (PDB), immediately preceding the table for reference. It is beyond the scope of this review to discuss each receptor in detail in the text and instead this table is intended to give a useful insight into how ligands interact with GPCRs. As far as possible each complex is shown in a similar orientation to aid comparisons of one structure with the next, but if this was not possible this is noted in the legend. Throughout this chapter and in Table 1.1 the amino acid residues are denoted both by their number in the sequence and also by the Ballesteros–Weinstein number, which is a system that gives the relative position of a residue within each of the seven transmembrane helices [58]. In the Ballesteros–Weinstein nomenclature, the first superscripted number is that of the helix and the value after the decimal point is the sequence position relative to the most conserved residue in each helix which is given the number 50. A number of excellent reviews describe in more detail the published GPCR complexes and discuss not only the ligand–protein interactions but also the structural features of the proteins themselves [2,4,5,14,15,23,59–67].

Crystallographic ligands from Table 1.1

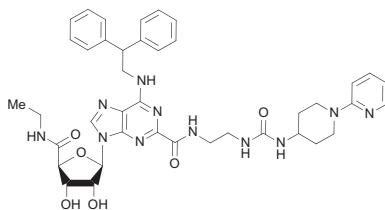




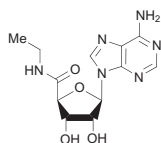
(7)
Isoprenaline
PDB = 2Y03



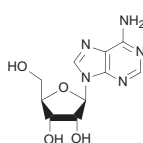
(8)
ZM241385
PDB = 4E1Y



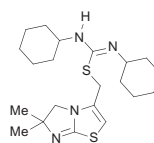
(9)
UK-432097
PDB = 3QAK



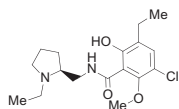
(10)
NECA
PDB = 2YDV



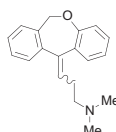
(11)
Adenosine
PDB = 2YDO



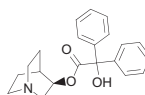
(12)
IT1t
PDB = 3ODU



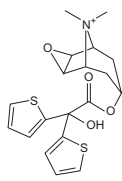
(13)
Eticlopride
PDB = 3PBL



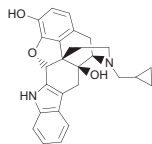
(14)
Doxepin
PDB = 3RZE



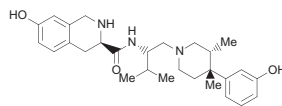
(15)
QNB
PDB = 3UON



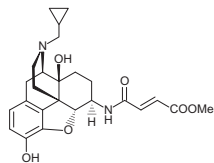
(16)
Tiotropium
PDB = 4DAJ



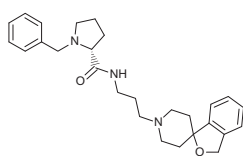
(17)
Naltindole
PDB = 4EJ4



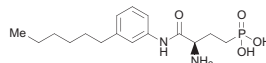
(18)
JDTric
PDB = 4DJH



(19)
Beta-funaltrexamine
PDB = 4DKL



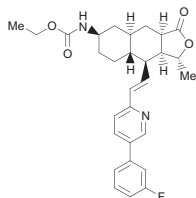
(20)
Compound-24
PDB = 4EA3



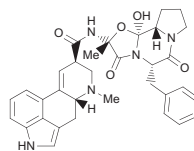
(21)
ML056
PDB = 3V2Y

H₂N-Arg-Arg-Pro-Tyr-Ile-Leu-OH

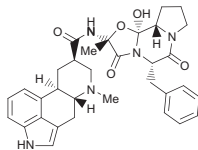
(22)
NTS₈₋₁₃
PDB = 4GRV



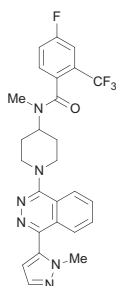
(23)
Vorapaxar
PDB = 3VW7



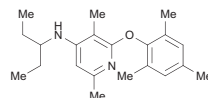
(24)
Ergotamine
PDB = 4IAR and PDB = 4IB4



(25)
Dihydroergotamine
PDB = 4IAQ



(26)
LY2940680
PDB = 4JKV



(27)
CP-376395
PDB = 4K5Y



4. MECHANISMS OF ACTIVATION: AGONIST BOUND STRUCTURES

Many of the most effective drugs targeted at GPCRs, unlike those for many other protein classes, mediate their therapeutic response through activation of the receptor; examples include the opioids, triptans and beta agonists [68]. SBDD for agonists is more complicated than simply increasing the affinity for the binding site. Agonist drugs that fully activate the receptor might actually have relatively weak affinity for the binding site of the ground state of the receptor (antagonist or inverse agonist form). Specific contacts between the receptor and agonist are sometimes a prerequisite to engage the activation process and trigger the conformational changes in the receptor required to bind and then activate intracellular signalling pathways. This conformational change can be ‘up-hill’ in energy, hence lowering the apparent overall binding affinity of the compound. To add further to this complexity, agonists can vary in efficacy, namely in their intrinsic ability to activate the receptor and downstream signalling pathways, ranging from

full agonists, which elicit the maximal response, to various degrees of partial agonists [69].

GPCRs are considered to exist in at least two conformational states that are in equilibrium and have been described by the ternary complex model [70]. R represents the ground or inactive state and R* the active conformation that can couple to G proteins. The baseline equilibrium between R and R* in the absence of a ligand determines the level of basal versus constitutive activity and varies among receptors. Agonist binding alters the equilibrium in favour of the R* form whilst inverse agonists favour the R state. It has long been understood that the affinity of agonist binding to the receptor is altered upon formation of the R* state. For example, in the case of agonist binding to the β_2 -adrenoceptor, biphasic binding affinity curves indicate a high (2 nM) and low affinity site (300 nM), which can be regulated by the addition of guanine nucleotides that promote dissociation of the G protein [71].

To apply structure-based design techniques to agonists, an understanding of the conformational changes that occur during receptor activation, and in particular the changes in the binding pocket resulting in high affinity binding, is of critical importance. The first active state GPCR structures obtained were of the light sensing receptor rhodopsin [72,73]. These structures were very informative with regard to the quite large transmembrane movements that occur upon receptor activation, particularly in TM6, which allow the G protein to bind to the intracellular face of the receptor. However, these structures have limited utility when modelling the ligand binding site of other GPCRs since rhodopsin is unique in having a covalently bound ligand, retinal, which is activated by light-induced isomerisation. In particular, retinal is encapsulated within the binding site as the extracellular loops of the receptor fold over the top of the ligand binding site.

Typically, binding of agonist alone to the receptor is not sufficient to fully stabilise the R* state and enable crystallisation. It is necessary to also have the G protein present, or a G protein mimetic, or alternatively to use mutagenesis to alter the equilibrium to the agonist state [74,75]. Four agonist-bound structures have been determined for an avian β_1 -adrenoceptor thermostabilised in the R state (Table 1.1). These structures did not reveal an obvious active state conformation with respect to, for example, movement of helices at the intracellular surface; an aspect most likely due to the thermostabilisation in the R state. Nevertheless, these structures were particularly useful for drug discovery as they included agonists with different efficacies ranging from the partial agonists dobutamine (5)

and salbutamol, to the full agonists isoprenaline (**7**) and carmoterol, with small but consistent changes evident within the binding pocket around the ligands [23]. These thermostabilised structures led to the first structural understanding of the basis of efficacy. For example, the full agonists were found to make a hydrogen bond to Ser215^{5.46} with a consequent small contraction of the binding pocket to generate the presumed high affinity state. In contrast, the partial agonists did not make this particular hydrogen bond and therefore were less able to stabilise the contraction of the ligand binding pocket. With regard to the equilibrium position between R and R^{*}, it could be inferred from these structures that the partial agonists are less able to drive the equilibrium to the R^{*} state than full agonists.

In 2011 Brian Kobilka and his team at Stanford solved the crystal structure of β_2 AR bound to the agonist BI-167107 (**3**) (Table 1.1) together with a single domain antibody (nanobody), which mimics the G protein. This was the first structure of a GPCR in the fully active state [76]. Binding of the nanobody to the receptor was shown to increase the affinity of agonist binding in a similar way to addition of the G protein. In this structure, there were further contractions of the binding site compared to the agonist bound structures of Warne *et al.* [22–24] and a change in rotamer conformation of Ser207^{5.46}. This was then followed by the agonist bound complex of the β_2 AR complexed with the G protein heterotrimer, showing for the first time the interactions between a G protein and the receptor at the intracellular surface in molecular detail (Table 1.1) [21]. This breakthrough contributed to the award of the 2012 Nobel Prize for chemistry to Kobilka and Lefkowitz [77].

The first GPCR structure to be solved in complex with its natural ligand was the adenosine A_{2A} receptor. To obtain a co-structure with such a weakly binding ligand (adenosine (**11**)) the receptor was thermostabilised by mutagenesis into the agonist state (Table 1.1) [26]. This approach enabled structures of the receptor to be solved both with adenosine and the related agonist NECA (5'-(*N*-ethylcarboxamido)adenosine (**10**)). Additionally, a structure of the very high affinity agonist UK-432097 (**9**) (Table 1.1) in complex with the adenosine A_{2A} receptor has also been solved, in this instance using a fusion protein approach to aid crystallisation and a large and very potent agonist ligand to trap the agonist conformation [25]. A common structural feature for adenosine agonists is that the ribose ring confers agonist activity. The ribose moiety sits deep within the receptor binding pocket with the 2' and 3' –OH groups making hydrogen bonds with His278^{7.43} and Ser277^{7.42}. In the UK-432097 structure, interaction with these residues results in a 2 Å

movement inwards of helix 7 towards helix 3 enabling hydrogen bonding interactions with Thr88^{3,36} and non-polar interactions with Val84^{3,32} and Leu85^{3,33}. These key interactions also result in a 2 Å upward movement of helix 3. The contraction in the binding site enabling high affinity binding also involves an inward bulge in helix 5 in conjunction with an outward movement of the cytoplasmic end of the helix. In contrast to agonists, inverse agonists such as ZM241385 (**8**) (Table 1.1) are not accommodated within the agonist binding site and serve to maintain the receptor in the inactive state whereas neutral antagonists [78,79] fit equally into both agonist and antagonist binding pockets of adenosine receptors and mediate their biological activity by simple displacement or prevention of agonist binding.

The neurotensin receptor (NTS₁) is activated by the relatively short (13 aa) peptide neurotensin. In 2012 a structure of a thermostabilised NTS₁ bound to NTS₈₋₁₃ (**22**) (Table 1.1) was solved in an active-like state. The peptide was found to bind in an extended conformation perpendicular to the plane of the membrane [37] although, in contrast to the receptors described earlier, the peptide was not found to reach deep into the receptor TMD binding pocket. Major interactions are with the N-terminus, all three extracellular loops and the upper portion of TM2–TM7 (Table 1.1). This structure revealed complementary charge interactions between the ligand and its binding pocket, extensive van der Waals interactions, hydrogen bonds and a salt bridge with Arg237^{6,54}. The entrance to the binding pocket appears to be quite open although it is partially capped by a β-hairpin from the second extracellular loop (ECL2) and part of the N-terminus. A full understanding of the changes within the peptide receptor binding pocket upon activation will require a structure of the antagonist bound receptor. Nevertheless from these data it would appear that the exact mechanisms of receptor activation for peptide receptors differ from those for aminergic receptors.

Two other members of the aminergic sub-family of Class A receptors (5-HT_{1B} and 5-HT_{2B}) have been crystallised in complex with the agonist anti-migraine drugs ergotamine (**24**) and dihydroergotamine (**25**) (Table 1.1) [39,40]. A comparison of these structures provides an understanding of subtype selectivity in serotonin receptors. This is particularly important since activity at the 5-HT_{2B} receptors is responsible for toxic heart valvulopathy [80]. Ergotamine (**24**) sits deep within the receptor, anchored through a salt bridge to Asp129^{3,32}, a residue highly conserved within the serotonin receptor sub-family. The cyclic tripeptide moiety of ergotamine extends outwards toward the extracellular side of the receptor, occupying an

‘extended pocket’, which would not normally be occupied by the endogenous ligand. Whilst the orthosteric binding pocket occupied by 5-HT is highly conserved across the serotonin family, the extended pocket is more diverse and allows the development of highly selective agonists and antagonists. Although this group of therapeutic compounds sits in a similar way in both the 5-HT_{1B} and 5-HT_{2B} receptors, the shape of the binding pockets differs significantly. For example, in the 5-HT_{2B} receptor the pocket is wider primarily due to differences in the position of the top of TM5 and also in the conformation of the phenyl group of the ergotamine tripeptide. Of note, the extended binding pocket occupied by the ergotamine tripeptide partially overlaps with the analogous site in the muscarinic M₂ structure (Table 1.1); this has been suggested to serve as the binding site for allosteric modulators [30].



5. BIASED AGONISM

GPCRs can activate multiple signalling pathways via both G protein dependent and independent mechanisms. Recently, it has been shown that some compounds can act as ‘biased’ agonists, which differentially trigger downstream pathways [5]. This feature raises the possibility that compounds can be designed to activate select pathways, mediating therapeutic benefits whilst having lower activity towards pathways associated with side effects. Compounds that differentially signal through G proteins and β -arrestin are of particular interest [81]. For example, μ -opioid agonists designed to signal via G proteins but not β -arrestins would be predicted to result in higher analgesic efficacy, yet less gastrointestinal dysfunction and reduced respiratory suppression compared with morphine [82]. SBDD that exploits this differential signalling potential of GPCRs, together with a precise understanding of GPCR structure, represents the ‘holy grail’ of GPCR pharmacology and drug discovery.

Presently, the structural basis of biased agonism is poorly understood, although it is presumed that biased ligands stabilise different receptor conformations that have an altered ability to interact with downstream signalling effectors. To gain insight, structures need to be solved of the same receptor complexed with a range of differently biased agonists. Some information has been provided by the structures of 5-HT_{1B} and 5-HT_{2B} receptors in complex with ergotamine (**24**) and dihydroergotamine (**25**) (discussed earlier and Table 1.1), since ergolines display strongly biased signalling towards β -arrestin via 5-HT_{2B} but are unbiased via 5-HT_{1B}. In the 5-HT_{2B}

structure, interactions between ergotamine and extracellular loop 2 (ECL2) are hypothesised to constrain the top of TM5 and TM6, potentially preventing rearrangements in these helices, proposed to be required to generate the active G protein coupled state.

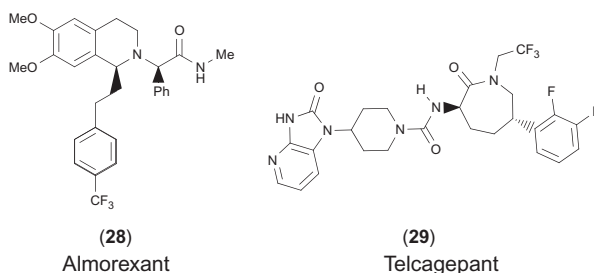


6. TRADITIONAL APPROACHES TO GPCR DRUG DISCOVERY AND THE NEED FOR CHANGE

Although up to 30% of drugs on the market are directed at GPCRs, the majority of these are targeted at the monoamine subfamily of receptors, which includes β -adrenergic receptors, dopamine receptors and 5-HT receptors [83]. These drugs were discovered primarily by screening analogues of the natural ligand using tissue-based assays [84,85]. Whilst this approach has been highly successful in identifying effective drugs, many of these compounds are poorly selective versus related receptors and are, in fact, active across multiple receptors within the monoamine family. Furthermore, when this approach has been applied to other GPCR families, the resulting drugs often suffer from problems associated with properties of the endogenous ligand. For example, drugs targeted at prostaglandin receptors are related to the prostanoid ligands, which are unstable and have poor pharmacokinetic properties. In addition, in cases where the natural GPCR ligands are peptides or larger hormones, it is often not possible to generate orally bioavailable drugs using a peptidic starting point for lead generation [15].

More recently, the availability of cloned GPCRs has led to development of miniaturised recombinant functional screening assays, enabling high-throughput screening (HTS) of large compound libraries of millions of compounds. However, the use of HTS in combination with GPCR functional screening has a number of problems. Firstly, the false positive hit rate in HTS is high due to non-receptor specific activation of downstream signalling pathways. Such compounds must be eliminated by running parallel screens in cells that lack the target receptor. A second problem is that selection of 'hits' is based primarily on compound potency, which creates a bias towards compounds with a higher molecular weight and higher lipophilicity; often not the best starting points for lead optimisation [86]. For as these hits undergo rounds of iterative chemistry to optimise potency, there is a tendency to add on further bulk, thereby increasing the molecular weight and lipophilicity. Such compounds have been shown to have an increased likelihood of toxicity and a high attrition rate during development [86]. Examples of GPCR drugs from HTS that have failed in clinical trials and

possess the aforementioned sub-optimal properties are the dual orexin antagonist almorexant (**28**), and the calcitonin gene-related peptide receptor (CGRP) antagonist telcagepant (**29**).



To date only 20% of non-olfactory GPCRs have been drugged with small molecules. The remaining receptors include many potential therapeutic targets according to biological rationale and clinical validation. For example, there are marketed peptides for many receptors including GLP-1 [87], GLP-2 [88], PTH1 [89] and growth hormone releasing hormone receptor (GHRH) [90], but no oral small molecule drugs have been identified for these receptors. SBDD in combination with fragment-based screening has proved very successful for drug discovery directed at enzyme targets [91–95]. Such approaches were previously not applicable to GPCRs due to the lack of X-ray structures and difficulty in obtaining purified protein for fragment screening by biophysical techniques. However, recent technological developments in the stabilisation of GPCRs (discussed earlier) now enable production of large quantities of correctly folded, purified protein suitable for biophysical and structural studies [96], as well as fragment screening [97]. Furthermore, additional breakthroughs in protein engineering and membrane protein crystallisation have facilitated the solution of GPCR X-ray structures (Table 1.1) [61,98].

7. POTENTIAL OF SBDD AND FBDD FOR GPCR DRUG DISCOVERY

It is intuitively obvious that a three-dimensional structure of a ligand bound to its receptor will be useful in the design of a drug. Therefore, the primary impact of SBDD on GPCR drug discovery is through more efficient identification, exploitation and optimisation of hits that result in higher quality lead compounds. However, GPCR medicinal chemists have long been used to working empirically, that is modifying features of a chemical

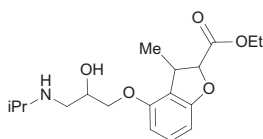
series iteratively and systematically rather than taking bold steps predicted from modelling or X-ray structural data. Additionally, the potency of a molecule is only one feature of its therapeutic properties and optimisation of solubility, pharmacokinetic and other pharmaceutical properties could be argued to be somewhat tangential to the insight given by protein–ligand binding information. However, there is now an increasing understanding in the medicinal chemistry community that smaller, more polar ligands have a much higher chance of becoming an approved drug and that SBDD can radically improve the opportunities to optimise molecules in an atom-efficient manner [86,94,99,100]. One factor that has driven this move towards multi-parameter optimisation is the advent of fragment-based drug design (FBDD) over the last 10–15 years, in which very small and weak but ligand efficient molecules are used as the starting points for structure-based design [99]. It is beyond the scope of this review to discuss the FBDD methodology and precedents but the reader is referred to a number of excellent reviews on the subject [93,94,101–104]. In the next section, some early examples of FBDD methodology applied to GPCRs are outlined, both regarding identification of fragment hits and also their optimisation to lead compounds.

A second impact of SBDD on GPCR drug discovery is likely to be the rational optimisation of receptor selectivity. This area is still in its infancy, but in our own research we have been able to use SBDD methods to design a selective adenosine A_{2A} antagonist and highly selective muscarinic M_1 agonists [105,106]. In the next section, a number of examples of FBDD and SBDD are described which encompass hit identification, hit and lead optimisation, as well as design and understanding of selectivity. Over the last 5 years there has been a plethora of published studies exploiting and building on the newly available GPCR structural data with modelling and drug design efforts. As such it is not possible for us to do justice to all of this work here. Therefore, in the following section we have focused on some representative examples and receptors, which serve to illustrate the approaches that are now possible. The reader is referred to a number of other review articles that describe further examples and some of the work below in more detail [4,15,60,62,107–112].

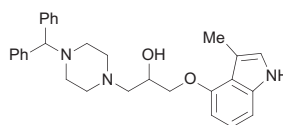
7.1. Beta Adrenergic Receptors

The crystal structures of both antagonist and agonist ligands complexed with beta adrenergic receptors β_1AR and β_2AR have facilitated virtual screening and hit generation for these targets, which now serve as paradigms of GPCR

drug design. Kolb *et al.* exploited the antagonist-bound structure of β_2 AR (2RH1) for virtual screening of one million compounds with lead-like properties, with the aim of demonstrating the utility of virtual screening for GPCR targets [113]. In a radioligand binding assay, 25 compounds selected from the *in silico* screen resulted in 6 hits (K_i values 9 nM–3.2 μ M; 24% hit rate), (30) being one example. Similarly, Topiol *et al.* performed docking and virtual screening for β_2 AR with in-house and external databases [114,115]. Hit rates were 36% and 12% for the in-house and commercial libraries, respectively (K_i values 0.1 nM–21 μ M and K_i 14 nM–4.3 μ M) whilst only a 0.3% hit rate was achieved with a control set of randomly selected compounds. Some familiar looking hydroxylamine chemotypes were re-discovered in the hit set but these included some highly potent examples, such as (31), offering opportunities for novel chemical optimisation. De Graaf and Rognan attempted to generate an agonist model based on the β_2 AR antagonist-bound structure in which the rotameric states of Ser212^{5.43} and Ser215^{5.46} within the binding site were adjusted to enable H-bonding of the receptor to the hydroxyl groups of agonist ligands [116]. Notably, this prediction was attempted before the agonist co-complex was published (Table 1.1). The modelled receptor binding site outperformed, during virtual screening, the original X-ray structure in docking of partial/full agonists from decoy ligands. This study demonstrates that, at least for some GPCRs, the active state of the receptor can be modelled with reasonable confidence. The agonist conformation has now been crystallised with agonist ligands (Table 1.1).



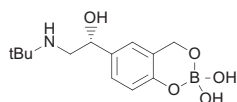
(30)
 β_2 AR antagonist
 $pK_i = 8.0$



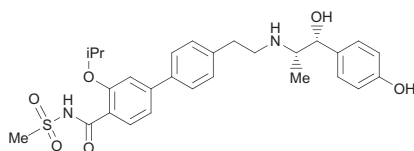
(31)
 β_2 AR antagonist
 $K_d = 0.3$ nM

In addition to docking and virtual screening studies, SBDD has also started to be applied to the β -adrenergic receptors. Soriano-Ursúa *et al.* investigated boron-containing analogues of β_2 AR agonists, their design based on the β_2 receptor structure [117]. One analogue (32) was found to have higher potency than the corresponding diol in a functional assay (relaxation of isolated guinea pig tracheal rings). Several analogues were also shown to be competitively antagonised by β_2 AR antagonists. Hattori *et al.*

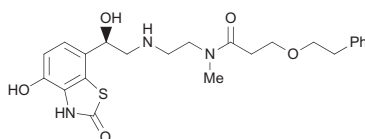
explored structure driven modifications of a series of biphenyl analogues containing acylsulfonamides, such as **(33)**, with the goal of obtaining potent and selective β_3 AR agonists [118]. The predicted binding pose was utilised to rationalise selectivity and potency and is presented as the basis for future design. A series of high efficacy β_2 AR agonists (e.g. **(34)**) derived from Sibenadet, notably devoid of the usual benzylic alcohol group found in most potent agonists, were generated by Stocks *et al.* [119]. The authors propose an induced fit whereby Trp286 moves to produce a new lipophilic pocket to accommodate the ligand.

**(32)**

β_2 AR agonist
 $K_d = 100$ nM

**(33)**

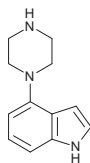
Selective β_3 AR agonist

**(34)**

High efficacy β_2 AR agonist

In a recent paper by Christopher *et al.*, the antagonist-stabilised conformation of β_1 AR (StaR β_1 AR) was successfully employed firstly for fragment screening and then for X-ray crystallographic studies of analogues of the fragment hits [120]. Simple phenyl piperazine hits were identified using surface plasmon resonance (SPR) screening of the StaR protein immobilised on a chip. Modelling of the binding modes of several related hits with affinities in the range of 10–50 μ M led to the purchase of selected analogues for further screening. In particular, an indole-containing derivative (**(35)**) was selected to interact with the OH of Ser 211^{5,42}. This compound had a significantly improved affinity of approximately 60 nM (assessed using a radioligand binding assay). Crystal structures were then solved with this ligand and another analogue from the same series, confirming the modelling hypothesis and establishing the basis for further optimisation (as yet not reported). This case study demonstrates, for the first time, that the principles and practise of fragment-based drug discovery (briefly outlined earlier) can

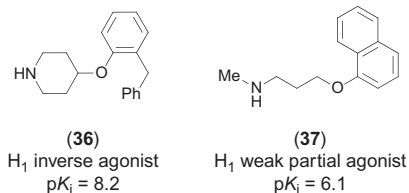
be applied to GPCRs and heralds enormous opportunities for future research in this area.



(35)
 β_1 AR antagonist
 $pK_i = 7.17$
LE = 0.65

7.2. Histamine Receptor

Publication of the histamine H_1 receptor structure (Table 1.1) was quickly followed by a virtual screening study using the ligand–protein binding data [121]. A large library of 757,728 fragment-like compounds (defined as containing fewer than 22 non-hydrogen atoms) was used as the test set. First the library was filtered to retain only molecules carrying a formal charge of +1 (after tautomers and protonation states were generated), which reduced the test set to 108,790 fragments. This was to ensure that the fragments had the potential to form ionic interactions with Asp107^{3.32} (TM3) with the assumption that this would be an absolute requirement for binding to the receptor. The docking program PLANTS was then used to carry out the virtual screen. Next, fragments forming an interaction with Asp107^{3.32} in the predicted binding pose were selected, leaving 95,147 molecules. Further post-processing was conducted, using interaction fingerprints derived from the contacts made by the ligand doxepin (present in the co-crystallised H_1 receptor structure). Finally, the most promising 354 fragments were subjected to Tanimoto-based similarity analysis with known H_1 antagonists and visually inspected, such that 30 fragments were finally selected for empirical study. Of the 26 compounds available for purchase, 19 fragments exhibited H_1 affinity, giving an impressive 73% experimental hit rate with hits in an affinity range of 10 μ M–6 nM. Compounds (36) and (37) are representative hit molecules. This case study corroborates that fragment-sized hit molecules can readily be identified for a number of Class A aminergic GPCRs, indicating that GPCRs are tractable to FBDD approaches that deliver hits with high ligand efficiency (LE) [99].

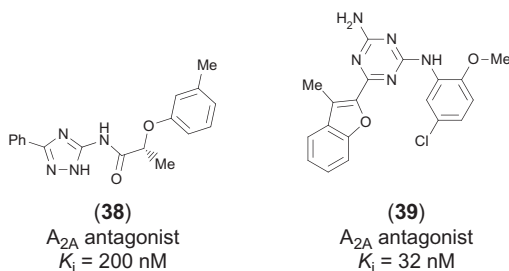


7.3. Adenosine Receptors

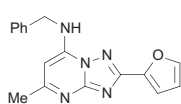
Drug discovery research concerning the adenosine receptor family (A_1 , A_{2A} , A_{2B} and A_3) encompasses a large body of work with multiple compounds (both agonists and antagonists) being investigated clinically for the treatment of cardiovascular disease, asthma, Parkinson's disease and cognitive disorders [112]. The multiple published crystal structures of the adenosine A_{2A} receptor bound to small molecule ligands in both antagonist and agonist receptor conformations are now having a considerable impact on the adenosine receptor field (Table 1.1). SBDD approaches to adenosine receptors are the subject of a very recent and excellent review by Jacobson [107].

Even before the first adenosine receptor X-ray structure was published (ZM241385 (8) complexed with A_{2A} -T4L [122]), its value was presaged by Michino *et al.* who initiated a community wide, blind prediction assessment of the ligand-receptor X-ray complex [123]. Indeed, 29 groups submitted 206 structural models before the release of the experimental X-ray co-ordinates. The best model had a ligand root mean squared deviation (RMSD) of 2.8 Å and a binding site RMSD of 3.4 Å. More generally, the results highlighted that ligand-binding pose predictions, and conformational modelling of extracellular loops, remain very challenging. The adenosine A_{2A} -T4L X-ray complex was subsequently successfully exploited for virtual screening by several groups. Carlsson *et al.* docked *in silico* 1.4 million compounds and selected 20 for screening [124]. Seven compounds (35%) were found to be hits using a radioligand binding assay, with affinities in the range 200 nM–8.8 μM. An example is compound (38). These hits were all shown to be antagonists in a functional assay and, in general, the hits exhibited selectivity with respect to the closely related adenosine A_1 and A_3 receptors, building confidence in their specificity of binding. The binding modes of the best hits were also assessed in more detail and H-bonding with Asn253^{6,55} and Glu169 (ECL2) seemed to be important. These residues are likely to be critical for binding of the X-ray ligand ZM241385 (8) (Table 1.1) to the receptor. In an analogous study, Katritch *et al.* performed

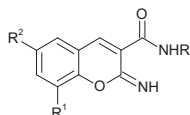
a virtual screen of adenosine A_{2A} -T4L with 4.3 million compounds [125]. In this case, 23 of the 56 molecules were found to be active (41%), with affinities in the range 32 nM–10 μ M (an example is compound (39)). The hits in this study were also shown to be antagonists, but a key difference was that selectivity was relatively low with respect to the adenosine A_1 receptor subtype. Taken together, these two virtual screening projects demonstrate that small and polar hits with respectable LE values can be identified for the adenosine receptor family by virtual screening.



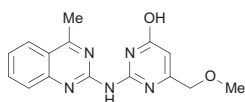
Van der Horst *et al.* carried out a sub-structure-based virtual screen of adenosine A_{2A} , employing a number of different ligand-based screening methods and compared their results with previous virtual screens [126]. Thirty-six compounds were selected and screened, of which eight were hits (>30% inhibition at 30 μ M; a 22% hit rate), including compound (40). Similarly Areias *et al.* used ligand-based *in silico* screening to efficiently identify a novel series of chromene A_{2A} antagonists (41) [127]. These studies support the utility of ligand-based data for a target of interest and would suggest there is value in considering both ligand-based and virtual screening approaches to hit identification. Indeed, Sanders *et al.* combined ligand based and virtual screening methods to study three receptors β_2AR , A_{2A} and the sphingosine 1-phosphate receptor (S1P1), selecting 300 compounds per target (using consensus scoring) but screening all 900 compounds in each of the three screening assays [128]. Screening hits were identified for each target: 6 for β_2AR , 18 for A_{2A} (e.g. (42)) and 3 for S1P1. However, a number of the hits were not actually against the target for which they were initially selected, highlighting how GPCR pharmacophores overlap, but also perhaps how serendipity is still an important part of drug discovery. Lastly, van Westen *et al.* very successfully employed a virtual screening protocol based on proteochemometric (PCM) modelling to identify nanomolar hits for A_{2A} and A_1 receptors, including compound (43) [129].



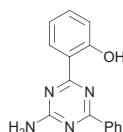
(40)
A_{2A} antagonist
K_i = 770 nM



R₁ — H, OH, OMe
R₂ — H, Cl, Br
R — H, alkyl, cycloalkyl,
heteroaromatic
(41)
A_{2A} antagonists



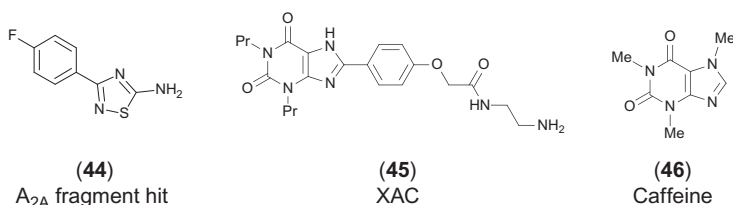
(42)
A_{2A} antagonist
pK_i = 6.2



(43)
Non-selective
A_{2A} antagonist
K_i = 43 nM

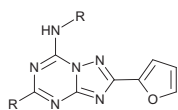
The adenosine A_{2A} receptor has been a test case for a number of biophysical fragment screening approaches. Target-immobilised NMR screening (TINS), is a sensitive method used to detect relatively weak interactions between proteins and small molecules [97]. The method is based on changes in the NMR spectrum of the ligand upon binding to the target protein. The thermostabilised A_{2A} Star2 protein was successfully immobilised on sepharose resin and screened at 500 μM with 531 fragment-sized molecules using the TINS method [97]. The screen identified 94 fragments binding specifically to A_{2A} Star2 and six fragments binding specifically to a reference protein OmpA. The A_{2A} hits were then screened in a binding assay with the wild-type receptor, using both [³H]-ZM241385 (8) and [³H]-NECA (10) radioligands [97]. Five competitive orthosteric ligands with diverse chemical structures (e.g. 44) were identified, with IC₅₀ values ranging between 70 and 1880 μM in concentration–response studies with [³H]-ZM241385. Another biophysical screening approach, SPR, already described earlier for β₁AR, has also been employed for the A_{2A} Star1 protein. The protein's suitability for SPR was validated initially using a set of standard ligands, with affinities ranging from 5.7 μM to 0.68 nM, to establish good agreement with values measured using wild-type A_{2A}R [130]. A library of fragments was then screened against A_{2A} Star1 at 200 μM, with standard ligand XAC (45) serving as a positive control. XAC was found to bind consistently and the receptor remained active throughout the study. The screen successfully identified multiple fragment hits binding significantly above background. The binding affinities of these hits were assessed using a

concentration–response format and were found to range from 10 to 5000 μM . A third biophysical screening approach, CEfrag, is a highly sensitive screening technique that uses capillary electrophoresis to identify low molecular weight (<300 Da), low affinity binders to a target protein [131]. The technique relies on the availability of a competitor probe ligand that interacts with the biological target of interest and changes in mobility upon binding, allowing detection [131,132]. In a proof of concept study, CEfrag was used to detect interactions between fragments and A_{2A} StaR1; ligands with a range of potencies, including the fragment-sized molecule caffeine (46), were successfully detected [112]. These three biophysical methods successfully applied to a stabilised GPCR protein, demonstrate that fragment screening using direct-binding methodologies, previously applied to soluble targets, has potential to facilitate GPCR drug discovery. Doubtless the utility of these more stable GPCR constructs with other biophysical methods will follow over time.

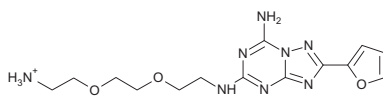


In a similar way to the $\beta_1\text{AR}$ case described earlier, A_{2A} protein–ligand structures are now being extensively utilised for drug design. Ivanov *et al.* have carried out a careful analysis of homology models of A_{2A} and concluded that modelling, extensively supported by a large body of site-directed mutagenesis data for this receptor, was reasonably predictive of the binding modes of several ligands [133]. Limitations in the models were found particularly in the extracellular loops, where ECL2 is involved in ligand binding. Pastorin and co-workers have reported a number of triazolotriazine derivatives (47) for which docking experiments, using the computational docking application GOLD and the A_{2A} crystal structure co-ordinates, were carried out [134]. Homology models were also generated of the closely related adenosine A_3 receptor. The structure–activity relationship (SAR) and selectivity for the series of compounds were rationalised and it was concluded that the presence of a relatively less bulky amino acid (Val169) in the ECL2 of the adenosine A_3 receptor seems to modulate potency and selectivity for the A_{2A} receptor versus the A_3 subtype. Further work on this series of compounds by the same team used SBDD to identify the best vector to introduce

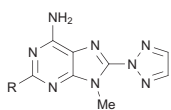
aqueous solubilising groups and in this way successfully generated highly potent and very soluble lead compounds, such as **(48)** [135]. Higgs *et al.* investigated the SAR of a series of low molecular weight triazolylpurines **(49)** and the role of binding site hydration using the programme WaterMap and the crystal structure: 3EML (PDB code) [136]. The observed SAR was explained by the finding that small substituents occupied a region containing stable waters, whilst larger groups accessed a sub-pocket to displace unstable waters. In a follow up to the virtual screening project described earlier, Carlsson and co-workers investigated the SAR across a series of 1,2,4-triazoles, again using modelling information [137]. Remarkably, close analogues of the original virtual screening hit were not more active, but instead more distantly related compounds selected by computational methods led to the identification of a 200 nM hit **50** with high LE. There have also been many studies of the A₃ receptor, using homology modelling starting from A_{2A} crystal structures. In one such study, Catarzi *et al.* investigated a series of pyrazoloquinazolines and carried out docking studies to rationalise the SAR and overall binding modes of the lead compounds, such as **(51)** [138]. In summary, homology modelling of closely related receptors can generate promising hit compounds and therefore the A_{2A} structures should facilitate the design of antagonists for all four adenosine receptors [139–150].



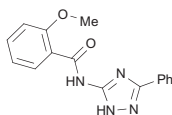
(47)
A_{2A} antagonist series



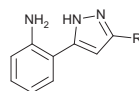
(48)
High solubility
A_{2A} antagonist
K_i = 11 nM



(49)
A_{2A} antagonist series



(50)
A_{2A} antagonist
K_i = 200 nM

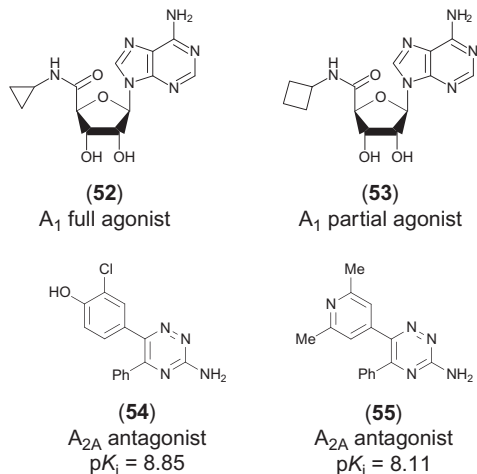


(51)
A₁ antagonist series

An active area of research is investigation of purine derived agonists of A_{2A} using the agonist-bound X-ray structures, either directly or in homology modelling of other adenosine receptor subtypes [151–156]. Adenosine

analogues have been studied for many years as agonists of adenosine receptors, but only now are their binding modes and interactions being rationalised. Deflorian *et al.* compared previous docking studies, aided by extensive SDM data, with the X-ray structure of UK-432,097 (**9**) and NECA (**10**) [157]. The base of the agonists, unsurprisingly, overlays the heterocyclic portion of antagonist ligands (Table 1.1), but there are key differences between agonists and antagonists in that the ribose moiety of agonists forms additional polar interactions with Thr88^{3,36}, His250^{6,52}, Ser277^{7,42} and His278^{7,43}, interactions that are largely absent in antagonists (Table 1.1). In an excellent study, Tosh and co-workers employed agonist-bound A_{2A} crystal structures to design modifications to the ribose group and create new agonist derivatives [156]. The optimisation process used *in silico* enumeration and docking of small groups coupled to the carboxylate functional group of the ribose, situated deep in the bottom of the binding pocket. A number of potent analogues were identified, such as (**52**) and (**53**), some of which exhibit interesting patterns of selectivity across the closely related adenosine A_{2A}, A₁ and A₃ receptors and various degrees of partial to full agonism. Historically, medicinal chemists have not been successful in replacing the metabolically susceptible ribose ring system in A_{2A} agonists with other groups. It is possible that further SBDD efforts will enable this problem to be resolved.

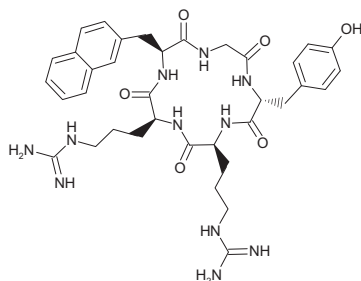
In the first GPCR SBDD case study in which crystal structures of analogues were solved and used as part of the lead optimisation process, Congreve *et al.* reported the identification and derivatisation of 1,2,4-triazine derivatives targeting the A_{2A} receptor [105]. The original hits had been discovered using virtual screening against a homology model of the receptor, enhanced using site-directed mutagenesis data [158]. The hit series was further characterised using a method called Biophysical MappingTM, whereby site-directed mutants of the receptor are made and the constructs captured onto a chip to carry out SPR screening [159]. In this way, a map of the binding mode of each compound was produced. One series of hits was then further developed [105]. Potent, ligand efficient, selective and orally efficacious 1,2,4-triazine derivatives were then designed via several iterations of medicinal chemistry optimisation supported by protein–ligand complexes. The X-ray crystal structures of two compounds, (**54**) and (**55**), bound to the GPCR illustrate that the molecules bind deeply inside the orthosteric binding cavity in a manner distinct from other classes of A_{2A} antagonists. *In vivo* pharmacokinetic and efficacy data for lead compounds support the potential of this series to treat Parkinson's disease.



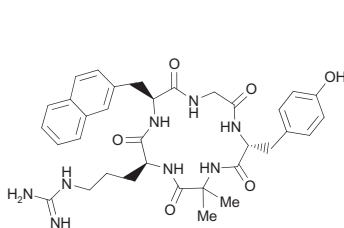
7.4. CXCR4 Receptor

Overexpression of the CXCR4 chemokine receptor is associated with multiple types of cancers, specifically with promotion of metastasis, angiogenesis and tumour growth [160]. Additionally, CXCR4 is involved in HIV pathogenesis as a co-receptor for viral cell entry [161]. The crystal structures of both small molecule and peptide ligands are starting to impact ligand design for this very challenging drug discovery target, which is a good example of a GPCR with relatively low historical tractability for drug design. Mungalpara *et al.* have used both peptide SAR analysis and modelling studies to rationally design conformationally constrained cyclopentapeptide antagonists of CXCR4 [162]. Docking into the X-ray structure of CXCR4, complexed with the 16-mer peptide antagonist CVX15 (PDB code: 3OEO), was conducted using induced-fit docking protocols and resulted in a binding pose consistent with the SAR [27]. Introduction of an α,α -disubstituted amino acid in position 1 of the peptide was found to improve activity, as illustrated by compounds (56)–(58). Aboye *et al.* have designed novel cyclotides to target CXCR4 using SBDD [163]. Cyclotides are globular microproteins (28–37 amino acids) stabilised by three intramolecular disulfide bonds, which provide a rigid molecular framework with improved metabolic stability *in vivo*. The most potent cyclotide was significantly more stable than the peptide CVX15 used in the X-ray study [27]. Finally, Yoshikawa *et al.* have modelled the three-dimensional complex of the cyclic peptide FC131 (56) with CXCR4, using a molecular dynamics simulation protocol [164]. The resulting predicted binding pose was consistent with experimental

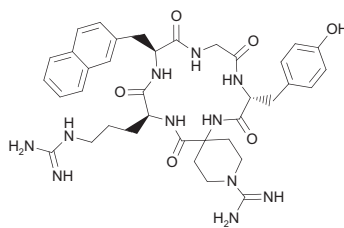
binding data and predicted a number of water-mediated interactions with the receptor. The ligand conformation was also supported by an NMR structure of the peptide FC131 [164].



(56)
CXCR4 antagonist
FC131
EC₅₀ = 0.47 μM



(57)
CXCR4 antagonist
EC₅₀ = 3.6 μM



(58)
CXCR4 antagonist
EC₅₀ = 0.26 μM

7.5. CRF₁ Receptor

As noted earlier, structures of the first two representatives of Class B receptors, the glucagon receptor and the corticotropin releasing factor receptor, CRF₁, have been solved recently [17,18]. Remarkably, small molecule ligands bind in the CRF₁ receptor much deeper inside the 7TM bundle and in a significantly different manner to any Class A receptor ((27), Table 1.1). The implications of this finding are only just being interpreted, but since the Class B receptor family is relatively homologous it is likely that this pocket exists in other Class B receptors. Therefore, it is likely the CRF₁ X-ray structure will facilitate design and virtual screening approaches for Class B receptors, opening the door to drug design for this very challenging class of drug targets.



8. CONCLUSIONS AND OUTLOOK

Recent progress in solving high resolution three-dimensional X-ray structures of GPCRs in complex with small molecule ligands is revolutionising approaches to GPCR drug discovery. Traditional methods of phenotypic or High throughput screening are being informed or replaced by structure-based rational drug design, familiar to those involved in enzyme drug discovery programmes. Visualisation of the complex and divergent shape and physico-chemical features of ligand binding sites enables computational and medicinal chemists to carry out virtual screening and to design optimised small molecule agonists and antagonists with improved potency, selectivity and LE. Based on the wealth of structural information, compounds can be developed with optimised physiochemical properties, including lower molecular weight and polarity, which should result in improved pharmacokinetics and safety. Techniques developed to obtain purified protein for structural studies are also enabling biophysical methods, which have the potential to support fragment screening.

Structural information obtained from agonist bound structures is informing our understanding of features that distinguish agonists from antagonists and partial agonists from full agonists. Complex parameters such as agonist efficacy, which previously could only be optimised via empirical rounds of compound synthesis and screening by cellular assays, can now be understood in the context of structural information, although this often requires multiple co-structures with ligands of different efficacies. The concept of biased agonism is gaining validity as an approach to obtain drugs with improved therapeutic potential. To date there is little structural understanding of what constitutes the basis of biased agonism but this is an area of great interest and we look forward to further co-structures of biased agonists in complex with GPCRs.

Advances in both structural and biophysical methods can also be expected to shed light on ligand receptor binding kinetics. Previously K_d values were often measured without consideration of the k_{on} and k_{off} parameters. For many GPCR targets, optimising the offrate of ligand binding can significantly impact the clinical profile with regard to both efficacy and side effects. Direct measurement of off rates can now be achieved using techniques such as SPR and rationalised by structural information. A future step will be to use structural information to proactively optimise receptor kinetics.

The field of SBDD for GPCRs is still in its infancy but its promise is enormous. Indeed, the growing number of available GPCR structures is triggering a renewed interest in GPCRs as drug targets across a wide range of therapeutic

areas. Highly validated targets previously considered intractable or 'undruggable' are now being revisited. As new structures emerge, most recently for Class B receptors, the list of medicines directed at GPCRs is sure to increase further. If the field of SBDD for enzymes serves as a paradigm, then many future medicines targeted at GPCRs are likely to be derived using SBDD.

ACKNOWLEDGMENTS

We thank Rebecca Nonoo for her contribution to compiling this manuscript and Tanya Gottlieb for editorial assistance.

REFERENCES

- [1] Hanson MA, Stevens RC. Discovery of new GPCR biology: one receptor structure at a time. *Structure* 2009;17:8–14.
- [2] Congreve M, Marshall FH. The impact of GPCR structures on pharmacology and structure-based drug design. *Br J Pharmacol* 2010;159(5):986–96.
- [3] Liu W, Chun E, Thompson AA, Chubukov P, Xu F, Katritch V, et al. Structural basis for allosteric regulation of GPCRs by sodium ions. *Science* 2012;337(6091):232–6.
- [4] Jacobson KA, Costanzi S. New insights for drug design from the X-ray crystallographic structures of G-protein-coupled receptors. *Mol Pharmacol* 2012;82(3):361–71.
- [5] Katritch V, Cherezov V, Stevens RC. Structure-function of the G protein-coupled receptor superfamily. *Annu Rev Pharmacol Toxicol* 2013;53:531–56.
- [6] Giraldo J, Pin J. G protein-coupled receptors. Cambridge, UK: RSC publishing; 2011.
- [7] Granier S, Kobilka B. A new era of GPCR structural and chemical biology. *Nat Chem Biol* 2012;8(8):670–3.
- [8] Muller DJ, Wu N, Palczewski K. Vertebrate membrane proteins: structure, function, and insights from biophysical approaches. *Pharmacol Rev* 2008;60:43–78.
- [9] Montaner S, Kufareva I, Abagyan R, Gutkind JS. Molecular mechanisms deployed by virally encoded G protein-coupled receptors in human diseases. *Annu Rev Pharmacol Toxicol* 2013;53:331–54.
- [10] Overington JP, Al-Lazikani B, Hopkins AL. How many drug targets are there? *Nat Rev Drug Discov* 2006;5(12):993–6.
- [11] Salon JA, Lodowski DT, Palczewski K. The significance of G protein-coupled receptor crystallography for drug discovery. *Pharmacol Rev* 2011;63:901–37.
- [12] Lagerström MC, Schiöth HB. Structural diversity of G protein-coupled receptors and significance for drug discovery. *Nat Rev Drug Discov* 2008;7:339–57.
- [13] Thomson Reuters Integrity database, <http://integrity.thomson-pharma.com/integrity/xmlxsl/>.
- [14] Katritch V, Cherezov V, Stevens RC. Diversity and modularity of G protein-coupled receptor structures. *Trends Pharmacol Sci* 2012;33(1):17–27.
- [15] Congreve M, Langmead CJ, Mason JS, Marshall FH. Progress in structure based drug design for G-protein-coupled receptors. *J Med Chem* 2011;54(13):4283–311.
- [16] Harmar AJ. Family-B G-protein-coupled receptors. *Genome Biol* 2001;2(12):reviews3013.1–reviews3013.10.
- [17] Siu FY, He M, de Graaf C, Han GW, Yang D, Zhang Z, et al. Structure of the class B human glucagon G protein coupled receptor. *Nature* 2013;499(7459):444–9.
- [18] Hollenstein K, Kean J, Bortolato A, Cheng RKY, Doré AS, Jazayeri A, et al. Structure of class B G-protein-coupled receptor corticotropin-releasing factor receptor 1. *Nature* 2013;499(7459):438–43.

- [19] Cherezov V, Rosenbaum DM, Hanson MA, Rasmussen SGF, Thian FS, Kobilka TS, et al. High resolution crystal structure of an engineered human β_2 -adrenergic G protein-coupled receptor. *Science* 2007;318(5854):1258–65.
- [20] Wacker D, Fenalti G, Brown MA, Katritch V, Abagyan R, Cherezov V, et al. Conserved binding mode of human β_2 adrenergic receptor inverse agonists and antagonist revealed by X-ray crystallography. *J Am Chem Soc* 2010;132(33):11443–5.
- [21] Rasmussen SGF, DeVree BT, Zou Y, Kruse AC, Chung KY, Kobilka TS, et al. Crystal structure of the β_2 adrenergic receptor–Gs protein complex. *Nature* 2011;477(7366):549–55.
- [22] Warne T, Serrano-Vega MJ, Baker JG, Moukhametzianov R, Edwards PC, Henderson R, et al. Structure of a β_1 -adrenergic G-protein coupled receptor. *Nature* 2008;454(7203):486–92.
- [23] Warne T, Moukhametzianov R, Baker JG, Nehmé R, Edwards PC, Leslie AGW, et al. The structural basis for agonist and partial agonist action on a β_1 -adrenergic receptor. *Nature* 2011;469(7329):241–4.
- [24] Warne T, Edwards PC, Leslie AGW, Tate CG. Crystal structures of a stabilized β_1 -adrenoceptor bound to the biased agonists bucindolol and carvedilol. *Structure* 2012;20:841–9.
- [25] Xu F, Wu H, Katritch V, Han GW, Jacobson KA, Gao ZG, et al. Structure of an agonist-bound human A2A adenosine receptor. *Science* 2011;332(6027):322–7.
- [26] Lebon G, Warne T, Edwards PC, Bennett K, Langmead CJ, Leslie AG, et al. Agonist bound adenosine A2A receptor structures reveal common features of GPCR activation. *Nature* 2011;474(7352):521–5.
- [27] Wu B, Chien EYT, Mol CD, Fenalti G, Liu W, Katritch V, et al. Structures of the CXCR4 chemokine GPCR with small-molecule and cyclic peptide antagonists. *Science* 2010;330(6007):1066–71.
- [28] Chien EYT, Liu W, Zhao Q, Katritch V, Han GW, Hanson MA, et al. Structure of the human dopamine D3 receptor in complex with a D2/D3 selective antagonist. *Science* 2010;330(6007):1091–5.
- [29] Shimamura T, Shiroishi M, Weyand S, Tsujimoto H, Winter G, Katritch V, et al. Structure of the human histamine H1 receptor complex with doxepin. *Nature* 2011;475(7354):65–70.
- [30] Haga K, Kruse AC, Asada H, Yurugi-Kobayashi T, Shiroishi M, Zhang C, et al. Structure of the human M2 muscarinic acetylcholine receptor bound to an antagonist. *Nature* 2012;482(7386):547–51.
- [31] Kruse AC, Hu J, Pan AC, Arlow DH, Rosenbaum DM, Rosemond E, et al. Structure and dynamics of the M3 muscarinic acetylcholine receptor. *Nature* 2012;482(7386):552–9.
- [32] Granier S, Manglik A, Kruse AC, Kobilka TS, Thian FS, Weis WI, et al. Structure of the δ -opioid receptor bound to naltrindole. *Nature* 2012;485(7398):400–5.
- [33] Wu H, Wacker D, Mileni M, Katritch V, Han GW, Vardy E, et al. Structure of the human κ -opioid receptor in complex with JD1c. *Nature* 2012;485(7398):327–32.
- [34] Manglik A, Kruse AC, Kobilka TS, Thian FS, Mathiesen JM, Sunahara RK, et al. Crystal structure of the μ -opioid receptor bound to a morphinan antagonist. *Nature* 2012;485(7398):321–6.
- [35] Thompson AA, Liu W, Chun E, Katritch V, Wu H, Vardy E, et al. Structure of the nociceptin/orphanin FQ receptor in complex with a peptide mimetic. *Nature* 2012;485(7398):395–401.
- [36] Hanson MA, Roth CB, Jo E, Griffith MT, Scott FL, Reinhart G, et al. Crystal structure of a lipid G protein-coupled receptor. *Science* 2012;335(6070):851–5.

- [37] White JF, Nojima N, Shibata Y, Love J, Kloss B, Xu F, et al. Structure of the agonist-bound neurotensin receptor. *Nature* 2012;490(7421):508–13.
- [38] Zhang C, Srinivasan Y, Arlow DH, Fung JJ, Palmer D, Zheng Y, et al. High-resolution crystal structure of human protease-activated receptor 1. *Nature* 2012;492(7429):387–92.
- [39] Wang C, Jiang Y, Ma J, Wu H, Wacker D, Katritch V, et al. Structural basis for molecular recognition at serotonin receptors. *Science* 2013;340(6132):610–4.
- [40] Wacker D, Wang C, Katritch V, Han GW, Huang XP, Vardy E, et al. Structural features for functional selectivity at serotonin receptors. *Science* 2013;340(6132):615–9.
- [41] Wang C, Wu H, Katritch V, Han GW, Huang XP, Liu W, et al. Structure of the human smoothed receptor bound to an antitumour agent. *Nature* 2013;497(7449):338–43.
- [42] DeLano WL. The PyMOL molecular graphics system, San Carlos, CA: DeLano Scientific; 2002. <http://www.PyMOL.org>.
- [43] Bjarnadóttir TK, Fredriksson R, Schiöth HB. The adhesion GPCRs: a unique family of G protein-coupled receptors with important roles in both central and peripheral tissues. *Cell Mol Life Sci* 2007;64(16):2104–19.
- [44] Niswender CM, Conn PJ. Metabotropic glutamate receptors: physiology, pharmacology, and disease. *Annu Rev Pharmacol Toxicol* 2010;50:295–322.
- [45] Gasparini F, Spooren W. Allosteric modulators for mGlu receptors. *Curr Neuropharmacol* 2007;5(3):187–94.
- [46] Gravius CA, Pietraszek M, Dekundy A, Danysz W. Metabotropic glutamate receptors as therapeutic targets for cognitive disorders. *Top Med Chem* 2010;10:187–206.
- [47] Urwyler S. Allosteric modulation of family C G-protein-coupled receptors: from molecular insights to therapeutic perspectives. *Pharmacol Rev* 2011;63:59–126.
- [48] Schulte G, Bryja V. The Frizzled family of unconventional G-protein-coupled receptors. *Trends Pharmacol Sci* 2007;28(10):518–25.
- [49] De Smaele E, Ferretti E, Gulino A. Vismodegib, a small-molecule inhibitor of the hedgehog pathway for the treatment of advanced cancers. *Curr Opin Investig Drugs* 2010;11(6):707–18.
- [50] Day PW, Rasmussen SGF, Parnot C, Fung JJ, Masood A, Kobilka TS, et al. A monoclonal antibody for G protein coupled receptor crystallography. *Nat Methods* 2007;4:927–9.
- [51] Rasmussen SGF, Choi HJ, Rosenbaum DM, Kobilka TS, Thian FS, Edwards PC, et al. Crystal structure of the human β_2 adrenergic G-protein-coupled receptor. *Nature* 2007;450(7163):383–7.
- [52] Serrano-Vega MJ, Magnani F, Shibata Y, Tate CG. Conformational thermostabilization of the β_1 -adrenergic receptor in a detergent-resistant form. *Proc Natl Acad Sci U S A* 2008;105(3):877–82.
- [53] Shibata Y, White JF, Serrano-Vega MJ, Magnani F, Aloia AL, Grishammer R, et al. Thermostabilization of the neurotensin receptor NTS1. *J Mol Biol* 2009;390(2):262–77.
- [54] Magnani F, Shibata Y, Serrano-Vega MJ, Tate CG. Co-evolving stability and conformational homogeneity of the human adenosine A_{2a} receptor. *Proc Natl Acad Sci U S A* 2008;105(31):10744–9.
- [55] Robertson N, Jazayeri A, Errey J, Baig A, Hurrell E, Zhukov A, et al. The properties of thermostabilised G protein-coupled receptors (StaRs) and their use in drug discovery. *Neuropharmacology* 2011;60(1):36–44.
- [56] Caffrey M, Cherezov V. Crystallizing membrane proteins using lipidic mesophases. *Nat Protoc* 2009;4:706–31.

- [57] Caffrey M, Li D, Drippati A. Membrane protein structure determination using crystallography and lipidic mesophases: recent advances and successes. *Biochemistry* 2012;51(32):6266–88.
- [58] Ballesteros JA, Weinstein H. Integrated methods for the construction of three dimensional models and computational probing of structure–function relations in G-protein coupled receptors. *Methods Neurosci* 1995;25:366–428.
- [59] Katritch V, Abagyan R. GPCR agonist binding revealed by modeling and crystallography. *Trends Pharmacol Sci* 2011;32(11):637–43.
- [60] Mason JS, Bortolato A, Congreve M, Marshall FH. New insights from structural biology into the druggability of G protein-coupled receptors. *Trends Pharmacol Sci* 2012;33(5):249–60.
- [61] Tate CG. A crystal clear solution for determining G-protein-coupled receptor structures. *Trends Biochem Sci* 2012;37(9):343–52.
- [62] Kontoyianni M, Liu Z. Structure-based design in the GPCR target space. *Curr Med Chem* 2012;19(4):544–56.
- [63] Zhua M, Lia M. Revisiting the homology modeling of G-protein coupled receptors: β 1-adrenoceptor as an example. *Mol BioSyst* 2012;8:1686–93.
- [64] Venkatakrisnan AJ, Deupi X, Lebon G, Tate CG, Schertler GF, Babu MM. Molecular signatures of G-protein-coupled receptors. *Nature* 2013;494(7436):185–94.
- [65] Deupi X, Standfuss J. Structural insights into agonist-induced activation of G-protein-coupled receptors. *Curr Opin Struct Biol* 2011;21:541–51.
- [66] Rosenbaum DM, Rasmussen SGF, Kobilka BK. The structure and function of G-protein-coupled receptors. *Nature* 2009;459(7245):356–63.
- [67] Rosenkilde MM, Benned-Jensen T, Frimurer TM, Schwartz TW. The minor binding pocket: a major player in 7TM receptor activation. *Trends Pharmacol Sci* 2010;31:567–74.
- [68] Deupi X, Standfuss J, Schertler G. Conserved activation pathways in G-protein-coupled receptors. *Biochem Soc Trans* 2012;40:383–8.
- [69] Hulme EC. GPCR activation: a mutagenic spotlight on crystal structures. *Trends Pharmacol Sci* 2013;34(1):67–84.
- [70] Kenakin T. Principles: receptor theory in pharmacology. *Trends Pharmacol Sci* 2004;25(4):186–92.
- [71] Cerione RA, Codina J, Benovic JL, Lefkowitz RJ, Birnbaumer L, Caron MG. The mammalian β 2-adrenergic receptor: reconstitution of functional interactions between pure receptor and pure stimulatory nucleotide binding protein of the adenylate cyclase system. *Biochemistry* 1984;23(20):4519–25.
- [72] Park JH, Scheerer P, Hofmann KP, Choe HW, Ernst OP. Crystal structure of the ligand-free G-protein-coupled receptor opsin. *Nature* 2008;454(7201):183–7.
- [73] Scheerer P, Park JH, Hildebrand PW, Kim YJ, Krauß N, Choe HW, et al. Crystal structure of opsin in its G-protein-interacting conformation. *Nature* 2008;455(7212):497–502.
- [74] Lebon G, Warne T, Tate CG. Agonist-bound structures of G-protein-coupled receptors. *Curr Opin Struct Biol* 2012;22(4):482–90.
- [75] Lebon G, Bennett K, Jazayeri A, Tate CG. Thermostabilisation of an agonist-bound conformation of the human adenosine A_{2A} receptor. *J Mol Biol* 2011;409(3):298–310.
- [76] Rasmussen SGF, Choi HJ, Fung JJ, Pardon E, Casarosa P, Chae PS, et al. Structure of a nanobody-stabilized active state of the β 2 adrenoceptor. *Nature* 2011;469(7329):175–80.
- [77] Roth BL, Marshall FH. NOBEL 2012 chemistry: studies of a ubiquitous receptor family. *Nature* 2012;492(7427):57.

- [78] Doré AS, Robertson N, Errey JC, Ng I, Hollenstein K, Tehan B, et al. Structure of the adenosine A_{2A} receptor in complex with ZM241385 and the xanthenes XAC and caffeine. *Structure* 2011;19(9):1283–93.
- [79] Bennett KA, Tehan B, Lebon G, Tate CG, Weir M, Marshall FH, et al. Pharmacology and structure of isolated conformations of the adenosine A_{2A} receptor define ligand efficacy. *Mol Pharmacol* 2013;83(5):949–58.
- [80] Rothman RB, Baumann MH. Serotonergic drugs and valvular heart disease. *Expert Opin Drug Saf* 2009;8(3):317–29.
- [81] Reiter E, Ahn S, Shukla AK, Lefkowitz RJ. Molecular mechanism of β -arrestin-biased agonism at seven-transmembrane receptors. *Annu Rev Pharmacol Toxicol* 2012;52:179–97.
- [82] DeWire SM, Yamashita DS, Rominger DH, Liu G, Cowan CL, Graczyk TM, et al. A G protein-biased ligand at the μ -opioid receptor is potently analgesic with reduced gastrointestinal and respiratory dysfunction compared with morphine. *J Pharmacol Exp Ther* 2013;344(3):708–17.
- [83] Tyndall JD, Sandilya R. GPCR agonists and antagonists in the clinic. *J Med Chem* 2005;1(4):405–21.
- [84] Black J. Drugs from emasculated hormones: the principle of syntopic antagonism. *Science* 1989;245(4917):486–93.
- [85] Humphrey PP, Feniuk W, Perren MJ, Connor HE, Oxford AW. The pharmacology of the novel 5-HT₁-like receptor agonist, GR43175. *Cephalalgia* 1989;9(Suppl 9):23–33.
- [86] Leeson PD, Springthorpe B. The influence of drug-like concepts on decision making in medicinal chemistry. *Nat Rev Drug Discov* 2007;6:881–90.
- [87] Bhavsar S, Mudaliar S, Cherrington A. Evolution of exenatide as a diabetes therapeutic. *Curr Diabetes Rev* 2013;9(2):161–93.
- [88] Norholm LM, Holst JJ, Jeppesen PB. Treatment of adult short bowel syndrome patients with teduglutide. *Expert Opin Pharmacother* 2012;13(2):235–43.
- [89] Blick SK, Dhillon S, Keam SJ. Teriparatide: a review of its use in osteoporosis. *Drugs* 2008;68(18):2709–37.
- [90] Dhillon S. Tesamorelin: a review of its use in the management of HIV-associated lipodystrophy. *Drugs* 2011;71(8):1071–91.
- [91] Congreve M, Murray C, Blundell T. Structural biology and drug discovery. *Drug Discov Today* 2005;10(13):895–907.
- [92] Rees DC, Congreve M, Murray CW, Carr R. Fragment-based lead discovery. *Nat Rev Drug Discov* 2004;3:660–72.
- [93] Congreve M, Chessari G, Tisi D, Woodhead AJ. Recent developments in fragment-based drug discovery. *J Med Chem* 2008;51(13):3661–80.
- [94] Murray CW, Verdonk ML, Rees DC. Experiences in fragment based drug discovery. *Trends Pharmacol Sci* 2012;33(5):224–32.
- [95] Scott DE, Coyne AG, Hudson SA, Abell C. Fragment-based approaches in drug discovery and chemical biology. *Biochemistry* 2012;51(25):4990–5003.
- [96] Cooke RM, Koglin M, Errey JC, Marshall FH. Preparation of purified GPCRs for structural studies. *Biochem Soc Trans* 2013;41(1):185–90.
- [97] Chen D, Errey JC, Heitman LH, Marshall FH, Ijzerman AP, Siegal G. Fragment screening of GPCRs using biophysical methods: identification of ligands of the adenosine A_{2A} receptor with novel biological activity. *Chem Biol* 2012;7(12):2064–73.
- [98] Cherezov V, Abola E, Stevens RC. Recent progress in the structure determination of GPCRs, a membrane protein family with high potential as pharmaceutical targets. *Methods Mol Biol* 2010;654:141–68.
- [99] Hopkins AL, Groom CR, Alex A. Ligand efficiency: a useful metric for lead selection. *Drug Discov Today* 2004;9(10):430–1.

- [100] Borshell N, Papp T, Congreve M. Deal watch: valuation benefits of structure-enabled drug discovery. *Nat Rev Drug Discov* 2011;10(3):166.
- [101] Erlanson DA, McDowell RS, O'Brien T. Fragment-based drug discovery. *J Med Chem* 2004;47(14):3463–82.
- [102] Jhoti H. A new school for screening. *Nat Biotechnol* 2005;23:184–6.
- [103] Schulz MN, Hubbard RE. Recent progress in fragment-based lead discovery. *Curr Opin Pharmacol* 2009;9:615–21.
- [104] Baker M. Fragment-based lead discovery grows up. *Nat Rev Drug Discov* 2013;12:5–7.
- [105] Congreve M, Andrews SP, Doré AS, Hollenstein K, Hurrell E, Langmead CJ, et al. Discovery of 1,2,4-triazine derivatives as adenosine A_{2A} antagonists using structure based drug design. *J Med Chem* 2012;55(5):1898–903.
- [106] Congreve M, Brown G, Cansfield J, Tehan B. Preparation of bipiperidinecarboxylates and piperidinylazepanecarboxylates as muscarinic M₁ receptor agonists. WO2013072705, A1; 2013.
- [107] Jacobson KA. Structure-based approaches to ligands for G-protein-coupled adenosine and P2Y receptors, from small molecules to nanoconjugates. *J Med Chem* 2013;56(10):3749–67.
- [108] Stevens RC, Cherezov V, Katritch V, Abagyan R, Kuhn P, Rosen H, et al. The GPCR network: a large-scale collaboration to determine human GPCR structure and function. *Nat Rev Drug Discov* 2013;12:25–34.
- [109] Costanzi S. Modeling G-protein-coupled receptors and their interactions with ligands. *Curr Opin Struct Biol* 2012;23(2):185–90.
- [110] Shoichet BK, Kobilka BK. Structure-based drug screening for G-protein-coupled receptors. *Trends Pharmacol Sci* 2012;33(5):268–72.
- [111] Costanzi S. Structure-based virtual screening for ligands of G protein-coupled receptors. *RSC Drug Discov Series* 2011;8:359–74.
- [112] Andrews SP, Tehan B. Stabilised G protein-coupled receptors in structure-based drug design: a case study with adenosine A_{2A} receptor. *MedChemComm* 2013;4(1):52–67.
- [113] Kolb P, Rosenbaum DM, Irwin JJ, Fung JJ, Kobilka BK, Shoichet BK. Structure based discovery of β_2 -adrenergic receptor ligands. *Proc Natl Acad Sci U S A* 2009;106(16):6843–8.
- [114] Topiol S, Sabio M. Use of the X-ray structure of the β_2 -adrenergic receptor for drug discovery. *Bioorg Med Chem Lett* 2008;18(5):1598–602.
- [115] Sabio M, Jones K, Topiol S. Use of the X-ray structure of the β_2 -adrenergic receptor for drug discovery Pt 2: identification of active compounds. *Bioorg Med Chem Lett* 2008;18(20):5391–5.
- [116] De Graaf C, Rognan D. Selective structure-based virtual screening for full and partial agonists of the β_2 adrenergic receptor. *J Med Chem* 2008;51(16):4978–85.
- [117] Soriano-Ursúa MA, McNaught-Flores DA, Nieto-Alamilla G, Segura-Cabrera A, Correa-Basurto J, Arias-Montaño JA, et al. Cell-based and in-silico studies on the high intrinsic activity of two boron-containing salbutamol derivatives at the human β_2 -adrenoceptor. *Bioorg Med Chem* 2012;20(2):933–41.
- [118] Hattori K, Orita M, Toda S, Imanishi M, Itou S, Nakajima Y, et al. Discovery of highly potent and selective biphenylacetylsulfonamide-based β_3 -adrenergic receptor agonists and molecular modeling based on the solved X-ray structure of the β_2 -adrenergic receptor: part 6. *Bioorg Med Chem Lett* 2009;19(16):4679–83.
- [119] Stocks MJ, Alcaraz L, Bailey A, Bonnert R, Cadogan E, Christie J, et al. Design driven H₁L: the discovery and synthesis of new high efficacy β_2 -agonists. *Bioorg Med Chem Lett* 2011;21(13):4027–31.

- [120] Christopher JA, Brown J, Doré AS, Errey JC, Koglin M, Marshall FH, et al. Biophysical fragment screening of the β_1 -Adrenergic receptor: identification of high affinity arylpiperazine leads using structure-based drug design. *J Med Chem* 2013;56(9):3446–55.
- [121] De Graaf C, Kooistra AJ, Vischer HF, Katritch V, Kuijter M, Shiroishi M, et al. Crystal structure-based virtual screening for fragment-like ligands of the human histamine H₁ receptor. *J Med Chem* 2010;54(23):8195–206.
- [122] Jaakola VP, Griffith MT, Hanson MA, Cherezov V, Chien EY, Lane JR, et al. The 2.6 angstrom crystal structure of a human A_{2A} adenosine receptor bound to an antagonist. *Science* 2008;322(5905):1211–7.
- [123] Michino M, Abola E, Brooks 3rd CL, Dixon JS, Moulton J, Stevens RC. Community-wide assessment of GPCR structure modelling and ligand docking: GPCR Dock 2008. *Nat Rev Drug Discov* 2009;8(6):455–63.
- [124] Carlsson J, Yoo L, Gao ZG, Irwin JJ, Shoichet BK, Jacobson KA. Structure-based discovery of A_{2A} adenosine receptor ligands. *J Med Chem* 2010;53(9):3748–55.
- [125] Katritch V, Jaakola VP, Lane JR, Lin J, Ijzerman AP, Yeager M, et al. Structure-based discovery of novel chemotypes for adenosine A_{2A} receptor antagonists. *J Med Chem* 2010;53(4):1799–809.
- [126] Van der Horst E, Van der Pijl R, Mulder-Krieger T, Bender A, Ijzerman AP. Substructure-based virtual screening for adenosine A_{2A} receptor ligands. *ChemMedChem* 2011;6:2302–11.
- [127] Areias F, Costa M, Castro M, Brea J, Gregori-Puigjané E, Proença MF, et al. New chromene scaffolds for adenosine A_{2A} receptors: synthesis, pharmacology and structure-activity relationships. *Eur J Med Chem* 2012;54:303–10.
- [128] Sanders MPA, Roumen L, van der Horst E, Lane JR, Vischer HF, van Offenbeek J, et al. A prospective cross-screening study on G-protein-coupled receptors: lessons learned in virtual compound library design. *J Med Chem* 2012;55(11):5311–25.
- [129] van Westen GJP, van den Hoven OO, van der Pijl R, Mulder-Krieger T, de Vries H, Wegner JK, et al. Identifying novel adenosine receptor ligands by simultaneous proteochemometric modeling of rat and human bioactivity data. *J Med Chem* 2012;55(16):7010–20.
- [130] Congreve M, Rich RL, Myszka DG, Figaroa F, Siegal G, Marshall FH. Fragment screening of stabilized G-protein-coupled receptors using biophysical methods. *Methods Enzymol* 2011;493:115–36.
- [131] Austin C, Pettit SN, Magnolo SK, Sanvoisin J, Chen W, Wood SP, et al. Fragment screening using capillary electrophoresis (CEfrag) for hit identification of heat shock protein 90 ATPase inhibitors. *J Biomol Screen* 2012;17(7):868–76.
- [132] Hughes D. Affinity capillary electrophoresis method for assessing biological interaction of a ligand/receptor pair such as a G protein coupled receptor and its targets as well as for drug screening. US Patent 20,120,175,255, A1; 2012.
- [133] Ivanov AA, Barak D, Jacobson KA. Evaluation of homology modeling of G-protein-coupled receptors in light of the A_{2A} adenosine receptor crystallographic structure. *J Med Chem* 2009;52(10):3284–92.
- [134] Pastorin G, Federico S, Paoletta S, Corradino M, Cateni F, Cacciari B, et al. Synthesis and pharmacological characterization of a new series of 5,7-disubstituted-[1,2,4]triazolo[1,5-*a*][1,3,5]triazine derivatives as adenosine receptor antagonists: A preliminary inspection of ligand-receptor recognition process. *Bioorg Med Chem* 2010;18(7):2524–36.
- [135] Federico S, Paoletta S, Cheong SL, Pastorin G, Cacciari B, Stragliotto S, et al. Synthesis and biological evaluation of a new series of 1,2,4-triazolo[1,5-*a*]-1,3,5-triazines as human A_{2A} adenosine receptor antagonists with improved water solubility. *J Med Chem* 2011;54(3):877–89.

- [136] Higgs C, Beuming T, Sherman W. Hydration site thermodynamics explain SARs for triazolylpurines analogues binding to the A_{2A} receptor. *Med Chem Lett* 2010;1:160–4.
- [137] Carlsson J, Tosh DK, Phan K, Gao ZG, Jacobson KA. Structure–activity relationships and molecular modeling of 1,2,4-triazoles as adenosine receptor antagonists. *Med Chem Lett* 2012;3(9):715–20.
- [138] Catarzi D, Colotta V, Varano F, Poli D, Squarcialupi L, Filacchioni G, et al. Pyrazolo [1,5-*c*]quinazoline derivatives and their simplified analogues as adenosine receptor antagonists: synthesis, structure–affinity relationships and molecular modeling studies. *Bioorg Med Chem* 2013;21(1):283–94.
- [139] Yaziji V, Rodríguez D, Coelho A, García-Mera X, El Maatougui A, Brea J, et al. Selective and potent adenosine A₃ receptor antagonists by methoxyaryl substitution on the N-(2,6-diarylpyrimidin-4-yl)acetamide scaffold. *Eur J Med Chem* 2013;59:235–42.
- [140] Sirci F, Goracci L, Rodríguez D, van Muijlwijk-Koezen J, Gutiérrez-de-Terán H, Mannhold R. Ligand-, structure- and pharmacophore-based molecular fingerprints: a case study on adenosine A₁, A_{2A}, A_{2B}, and A₃ receptor antagonists. *J Comput Aided Mol Des* 2012;26(11):1247–66.
- [141] Yaziji V, Rodríguez D, Gutiérrez-de-Terán H, Coelho A, Caamaño O, García-Mera X, et al. Pyrimidine derivatives as potent and selective A₃ adenosine receptor antagonists. *J Med Chem* 2011;54(2):457–71.
- [142] Lenzi O, Colotta V, Catarzi D, Varano F, Poli D, Filacchioni G, et al. 2-Phenylpyrazolo[4,3-*D*]pyrimidin-7-one as a new scaffold to obtain potent and selective human A₃ adenosine receptor antagonists: new insights into the receptor-antagonist recognition. *J Med Chem* 2009;52(23):7640–52.
- [143] Federico S, Ciancetta A, Sabbadin D, Paoletta S, Pastorin G, Cacciari B, et al. Exploring the directionality of 5-substitutions in a new series of 5-alkylaminopyrazolo[4,3-*e*]1,2,4-triazolo[1,5-*c*]pyrimidine as a strategy to design novel human A₃ adenosine receptor antagonists. *J Med Chem* 2012;55(22):9654–68.
- [144] Cheong SL, Dolzhenko A, Kachler S, Paoletta S, Federico S, Cacciari B, et al. The significance of 2-furyl ring substitution with a 2-(para-substituted) Aryl group in a new series of pyrazolo–triazolo–pyrimidines as potent and highly selective hA₃ adenosine receptors antagonists: new insights into structure–affinity relationship and receptor–antagonist recognition. *J Med Chem* 2010;53(8):3361–75.
- [145] Baraldi PG, Preti D, Zaid AN, Saponaro G, Tabrizi MA, Baraldi S, et al. New 2-heterocycl-yl-imidazo[2,1-*i*]purin-5-one derivatives as potent and selective human A₃ adenosine receptor antagonists. *J Med Chem* 2011;54(14):5205–20.
- [146] Taliani S, Pugliesi I, Barresi E, Simorini F, Salerno S, La Motta C, et al. 3-Aryl-[1,2,4] triazino[4,3-*a*]benzimidazol-4(10H)-one: a novel template for the design of highly selective A_{2b} adenosine receptor antagonists. *J Med Chem* 2012;55(4):1490–9.
- [147] Kolb P, Phan K, Gao ZG, Marko AC, Sali A, Jacobson KA. Limits of ligand selectivity from docking to models: in silico screening for A₁ adenosine receptor antagonists. *PLoS ONE* 2012;7(11):e49910.
- [148] Gaspar A, Reis J, Kachler S, Paoletta S, Uriarte E, Klotz KN, et al. Discovery of novel A₃ adenosine receptor ligands based on chromone scaffold. *Biochem Pharmacol* 2012;84:21–9.
- [149] Inamdar GS, Pandya AN, Thakar HM, Sudarsanam V, Kachler S, Sabbadin D, et al. New insight into adenosine receptors selectivity derived from a novel series of [5-substituted-4-phenyl-1,3-thiazol-2-yl] benzamides and furamides. *Eur J Med Chem* 2013;63:924–34.
- [150] Squarcialupi L, Colotta V, Catarzi D, Varano F, Filacchioni G, Varani K, et al. 2-Arylpyrazolo[4,3-*d*]pyrimidin-7-amino derivatives as new potent and selective human

- A₃ adenosine receptor antagonists. Molecular modeling studies and pharmacological evaluation. *J Med Chem* 2013;56(6):2256–69.
- [151] Tosh DK, Paoletta S, Deflorian F, Phan K, Moss SM, Gao ZG, et al. Structural sweet spot for A₁ adenosine receptor activation by truncated (N)-methanocarpa nucleosides: receptor docking and potent anticonvulsant activity. *J Med Chem* 2012;55(18):8075–90.
- [152] Tosh DK, Deflorian F, Phan K, Gao ZG, Wan TC, Gizewski E, et al. Structure-guided design of A₃ adenosine receptor-selective nucleosides: combination of 2-arylethynyl and bicyclo[3.1.0]hexane substitutions. *J Med Chem* 2012;55(10):4847–60.
- [153] Tosh DK, Phan K, Gao ZG, Gakh AA, Xu F, Deflorian F, et al. Optimization of adenosine 5'-carboxamide derivatives as adenosine receptor agonists using structure-based ligand design and fragment screening. *J Med Chem* 2012;55(9):4297–308.
- [154] Dal Ben D, Buccioni M, Lambertucci C, Marucci G, Thomas A, Volpini R, et al. Molecular modeling study on potent and selective adenosine A₃ receptor agonists. *Bioorg Med Chem* 2010;18(22):7923–30.
- [155] Hou X, Majik MS, Kim K, Pyee Y, Lee Y, Alexander V, et al. Structure-activity relationships of truncated C2- or C8-substituted adenosine derivatives as dual acting A_{2A} and A₃ adenosine receptor ligands. *J Med Chem* 2012;55(1):342–56.
- [156] Tosh DK, Paoletta S, Phan K, Gao ZG, Jacobson KA. Truncated nucleosides as A₃ adenosine receptor ligands: combined 2-arylethynyl and bicyclohexane substitutions. *Med Chem Lett* 2012;3:596–601.
- [157] Deflorian F, Kumar TS, Phan K, Gao ZG, Xu F, Wu H, et al. Evaluation of molecular modeling of agonist binding in light of the crystallographic structure of an agonist-bound A_{2A} adenosine receptor. *J Med Chem* 2012;55(1):538–52.
- [158] Langmead CJ, Andrews SP, Congreve M, Errey JC, Hurrell E, Marshall FH, et al. Identification of novel adenosine A_{2A} receptor antagonists by virtual screening. *J Med Chem* 2012;55(5):1904–9.
- [159] Zhukov A, Andrews SP, Errey JC, Robertson N, Tehan B, Mason JS, et al. Biophysical mapping of the adenosine A_{2A} receptor. *J Med Chem* 2011;54(13):4312–23.
- [160] Fulton AM. The chemokine receptors CXCR4 and CXCR3 in cancer. *Curr Oncol Rep* 2009;11:125–31.
- [161] Oberlin E, Amara A, Françoise B, Bessia C, Virelizier J, Arenzana-Seisdedos F, et al. The CXC chemokine SDF-1 is the ligand for LESTR/fusin and prevents infection by T-cell-line-adapted HIV-1. *Nature* 1996;382(6606):833–5.
- [162] Mungalpara J, Thiele S, Eriksen Ø, Eksteen J, Rosenkilde MM, Våbenø J. Rational design of conformationally constrained cyclopentapeptide antagonists for C-x-C chemokine receptor 4 (CXCR4). *J Med Chem* 2012;55(22):10287–91.
- [163] Aboye TL, Ha H, Majumder S, Christ F, Debyser Z, Shekhtman A, et al. Design of a novel cyclotide-based CXCR4 antagonist with anti-human immunodeficiency virus (HIV)-1 activity. *J Med Chem* 2012;55(23):10729–34.
- [164] Yoshikawa Y, Kobayashi K, Oishi S, Fujii N, Furuya T. Molecular modeling study of cyclic pentapeptide CXCR4 antagonists: new insight into CXCR4-FC131 interactions. *Bioorg Med Chem Lett* 2012;22(6):2146–50.



P2X7 Antagonists as Potential Therapeutic Agents for the Treatment of CNS Disorders

Christa C. Chrovian, Jason C. Rech, Anindya Bhattacharya,
Michael A. Letavic

Janssen Research and Development, LLC, San Diego, CA, USA

Contents

1. Introduction	65
2. P2X7 in the CNS	66
2.1 Neuropsychiatric Disorders	67
2.2 Neurodegenerative Disorders	68
2.3 Pain	69
3. P2X7 Modulators in Clinical Trials	70
4. P2X7 Receptor Antagonists	72
4.1 Monocyclic Hetero and Carbocyclic Antagonists	73
4.2 Heteroaromatic-Fused Core Antagonists	81
4.3 P2X7 Antagonists in Animal Models of the CNS	88
5. Conclusion	93
References	93

Keywords: Purinergic, Neuroinflammation, IL-1 β , Patent, Heterocyclic, Heteroaromatic, Brain penetrant, Pre-clinical, Clinical



1. INTRODUCTION

P2X7 is a member of the purinergic family of receptors. It is an adenosine triphosphate (ATP)-gated ion channel expressed predominantly on cells of haematopoietic lineage, including macrophages and monocytes in the periphery and microglia and astrocytes in the central nervous system (CNS). The channel presents itself primarily as a homotrimer, with three alpha subunits assembling together to form a functional channel. Each

subunit has an intracellular N-terminal domain, a bulky extracellular loop that hosts the ATP-binding site(s) and a long C-terminal region [1–3]. ATP-mediated P2X7 activation leads to opening of the channel pore, followed by non-selective cation flux. Prolonged exposure to ATP leads to formation of a large opening (termed a macropore) *in vitro*, although the physiological significance of this macropore formation is not clearly understood.

One of the hallmark features of P2X7 activation is release of the pro-inflammatory cytokine IL-1 β , known to be involved in a number of cellular activities. In addition to IL-1 β , experimental data links activation of P2X7 to the release of IL-18, IL-6 and TNF- α (the latter two are indirectly modulated), chemokines [4–6], cathepsins [7,8], glutamate [9–12] and nitric oxide [13]. Within the CNS, IL-1 β is thought to contribute to neuroinflammatory tone leading to neuropsychiatric and neurodegenerative disorders [14].

In recent years there has been a surge of literature supporting the role of P2X7 in neuroinflammatory pathways. Studies have been reported that demonstrate the use of P2X7 antagonists as a viable approach to treating neuroinflammatory disorders and will be highlighted in this chapter. In addition, a number of recent patent applications and medicinal chemistry publications have described novel compounds and their activity as P2X7 antagonists; many of these reports highlight the compounds' efficacy in pre-clinical *in vivo* models of pain, inflammation and arthritis. Further studies from Pfizer, GlaxoSmithKline (GSK) and Janssen have demonstrated the ability of small molecule P2X7 antagonists to penetrate the CNS in the rat. Given the recent data supporting the role of P2X7 as a viable CNS target, the focus of this chapter will be on developments since 2009 towards the use of P2X7 antagonists for the treatment of CNS disorders.



2. P2X7 IN THE CNS

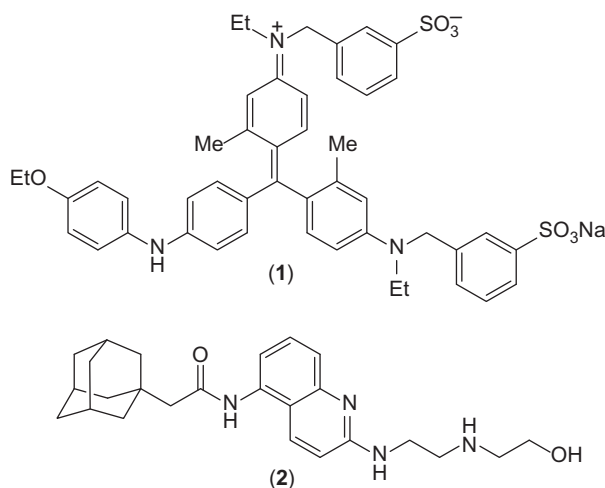
P2X7-mediated signalling has been most extensively studied in terms of its role in IL-1 β regulation in the periphery. However, it has been postulated that CNS P2X7 activation contributes to microglial activation, astrogliosis and neurodegeneration [3,15–18] although this hypothesis remains to be tested *in vivo*. Given the recent interest in P2X7 antagonism as a pharmacological intervention for CNS disorders, it is anticipated that new biological understanding will continue to emerge that correlates effects of P2X7 modulation on the release of cytokines, chemokines and neurotransmitters, as well as its role in neurogenesis and axonal sprouting [19]. This research is expected to reveal the role of P2X7-mediated signalling in neurophysiology.

ATP is a major neurotransmitter (and a gliotransmitter) within the CNS and plays an important role in neuroglia crosstalk [20] via a plethora of cell-surface ATP-sensitive G-protein-coupled receptors and ion channels. While the role of ATP-induced P2X7 activation in CNS pathology is clinically untested, emerging pre-clinical research supports the hypothesis. For example, in disease states involving cell death and necrosis such as neurodegenerative disorders, ATP is released from intracellular compartments in millimolar concentrations, probably over 10^4 -fold higher than under normal physiological conditions [21–23]. The elevated ATP levels activate P2X7 channels, resulting in IL-1 β release and contributing to a neuroinflammatory tone of the brain. Likewise, during chronic stress ATP release has been postulated to enhance the P2X7 tone. As such, CNS penetrable P2X7 antagonists would be a novel therapeutic approach for treating neuropsychiatric [24] and neurodegenerative diseases [25].

2.1. Neuropsychiatric Disorders

There is growing evidence that strengthens the role of P2X7 in mood disorders. Several human genetic studies have associated the highly polymorphic *P2RX7* gene with both bipolar disorder and depression [26–29] and some of these mutations have been linked to modulation of P2X7 channel function *in vitro* [30,31]. In contrast, there have also been reports that show a lack of correlation of *P2RX7* with mood disorders [32,33]. The lack of clarity for a genetic association of P2X7 in precipitating mood disorders is perhaps not surprising as the underlying factors of such pathologies are often a result of interplay between genetic (often many genes), environmental and developmental factors. In addition to the equivocal human genetic literature, several independent laboratories have demonstrated a protective phenotype of P2X7 knockout mice in models of depression and mania, strengthening the hypothesis that P2X7 antagonism may be therapeutically beneficial in mood disorders [34,35]. The phenotype of the knockout animals has since been validated using P2X7 selective antagonists. For example, systemic administration of the P2X7 antagonist brilliant blue G (1) attenuated amphetamine-induced hyperactivity and decreased immobility in a tail suspension test [36]. Moreover, in a model of sucrose consumption that is more reflective of anhedonic behaviour, pharmacological antagonism of P2X7 by AZ-10606120 (2) restored the deficit observed in drinking sucrose-water (anhedonia) either under chronic stress or by systemic administration of lipopolysaccharides (LPS) [37]. In addition, there is an overwhelming body of literature suggesting that manipulation of central

IL-1 β (either by exogenous administration or by selective ablation of signaling by pharmacology or genetics) results in animal behaviours akin to clinical depression when IL-1 β is increased, and a diminished depressed state when IL-1 β is decreased [38–41]. In addition, increased levels of IL-1 β have been measured in plasma, cerebrospinal fluid and in post-mortem brain tissue of mood disorder patients [42–44]. Taken together, it remains plausible that a selective and brain penetrant P2X7 antagonist may be therapeutically beneficial in neuropsychiatric conditions. Such a mechanism would be a novel treatment for psychiatric disorders.



2.2. Neurodegenerative Disorders

It is well established that neuroinflammation, microglial activation and astrogliosis may all contribute to several neurodegenerative disorders. Since P2X7 is expressed primarily in glial cells and is possibly activated by degenerating and/or necrotic cells releasing high local concentrations of ATP, it has been speculated that P2X7 antagonism will be therapeutically beneficial in Alzheimer's disease [45–47], multiple sclerosis (MS) [48], epilepsy [49] and Huntington's disease [50].

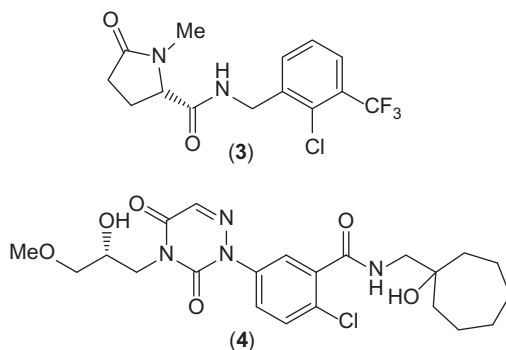
In 2003 it was reported that P2X7 immunoreactivity in transgenic mouse models of Alzheimer's disease was up-regulated near β -amyloid (A β) plaques [51]. Since then several groups have presented mechanistic data suggesting an association of P2X7 with the biology of the disease. For example, A β induced IL-1 β release in primary microglia has been shown to be P2X7 dependent [52,53]. In addition, exogenous administration of A β

in the mouse brain was found to cause an increase in IL-1 β in a P2X7-dependent manner [54]. Another report showed silencing of the *P2RX7* gene promoted microglia-induced A β phagocytosis *in vitro* [46], suggesting a possible mechanism for clearing A β . This hypothesis has been further strengthened *in vivo* [45]. The role of P2X7 is corroborated by a report showing *P2RX7* up-regulation in post-mortem brain tissue that had a clinical diagnosis of Alzheimer's disease [54].

The role of P2X7 in MS has been probed in the rat using experimental autoimmune encephalomyelitis (EAE) models. In one study, P2X7 expressed on oligodendrocytes caused cell death and MS lesions during the disease progression, and administration of a P2X7 antagonist resulted in attenuated neurological scores [55]. Because the EAE model of MS is known to cause microglial activation [56], it is a reasonable hypothesis that P2X7 is an important player in disease progression. Moreover, P2X7 knock out animals are protected against MS [57], and gain-of-function P2X7 single nucleotide polymorphisms have been linked to increased incidence of the disease [48]. It remains to be seen whether these pre-clinical findings will be translated into robust efficacy and proof-of-concept clinical studies.

2.3. Pain

The therapeutic effect of modulating P2X7 has been most widely studied pre-clinically with respect to its potential role in managing a variety of pain disorders [58]. Modulating P2X7 activity as a potential approach to treating inflammatory and neuropathic pain was demonstrated in knockdown studies of *P2RX7* [59,60] and IL-1 β [61]. An unanswered question, however, is whether CNS occupancy of a P2X7 by an antagonist is necessary in order to achieve this desired therapeutic effect. Recent reports have emerged validating the use of brain penetrant P2X7 antagonists in animal models of neuropathic and inflammatory pain [62–64]. In addition, the brain penetrant P2X7 antagonist GSK1482160 (**3**) advanced into the clinic for neuropathic and inflammatory pain [65]. Although the pre-clinical studies involving genetic and pharmacological attenuation of P2X7 predict clinical efficacy in rheumatoid arthritis (RA) pain, two other clinical compounds, CE-224,535 (**4**) and AZD9056 failed in Phase II RA trials due to lack of efficacy [66,67]. The exact mechanism by which P2X7 contributes to mechanical allodynia in neuropathic pain remains unclear but it has been speculated that microglial P2X7 drives neuroglia [68] crosstalk via glutamate release [10], cathepsins [8] and IL-1 β [69], contributing to the increased pain sensitivity.



Neuropathic pain remains an unmet medical need. Although recent literature demonstrates the efficacy of P2X7 antagonists in pre-clinical pain models [70,71], including with compounds that are CNS permeable [64], it has yet to be determined whether administration of a P2X7 antagonist will translate into positive clinical outcomes for neuropathic pain.

3. P2X7 MODULATORS IN CLINICAL TRIALS

A number of clinical studies with P2X7 antagonists have been conducted that target peripheral inflammatory indications; however, there are only a few reports to date in which a CNS condition is identified. GSK reported results from a Phase I study in which the target indications were neuropathic and inflammatory pain. The study aim was to assess safety and tolerability of the pyroglutamic acid amide GSK1482160 (3) [62,64,65,72–74], a negative allosteric modulator, in healthy human subjects and to determine whether increased levels of GSK1482160 correlate with decreased *ex vivo* plasma IL-1 β concentrations. The study was carried out in 29 volunteers. A single dose escalation of up to 1000 mg was well tolerated, with a measured drug half-life of 4.5 h. In order to establish a PK/PD relationship at this stage in the clinic, IL-1 β release in the plasma was measured after *ex vivo* stimulation with LPS and ATP; IL-1 β release was found to be dependent upon compound dose and ATP concentrations. That is, in the absence of ATP, no IL-1 β was measured and higher doses of GSK1482160 (100–1000 mg) resulted in nearly complete suppression of IL-1 β at all ATP concentrations. It is of note that IL-1 β release was found to be lower in subjects containing the Glu496 to Ala polymorphism, corroborating earlier reports [75]. Nonetheless, the model could be used to assess P2X7 receptor engagement at specific measured human exposures. The authors hypothesise

that greater than 90% inhibition of IL-1 β release is pharmacologically necessary in order to test the P2X7 mechanism; however, sufficient safety margins were not attained to reach this level of inhibition safely with GSK1482160. For this reason the development of GSK1482160 was terminated.

Disclosed in 2010, Pfizer Inc. conducted a Phase IIa study with CE-224,535 (**4**) [66,76,77] in order to assess its effect in patients with RA inadequately controlled by methotrexate. This compound displays exceptionally high potency in several *in vitro* assays measuring P2X7 IC₅₀ values; in human whole blood, for example, IL-1 β IC₅₀ = 0.8 nM. Due to weak potency in rodents however, Pfizer reported that pre-clinical disease models were not assessed. The compound was evaluated in a trial of 100 RA patients over 12 weeks. Patients taking the drug received 500 mg of CE-224,535 twice a day. The compound was found to be generally safe and well tolerated. However, these patients showed no significant improvement in American College of Rheumatology 20% response rate (ACR20) compared to the placebo group. It was noted that plasma concentrations of CE-224,535 were estimated to be 25 times the IC₉₀ for IL-1 β inhibition, as measured *ex vivo* in a previous study, suggesting that P2X7 receptor blockade is not an effective approach to treating RA.

AstraZeneca's AZD9056, an adamantane-based antagonist (**5**) of undisclosed structure, was the subject of a 75 person Phase IIa study also targeting RA [67]. This was a 4-week trial and the compound was also found to be safe and well tolerated at the two doses assessed. In addition, statistically significant improvement in several parameters of clinical relevance compared to placebo was reported, with the most significant results seen in reduction of tender and swollen joint counts. AZD9056-treated healthy human volunteers exhibited significant inhibition of *ex vivo* ATP-induced monocyte IL-1 β release. A subsequent Phase IIb trial in 385 patients did not demonstrate efficacy versus placebo in all doses while the positive control etanercept elicited distinguishable improvements. The negative outcome of this study was similar to Pfizer's results in their later Phase IIa study (*vide supra*).

Evotec reported results of a Phase I trial in 96 healthy volunteers with EVT 401, a compound of undisclosed structure [78]. This study was conducted in healthy males who received single ascending doses. The compound was found to be safe and well tolerated, and as was shown by GSK, Pfizer and AstraZeneca's compounds, it also prevented ATP-stimulated release of IL-1 β . The authors state that the oral dosage needs

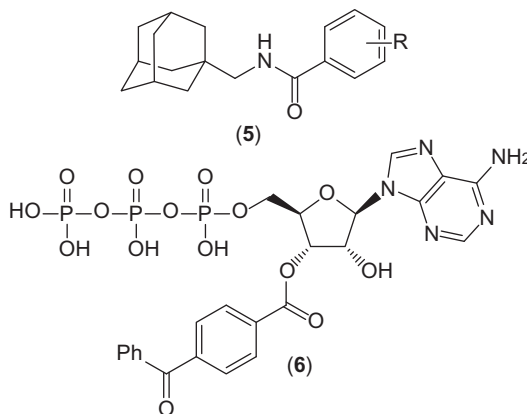
further optimisation; however, they anticipate Phase II studies in patients with RA will proceed once this adjustment has been made [79]. Further studies will probably also be initiated by Conba Pharmaceuticals, who have an agreement with Evotec to develop and commercialise the compound for the Chinese market [78]. Disease areas reported to be pursued by Conba are ophthalmological, chronic obstructive pulmonary disease and endometriosis.



4. P2X7 RECEPTOR ANTAGONISTS

A number of recent reports describing novel P2X7 antagonists are differentiated from previous disclosures, which had commonly featured amide-based chemotypes such as Pfizer's phenyl-6-azauracil amides (4) [77] and AstraZeneca's adamantanes (5) [80]. In addition, many of the recent compounds are not only potent human P2X7 antagonists but have desirable potency at the rat receptor as well. Molecules with several different structural features have been exemplified, and for the purposes of this review are described in two groupings—those featuring one or more monocyclic core systems, and those containing bicyclic systems. However, it will be recognised that many compounds in these two groups share key functionality and pharmacophore similarity. Nonetheless, these structural advances have allowed for the application of pre-clinical models to probe the role of P2X7 in various inflammatory diseases and the final section of this review describes antagonists from a variety of pharmacophores with recent data in animal models of CNS disorders. It is still the case, however, that much of the data described in the patent applications only details potency for the human receptor.

The studies reviewed herein typically report *in vitro* inhibition by measuring recombinant human or rat P2X7-mediated calcium flux in the presence of synthetic agonist benzoylbenzoyl ATP (Bz-ATP) (6). As an alternative method, sustained activation of P2X7 by ATP or Bz-ATP leads to a macropore opening, which allows for accumulation of dyes such as Yo-Pro-1 or ethidium bromide. Either calcium flux or dye accumulation can be measured by fluorescence to determine IC_{50} values. Less common is the use of native whole cells such as monocytes to measure IL-1 β release. Radioligand binding assays have also been utilised with recombinant human and rat P2X7 and results are reported as K_i values. Note that caution should be applied when attempting to compare IC_{50} values across assays due to differences in experimental conditions.



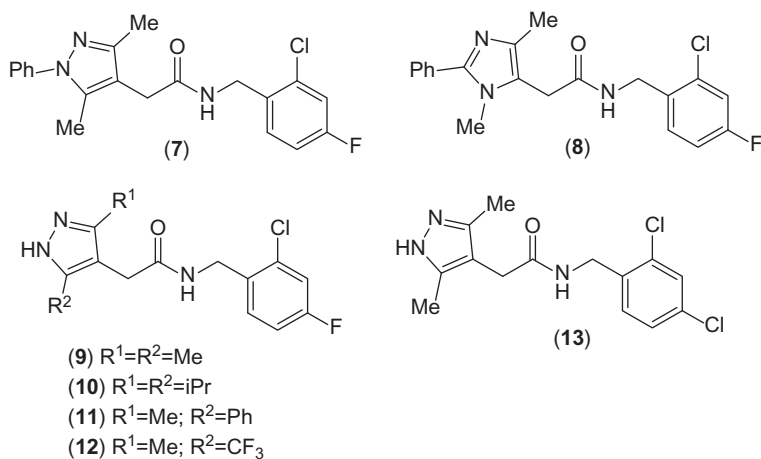
4.1. Monocyclic Hetero and Carbocyclic Antagonists

GSK has been one of the most active research groups over the past several years in submitting new P2X7 patent applications and publications. One area of focus of their P2X7 medicinal chemistry programme has been on compounds that feature *N*-benzyl- or piperazine-based amides. In 2009, they reported the use of pyrazolyl or isoxazolyl P2X7 modulators in combination therapy for several indications, including for the treatment of pain in combination with opioids, monoamine reuptake inhibitors or other pain therapies [81,82].

GSK's pyrazole and oxazole-based antagonists were identified from a high-throughput screen [63]. The pyrazolyl acetamide (7) was identified as a reasonable starting point for further optimisation, demonstrating good P2X7 potency in an ethidium bromide accumulation assay (human $pIC_{50} = 7.4$, rat $pIC_{50} = 7.0$) and good ligand efficiency (0.39) [83]. Modifications to (7) included altering the *N*-benzyl substituents, changing the amide linker (such as urea incorporation and reversing the amide) as well as modifying the pyrazole or pyrazole N1 substitution. Most of these changes led to reduced P2X7 potency relative to (7), with some notable exceptions. First, pyrazole replacement by imidazole (8) was found to be equipotent to compound (7) (human $pIC_{50} = 7.3$). Second, dichloro-substituents on the benzamide resulted in maintained or improved human pIC_{50} values and third, removal of the N1 phenyl group to give the pyrazole (9) demonstrated a modest increase in P2X7 human potency ($pIC_{50} = 7.7$). Based on *in silico* profiling, it was hypothesised that this pyrazole *N*-phenyl group was the likely site of metabolism. Indeed nearly every attempt to replace the pyrazole N1 phenyl group resulted in lowering *in vitro* clearance. The pyrazole (9)

was chosen for *in vivo* studies in rat. It demonstrated an *in vivo* i.v. clearance of 15 mL/min/kg, a volume of distribution of 1.6 L/kg and bioavailability of 90%. It should be noted that the heteroaromatic change from pyrazole to imidazole also led to an improvement in metabolic stability *in vitro* ($CL_{int} = 9.5$ mL/min/g in human liver microsomes) in the case of **(8)** [84].

Further optimisation of the pyrazole group and the *N*-benzyl substituent of **(9)** was conducted [74]. Modifications to the 3,5-dimethyl pyrazole led to a 3,5-diethyl substituted pyrazole with an improved human P2X7 pIC_{50} of 8.0. However, further bulkiness was not well tolerated as the 3,5-diisopropyl pyrazole **(10)** displayed diminished potency ($pIC_{50} = 6.9$) and the 3-methyl-5-phenyl pyrazole **(11)** was even weaker ($pIC_{50} < 6$). Compound **(12)** containing a 3-methyl-5-trifluoromethyl pyrazole was found to be a potent P2X7 antagonist ($pIC_{50} = 7.9$) and demonstrated improved *in vitro* stability in rat microsomes ($CL_{int} = 1.6$ mL/min/g). Further improvements were achieved by modifying the *N*-benzyl substituents to 2-chloro-3-trifluoromethyl in place of the previously favoured 2-chloro-4-fluoro (pIC_{50} of 8.6 compared to 7.7). It was noted that compounds within this series generally have reasonable rat oral pharmacokinetic profiles only when the clearance in liver microsomes is lower than 2 mL/min/g liver. Ultimately **(13)** was chosen for *in vivo* studies based on its favourable balance of human and rat P2X7 pIC_{50} (8.1 and 7.1, respectively) as well as low rat *in vitro* clearance of 1.3 mL/min/g. Indeed **(13)** demonstrated low blood clearance in rat (9 mL/min/kg) and an oral bioavailability of close to 100%.



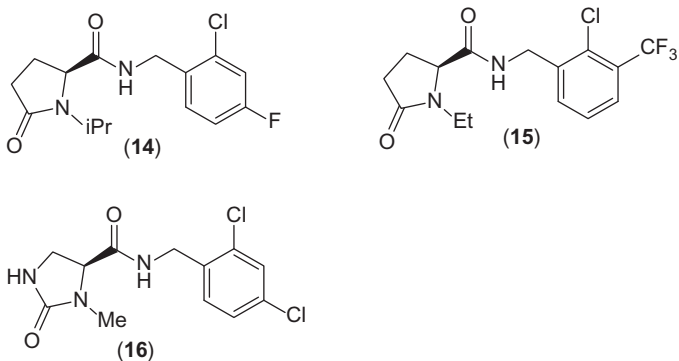
Compound **(13)** was dosed orally in the rat acute complete Freund's adjuvant (CFA) model of inflammatory pain in order to study target validation in a pain model. The compound was found to exhibit a dose-dependent

reversal of induced hypersensitivity with an ED_{50} of 2.5 mg/kg, with efficacy comparable to 10 mg/kg of the celecoxib standard. It is of note that rat brain concentrations of (**13**) were measured at 10 mg/kg and determined to be 4.9 μM . However, later studies showed the methyl pyrazoles to be prone to time-dependent inhibition (TDI) of the CYP3A4 isozyme [62]. Metabolism studies indicated that oxidation of the methyl substituents was the most likely cause of the TDI.

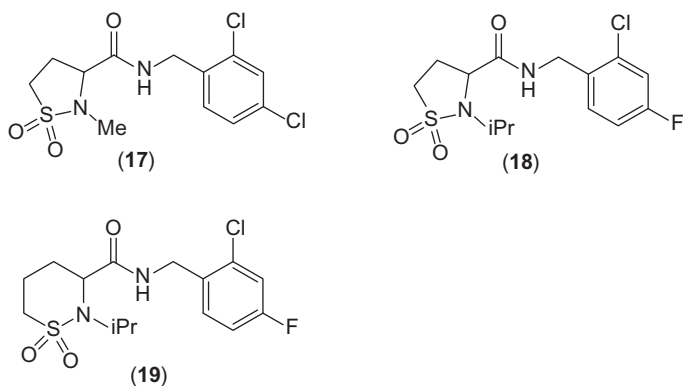
GSK's clinical compound GSK1482160 (**3**) was part of a series of pyroglutamic acid amide P2X7 receptor antagonists that were identified using a fingerprint-based similarity search [62,72,73,85]. These compounds feature a proline amide in place of the dimethyl pyrazole moiety of (**9**). The fingerprint screen sought to maintain a hydrogen bond acceptor in the pyrazole N1 position as well as at the carbonyl of the amide. The authors suggest that the hydrogen bond acceptors are likely to be beneficial for P2X7 activity, based on findings from the pyrazole GSK1482160 overlaid with other chemotypes of P2X7 antagonists previously identified. The pyroglutamic acid amide (**14**) was identified and pursued based on its promising human P2X7 potency ($pIC_{50}=6.5$) and good ligand efficiency (0.43) [83]. A range of substituents on the proline nitrogen as well as on the *N*-benzylamide were investigated. This led to the discovery of (**15**) and the clinical candidate GSK1482160, which have human P2X7 pIC_{50} values of 8.8 and 8.5, respectively. GSK1482160 was found to have 100-fold lower affinity for the rat receptor over human but also showed low clearance in rat and human liver microsomes and no appreciable inhibition of the CYP450 enzyme isoforms or TDI of any of these isoforms. It was also found to have excellent solubility and low protein binding. The combination of these desirable properties prompted further *in vivo* profiling.

In a rat pharmacokinetic study, GSK1482160 was found to have a low *i.v.* clearance (9 mL/min/kg), a half-life of 1.5 h and 65% oral bioavailability. However, short half-lives were measured in dog and monkey, potentially indicative of a short human half-life [64]. For this reason, further SAR was conducted on the pyroglutamate moiety, which was where the metabolism was thought to be occurring. Reasonable success was attained by replacing one of the methylene groups with nitrogen to form a cyclic urea [62]. Indeed urea (**16**) displayed a 7-h half-life in monkey, which is a significant improvement over the 0.9-h half-life of GSK1482160. It also showed a highly significant reversal of CFA-induced hypersensitivity in the knee joint model of chronic inflammatory pain in rats at a dose of 20 mg/kg. This is despite a relatively low rat P2X7 pIC_{50} of 6.4 (human P2X7 $pIC_{50}=8.0$) and P-glycoprotein 9 (Pgp) efflux ratio of 2.3. Substituted cyclic ureas were also

prepared and profiled (adding heterocyclic substituents on the unsubstituted urea nitrogen of **(16)**); human P2X7 pIC₅₀ values ranged from 7.1 to 8.6. Most of these analogues had Pgp efflux ratios greater than 2.0.

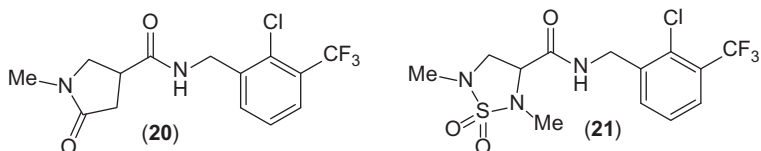


Further work was reported in a 2009 patent application in which the carbonyl of the pyrrolidinic acid amides was replaced by a sulfone [86]. Several of these compounds including **(17)** and **(18)** have human pIC₅₀ values in the range of 6.5–8.0. Expanding the ring of **(18)** to an oxo-piperidine as in compound **(19)** resulted in loss of activity (P2X7 pIC₅₀ 4.8–5.4).



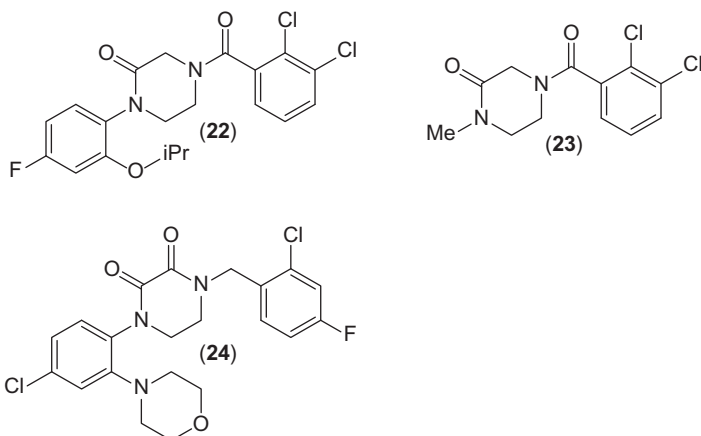
Other patent applications published by GSK detail modifications of the oxo-pyrrolidine system [87,88]. Exemplified in these patents are 14 compounds comprised of 5-oxo-3-pyrrolidinecarboxamides and sulphonyl ureas. Two of the most potent examples are **(20)** and **(21)**, with reported pIC₅₀ values in the range of 7.2–7.3 and 7.5–7.9, respectively. It should be noted that these compounds maintain the two carbonyl hydrogen bond acceptor positions proposed to be beneficial based in earlier modelling studies. Similar to the other GSK patent applications discussed in this review, a

broad range of proposed clinical indications were outlined for their P2X7 antagonists including pain, inflammatory conditions, bone disease, cardiovascular disease and neurodegenerative disease.



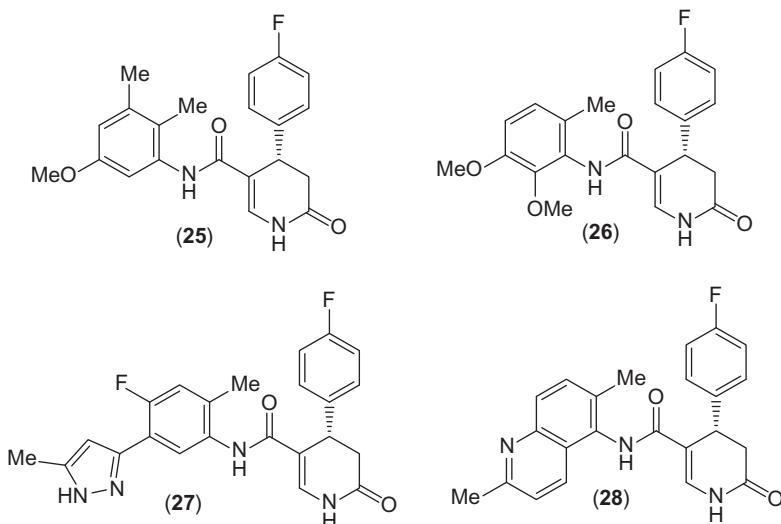
Two series of piperazinones were also reported by GSK in 2009 and 2010 [89,90]. Aromatic-substituted piperazinones such as (22) were claimed, most of which contain chloro-, fluoro- or trifluoromethyl-benzamides [89]. Forty compounds were reported with human P2X7 pIC_{50} values greater than 7.0 and over 30 of them, such as (22), have an ortho-substituted *N*-aryl group. Three examples contain an *N*-substituted methylpyridine and are likely to be less potent, with reported pIC_{50} values of 6.2–7.0. However, the presence of an *N*-aryl substituent was not required on the internal amide for P2X7 activity, as exemplified by *N*-methyl piperazinone (23). This molecule has a low molecular weight of 287 and a $pIC_{50} > 7.0$.

Moving the amide carbonyl group from the exocyclic to endocyclic position of the piperazinone resulted in active P2X7 diketopiperazine amide antagonists [90]. Numerous compounds were reported as having human P2X7 pIC_{50} values above 6.5, including the 4-chloro-2-morpholinophenyl substituted diketopiperazine (24). This patent application includes compounds with substantial variation on the *N*-phenyl substituent while maintaining a P2X7 pIC_{50} of greater than 6.5. No examples of *N*-alkyl substituted piperazines were reported in this application.



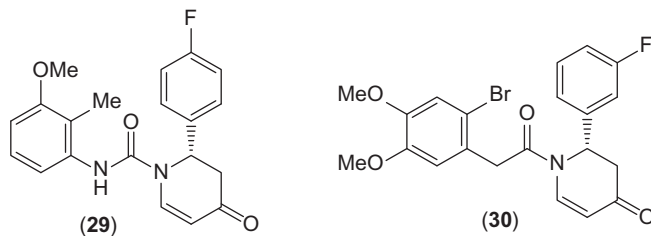
Between 2010 and 2011, Hoffman-La Roche disclosed in six patent applications examples of over 600 P2X7 antagonists that contain an amide or urea in conjugation with a six-membered heterocycle, such as a δ -lactam, six-membered urea or α,β -unsaturated ketone [91–96]. The target indications are peripheral inflammatory diseases such as RA and pain. Respiratory and gastrointestinal disorders are also indicated, as well as memory disorders and treatments for the enhancement of cognitive function. Several of the applications describe an *in vivo* asthma challenge model to assess lung function when a P2X7 antagonist is administered. Two protocols are outlined in the applications for measuring P2X7 IC₅₀ values: inhibition of human P2X7-mediated calcium flux and rat and human whole blood IL-1 β release. It was not specified which of them was used to determine the IC₅₀ values reported therein.

Three of the applications claim the use of 3,4-dihydropyridin-2-ones as P2X7 antagonists. In addition to having good P2X7 potency, examples are generally CNS drug-like, many with molecular weights less than 430 and cLogP values of about 3. Frequently featured is an (*S*)-4-fluorophenyl-substituted dihydropyridone and all compounds have a benzamide, either minimally substituted [91], substituted with a heteroaryl [92] or as part of a fused heterocyclic system [93]. The location of the benzamide substituents appears to be important for potency. For example, compound (**25**) has a P2X7 pIC₅₀ of 8.0 but changing the placement of the methyl- and methoxy-groups to give (**26**) results in a compound with 100 times lower potency (P2X7 pIC₅₀=6.0) [91]. The biaryl systems have P2X7 pIC₅₀ values in the range of about 6–8 for the 159 exemplified compounds. One of the most potent examples is (**27**), with a P2X7 IC₅₀ of 8.0 [92]. It is interesting to note that benzamides containing an ortho-substituent typically showed improved activity over their unsubstituted counterparts. This trend was also evident in the other Roche patent applications, including one claiming fused aryls [93], where all but one of the compounds exemplified contain an ortho-substituent on the benzo-fused amide. A particularly potent compound is the dimethylquinoline (**28**) (P2X7 pIC₅₀=7.9). Many examples of other types of fused heterocycles including isoquinolines and indazoles as well as di- and tetra-hydroisoquinolinones were also included.



A pilot plant preparation of the (*S*)-4-fluorophenyl-substituted 3,4-dihydropyridin-2-one core was also disclosed [97]. A catalytic desymmetrisation of an anhydride precursor with a bifunctional thiourea-based organocatalyst was utilised as a key step. This intermediate was prepared on a multikilogram scale to give 5.75 kg of the key intermediate. It contains an ester handle and would be amenable to accessing the compounds described in the three applications described previously.

Another patent application establishes dihydropyridones appended to an aromatic group by a urea linkage as P2X7 antagonists [94]. In this publication, compounds show improved P2X7 activity when the *N*-aryl urea ortho-substituent is –Me, –OMe, –Cl or –Br. For example, (29) has a pIC₅₀ of 8.6 and a molecular weight of 354. A second application disclosing dihydropyridones replaces the exocyclic nitrogen of the ureas with carbon [95]. These compounds have similar SAR trends to the ureas but are generally less potent. One particularly active example is (30) which has a pIC₅₀ of 7.9.



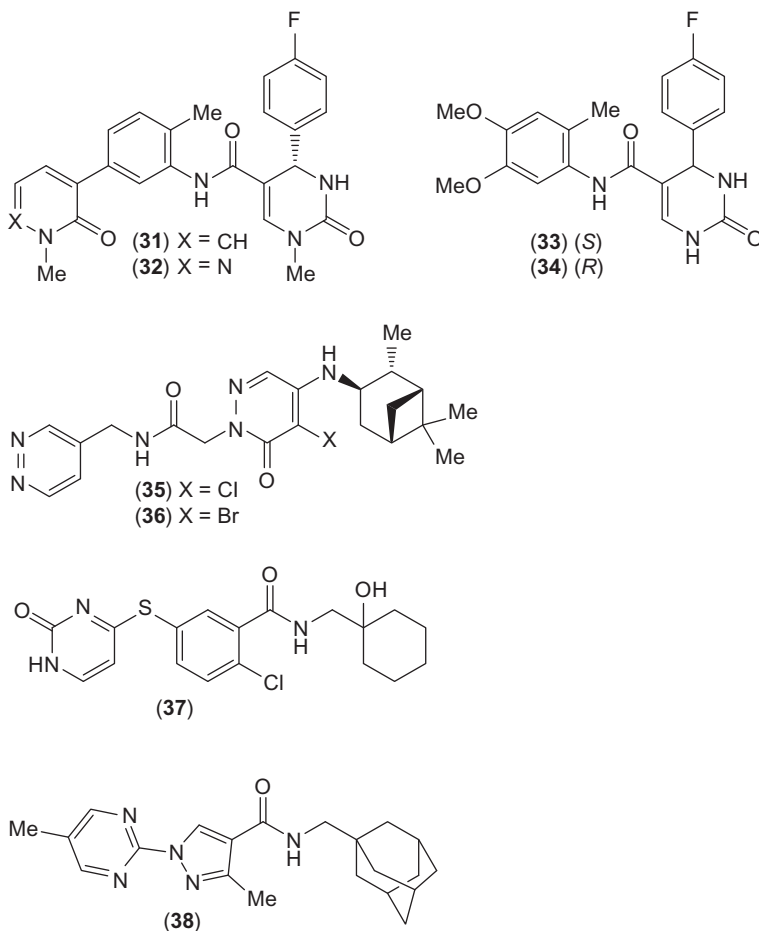
Roche's dihydropyridone patent application claiming cyclic ureas exemplifies 78 P2X7 antagonists, many with molecular weights above 450. Besides high molecular weight, the cyclic urea moiety has the potential to reduce their ability to cross the blood–brain barrier. Even so, their use in the treatment of memory disorders is declared [96]. Compound (**31**) has a P2X7 pIC₅₀ of 8.3. Typified by (**31**), nearly all of the exemplified compounds contain an (*S*)-4-fluorophenyl group and have a 1-methyl-substituent on a cyclic urea. Changing the pyridinone (**31**) to the pyridazinone (**32**) reduces the affinity by more than 500-fold, resulting in a pIC₅₀ of 5.5. The (*R*)-enantiomer was shown to be less potent than (*S*) in the single direct comparison given; compounds (**33**) and (**34**) demonstrated pIC₅₀ values of 7.2 and 6.4, respectively.

Recent patent applications from Nissan Chemical disclose pyridazinone P2X7 inhibitors for the treatment of inflammatory and immunological disorders. The inventors indicate they sought low molecular weight antagonists [98,99]. A number of highly potent compounds were exemplified; however, most have molecular weights of 450–500. The exemplified compounds contain a chloro- or bromo-substituted pyridazinone and a bridged amino carbocycle. Many were reported to have human P2X7 IC₅₀ values below 10 nM in a Yo-Pro-1 dye uptake assay. Two examples are (**35**) and (**36**), which differ only by their halogen substitution and both exhibit P2X7 IC₅₀ values of 4 nM [98]. Other examples include amides or substituted imines in place of the halogen, several of which are extremely potent P2X7 antagonists with IC₅₀ values of less than 1 nM [99].

A 2012 patent application from Actelion features chemotypes similar to that of Pfizer's clinical compound (**4**) with a benzamide linked to a hydroxymethylcarbocycle [100]. Thioether (**37**) was found to be the most potent antagonist with a human IC₅₀ of 8 M in a Yo-Pro-1 dye uptake assay. The application claims use of a P2X7 antagonist for the treatment or prevention of pain and of neurodegenerative or neuroinflammatory disorders.

Scientists at Neurogen in 2009 reported pyrazole and thiazole core compounds containing amide-linkages to adamantanes or other carbocycles or heterocycles [101]. Several indications are suggested in this application, including neuropathic pain, Alzheimer's disease and traumatic brain injury. A number of the exemplified compounds have potential for CNS penetration, some with molecular weights as low as 288. However, the molecular weights of the exemplified compounds vary greatly, to more than 500, and the relative potencies of the molecules are difficult to ascertain, given that all compounds were reported to have human P2X7 IC₅₀ values below 2 μM in

a calcium flux assay. Compound (**38**) is an example of one of the lower molecular weight compounds reported.



4.2. Heteroaromatic-Fused Core Antagonists

In the years 2009–2012, Affectis Pharmaceuticals detailed their interest in P2X7 antagonists for the treatment of a variety of inflammatory disorders in a series of five patent applications. These included CNS-specific indications such as Alzheimer's and Parkinson's diseases [102–106]. Four of the Affectis applications describe a number of *N*-indol-3-yl-acetamide and *N*-indazol-3-yl-acetamide P2X7 antagonists [102,103,105,106] while a fifth patent describes the large-scale synthesis of the indole NTR-035 (**39**) [103].

All compounds were reported to inhibit human P2X7 in a calcium flux assay with *in vitro* IC₅₀ values ranging from 1 nM to 1 μM.

The first Affectis patent application describing P2X7 antagonists appeared in 2009 and contains nearly 300 compounds [102], exemplified by (40). A majority of the exemplified compounds in this disclosure are indol-3-carboxamides containing an aliphatic amide, alkyl or alkoxy moiety, the indole nitrogen and a substituent (commonly a halide) in the indole 4-position. Affectis also reported that four unspecified compounds in this invention significantly reduced the P2X7-mediated release of IL-1β in the human monocyte cell line THP-1 when treated with 1 μg/mL LPS followed by 2 mM ATP. An unspecified compound with a human IC₅₀ of approximately 134 nM was administered orally 1 h following carrageenan (1% suspension, 0.1 mL) challenge and showed a significant decrease in paw withdrawal latency and decrease in paw volume with respect to vehicle in a mouse paw edema model [102].

In 2012, Affectis reported that AFC-5128, a compound of undisclosed structure claimed in the 2009 application [102], was nominated for Investigational New Drug filing [107]. They reported that it is a highly potent P2X7 antagonist that crosses the blood-brain barrier. In addition, they reported efficacy in an undisclosed mouse model of multiple sclerosis as well as in animal models of neuropathic and inflammatory pain. Its expected development for the treatment of neuropathic pain and multiple sclerosis was noted [107].

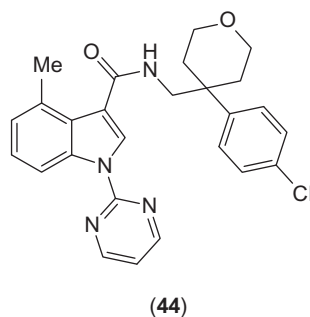
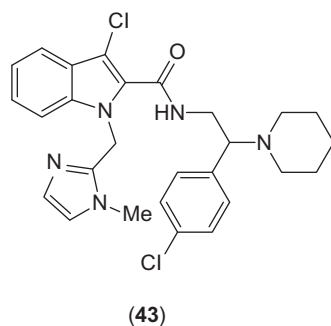
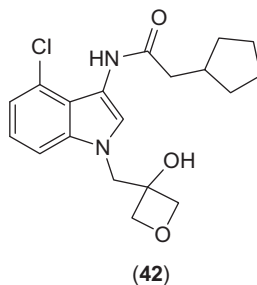
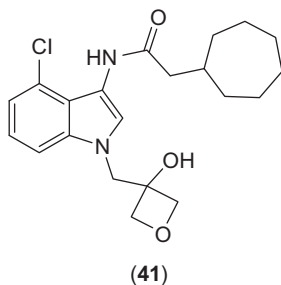
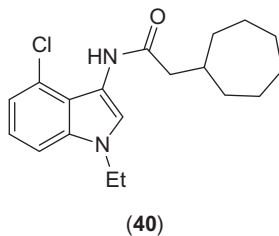
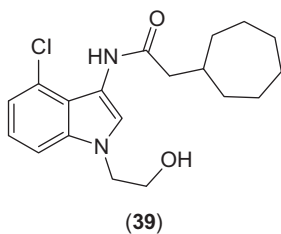
The second Affectis patent application describing P2X7 antagonists was published in 2010 and claims both *N*-indole-3-yl-acetamides and *N*-azaindole-3-yl-acetamides [103]. The exemplified compounds are similar to (in some cases identical to) their 2009 application [102]; only *N*-indole-3-yl-acetamides are exemplified, most of which contain a hydroxyl or amine moiety attached to the indole nitrogen, an aliphatic amide, and a substituent in the 4-position of the indole. Compound (39) was reported to have an IC₅₀ value of approximately 3.8 nM and was shown to dose dependently reduce the P2X7-mediated release of IL-1β at 30 and 100 nM in isolated human monocytes treated with 1 μg/mL LPS followed by 100 μM Bz-ATP. In addition, (39) was reported to have both analgesic and anti-inflammatory effects in the carrageenan-induced mouse paw oedema model. In this model, (39) was administered orally 1 h following carrageenan (1% suspension, 0.1 mL) challenge and showed a significant decrease in paw withdrawal latency and decrease in paw volume comparable to that achievable with indomethacin [103]. A novel method for the

synthesis of (39) (NTR-035) was claimed and the preparation of 29 g described [104].

Two Affectis patent applications detailing P2X7 antagonists were published in 2012 and disclose very similar, often identical, sets of compounds with only subtle differences in the structural claims. Compound (41) appears in both applications and was reported to have an IC_{50} of 18 nM [105,106]. It was also reported to have analgesic and anti-inflammatory effects in the carrageenan-induced paw oedema model. The compound was administered by i.p. injection (50 mg/kg) 1.5 h following carrageenan (1% suspension, 0.1 mL) challenge and showed around a 42% reduction in paw withdrawal latency and an approximately 47% decrease in paw volume with respect to vehicle. The biological data provided showed (42) to have both *in vitro* human efficacy and *in vivo* mouse efficacy [106]. Compound (42) was also found to inhibit the P2X7-mediated release of IL-1 β in human whole blood from four different donors, induced by treatment with LPS and ATP with IC_{50} values of 3.8, 3.8, 5.3 and 6.1 μ M. In mice, oral dosing of (42) was shown to decrease IL-1 β release in a dose-dependent manner in response to LPS/ATP challenge in both the plasma and peritoneal lavage. A 150 mg/kg dose resulted in an 81% and 92% reduction in IL-1 β release in the plasma and peritoneal lavage, respectively. Treatment with dexamethasone resulted in similar reductions in IL-1 β in both the plasma and peritoneal lavage. A 50 mg/kg dose of (42) resulted in 55% and 52% reduction in IL-1 β release plasma and peritoneal lavage, respectively. No significant decrease was observed with a 15 mg/kg dose [105].

In early 2009, Neurogen Corporation published a patent application detailing their interest in P2X7 receptor agonists for the treatment of a variety of disorders including pain, inflammation and neuropsychiatric diseases [108]. The *in vivo* efficacy model described is the carrageenan-induced mechanical hyperalgesia assay for determining pain relief. However, no efficacy data for any specific antagonist exemplified in this invention is provided.

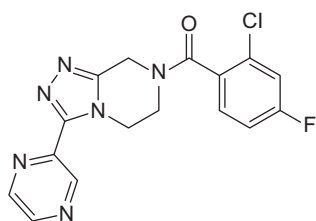
The Neurogen application describes a series of heteroaryl amides, for example, the indoles (43) and (44). The compounds exemplified in the disclosure were reported as belonging to one of two categories, either inhibiting human P2X7-mediated calcium flux with IC_{50} values of 2 μ M or less, or greater than 2 μ M. No additional biological characterisation is provided in this invention. The same inventors, now associated with Lundbeck, filed an identical application with an expanded set of antagonists in February 2009 [109].



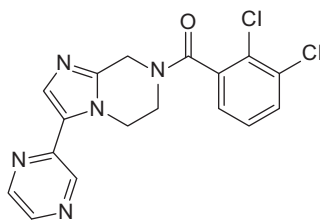
In 2010, GSK filed two patent applications detailing their interest in two series of P2X7 antagonists, tetrahydrotriazolopyrazines and tetrahydroimidazopyrazines, typified by (45) and (46), respectively [110,111]. The potency of the patent's exemplified compounds was evaluated in an ethidium bromide accumulation assay and was reported as a pIC_{50} range of less than 6.0, 6.3 or greater, 7.0 or greater or 8.0 or greater. No additional biological data or efficacy data were provided in these disclosures. Both (45) and (46) were reported to have pIC_{50} values greater than 8.0 [110,111].

The GSK disclosure containing tetrahydrotriazolopyrazines [110] has the larger compound set of the two disclosures. It contains 207 examples,

71 of which were reported to have a pIC_{50} value of 8.0 or greater at the human P2X7 receptor. The disclosure containing tetrahydroimidazolopyrazines contains 45 compounds of which 15 compounds were reported to have pIC_{50} values of 8.0 or greater [110]. While it is difficult to gain specific SAR from these disclosures, common structural features of the more potent compounds include a heteroaryl moiety on the 3-position of the 1,2,4-triazole or imidazole, and substitution at the 2-position of the benzamide. Prominent across all exemplified compounds are 2-halo-substituted benzamides, with chloro-, fluoro- and trifluoromethyl-substituents most often recurring in the 2-, 3- and 4-positions of the benzamide ring.



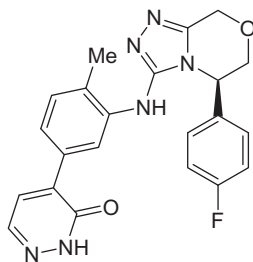
(45)



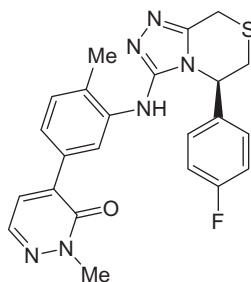
(46)

A 2011 patent application from Hoffman-La Roche claims a series of fused triazole amines as P2X7 antagonists for use in treating a variety of conditions associated with inflammatory cytokine release [112]. A total of 66 compounds are exemplified in the application with pIC_{50} values ranging from 5.1 to 8.3. The antagonists in this disclosure are typified by (47) and (48). As in the Roche application described earlier in this chapter, it was not specified which of the described methods was used to determine the IC_{50} values reported (P2X7-mediated calcium flux, or rat or human whole blood IL-1 β release).

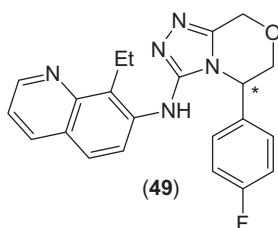
The two most potent antagonists reported by Roche are (47) and (48). The compounds in the Roche disclosure all contain a phenyl, 4-fluorophenyl or 3-fluorophenyl moiety adjacent to the triazole and the stereochemistry of the benzylic carbon was shown to have a significant impact on the potency of the antagonists. Compounds containing the *S*-configuration were shown to have superior potency, exemplified by (49). All compounds exemplified in this disclosure have either an aryl or a heteroaryl moiety appended to the 3-position of the triazole with an amino-linkage, despite the variety of other linkages present in the claims [112].



(47)



(48)



(49)

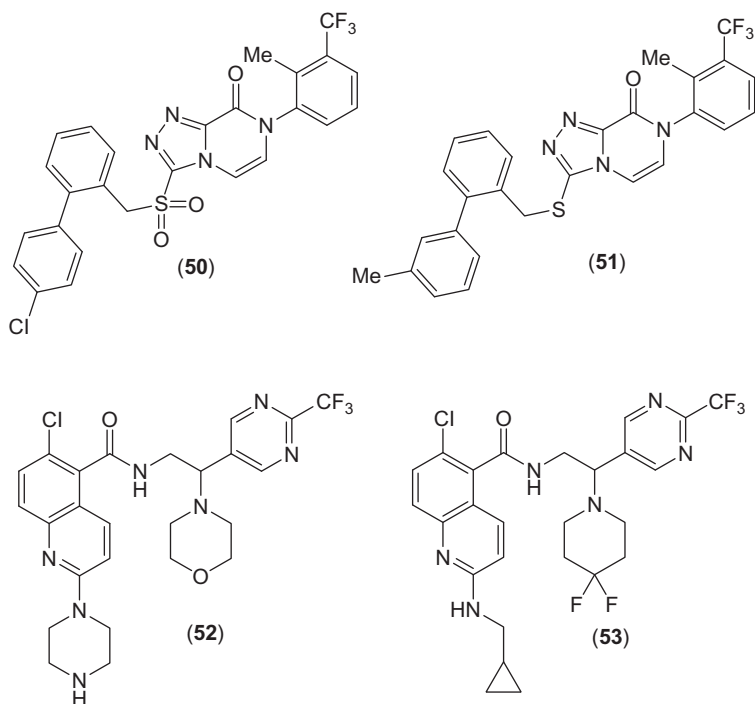
config	pIC ₅₀
rac	7.5
S	7.7
R	5.2

In 2012, Schering Corporation reported a series of triazolopyrazinone P2X7 antagonists, exemplified by (50) and (51), for use in the treatment of inflammatory disease and pain [113]. A total of 171 compounds were included in the Schering disclosure with IC₅₀ values measuring P2X7-mediated calcium flux ranging from 7.0 nM to 6.0 μM.

The two most potent antagonists in this disclosure are (50) and (51) (IC₅₀ = 7 and 30 nM, respectively). In general, having a 2-methyl-3-trifluoromethylphenyl substituent appended to the pyrazinone nitrogen appears to be optimal and is present in a high proportion of the compounds. Small variations to this moiety were found to result in significant losses in potency. Additionally, a lipophilic moiety linked to the 3-position of the triazole via a benzylic sulfone (50) or benzylic thioether (51) produced the most potent antagonists [113].

In 2009, Janssen Pharmaceuticals reported a series of quinoline- and isoquinoline-based compounds, exemplified by (52) and (53), for use in the treatment of diseases related to the P2X7 channel [114]. The disclosure contains 654 quinolone or isoquinoline compounds. The examples are predominantly quinolones with substitution at the 2-position and

an amide at the 5-position. All compounds described have at least one chiral centre; most are reported as either racemic or a mixture of diastereomers (**52**) and (**53**). Polar functionality appended to the 2-position of the quinoline via an amino-linkage appears to provide the most potent compounds. However, an oxygen-linkage at the 2-position of the quinoline also appears to be tolerated. Substitution at the 6-position of the quinoline, often a halogen, is common among the compounds in the disclosure but was not found to be required for potency. The amide fragments of the antagonists are geminally substituted ethylamines with an aryl or heteroaryl moiety and a cyclic amine. Examples (**52**) and (**53**) contain the two amide fragments most commonly present in the exemplified compounds and were reported to have human pIC₅₀ values of 8.2 and 7.9, respectively, in a Yo-Pro-1 uptake assay. All tested antagonists have human P2X7 pIC₅₀ values ranging from less than 5 to more than 9 and the potency of the compounds was assessed through the inhibition of human P2X7-mediated calcium flux or Yo-Pro-1 uptake.



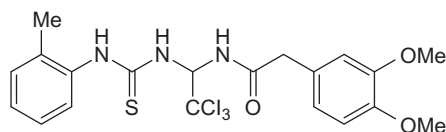
4.3. P2X7 Antagonists in Animal Models of the CNS

The literature reports reviewed in this section describe P2X7 antagonists that have been shown to be efficacious in CNS rat models of neuropathic pain, nerve injury or diabetic neuropathy, or antagonists that have been measured in the brain of the rat at potentially therapeutic levels.

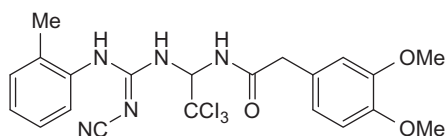
Measurement of the brain penetration of GSK's clinical compound was carried out in conjunction with a pain model in which GSK1482160 (**3**) was administered in a CFA-induced hypersensitivity in the knee joint model of chronic inflammatory pain [62]. Brain concentrations of GSK1482160 at a dose of 50 mg/kg were measured to be 12.9 μM at 1.5 h post-dose. In this study, GSK1482160 produced a maximal reversal of hypersensitivity at 20 mg/kg, although the effect was not statistically different from the positive control celecoxib. The compound was also administered to a rat in a chronic constriction injury (CCI) model of nerve injury-induced allodynia. Efficacy of GSK1482160 in this model was observed to be on par with that of the gabapentin standard. In this experiment, compound blood and brain concentrations measured were 5.91 and 3.36 μM , respectively, and efficacy was confirmed at free exposures higher than the rat pIC_{50} in both the periphery and CNS in *in vivo* studies. Based on its excellent pre-clinical, physicochemical and pharmacokinetic profile in rats, GSK1482160 (**3**) was selected for clinical studies [62].

Abbott Laboratories recently reported on a series of cyanoguanidine P2X7 antagonists as potential treatments for neuropathic pain [115]. The authors revealed that a high-throughput screening campaign led to the discovery of the thiourea (**54**) with human and rat P2X7 pIC_{50} values of 6.8 and 6.3, respectively, in a calcium flux assay. Because of the potential toxicity of the thiourea moiety the authors focused on cyanoguanidine replacements for the thiourea. This work generated a number of interesting structures including (**55**) (human and rat P2X7 pIC_{50} values of 6.9 and 7.9, respectively), (**56**) (human and rat P2X7 pIC_{50} values of 6.9 and 7.9, respectively) and (**57**) (human and rat P2X7 pIC_{50} values of 8.0 and 8.2, respectively). It should be noted that although (**54**) showed a strong enantioselectivity with respect to P2X7 affinity, all the SAR and *in vivo* experiments used racemic material as the drug substance. The authors also note that for the cyanoguanidines prepared, a single geometric isomer was obtained in each case; however, they did not prove that the isomer shown was the one synthesised. All three compounds were shown to reduce tactile allodynia in the Chung model of neuropathic pain following i.p. administration. Compound (**56**) was the most potent compound in this assay with an ED_{50} of 38 $\mu\text{mol/kg}$. The compound was also efficacious following p.o. administration and this effect was retained upon chronic administration.

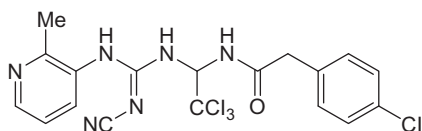
Investigators from Abbott also recently disclosed A-804598 (**58**), a very potent and selective ATP competitive P2X7 antagonist that was labelled with tritium in order to study its binding to rat recombinant P2X7 receptors [116]. The authors showed that (**58**) effectively blocked Bz-ATP-induced calcium concentrations in cells expressing human, rat or mouse P2X7 receptors (IC_{50} 10.9, 9.9 and 8.9 nM, respectively). They also demonstrated high selectivity for (**58**) over a variety of transporters, ion channels and receptors. Unlike many earlier compounds, (**58**) is a very potent P2X7 antagonist at the rodent and human receptor, and as such the authors propose the use of this compound to further study the function of rodent P2X7 receptors.



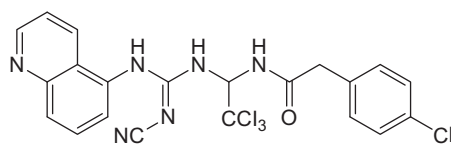
(54)



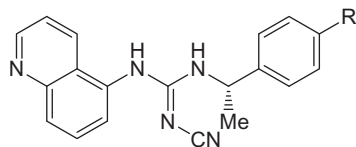
(55)



(56)



(57)

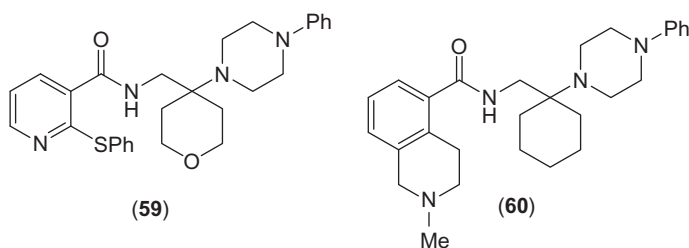


(58) R=H

³H-58) R=³H

Janssen Research and Development recently reported on the discovery of two piperazine-based brain-penetrating P2X7 antagonists [117]. These

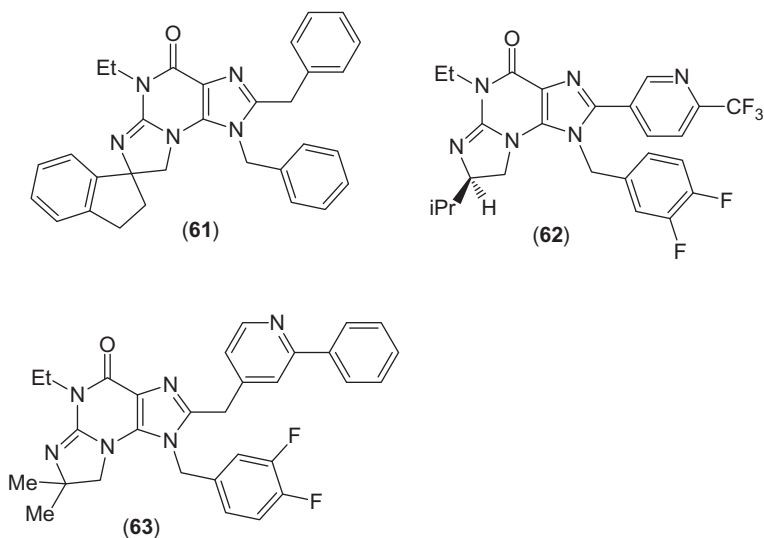
compounds are proposed as tools to determine the role of the P2X7 receptor on neuroimmune modulation. Compounds (**59**) and (**60**) were found to have high affinity for both the human and rat P2X7 receptors ((**59**): human $pK_i = 7.9$, rat $pK_i = 8.7$; (**60**): human $pK_i = 7.9$, rat $pK_i = 9.1$). Compound (**60**) also has high affinity for the serotonin reuptake transporter with a reported pK_i of 7.7. This presumably could have interesting implications for CNS indications, particularly in the area of mood disorders. Focusing on (**59**), the authors demonstrate dose-dependent P2X7 target engagement in rat via *ex vivo* autoradiography with an ED_{50} of 2.5 mg/kg following s.c. dosing. This robust target engagement makes (**59**) a compound suitable for characterisation in pre-clinical models of depression and other mood disorders.



Starting with a rather high molecular weight lead identified by high-throughput screening ((**61**), MW = 487), with a weak P2X7 human IC_{50} of 248 nM (calcium flux) and human whole blood IC_{50} of 3372 nM (IL-1 β), scientists at the Merck Research Laboratory optimised this 7,8-dihydro-1*H*-imidazo[2,1-*b*]purin-4(5*H*)-one core which led to the discovery of compound (**62**) [71]. Their optimisation efforts focused on improving the human whole blood activity and pharmacokinetic properties of the lead molecule in order to assess utility for the treatment of pain and neurodegenerative diseases. As such, compound (**62**) has much improved human P2X7 affinity (human P2X7 $IC_{50} = 50$ nM, human whole blood (IL-1 β) $IC_{50} = 82$ nM) and even better rat whole blood affinity ($IC_{50} = 17$ nM). The authors also demonstrated that (**62**) was efficacious in the monoiodoacetate (MIA) model of pain (p.o. 30 mg/kg). However, the compound showed only marginal activity in the rat CCI model of pain at 100 mg/kg p.o. The authors contend that this is probably due to the fact that (**62**) does not efficiently penetrate the CNS.

In a second report, the same group at Merck further optimised the 7,8-dihydro-1*H*-imidazo[2,1-*b*]purin-4(5*H*)-one core with a focus on improved exposure and efficacy in models of neuropathic pain. This work led to the discovery of (**63**). Compound (**63**) has a human whole blood IC_{50} of 24 nM, as measured by IL-1 β inhibition [70]. It was efficacious in a streptozocin-induced diabetic neuropathy model at 10 mg/kg p.o. and showed efficacy in both the

MIA and CCI models in rat at 1–3 mg/kg p.o. Although (63) had promising *in vivo* efficacy in rat, the authors report that glutathione adducts were observed in higher species, precluding further development.

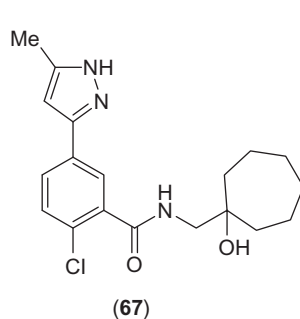
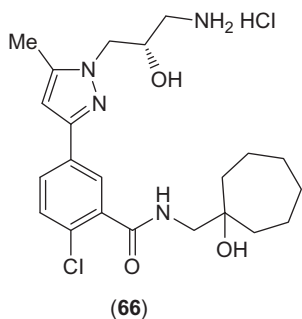
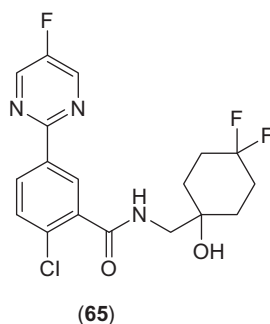
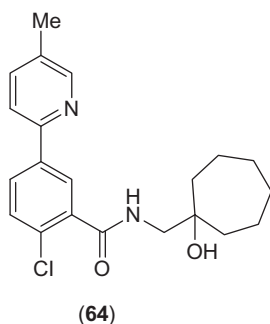


Pfizer Global Research and Development recently reported on the use of [^3H]-A-804598 (^3H -58) as a tracer useful for determining *ex vivo* receptor occupancy of centrally penetrating P2X7 antagonists [118]. This work represents the first report demonstrating native tissue P2X7 binding. In agreement with earlier work, the authors showed widespread specific binding throughout the CNS, with moderate to high binding in the colliculus and areas of the cerebral cortex. As *ex vivo* receptor occupancy is a powerful technique for assessing target engagement for CNS drugs, this report is also an important advance in determining the utility of centrally penetrating P2X7 antagonists in CNS disorders.

A different research group at Pfizer utilised the 2-chlorobenzamide lead (64) as a starting point with the goal of discovering brain penetrant P2X7 antagonists for the treatment of inflammatory and/or neuropathic pain [119]. According to their report, (64) is a potent drug-like lead ($\text{IC}_{50} = 32 \text{ nM}$, $\text{cLogD} = 3.5$, human liver microsomes (HLM) $\text{CL}_{\text{int}} = 80 \text{ mL/min/kg}$); however, the compound suffered from poor metabolic stability. Efforts to improve the metabolic profile of this series of compounds led to the discovery of (65), a potent P2X7 antagonist with reduced cLogD and with much improved metabolic stability ($\text{IC}_{50} = 27 \text{ nM}$, $\text{cLogD} = 1.8$, HLM $\text{CL}_{\text{int}} < 8.8 \text{ mL/min/kg}$). This was accomplished by strategically locating fluorine atoms at two potential metabolically susceptible positions, namely the methyl pyridine and cycloheptanol moieties. Compound (65) had low clearance *in vivo* in rat (3.3 mL/min/kg),

an acceptable half-life of 4.6 h and high bioavailability (84%). Based on this data and the fact that (**65**) was shown to effectively penetrate the CNS (brain : plasma concentration ratio of 1.3), the authors report that the compound was endorsed for development.

Yet another research group at Pfizer sought to improve the predicted pharmacokinetic profile of a related series of compounds derived from the clinical candidate CE-224,535 (**4**) (IL-1 β IC₅₀ = 1.3 nM) via modifications of the 6-azauracil ring. The authors assert that it was the acidic nature of this ring which presumably led to a low V_{dss} *in vivo*, as well as the short half-life observed [120]. This work led to the discovery of (**66**), in which the azauracil is replaced by a methyl pyrazole. Compound (**66**) was found to be a potent P2X7 antagonist with an IC₅₀ of 0.5 nM (Yo-Pro-1) and whole blood IC₅₀ of 3 nM. It demonstrated a high V_{dss} (11.7 L/kg) and suitable half-life (8.36 h) but suffered from a low bioavailability (9%), believed to be due to poor cell permeability (as measured by Caco-2). Compound (**67**) contains no pyrazole *N*-alkyl substitution and has an improved bioavailability of 59%. It was found to be a potent P2X7 antagonist with an IC₅₀ of 3 nM (Yo-Pro-1) and whole blood IC₅₀ of 121 nM. Its relatively poor rodent potency precluded its evaluation in standard rodent inflammation but a specialised mouse model measuring ATP-induced IL-1 β output was developed in which (**67**) demonstrated *in vivo* activity.





5. CONCLUSION

Recently, there have been many reports detailing novel P2X7 antagonists and their potential to treat diseases of the CNS. The ability of a P2X7 antagonist to reduce or eliminate IL-1 β production in the periphery has been demonstrated several times in the clinic. However, Phase II trials from two companies have resulted in the failure of human P2X7 selective antagonists to improve symptoms in patients whose RA was not well controlled by other therapies. Given these disappointing results, the discovery of novel antagonists that allow for pre-clinical determination of efficacy in animal models has been an important advance. Many of the novel antagonists have excellent P2X7 *in vitro* potency both in human and rat and some have been measured in the CNS. In addition, there is significant data indicating that IL-1 β ablation in *P2RX7* knockout studies and from P2X7 antagonists attenuates the negative effects of neuropsychiatric conditions, neurodegeneration and pain. However, it remains to be seen whether these pre-clinical observations will translate into the clinic.

REFERENCES

- [1] Jiang LH, Baldwin JM, Roger S, Baldwin SA. Insights into the molecular mechanisms underlying mammalian P2X7 receptor functions and contributions in diseases, revealed by structural modeling and single nucleotide polymorphisms. *Front Pharmacol* 2013;4:55.
- [2] North RA, Jarvis MF. P2X receptors as drug targets. *Mol Pharmacol* 2013;83(4):759–69.
- [3] Volonte C, Apolloni S, Skaper SD, Burnstock G. P2X7 receptors: channels, pores and more. *CNS Neurol Disord Drug Targets* 2012;11(6):705–21.
- [4] Kataoka A, Tozaki-Saitoh H, Koga Y, Tsuda M, Inoue K. Activation of P2X7 receptors induces CCL3 production in microglial cells through transcription factor NFAT. *J Neurochem* 2009;108(1):115–25.
- [5] Panenka W, Jijon H, Herx LM, Armstrong JN, Feighan D, Wei T, et al. P2X7-like receptor activation in astrocytes increases chemokine monocyte chemoattractant protein-1 expression via mitogen-activated protein kinase. *J Neurosci* 2001;21(18):7135–42.
- [6] Shiratori M, Tozaki-Saitoh H, Yoshitake M, Tsuda M, Inoue K. P2X7 receptor activation induces CXCL2 production in microglia through NFAT and PKC/MAPK pathways. *J Neurochem* 2010;114(3):810–9.
- [7] Clark AK, Wodarski R, Guida F, Sasso O, Malcangio M. Cathepsin S release from primary cultured microglia is regulated by the P2X7 receptor. *Glia* 2010;58(14):1710–26.
- [8] Lopez-Castejon G, Theaker J, Pelegrin P, Clifton AD, Braddock M, Surprenant A. P2X(7) receptor-mediated release of cathepsins from macrophages is a cytokine-independent mechanism potentially involved in joint diseases. *J Immunol* 2010;185(4):2611–9.
- [9] Patti L, Raiteri L, Grilli M, Parodi M, Raiteri M, Marchi M. P2X(7) receptors exert a permissive role on the activation of release-enhancing presynaptic alpha7 nicotinic

- receptors co-existing on rat neocortex glutamatergic terminals. *Neuropharmacology* 2006;50(6):705–13.
- [10] Ando RD, Sperlagh B. The role of glutamate release mediated by extrasynaptic P2X7 receptors in animal models of neuropathic pain. *Brain Res Bull* 2013;93:80–5.
 - [11] Sperlagh B, Kofalvi A, Deuchars J, Atkinson L, Milligan CJ, Buckley NJ, et al. Involvement of P2X7 receptors in the regulation of neurotransmitter release in the rat hippocampus. *J Neurochem* 2002;81(6):1196–211.
 - [12] Deuchars SA, Atkinson L, Brooke RE, Musa H, Milligan CJ, Batten TF, et al. Neuronal P2X7 receptors are targeted to presynaptic terminals in the central and peripheral nervous systems. *J Neurosci* 2001;21(18):7143–52.
 - [13] Codocedo JF, Godoy JA, Poblete MI, Inestrosa NC, Huidobro-Toro JP. ATP induces NO production in hippocampal neurons by P2X(7) receptor activation independent of glutamate signaling. *PLoS One* 2013;8(3):e57626.
 - [14] Iwata M, Ota KT, Duman RS. The inflammasome: pathways linking psychological stress, depression, and systemic illnesses. *Brain Behav Immun* 2013;31:105–14.
 - [15] Monif M, Burnstock G, Williams DA. Microglia: proliferation and activation driven by the P2X7 receptor. *Int J Biochem Cell Biol* 2010;42(11):1753–6.
 - [16] Choi HB, Ryu JK, Kim SU, McLamon JG. Modulation of the purinergic P2X7 receptor attenuates lipopolysaccharide-mediated microglial activation and neuronal damage in inflamed brain. *J Neurosci* 2007;27(18):4957–68.
 - [17] Sperlagh B, Illes P. Purinergic modulation of microglial cell activation. *Purinergic Signal* 2007;3(1–2):117–27.
 - [18] Sperlagh B, Vizi ES, Wirkner K, Illes P. P2X₇ receptors in the nervous system. *Prog Neurobiol* 2006;78(6):327–46.
 - [19] Diaz-Hernandez M, Del Puerto A, Diaz-Hernandez JI, Diez-Zaera M, Lucas JJ, Garrido JJ, et al. Inhibition of the ATP-gated P2X7 receptor promotes axonal growth and branching in cultured hippocampal neurons. *J Cell Sci* 2008;121(Pt. 22):3717–28.
 - [20] Fields RD, Stevens B. ATP: an extracellular signaling molecule between neurons and glia. *Trends Neurosci* 2000;23(12):625–33.
 - [21] Skaper SD, Debetto P, Giusti P. The P2X7 purinergic receptor: from physiology to neurological disorders. *FASEB J* 2009;24(2):337–45.
 - [22] Gombault A, Baron L, Couillin I. ATP release and purinergic signaling in NLRP3 inflammasome activation. *Front Immunol* 2012;3:414.
 - [23] Corriden R, Insel PA. Basal release of ATP: an autocrine-paracrine mechanism for cell regulation. *Sci Signal* 2010;3(104):re1.
 - [24] Sperlagh B, Csölle C, Ando RD, Goloncser F, Kittel A, Baranyi M. The role of purinergic signaling in depressive disorders. *Neuropsychopharmacol Hung* 2012;14(4):231–8.
 - [25] Le Feuvre R, Brough D, Rothwell N. Extracellular ATP and P2X7 receptors in neurodegeneration. *Eur J Pharmacol* 2002;447(2–3):261–9.
 - [26] Soronen P, Mantere O, Melartin T, Suominen K, Vuorilehto M, Rytsala H, et al. P2RX7 gene is associated consistently with mood disorders and predicts clinical outcome in three clinical cohorts. *Am J Med Genet B Neuropsychiatr Genet* 2011;156B(4):435–47.
 - [27] Backlund L, Nikamo P, Hukic DS, Ek IR, Traskman-Bendz L, Landen M, et al. Cognitive manic symptoms associated with the P2RX7 gene in bipolar disorder. *Bipolar Disord* 2011;13(5–6):500–8.
 - [28] Barden N, Harvey M, Gagne B, Shink E, Tremblay M, Raymond C, et al. Analysis of single nucleotide polymorphisms in genes in the chromosome 12Q24.31 region points to P2RX7 as a susceptibility gene to bipolar affective disorder. *Am J Med Genet B Neuropsychiatr Genet* 2006;141B(4):374–82.

- [29] McQuillin A, Bass NJ, Choudhury K, Puri V, Kosmin M, Lawrence J, et al. Case-control studies show that a non-conservative amino-acid change from a glutamine to arginine in the P2RX7 purinergic receptor protein is associated with both bipolar- and unipolar-affective disorders. *Mol Psychiatry* 2009;14(6):614–20.
- [30] Stokes L, Fuller SJ, Sluyter R, Skarratt KK, Gu BJ, Wiley JS. Two haplotypes of the P2X7 receptor containing the Ala-348 to Thr polymorphism exhibit a gain-of-function effect and enhanced interleukin-1 β secretion. *FASEB J* 2010;24(8):2916–27.
- [31] Roger S, Mei Z-Z, Baldwin JM, Dong L, Bradley H, Baldwin SA, et al. Single nucleotide polymorphisms that were identified in affective mood disorders affect ATP-activated P2X7 receptor functions. *J Psychiatr Res* 2010;44(6):347–55.
- [32] Green EK, Grozeva D, Raybould R, Elvidge G, Macgregor S, Craig I, et al. P2RX7: a bipolar and unipolar disorder candidate susceptibility gene? *Am J Med Genet B Neuropsychiatr Genet* 2009;150B(8):1063–9.
- [33] Grigoriu-Serbanescu M, Herms S, Muhleisen TW, Georgi A, Diaconu CC, Strohmaier J, et al. Variation in P2RX7 candidate gene (rs2230912) is not associated with bipolar I disorder and unipolar major depression in four European samples. *Am J Med Genet B Neuropsychiatr Genet* 2009;150B(7):1017–21.
- [34] Boucher AA, Arnold JC, Hunt GE, Spiro A, Spencer J, Brown C, et al. Resilience and reduced c-Fos expression in P2X7 receptor knockout mice exposed to repeated forced swim test. *Neuroscience* 2011;189:170–7.
- [35] Basso AM, Bratcher NA, Harris RR, Jarvis MF, Decker MW, Rueter LE. Behavioral profile of P2X7 receptor knockout mice in animal models of depression and anxiety: relevance for neuropsychiatric disorders. *Behav Brain Res* 2009;198(1):83–90.
- [36] Csölle C, Ando RD, Kittel A, Gölöncsér F, Baranyi M, Soproni K, et al. The absence of P2X7 receptors (P2rx7) on non-haematopoietic cells leads to selective alteration in mood-related behaviour with dysregulated gene expression and stress reactivity in mice. *Int J Neuropsychopharmacol* 2013;16(1):213–33.
- [37] Csölle C, Baranyi M, Zsilla G, Kittel A, Gölöncsér F, Illes P. Neurochemical changes in the mouse hippocampus underlying the antidepressant effect of genetic deletion of P2X7 receptors. *PLoS One* 2013;8(6):e66547.
- [38] Koo JW, Duman RS. IL-1 β is an essential mediator of the antineurogenic and anhedonic effects of stress. *Proc Natl Acad Sci USA* 2008;105(2):751–6.
- [39] Koo JW, Duman RS. Evidence for IL-1 receptor blockade as a therapeutic strategy for the treatment of depression. *Curr Opin Investig Drugs* 2009;10(7):664–71.
- [40] Koo JW, Duman RS. Interleukin-1 receptor null mutant mice show decreased anxiety-like behavior and enhanced fear memory. *Neurosci Lett* 2009;456(1):39–43.
- [41] Goshen I, Kreisel T, Ben-Menachem-Zidon O, Licht T, Weidenfeld J, Ben-Hur T, et al. Brain interleukin-1 mediates chronic stress-induced depression in mice via adrenocortical activation and hippocampal neurogenesis suppression. *Mol Psychiatry* 2008;13(7):717–28.
- [42] Jones KA, Thomsen C. The role of the innate immune system in psychiatric disorders. *Mol Cell Neurosci* 2013;53:52–62.
- [43] Rao JS, Harry GJ, Rapoport SI, Kim HW. Increased excitotoxicity and neuro-inflammatory markers in postmortem frontal cortex from bipolar disorder patients. *Mol Psychiatry* 2010;15(4):384–92.
- [44] Soderlund J, Olsson SK, Samuelsson M, Walther-Jallow L, Johansson C, Erhardt S, et al. Elevation of cerebrospinal fluid interleukin-1ss in bipolar disorder. *J Psychiatry Neurosci* 2011;36(2):114–8.
- [45] Diaz-Hernandez JI, Gomez-Villafuertes R, Leon-Otegui M, Hontecillas-Prieto L, Del Puerto A, Trejo JL, et al. In vivo P2X7 inhibition reduces amyloid plaques in

- Alzheimer's disease through GSK3beta and secretases. *Neurobiol Aging* 2012;33(8):1816–28.
- [46] Ni J, Wang P, Zhang J, Chen W, Gu L. Silencing of the P2X7 receptor enhances amyloid-beta phagocytosis by microglia. *Biochem Biophys Res Commun* 2013;434(2):363–9.
- [47] Delarasse C, Auger R, Gonnord P, Fontaine B, Kanellopoulos JM. The purinergic receptor P2X7 triggers alpha-secretase-dependent processing of the amyloid precursor protein. *J Biol Chem* 2011;286(4):2596–606.
- [48] Oyanguren-Desez O, Rodriguez-Antiguedad A, Villoslada P, Domercq M, Alberdi E, Matute C. Gain-of-function of P2X7 receptor gene variants in multiple sclerosis. *Cell Calcium* 2011;50(5):468–72.
- [49] Engel T, Gomez-Villafuertes R, Tanaka K, Mesuret G, Sanz-Rodriguez A, Garcia-Huerta P, et al. Seizure suppression and neuroprotection by targeting the purinergic P2X7 receptor during status epilepticus in mice. *FASEB J* 2012;26(4):1616–28.
- [50] Diaz-Hernandez M, Diez-Zaera M, Sanchez-Nogueiro J, Gomez-Villafuertes R, Canals JM, Alberch J, et al. Altered P2X7-receptor level and function in mouse models of Huntington's disease and therapeutic efficacy of antagonist administration. *FASEB J* 2009;23(6):1893–906.
- [51] Parvathenani LK, Tertysnikova S, Greco CR, Roberts SB, Robertson B, Posmantur R. P2X7 mediates superoxide production in primary microglia and is up-regulated in a transgenic mouse model of Alzheimer's disease. *J Biol Chem* 2003;278(15):13309–17.
- [52] Rampe D, Wang L, Ringheim GE. P2X7 receptor modulation of beta-amyloid- and LPS-induced cytokine secretion from human macrophages and microglia. *J Neuroimmunol* 2004;147(1–2):56–61.
- [53] Sanz JM, Chiozzi P, Ferrari D, Colaianna M, Idzko M, Falzoni S, et al. Activation of microglia by amyloid beta requires P2X7 receptor expression. *J Immunol* 2009;182(7):4378–85.
- [54] McLarnon JG, Ryu JK, Walker DG, Choi HB. Upregulated expression of purinergic P2X(7) receptor in Alzheimer disease and amyloid-beta peptide-treated microglia and in peptide-injected rat hippocampus. *J Neuropathol Exp Neurol* 2006;65(11):1090–7.
- [55] Matute C, Torre I, Perez-Cerda F, Perez-Samartin A, Alberdi E, Etxebarria E, et al. P2X₇ receptor blockade prevents ATP excitotoxicity in oligodendrocytes and ameliorates experimental autoimmune encephalomyelitis. *J Neurosci* 2007;27(35):9525–33.
- [56] Abourbeh G, Theze B, Maroy R, Dubois A, Brulon V, Fontyn Y, et al. Imaging microglial/macrophage activation in spinal cords of experimental autoimmune encephalomyelitis rats by positron emission tomography using the mitochondrial 18 kDa translocator protein radioligand [(1)(8)F]DPA-714. *J Neurosci* 2012;32(17):5728–36.
- [57] Sharp AJ, Polak PE, Simonini V, Lin SX, Richardson JC, Bongarzone ER, et al. P2x7 deficiency suppresses development of experimental autoimmune encephalomyelitis. *J Neuroinflammation* 2008;5(1):33.
- [58] Donnelly-Roberts DL, Jarvis MF. Discovery of P2X7 receptor-selective antagonists offers new insights into P2X7 receptor function and indicates a role in chronic pain states. *Br J Pharmacol* 2007;151(5):571–9.
- [59] Chessell IP, Hatcher JP, Bountra C, Michel AD, Hughes JP, Green P, et al. Disruption of the P2X7 purinoceptor gene abolishes chronic inflammatory and neuropathic pain. *Pain* 2005;114(3):386–96.
- [60] Labasi JM, Petrushova N, Donovan C, McCurdy S, Lira P, Payette MM, et al. Absence of the P2X7 receptor alters leukocyte function and attenuates an inflammatory response. *J Immunol* 2002;168(12):6436–45.

- [61] Honore P, Wade CL, Zhong C, Harris RR, Wu C, Ghayur T, et al. Interleukin-1 α gene-deficient mice show reduced nociceptive sensitivity in models of inflammatory and neuropathic pain but not post-operative pain. *Behav Brain Res* 2006;167(2):355–64.
- [62] Abdi MH, Beswick PJ, Billinton A, Chambers LJ, Charlton A, Collins SD, et al. Discovery and structure–activity relationships of a series of pyroglutamic acid amide antagonists of the P2X7 receptor. *Bioorg Med Chem Lett* 2010;20:5080–4.
- [63] Chambers LJ, Stevens AJ, Moses AP, Michel AD, Walter DS, Davies DJ, et al. Synthesis and structure–activity relationships of a series of (1H-pyrazol-4-yl)acetamide antagonists of the P2X7 receptor. *Bioorg Med Chem Lett* 2010;20:3161–4.
- [64] Abberley L, Bebius A, Beswick PJ, Billinton A, Collis KL, Dean DK, et al. Identification of 2-oxo-N-(phenylmethyl)-4-imidazolidinecarboxamide antagonists of the P2X(7) receptor. *Bioorg Med Chem Lett* 2010;20(22):6370–4.
- [65] Ali Z, Laurijssens B, Ostenfeld T, McHugh S, Stylianou A, Scott-Stevens P, et al. Pharmacokinetic and pharmacodynamic profiling of a P2X7 receptor allosteric modulator GSK1482160 in healthy human subjects. *Br J Clin Pharmacol* 2012;75:197–207.
- [66] Stock TC, Bloom BJ, Wei N, Ishaq S, Park W, Wang X, et al. Efficacy and safety of CE-224,535, an antagonist of P2X7 Receptor, in treatment of patients with rheumatoid arthritis inadequately controlled by methotrexate. *J Rheumatol* 2012;39(4):720–7.
- [67] Keystone EC, Wang MM, Layton M, Hollis S, McInnes IB. Clinical evaluation of the efficacy of the P2X7 purinergic receptor antagonist AZD9056 on the signs and symptoms of rheumatoid arthritis in patients with active disease despite treatment with methotrexate or sulphasalazine. *Ann Rheum Dis* 2012;71:1630–5.
- [68] Inoue K, Tsuda M. Purinergic systems, neuropathic pain and the role of microglia. *Exp Neurol* 2012;234(2):293–301.
- [69] Clark AK, Staniland AA, Marchand F, Kaan TK, McMahan SB, Malcangio M. P2X7-dependent release of interleukin-1 β and nociception in the spinal cord following lipopolysaccharide. *J Neurosci* 2010;30(2):573–82.
- [70] Brumfield S, Matasi JJ, Tulshian D, Czarniecki M, Greenlee W, Garlisi C, et al. Synthesis and SAR development of novel P2X7 receptor antagonists for the treatment of pain: part 2. *Bioorg Med Chem Lett* 2011;21(24):7287–90.
- [71] Matasi JJ, Brumfield S, Tulshian D, Czarniecki M, Greenlee W, Garlisi CG, et al. Synthesis and SAR development of novel P2X7 receptor antagonists for the treatment of pain: part 1. *Bioorg Med Chem Lett* 2011;21(12):3805–8.
- [72] Michel AD, Walter DS, inventors; Glaxo Group Limited, assignee. Combinations of prolinamide P2X7 modulators with further therapeutic agents. Patent WO 2009074518A1; 2009.
- [73] Chambers LJ, Gleave R, Senger S, Walter DS, inventors; Glaxo Group Limited, assignee. Preparation of N-(phenylmethyl)-5-oxoprolinamides derivatives as P2X7 antagonists for the treatment of pain, inflammation and neurodegeneration. Patent WO 2008003697A1; 2008.
- [74] Beswick PJ, Billinton A, Chambers LJ, Dean DK, Fonfria E, Gleave RJ, et al. Structure–activity relationships and in vivo activity of (1H-pyrazol-4-yl)acetamide antagonists of the P2X7 receptor. *Bioorg Med Chem Lett* 2010;20:4653–6.
- [75] Sluyter R, Shemon A, Wiley J. Glu496 to Ala polymorphism in the P2X7 receptor impairs ATP-induced IL1 β release from human monocytes. *J Immunol* 2004;172:3399–405.
- [76] Stock T, Bloom BJ, Wang X, Gupta P, Mebus C. European League Against Rheumatism, Rome, Italy, June 16–19; 2010.
- [77] Duplantier AJ, Dombroski MA, Subramanyam C, Beaulieu AM, Chang S-P, Gabel CA. Optimization of the physicochemical and pharmacokinetic attributes in

- a 6-azauracil series of P2X7 receptor antagonists leading to the discovery of the clinical candidate CE-224,535. *Bioorg Med Chem Lett* 2011;21:3708–11.
- [78] Evotec. Evotec development partnerships, http://evotec.com/article/en/Alliances-Projects/EVT401-P2X7-Antagonists/67/4?selected_category_id=6.
- [79] Biopharmaceutiques clinical studies archives, http://www.biopharmaceutiques.com/en/article/113_1981.html>.
- [80] Guile SD, Alcaraz L, Birkinshaw TN, Bowers KC, Ebden MR, Furber M, et al. Antagonists of the P2X(7) receptor. From lead identification to drug development. *J Med Chem* 2009;52(10):3123–41.
- [81] Michel AD, Walter DS, inventors; Glaxo Group Limited, assignee. Combinations of pyrazolyl or isoxazolyl P2X7 modulators with further therapeutic agents. Patent WO 2009074519A1; 2009.
- [82] Beswick PJ, Chambers LJ, Davies DJ, Dean DK, Demont EM, Roomans S, et al., inventors; Glaxo Group Limited, assignee. N-(phenylmethyl)-2-(1H-pyrazol-4-yl) Acetamide derivatives as P2X7 antagonists for the treatment of pain, inflammation and neurodegeneration. Patent WO 2007141267A1; 2007.
- [83] Abad-Zapatero C. Ligand efficiency indices for effective drug discovery. *Expert Opin Drug Discov* 2007;2(4):469–88.
- [84] Gleave RJ, Walter DS, Beswick PJ, Fonfria E, Michel AD, Roman SA, et al. Synthesis and biological activity of a series of tetrasubstituted-imidazoles as P2X7 antagonists. *Bioorg Med Chem Lett* 2010;20:4951–4.
- [85] Chambers L, Gleave R, Senger S, Walter DS, inventors; Glaxo Group Limited, assignee. Novel receptor antagonists and their methods of use. US patent 20080009541A1; 2009.
- [86] Walter DS, inventor; Glaxo Group Limited, assignee. Isothiazolidine 1,1-dioxide and tetrahydro-2H-1,2-thiazine 1,1-dioxide derivatives as P2X7 modulators. Patent WO 2009077362A1; 2009.
- [87] Steadman JGA, Walter DS, inventors; Glaxo Group Limited, assignee. 5-Oxo-3-pyrrolidinecarboxamide derivatives as P2X7 modulators. Patent WO 2009077559A2; 2009.
- [88] Dean DK, Walter DS, inventors; Glaxo Group Limited, assignee. Thiazolidinedioxide P2X7 receptor antagonists. Patent WO 2011054947A1; 2011.
- [89] Chambers LJ, Collis KL, Dean DK, Munoz-Muriedas J, Steadman JGA, inventors; Glaxo Group Limited, assignee. 4-Benzoyl-1-substituted-piperazine-2-one derivatives as P2X7 modulators. Patent WO 2009053459A1; 2009.
- [90] Chambers LJ, Dean DK, Munoz-Muriedas J, Steadman JGA, Walter DS, inventors; Glaxo Group Limited, assignee. Diketopiperazine derivatives as P2X7 modulators. Patent WO 2010125103A1; 2010.
- [91] Berger J, Caroon JM, Lopez-Tapia FJ, Nitzan D, Walker KAM, Zhao S-H, inventors; Roche Palo Alto LLC, assignee. Dihydropyridone amides as P2X7 modulators. US patent 20100160389A1; 2010.
- [92] Berger J, Brotherton-Pleiss CE, Lopez-Tapia FJ, Walker KAM, Zhao S-H, inventors; Roche Palo Alto LLC, assignee. Dihydropyridone amides as P2X7 modulators. US patent 20100160384A1; 2010.
- [93] Berger J, Caroon JM, Krauss NE, Walker KAM, Zhao S-H, Lopez-Tapia FJ, inventors; Roche Palo Alto LLC, assignee. Dihydropyridone amides as P2X7 modulators. US patent 20100160373A1; 2010.
- [94] Brotherton-Pleiss CE, Caroon JM, Lopez-Tapia FJ, inventors; Roche Palo Alto LLC, assignee. Dihydropyridone ureas as P2X7 modulators. US patent 20100160388A1; 2010.
- [95] Lopez-Tapia FJ, Walker KAM, Zhao S-H, inventors; Roche Palo Alto LLC, assignee. Dihydropyridone amides as P2X7 modulators. US patent 20100160387A1; 2010.
- [96] Brotherton-Pleiss CE, Caroon JM, Lopez-Tapia FJ, Walker KAM, inventors; F. Hoffmann-La Roche AG, assignee. Dihydropyridone ureas as P2X7 modulators. Patent WO 2011012592A1; 2011.

- [97] Huang X, Broadbent S, Dvorak C, Zhao S-H. Pilot-Plant Preparation of 3,4-Dihydropyridin-2-one derivatives, the core structures of P2X7 receptor antagonists. *Org Process Res Dev* 2010;14:612–6.
- [98] Shigeta Y, Hirokawa Y, Nagai H, Nagae K, Watanabe T, Io M, et al., inventors; Nissan Chemical Industries Ltd., assignee. Pyridazinone derivatives as P2X7 receptor inhibitors and their preparation, pharmaceutical compositions and use in the treatment of rheumatoid arthritis. Patent WO 2009057827A1; 2009.
- [99] Io M, Shintani Y, Shigeta Y, Kamon J, inventors; Nissan Chemical Industries Ltd., assignee. Preparation of 4-substituted pyridazinone compounds as P2X7 receptor inhibitors. Patent WO 2010126104A1; 2010.
- [100] Hilpert K, Hubler F, Murphy M, Renneberg D, inventors; Actelion Pharmaceuticals Ltd., assignee. Benzamide derivatives as P2X7 preceptor antagonists. Patent WO 2012114268A1; 2012.
- [101] Li H, Yuan J, Bakthavatchalam R, Hodgetts KJ, Capitosti SM, Mao J, et al., inventors; Neurogen Corporation, assignee. Preparation of 5-membered heterocyclic amides and related compounds as specific receptor activity modulators. Patent WO 2009012482A2; 2009.
- [102] Bos M, inventor; Affectis Pharmaceuticals AG, assignee. Novel P2X₇ antagonists and their use. Patent WO 2009118175A1; 2009.
- [103] Bos M, inventor; Affectis Pharmaceuticals AG, assignee. Novel P2X₇ antagonists and their use. Patent WO 2010118921A1; 2010.
- [104] Bos M, inventor; Affectis Pharmaceuticals AG, assignee. Novel methods for the preparation of P2X₇ antagonists. Patent WO 2011141194A1; 2011.
- [105] Boes M, inventor; Affectis Pharmaceuticals AG, assignee. Novel P2X₇ antagonists and their use. Patent WO 2012163456A1; 2012.
- [106] Boes M, inventor; Affectis Pharmaceuticals AG, assignee. Novel P2X₇ antagonists and their use. Patent WO 2012163792A1; 2012.
- [107] Affectis. Affectis News and Events. Affectis granted patent for AFC-5128, other P2X7 antagonists http://www.affectis.com/attachments/035_Press%20Release%20Affectis_EP%20patent%20AFC-5128%2020120125.pdf.
- [108] Bakthavatchalam R, Ihle DC, Capitosti SM, Trow DJ, Yuan J, inventors; Neurogen Corporation, assignee, Heteroaryl amide analogues. International Patent 2009023623 A1; 2009.
- [109] Bakthavatchalam R, Ihle DC, Capitosti SM, Trow DJ, Yuan J, inventors; H. Lundbeck A/S, assignee, Heteroaryl amide analogues. Patent WO 2009108551A2; 2009.
- [110] Dean DK, Munoz-Muriedas J, Sime M, Steadman JGA, Thewlis REA, Trani C, et al., inventors; Glaxo Group Limited, assignee, 5,6,7,8-Tetrahydroimidazo[1,2-a]pyrazine derivatives as P2X₇ Modulators. Patent WO 2010125101; 2010.
- [111] Dean DK, Munoz-Muriedas J, Sime M, Steadman JGA, Thewlis REA, Trani C, et al., inventors; Glaxo Group Limited, assignee, 5,6,7,8-Tetrahydro[1,2,4]triazolo[4,3-a]pyrazine derivatives as P2X₇ Modulators. Patent WO 2010125102 A1; 2010.
- [112] Brotherton-Pleiss C, Harris RN III, Loe BE, Lopez-Tapia FJ, Rege PD, Repke DB, et al., inventors; F. Hoffman-La Roche AG, assignee. Fused triazole amines as P2X₇ modulators. Patent WO patent 2011033055 A1; 2011.
- [113] Labroli M, Czarniecki MF, Poker CS, inventors; Schering Corporation, assignee. Triazolopyrazinones as P2X₇ receptor antagonists. Patent WO 2012040048 A2; 2010.
- [114] Love CJ, Leenaerts JE, Coymans LP, Lebsack AD, Branstetter BJ, Rech JC, inventors; Janssen Pharmaceuticals, assignee. Quinoline or isoquinoline substituted P2X₇ antagonists. Patent WO 2009132000 A1; 2009.
- [115] Perez-Medrano A, Donnelly-Roberts DL, Honore P, Hsieh GC, Namovic MT, Peddi S, et al. Discovery and biological evaluation of novel cyanoguanidine P2X₇ antagonists with analgesic activity in a rat model of neuropathic pain. *J Med Chem* 2009;52:3366–76.

- [116] Donnelly-Roberts DL, Namovic MT, Surber B, Vaidyanathan SX, Perez-Medrano A, Wang Y, et al. [3H]A-804598 ([3H]2-cyano-1-[(1S)-1-phenylethyl]-3-quinolin-5-ylguanidine) is a novel, potent, and selective antagonist radioligand for P2X₇ receptors. *Neuropharmacology* 2009;56:223–9.
- [117] Letavic MA, Lord B, Bischoff F, Hawryluk HA, Pieters S, Rech JC, et al. Synthesis and pharmacological characterization of two novel, brain penetrating P2X₇ antagonists. *ACS Med Chem Lett* 2013;4:419–22.
- [118] Able SL, Fish RL, Bye H, Logan YR, Nathaniel C, Hayter P, et al. Receptor localization, native tissue binding and ex vivo occupancy for centrally penetrant P2X₇ antagonists in the rat. *Br J Pharmacol* 2011;162:405–14.
- [119] Chen X, Pierce B, Naing W, Grapperhaus ML, Phillion DP. Discovery of 2-chloro-N-((4,4-difluoro-1-hydroxycyclohexyl)methyl)-5-(5-fluoropyrimidinyl-2-yl)benzamide as a potent and CNS penetrable P2X₇ antagonist. *Bioorg Med Chem Lett* 2010;20:3107–11.
- [120] Subramanyam C, Duplantier AJ, Combroski MA, Chang S-P, Gabel CA, Whintey-Pickett C, et al. Discovery, synthesis and SAR of azinyl- and azolylbenzamides antagonists of the P2X₇ receptor. *Bioorg Med Chem Lett* 2011;21:5475–9.



γ -Secretase Modulators: Current Status and Future Directions

Adrian Hall^{*}, Toshal R. Patel[†]

^{*}Department of Chemistry, Discovery Research, Neuroscience and General Medicine Product Creation Unit, Eisai Ltd., EMEA Knowledge Centre, Mosquito Way, Hatfield, United Kingdom

[†]Department of BioPharmacology, Discovery Research, Neuroscience and General Medicine Product Creation Unit, Eisai Ltd., EMEA Knowledge Centre, Mosquito Way, Hatfield, United Kingdom

Contents

1. Introduction	101
1.1 Alzheimer's Disease	101
1.2 γ -Secretase Biology	102
2. GSMs: Chemical Classes	104
2.1 Acid Derivatives	104
2.2 Imidazoles and Related Analogues	111
2.3 Natural Products	129
3. Chemical Biology	132
4. Outlook	135
5. Clinical Studies	137
6. Conclusions	139
References	140

Keywords: Alzheimer's disease, γ -Secretase, γ -Secretase modulators, γ -Secretase inhibitors



1. INTRODUCTION

1.1. Alzheimer's Disease

Alzheimer's disease (AD) is a progressive, neurodegenerative disease of unknown cause and is the most common form of dementia among older people. An estimated 11% of people over the age of 65 and a third of those over age 85 have AD [1]. More than 5 million people in the United States and more than 15 million people worldwide currently suffer from the disease, with numbers expected to increase with ageing populations [1].

The hallmark of AD is the degeneration and loss of neurons in cortical and subcortical regions, associated with the formation of senile plaques and neurofibrillary tangles. Currently, only the symptoms of Alzheimer's disease are treated using agents typified by acetylcholinesterase inhibitors (donepezil, galantamine or rivastigmine) or glutamate antagonists (memantine). These therapeutics improve the symptoms of AD, noticeably in those where declining cognitive function affects the activities of daily living and behaviour, but do not alter the underlying pathology of the disease. The search for a therapeutic that can stem the progression of the disease, or a method for controlling the causative pathology of Alzheimer's disease, is an area of focus by a number of pharmaceutical and biotechnology companies.

The plaques and tangles associated with AD pathology have been identified as containing β -amyloid ($A\beta$) and tau proteins, respectively. It is believed that $A\beta$ -proteins, as proteolytic degradants of amyloid precursor protein (APP), are critical to the degeneration and loss of neurons and the onset of symptoms of dementia. APP is processed in a two-step proteolytic process. The primary cleavage of APP is performed by β -secretase which results in soluble β -APP and a membrane-bound C-99 fragment. This C-99 fragment serves as a substrate for a secondary cleavage performed by γ -secretase. The result of the secondary cleavage is an APP intracellular domain and fragments of $A\beta$ with varying lengths of amino acids including peptides of 40 ($A\beta_{40}$) and 42 ($A\beta_{42}$) amino acids. The $A\beta_{40}$ and $A\beta_{42}$ proteins are known to be highly prone to aggregation and to be the main components of the senile plaques linked to AD [2].

1.2. γ -Secretase Biology

γ -Secretase is a member of the aspartyl protease family of enzymes and consists of multiple units. The mechanism of action of γ -secretase is thought to be via an intramembrane proteolysis at specific transmembrane residues. One of the hallmarks of γ -secretase is that it targets multiple substrates in addition to APP, including Notch, Jagged and other cell proliferation proteins. The γ -secretase complex consists of four main components: anterior pharynx-defective 1, presenilin enhancer protein-2, presenilin and nicastrin, with presenilin constituting the protease catalytic subunit [3]. There are two types of presenilin (PS-1 and -2) both of which are encoded on human chromosome 14. The four protein components exist as a monomeric complex which uses water to hydrolyse substrates. Initial structural identification

has been performed using transmission electron microscopy, however, as yet no detailed NMR or X-ray crystal structure has been elucidated [4,5].

A number of mutations have been identified in APP that lead to early onset of familial forms of AD. The common thread between the various mutations is the resultant increased production of the $A\beta_{42}$ peptide which is more prone to aggregation than $A\beta_{40}$. The amyloid hypothesis proposes that the processing of APP to form amyloid peptides is the central component of the aetiology and pathophysiology of AD. In support of this, mutations have been identified in presenilin-1 and -2 which lead to increased $A\beta$ production and increases in the ratio of $A\beta_{42}:A\beta_{40}$. In addition, mutations have been identified on APP, proximal to the β -secretase cleavage site, which lead to either increased (A673V) or decreased (A673T) amyloid (both $A\beta_{x-40}$ and $A\beta_{x-42}$) production and correlate with increased or decreased risk of developing AD, respectively [6].

Recent findings have implicated $A\beta_{42}$ as a potential causative agent in AD and have suggested that reducing $A\beta$ levels in the brain, in particular $A\beta_{42}$ levels, is a viable therapeutic strategy for the treatment of AD. One major therapeutic approach, based on the amyloid hypothesis, has been the development of γ -secretase inhibitors. A review of the status of the main γ -secretase inhibitors has been previously published by Oehlrich and colleagues [7]. A number of γ -secretase inhibitors have advanced into Phase II and Phase III clinical trials; Lilly (Semagacestat/LY 450149), Elan (ELND006), Bristol Myers Squibb (Avagacestat/BMS 708163) and Wyeth (Begacestat/GSI-953) have all terminated clinical trials with their respective agents [8–11]. The reasons for termination were varied with liver toxicity, gastrointestinal (GI) effects, dermatological effects and absence of an effect on cognition amongst those described [8–10].

The termination of these trials has been a setback to the continued targeting of the amyloid hypothesis. Adverse events have been related to the possible non-selective nature of these inhibitors and this has focussed efforts on the identification of γ -secretase modulators (GSMs) which may offer selective targeting of amyloid cleavage over other substrates, such as Notch. Their mode of action is thought to be via modulation of the proteolytic activity of the enzyme complex leading to either the production of shorter length $A\beta$ peptides, which would have lower propensity to aggregate, or to compounds that are termed 'Notch-sparing' as they prevent the processing of APP to $A\beta$ peptides but do not have any effect on the activity towards Notch [12]. In addition, various modes of action are possible,

such as selective lowering of $A\beta_{42}$, or simultaneous lowering of $A\beta_{42}$ and $A\beta_{40}$, which can force scientists to make a strategic decision about which may be the main pathogens. In addition to this, the levels of shorter amyloid species such as $A\beta_{37}$ and $A\beta_{38}$ are increased, which again forces questions about the functional importance and potential adverse consequences due to increased levels of these lesser studied peptides.

The current chapter provides an overview of recent progress in the development of GSMs, focussing mainly on the peer reviewed literature, but drawing on the patent literature where necessary. In addition, this summary does not seek to recapitulate everything that has been covered recently in three excellent review articles [7,13,14] but offers some context to the data and studies that have been published and summarises the authors' opinions on the current state of research in the field.



2. GSMs: CHEMICAL CLASSES

The search for GSMs has led to the identification of multiple pharmacophores that have formed the basis of medicinal chemistry efforts to identify potent and safe molecules. A discussion of the characteristics of the compounds is described below.

For the purposes of this chapter, unless otherwise stated, cLogP values have been calculated using ChemDraw™. Note that in certain instances there is a marked difference between these and the literature values.

2.1. Acid Derivatives

2.1.1 *Myriad and Chiesi*

The original report that non-steroidal anti-inflammatory drug (NSAID) derivatives modulate γ -secretase activity [15,16] sparked numerous researchers to discover novel carboxylic acid derivatives with increased γ -secretase modulatory potency. Unsurprisingly, most of the structures of

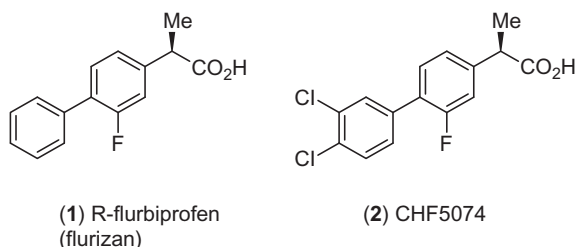


Figure 3.1 Structures of flurbiprofen and CHF5074.

the early derivatives were closely related to NSAIDs such as ibuprofen; the most prominent of these being flurbiprofen (FlurizanTM) (1) developed by Myriad [17] and CHF5074 (2) developed by Chiesi [18] (Figure 3.1). These early compounds showed weak modulatory potency *in vitro* and although pre-clinical efficacy was demonstrable, the corresponding concentrations appeared somewhat discrepant with the *in vitro* data. Furthermore, these compounds have failed to show an effect on amyloid levels in the clinic, adding credence to the scepticism over their pre-clinical efficacy.

2.1.2 Janssen

Still closely related to the NSAID class is JNJ-40418677 (3) (Figure 3.2) which was developed by Cellzome in collaboration with Janssen. This compound shows much improved potency over the above compounds with an A β_{42} IC₅₀ of 200 nM (SKNBE-2 neuroblastoma cells expressing wild-type APP, 16 h incubation) and an A β_{42} IC₅₀ of 185 nM in rat primary cortical neurons (48 h incubation) (Figure 3.2) [19]. Efficacy has been demonstrated in a range of studies. In a single time-point study (4 h post-dose) in the mouse (non-transgenic), (3) showed a dose-dependent reduction in brain A β_{42} (18%, 36%, 61% and 69% at 10, 30, 100 and 300 mg/kg, respectively, with brain being extracted using diethylamine (DEA)). In a time course study in non-transgenic mice at 30 mg/kg p.o. (3) had a maximal effect on brain amyloid 6 h post-dose. Interestingly, the T_{max} of the compound in brain was 4–8 h, thus showing a minimal PK–PD lag. Brain A β_{38} levels were increased, in line with the *in vitro* profile. In a 7-month efficacy study in Tg2576 mice, starting from 6 months of age, doses of 60 and 120 mg/kg p.o.

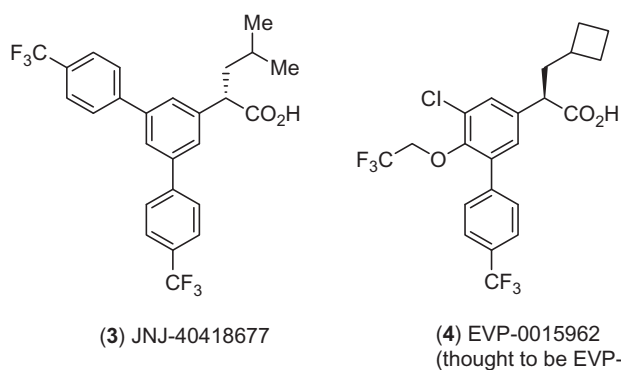


Figure 3.2 Structures of JNJ-40418677 (3) and EVP-0015962 (4) (thought to be EVP-0962).

caused a large reduction in brain $A\beta_{42}$, both soluble and deposited, 20 mg/kg did not affect $A\beta_{42}$. In contrast to the *in vitro* profile, brain $A\beta_{40}$ levels were also reduced in a similar manner including at the 20 mg/kg dose. Surprisingly, it was found that the levels of deposited $A\beta_{38}$ were decreased in brain while the levels of soluble $A\beta_{38}$ were unaffected. These results are in contrast to the *in vitro* profile where the compound shows an increase in $A\beta_{38}$. Further analysis showed a reduction in plaque burden. Although the total brain concentration (0.42, 2.4 and 12 μM after 20, 60 and 120 mg/kg, respectively) and total plasma concentration (0.38, 2.7 and 13 μM after 20, 60 and 120 mg/kg, respectively) are above the *in vitro* IC_{50} values for $A\beta_{42}$, it is unlikely that the free concentrations in either compartment would be higher than the IC_{50} and therefore sufficient to cause the observed effect. The progression of JNJ-40418677 (**3**) was halted before Phase I due to toxicological findings, mainly in the liver, which may be related to its high lipophilicity (cLogP 8.5) [20]. It is also noteworthy that this compound has (*S*)-stereochemistry at the chiral centre α to the carboxylic acid, in contrast to all other acid GSMs which have (*R*)-stereochemistry. Early research showed that the (*R*)-stereochemistry does not affect γ -secretase activity but generally abolishes cyclooxygenase (COX) activity, whereas (*S*)-stereochemistry retains COX activity. Despite having an (*S*)-stereocentre, (**3**) is reported to be inactive at both COX-1 and -2 up to and including a concentration of 60 μM .

2.1.3 *EnVivo*

The pre-clinical profile of EVP-0015962 (**4**) (Figure 3.2), thought to be the Phase II development compound EVP-0962, has recently been disclosed [21]. In a cellular assay (human neuroglioma H4 cells stably transfected with wild-type human APP751), the compound lowered $A\beta_{42}$ with an IC_{50} of 67 nM and increased $A\beta_{38}$ with an EC_{50} of 33 nM, thus making it one of the most potent acid-derived GSMs, although it is not clear from the structure how this high level of potency is gained. Cellular mass spectroscopic analysis (MALDI-TOF) revealed that $A\beta_{42}$ and $A\beta_{39}$ were decreased while $A\beta_{38}$ and $A\beta_{33}$ levels were increased. In rat primary neocortical cultures, the potency was found to be almost 10-fold lower with an $A\beta_{42}$ IC_{50} of 427 nM and an $A\beta_{38}$ EC_{50} of 384 nM. In Tg2576 mice (21 weeks old), 4 h post 30 mg/kg dose, brain $A\beta_{42}$ levels were reduced by 39% with corresponding brain concentrations of 4.3 μM ; however, the effect at 10 mg/kg was not statistically significant, despite brain levels of 1.3 μM . A follow-up 50-week study in Tg2576 mice, starting from 17 to 26 weeks of age, was conducted at doses of 20 and 60 mg/kg p.o. which resulted in corresponding brain

concentrations of 2.5 and 8.3 μM , respectively. Interestingly, the compound showed a reversal in the contextual fear conditioning model following 11 weeks treatment at 20 and 60 mg/kg in Tg2576 mice, when dosing started at 19–22 weeks of age.

In 2006, scientists at Merck disclosed a novel series of zwitterionic GSMs in which the phenyl acetic acid moiety has been replaced by a piperidin-4-yl acetic acid, such as in (5) [22] (Figure 3.3). The consequence of this is a reduction in aromaticity, increased sp^3 character and addition of a basic centre. These salient points have sparked a new area of chemical optimisation by many other companies.

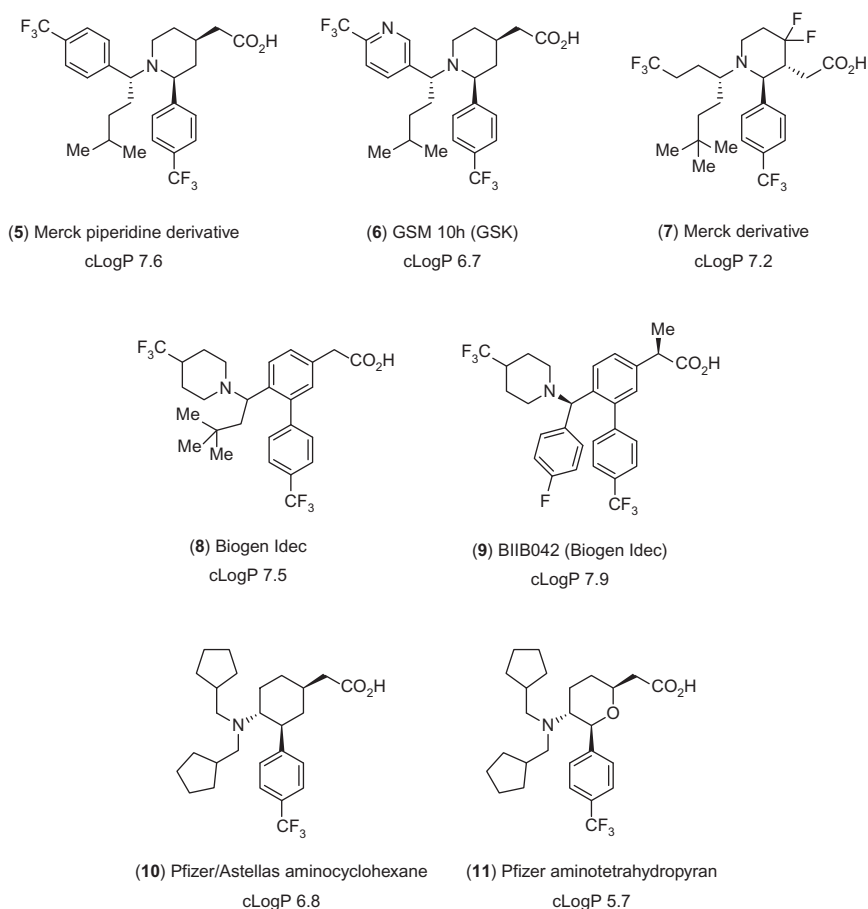


Figure 3.3 Acid derivatives from Merck, GSK, Biogen Idec and Pfizer/Astellas.

2.1.4 GSK

GSK have disclosed their investigations into related compounds, in which the goal was to incorporate heteroatoms in order to reduce lipophilicity. The best characterised compound of this series is GSM 10h (**6**) [23] (Figure 3.3). In SH-SY5Y neuroblastoma cells stably expressing human APPSwe (48 h incubation) (**6**) reduced $A\beta_{42}$ production with an IC_{50} of 300 nM and $A\beta_{40}$ with an IC_{50} of 6.3 μ M [24]. In the same assay, but using a shorter (24 h) incubation period, the compound reduced $A\beta_{42}$ production with an IC_{50} of 1 μ M and increased $A\beta_{38}$ with an EC_{50} of 500 nM [25]. In a primary rat cortical neuron assay (48 h incubation) (**6**) reduced $A\beta_{42}$ with an IC_{50} of 350 nM [24]. In a mouse central nervous system (CNS) penetration study at 5 mg/kg p.o., the compound showed good CNS penetration with concentrations of 5.6 and 4.2 μ M in brain and blood, respectively, 2 h post-dose. Pharmacokinetic (PK) parameters were evaluated in mouse, rat and dog where (**6**) displayed low blood clearance (Cl_b) values of 4 mL/min/kg (mouse and rat) and 3 mL/min/kg (dog), moderate distribution volumes (V_{dss}) values of 1.4, 2.3 and 1.1 L/kg in mouse, rat and dog, respectively, which are in excess of total body water, a moderate half-life (4.3–6.6 h) and high oral bioavailability. Profiling of (**6**) was conducted in TASTPM mice [25] and rat [24]. In an acute study in the rat at doses of 3, 10, 30 and 100 mg/kg, with sampling 6 h post-dose, (**6**) showed strong reduction of plasma and cerebrospinal fluid (CSF) $A\beta_{42}$ but weaker efficacy in brain $A\beta_{42}$ with only 21% and 30% reductions at doses of 30 and 100 mg/kg, respectively. However, it should be noted that brain amyloid was extracted with guanidine hydrochloride, which extracts both soluble and deposited amyloid. It would be expected that the compound could only reduce soluble amyloid levels which would be a small proportion of the extracted amyloid. At the 100 mg/kg dose, the brain and blood concentrations were 34 and 28 μ M, respectively. In a 5-day study, with samples taken 6 h after the final dose, a somewhat increased effect was observed in the brain, but not in plasma or CSF, with reductions of brain $A\beta_{42}$ of 38% and 48% at 30 and 100 mg/kg, respectively. However, it should be noted that the brain and plasma concentrations, at 52 and 79 μ M, respectively, were higher than in the acute study, which could account for the marginal increase in efficacy. Finally, a time course study at 30 mg/kg showed the T_{max} occurred about 3 h post-dose whereas the maximal pharmacodynamic effect occurred 6 h post-dose in all three compartments. Furthermore, after 24 h, the amyloid levels had returned to baseline and showed no rebound, unlike the effects observed with γ -secretase inhibitors.

2.1.5 Merck

Working in a related series, Merck have disclosed optimisation efforts around (5) leading to compound (7) [26] (Figure 3.3), in which the acetic acid moiety is translocated one position around the piperidine ring relative to (5). This compound shows the high tolerance of structural variation on GSM templates as not only has the acid been moved, but a trifluorophenyl ring has been replaced by a trifluoroethyl group. Compound (7) was found to exhibit moderate potency in a cellular assay with an $A\beta_{42}$ IC_{50} of 600 nM and good rodent (species not specified) PK, similar to that of (6), plasma clearance (Cl_p) = 3.8 mL/min/kg, volume of distribution (V_{dss}) = 1.9 L/kg, half life ($t_{1/2}$) = 5.1 h and oral bioavailability (F_{po}) = 160%. Again the volume of distribution and oral bioavailability are perhaps indicative of extra-hepatic recirculation. In the APP-YAC mouse, (7) demonstrated an 84% reduction of brain $A\beta_{42}$ (10 mg/kg, p.o.) 7 h post-dose, with corresponding brain and plasma concentrations of 0.58 and 1.1 μ M, respectively. In a follow-up dose-response study (1, 3, 10 and 30 mg/kg), the calculated ED_{50} was 5 mg/kg, the brain EC_{50} was calculated to be 1 μ M and the plasma EC_{50} 3.7 μ M. It was also noted that (7) showed no Notch effects in a 7-day rat study at doses of up to 250 mg/kg; however, no mention was made about effects in the liver.

2.1.6 Biogen Idec

Biogen Idec has recently described the research efforts which led to the identification of the clinical candidate BIIB042 (9) [27] (Figure 3.3). In a preliminary disclosure, the group described the identification of phenylacetic acid (8) (Figure 3.3), which is structurally related to (5), except that the piperidine has been exchanged with one of the phenyl rings [28]. Compound (8) reduced $A\beta_{42}$ in CHO cells expressing V717F APP with an IC_{50} of 630 nM. In a single-dose study in the mouse at 30 mg/kg, brain amyloid was reduced by 50% 4 h post-dose, with corresponding brain and plasma concentrations of 32 and 37 μ M, respectively. Pharmacokinetic assessment in rat and dog revealed very low clearances of 2.5 and 0.6 mL/min/kg, respectively. In follow-up work, the same group identified the development compound (9) [27] (Figure 3.3). In CHO cells expressing V717F APP, (9) reduced $A\beta_{42}$ with an IC_{50} of 170 nM, while showing no effect on $A\beta_{40}$ and increasing $A\beta_{38}$ with an EC_{50} of 150 nM, while in human H4 cells, which express wild-type APP, the calculated $A\beta_{42}$ IC_{50} was 70 nM. In non-transgenic (CF-1) mouse at a dose of 10 mg/kg (9) reduced brain $A\beta_{42}$ by 40% 4 h post-dose. Bioanalysis indicated good brain (4.6 μ M) and plasma

(10 μM) exposure. In Fischer rats (**9**) reduced brain $\text{A}\beta_{42}$ by 30% 4 h post-dose, while in the monkey it reduced plasma $\text{A}\beta_{42}$ by 30% 5 h post-dose, with both species receiving an oral dose of 10 mg/kg. Compound (**9**) had low Cl_p values of 1.5 and 3.7 mL/min/kg in rat and monkey, respectively, but showed moderate Cl_p in the dog (14 mL/min/kg). The V_{ss} was around total body water in rat (0.8 L/kg) and in dog (0.9 L/kg) but was higher in monkey (1.7 L/kg). These parameters were associated with long half-lives in the rat (7.2 h) and monkey (11.2 h), but a shorter half-life in the dog (1.3 h). As a result, bioavailability was good in both rat and dog (44–47%) and high in the monkey (106%). Further profiling revealed CYP450 IC_{50} values $>35 \mu\text{M}$ and weak hERG inhibition with an IC_{50} of 15 μM . However, these off-target effects need to be put into context as the *in vivo* efficacy concentrations are approximately 10 μM , although plasma protein binding (ppb) is very high with $<0.1\%$ free across species. Based on these data (**9**) was advanced into pre-clinical development; however, it is assumed that progression has been terminated as the compound has not appeared in Biogen Idec's published pipeline.

2.1.7 Pfizer/Astellas

A recent patent application from Pfizer [29] has detailed related to aminocyclohexane derivatives such as (**10**), which has an $\text{A}\beta_{42}$ IC_{50} of 229 nM, and aminotetrahydropyran derivative (**11**), with an $\text{A}\beta_{42}$ IC_{50} of 357 nM (Figure 3.3). This latter compound represents one of the least lipophilic derivatives in the acid series. Closely related compounds, including (**10**) have also recently been disclosed by Astellas [30]. In this publication (**10**) was reported to reduce hippocampal $\text{A}\beta_{42}$ in mouse in a dose-dependent manner with 25%, 45% and 61% reductions at doses of 3, 10 and 30 mg/kg, respectively.

2.1.8 Summary

Despite extensive research for a sustained period, few derivatives from the acid series of modulators have entered clinical development, although several publications describe potential development candidates. Only EnVivo and Chiesi have managed to advance a compound through the clinical phases, compound (**2**) has since failed to show efficacy on its primary biomarkers and (**3**) is the sole remaining hope to modulate amyloid levels in humans from this acid class.

It is clear from the literature that scientists have struggled to contain lipophilicity in this series, and to balance this with potency, which with

the exception of (3) appears limited. Many of the interactions seem somewhat non-specific. There is a wide tolerance of lipophilic groups and large structural changes lead to only moderate increases or decreases in potency. Furthermore, although the total plasma and brain concentrations are considerably in excess of the *in vitro* IC₅₀ values when *in vivo* efficacy is observed, the free concentrations are certainly not, and most compounds have very low unbound concentrations, typically less than 0.5%. For example, in the case of BIIB042 (9) less than 0.1% is free in plasma, and for GSM 10 h (6) 0.5% is free in blood and 0.2% free in brain tissue. Thus, there is no correlation with either total or free concentrations and efficacy. In addition, while compounds from this series demonstrate very good pharmacokinetic parameters and yield very high *in vivo* concentrations, this may be a consequence of high ppb, which may also result in consequences in safety studies. Thus, it appears that the chances of a compound from this class being able to balance efficacy and safety and make it to the market are limited.

2.2. Imidazoles and Related Analogues

Research on this chemotype of GSMs was pioneered by TorreyPines Therapeutics and Eisai. An Eisai patent application published in 2005 [31] has seeded an entire field of research. Although Eisai has not yet disclosed the structures of the Phase I GSMs E2012 and E2212, it is widely accepted in the literature that the structure of E2012 is represented by (12), while others have speculated that the structure of E2212 is that represented by (13) [32,33], (Figure 3.4). The pharmacophore of this series is exemplified by (12) and consists of a hydrogen bond acceptor (HBA) on the left-hand side (imidazole), a HBA in the central region, fulfilled by the amide and a lipophilic/aromatic moiety on the right-hand side. In addition, the methoxy group and the methyl group on the imidazole tend to increase potency slightly, presumably by forming lipophilic interactions and/or by subtly modulating the HBA strength of the imidazole.

2.2.1 TorreyPines

TorreyPines Therapeutics recently disclosed their work, in which (14) (Figure 3.4) was identified from an 80,000 compound HTS follow up and was found to reduce A β ₄₂ in SH-SY5Y neuroblastoma cells stably over-expressing human APP751 with an IC₅₀ of 1512 nM [34]. Optimisation of (14) led to (15) (Figure 3.4). Profiling in a range of cellular assays revealed (15) to be a potent modulator. In SH-SY5Y cells (15) had an IC₅₀ of 10 nM, whereas in mixed brain cultures from Tg2576 mice (15) displayed an A β ₄₂

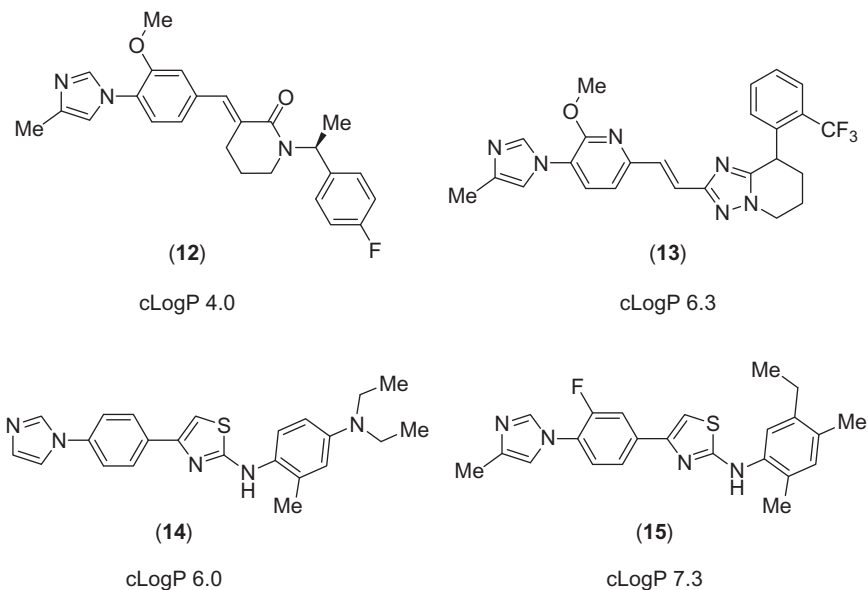


Figure 3.4 Literature consensus of the structures of E2012 (**12**) and E2212 (**13**), and compounds (**14**) and (**15**) from TorreyPines Therapeutics.

IC₅₀ of 29 nM, an Aβ₄₀ IC₅₀ of 90 nM and an Aβ₃₈ EC₅₀ of 170 nM. Slightly weaker activity was observed in a HeLa cell membrane assay (Aβ₄₂ IC₅₀ = 131 nM, Aβ₄₀ IC₅₀ = 531 nM). Dosing to female C57BL/6 mice, 2–3 months of age with 50 mg/kg for 3 days showed that the compound penetrated the CNS, with a brain to plasma ratio (Br:Pl) of 0.93. Dosing for 3 days to Tg2576 mice, 3–4 months of age, at 12.5, 25, 50 and 100 mg/kg showed a large reduction of plasma Aβ₄₂ at all doses, but only moderate, approximately 30% and 40%, reductions in brain Aβ₄₂, at the two highest doses, despite high total brain concentrations of approximately 12 and 27 nmol/g, respectively. A subsequent study investigated a dose of approximately 50 mg/kg/day p.o. for a period of 7 months to 8-month-old (pre-plaque bearing) Tg3576 mice. There were no observed GI abnormalities or changes in bodyweight gain relative to vehicle-treated animals. GI changes are a hallmark of GSI treatment, whereas decreased bodyweight gain has been observed with some GSIs. Upon completion of the study, the brains were serially extracted with DEA, sodium dodecyl sulfate (SDS) and then formic acid, to allow quantitation of the effects on soluble and total amyloid pools. Surprisingly, Aβ₃₈ levels were reduced to a similar level to Aβ₄₀ and Aβ₄₂, in contrast to the *in vitro* profile. Thus, reductions in

DEA-extracted amyloid levels were 76%, 73% and 76% for $A\beta_{38}$, $A\beta_{40}$ and $A\beta_{42}$, respectively, while formic acid extraction revealed reductions of 45%, 48% and 55%, respectively. In concordance with these data, the compound reduced plaque area in the cortex and hippocampus relative to vehicle-treated control. Despite having an encouraging profile, no further characterisation or development of this compound or related derivatives has been reported.

2.2.2 GSK

In addition to divulging medicinal chemistry and pharmacological characterisation of selective $A\beta_{42}$ modulators from the carboxylic acid series, GSK has recently disclosed work on non-acid imidazole derivatives. The first paper [35] detailed compounds such as (16) ($A\beta_{42}$ IC_{50} = 60 nM, $A\beta_{40}$ IC_{50} = 200 nM) and the optimised derivative (17) ($A\beta_{42}$ IC_{50} = 60 nM, $A\beta_{40}$ IC_{50} = 200 nM) (Figure 3.5). Assessment of the rat pharmacokinetics of (17) showed a low Cl_b (5.1 mL/min/kg), a moderate V_{dss} (1.4 L/kg), a half-life of 3.1 h and excellent oral bioavailability (98%) when dosed as the HCl salt in 1% methylcellulose. Administration of a 30 mg/kg oral dose to rats revealed a high blood and brain exposure 5 h post-dose, 16 and 9 μ M, respectively. This compound was also specifically claimed in a patent application [36].

A subsequent paper [37] detailed replacements of the central pyridazine group and showed that a range of nitrogen-containing six-membered rings were tolerated including compound (18) ($A\beta_{42}$ IC_{50} = 126 nM, $A\beta_{40}$ IC_{50} = 794 nM) (Figure 3.5). This compound also demonstrated good

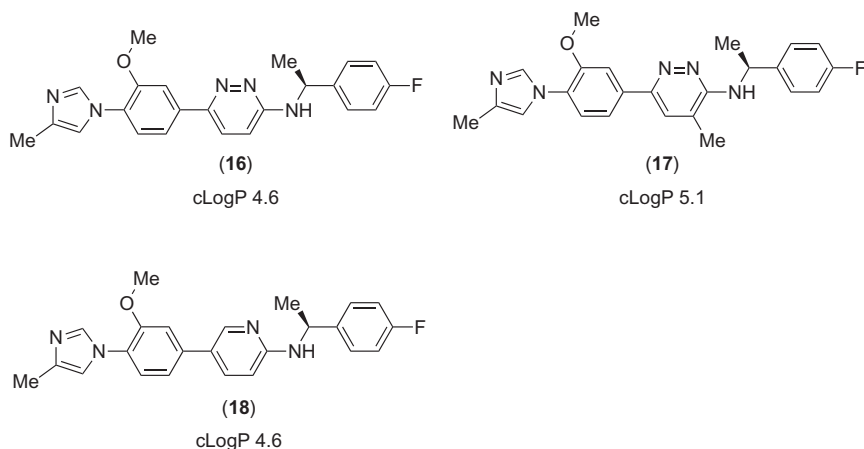


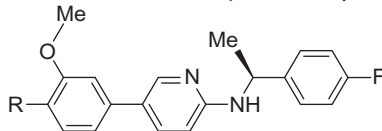
Figure 3.5 GSK heterocyclic derivatives.

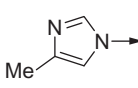
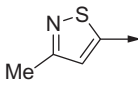
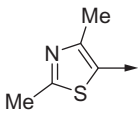
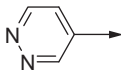
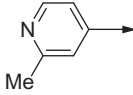
pharmacokinetic parameters in the rat ($Cl_b = 12.2$ mL/min/kg, $V_{dss} = 3.7$ L/kg, $t_{1/2} = 3.3$ h, oral bioavailability (F_{po}) 100% as the HCl salt administered in 1% methylcellulose). Using the same CNS penetration study design as for compound (17), (18) showed good concentration in blood and brain, 5 and 8.7 μ M, respectively, with an apparent increase in CNS penetration, (Br:Bl = 1.74 cf (17) Br:Bl = 0.49). Further characterisation of (17) and (18) (also known respectively as GSM-C and GSM-D) has recently been published [38]. The *in vitro* activity was confirmed in rat primary cortical neurons (48 h incubation) where (17) showed an $A\beta_{42}$ IC_{50} of 100 nM and an $A\beta_{40}$ IC_{50} of 63 nM. (18) showed similar $A\beta_{42}$ activity ($IC_{50} = 63$ nM), but a weaker effect on $A\beta_{40}$ (IC_{50} 398 nM). The modulatory profile of both compounds was confirmed by spectroscopy (LC-MS/MS) which showed relative increases in $A\beta_{37}$ and $A\beta_{38}$ concentrations. Both compounds were found to have high brain tissue binding (btb) and ppb with (17) showing ppb of 99.07% (Fraction unbound (F_u) = 0.0093) and btb of 99.21% ($F_u = 0.0079$) while (18) gave a ppb of 99.85% ($F_u = 0.0015$) and a btb of 99.89% ($F_u = 0.0011$). Correction of the total Br:Bl ratios above results in unbound concentration $Br_u:Bl_u$ values of 0.41 and 1.10 for (17) and (18), respectively. Dosing *in vivo* revealed much better efficacy for (17) than for (18). In an acute study at doses of 3, 10, 30 and 100 mg/kg, with sampling 6 h post-dose, (17) demonstrated a dose-dependent reduction in amyloid in plasma, CSF and brain, although CSF reductions were significant only at 30 and 100 mg/kg whereas brain and plasma reductions were apparent at all doses. The magnitude of the effect was greater in plasma than brain. In contrast, (18) showed very weak effects in brain and CSF. In a time course study at 30 mg/kg neither compound showed a rebound of $A\beta_{40}$ or $A\beta_{42}$ in plasma or brain. Compound (17) showed a maximal reduction (91%) in plasma $A\beta_{42}$, approximately 16 h post-dose and a maximal reduction of brain amyloid about 8–10 h post-dose, 54% and 40% reductions of $A\beta_{40}$ and $A\beta_{42}$, respectively. Again, the efficacy of (17) was found to be superior to that of (18). In a sub-chronic, 5-day u.i.d. dosing regimen, (17) reduced brain $A\beta_{42}$ levels by 58% and brain $A\beta_{40}$ levels by 63% whereas (18) caused reductions of 23% and 17% in brain $A\beta_{42}$ and $A\beta_{40}$, respectively. Using the concentration data from earlier publications, brain concentrations were found to be 9.1 μ M for (17) and 8.7 μ M for (18), resulting in a calculated free brain concentrations of 72 and 10 nM. These data highlight a recurring theme for GSMs of this class, as pointed out for the acid class, that there is a poor correlation between *in vivo* efficacious concentrations and *in vitro* activity. While the total brain concentrations for both compounds are

very high and considerably in excess of their *in vitro* activity, ((**17**); $A\beta_{42}$ $IC_{50} = 60$ nM, (**18**); $A\beta_{42}$ $IC_{50} = 125$ nM), the free concentrations are in line with the IC_{50} for (**17**) but not for (**18**). Thus, the free concentrations do not appear to correlate with efficacy. Additionally if one assumes that the compound T_{max} is 2 h, based on the compounds' half-lives one would expect C_{max} values to be two to three times higher than the 6 h concentrations, which may explain the efficacy for (**17**) but again the free concentrations for (**18**) would still be inferior to the *in vitro* levels necessary to modulate amyloid.

Replacement of the imidazole in (**18**) was also investigated [37]. Replacements were designed to mimic the HBA ability of the imidazole and several active derivatives were identified. These included isothiazole (**19**), thiazole (**20**), pyridazine (**21**) and pyridine (**22**) (Table 3.1). Activity correlated well with the HBA strength of the heterocycle, supporting the pharmacophore as discussed earlier. However, all suffer from decreased solubility owing to the removal of the ionisable imidazole group.

Table 3.1 Variation of Imidazole Group on GSK Pyridine Template



Compound	R	$A\beta_{42}$ IC_{50} (nM)
18		126
19		251
20		398
21		398
22		501

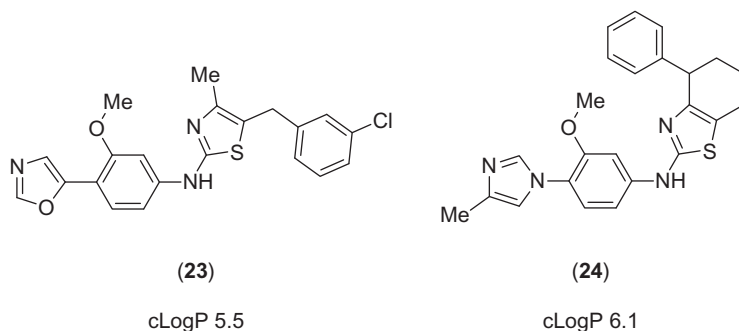


Figure 3.6 Structures of hit **(23)** and optimised derivative **(24)** from Roche.

2.2.3 Roche

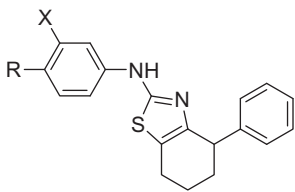
In 2011, Roche published some of their work detailing an HTS hit **(23)** ($A\beta_{42}$ IC_{50} = 815 nM, $A\beta_{40}$ IC_{50} = 3.7 μ M, $A\beta_{38}$ EC_{50} = 1.5 μ M in human neuroglioma H4 cells overexpressing human APP, 22 h incubation) [39] (Figure 3.6). Optimisation of **(23)** resulted in the identification of **(24)** ($A\beta_{42}$ IC_{50} = 44 nM) (Figure 3.6) which displayed acceptable mouse pharmacokinetics (Cl_p = 18.3 mL/min/kg, V_{dss} 4.6 = L/kg, $t_{1/2}$ = 2.5 h, F_{po} = 25%, Br:PI = 0.4–2.1). Profiling *in vivo* (APPSwe Tg mouse) at 10, 30 and 100 mg/kg demonstrated reductions in brain $A\beta_{42}$ of 18%, 35% and 65%, respectively (DEA extraction) leading to a calculated ED_{50} of 40 mg/kg.

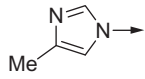
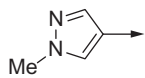
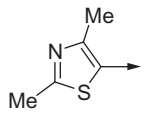
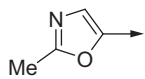
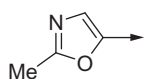
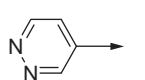
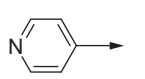
The Roche group also investigated some imidazole replacements, a summary of which is presented in Table 3.2. Again, a HBA in this region of the molecule was found to be important. The nitrile group was significantly weaker than the heteroaromatic rings, (R = CN, X = OMe, IC_{50} = 3358 nM), despite providing a good pharmacophoric overlap.

The oxazole derivative **(27)** was also evaluated *in vivo* in APPSwe Tg mice and produced a 47% reduction in brain $A\beta_{42}$ 4 h after a 100 mg/kg oral dose. Bioanalysis revealed a Br:PI ratio of 0.34.

2.2.4 Janssen

The Janssen research group has been active in the GSM area for a considerable period of time. In recent times, their focus appears to have changed to the imidazole series. A recent publication [40] details some of their work. Starting from Eisai derivative **(12)** (Figure 3.4), the primary objective was to generate novel compounds without an α,β -unsaturated amide and this

Table 3.2 Variation of Imidazole on Roche Template

Compound	R	X	A β ₄₂ IC ₅₀ (nM)
24		MeO	44
25		MeO	244
26		MeO	212
27		MeO	86
28		H	133
29		H	376
30		H	319

resulted in the identification of aminopyridone (**31**) (Figure 3.7) which was considerably less active (A β ₄₂ IC₅₀ = 550 nM in SKNBE2 cells which express wild-type APP695) than (**12**) (A β ₄₂ IC₅₀ = 81 nM).

Maintaining the putative HBA of (**31**) and cyclisation gave imidazopyridine (**32**) (Figure 3.7) which displayed improved potency (A β ₄₂ IC₅₀ = 182 nM), albeit at the cost of increased lipophilicity. Further optimisation resulted in the identification of aminobenzimidazole derivative (**33**)

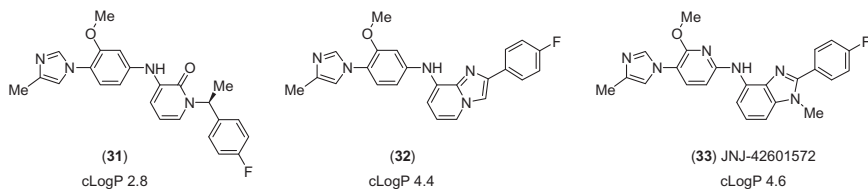


Figure 3.7 Initial lead compounds **(31)** and **(32)**, and subsequent optimised analogue **(33)** from Janssen.

(JNJ-42601572) with an $A\beta_{42}$ IC_{50} of 16 nM (Figure 3.7). **(33)** proved to be effective *in vivo* and produced a 62% reduction of brain $A\beta_{42}$ after a 30 mg/kg oral dose in non-transgenic CD1 mice 4 h post-dose. Further profiling revealed that the compound was not genotoxic although it had moderate hERG activity (30% inhibition at 3 μ M), moderate CYP activity (2C19 IC_{50} = 3.5 μ M, 2D6 IC_{50} = 3.6 μ M, 3A4 IC_{50} = 2.9 μ M) and showed very high ppb (0.13% free in human, 0.04% free in mouse and rat and 0.03% free in dog). Despite suffering from very low solubility, **(33)** displayed good pharmacokinetic parameters across mouse, rat and dog (Cl = 0.94, 0.53 and 2.4 L/h/kg, respectively, V_{dss} = 2.4, 1.8 and 4.6 L/kg, respectively, $t_{1/2}$ = 1.7, 2.3 and 1.6 h). Oral bioavailability was high: >100% in mouse, 95% in rat and 64% in dog, when administered in 20% captisol at pH 4. A time course study in the mouse at 10 and 30 mg/kg resulted in a large reduction of brain $A\beta_{42}$, 50% and 71%, respectively at 8 h post-dose. Brain $A\beta_{38}$ showed a maximal effect 4 h post-dose, with a 41% increase at 10 mg/kg and a 65% increase at 30 mg/kg. The brain concentration was found to be 15.6 μ M 4 h post-dose and 10.5 μ M 8 h post-dose in the 30 mg/kg group, and 2.8 and 1.9 μ M 4 and 8 h after a 10 mg/kg dose, with the Br:Pl ratio ranging from 0.53 to 1.14 across all time points and doses. Furthermore, no rebound in amyloid was observed and levels returned to baseline within 48 h. In the dog, following a 20 mg/kg oral dose, CSF $A\beta_{42}$ decreased by 19% at 4 h and 48% at 8 h, with $A\beta_{38}$ levels increased by 34% at 4 h and 84% at the 8 h time point. In a rat time course study at 10 mg/kg, **(33)** showed a Br:Pl ratio of approximately 0.5 at all time points with a very flat exposure profile with brain concentrations of 2.5, 2.2 and 2.0 μ M at 2, 4 and 7 h post-dose, respectively. Brain $A\beta_{42}$ levels were reduced by 25%, 36% and 34% at the 2, 4 and 7 h time points, whereas CSF $A\beta_{42}$ levels were reduced by 35%, 34% and 43% at the same time points. The $A\beta_{40}$ levels in both compartments showed almost identical effects. Brain $A\beta_{38}$ levels were affected less than CSF $A\beta_{38}$, which showed increases of 62%, 79% and 53% at 2, 4 and 7 h post-dose. Interestingly, $A\beta_{37}$

in CSF and brain levels showed much more dramatic increases than $A\beta_{38}$ at all time points in CSF and brain and the peak increase in CSF of 855% occurred 4 h post-dose. Further profiling of (33) revealed several issues which resulted in the termination of its development [41]. (33) caused increases in alanine transaminase (ALT) and aspartate aminotransferase (AST) plasma levels at 20 mg/kg in the dog in one in six animals. This effect was also produced by (12) at 80 mg/kg and indicates liver damage or impaired liver function. Furthermore, gene expression profiling revealed that (33) affected gene levels in multiple pathways, including bile transport, lipid transport and inflammation.

In subsequent publications, the Janssen group has detailed further work which resulted in the identification of fused triazole derivatives such as (34) and (35) [42] (Figure 3.8). Both of these compounds displayed potent *in vitro* activity ($A\beta_{42}$ IC_{50} = 71 and 28 nM, respectively). Four hours after a 30 mg/kg oral dose to mice, (34) showed a concentration of 3.6 μ M in plasma and 3.4 μ M in brain, resulting in a Br:Pl ratio of 0.93. This gave a 22% decrease in brain $A\beta_{42}$ and a 17% increase in brain $A\beta_{38}$ levels. In the same study, (35) showed similar brain levels of 2.8 μ M, but much higher plasma levels at 12.3 μ M, which resulted in a Br:Pl ratio of 0.23. This compound was more active and decreased brain $A\beta_{42}$ by 62% and gave a 66% increase in brain $A\beta_{38}$. It was also found that (35) showed a much higher free fraction in plasma (8.5%) and brain (2.2%) compared with other GSMs. Thus, the calculated free plasma and brain concentrations from the *in vivo* mouse study are 1046 and 62 nM, respectively, which results in a $Br_u:Pl_u$ ratio of 0.06. This implies that the compound is actively effluxed from the CNS. There also appears to be a good correlation between the free brain concentration and the *in vitro* activity for this compound. However, peripheral side effects such as cardiovascular activity may be an issue due to the high peripheral concentrations relative to those in the CNS. In the dog, a dose of 20 mg/kg resulted in a plasma concentration of 19 μ M with a concomitant reduction in CSF $A\beta_{42}$ of 50% and an increase in CSF $A\beta_{38}$ of 28%.

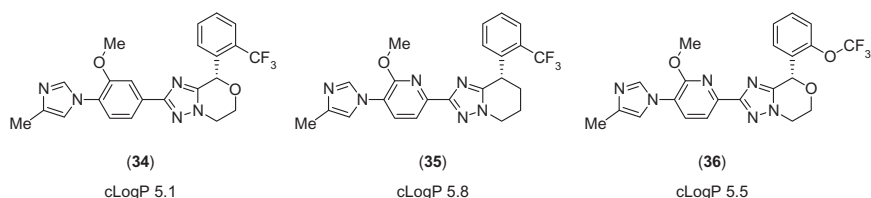


Figure 3.8 Fused triazole derivatives from Janssen.

In the same study, there were no changes in bilirubin or ALT levels, representing an improvement over predecessor compounds. In a subsequent publication [41], (36) (Figure 3.8) has been described as a ‘next-generation GSM’ as it combines potency ($A\beta_{42}$ IC_{50} = 56 nM) with lower lipophilicity (Janssen $cLogP$ = 3.1, ChemDraw $cLogP$ = 5.5) and an increased free fraction in brain at 3.9%. For comparison purposes, note the disparity between ChemDraw $cLogP$ values for (34), (35) and (36), (Figure 3.8) versus Janssen values; $cLogP$ 3.4 for (34), 4.5 for (35) and 3.1 for (36).

2.2.5 BMS

At a recent investor meeting [43], BMS claimed to have a GSM in the pre-clinical development phase. As this group has not yet released any peer reviewed publications, only patent literature is available and discussed here in chronological order. In 2010, the group described fused aminotriazole derivatives (37) and (38) with $A\beta_{42}$ IC_{50} s of 8 and 4 nM, respectively (human H4 cells transfected with APP751 containing Swe mutations, incubated for 19 h) [44] (Figure 3.9). The tolerance of the chloro-imidazole moiety is noteworthy as this group has not frequently been employed by other research groups. Furthermore, the Cl atom on the imidazole should significantly decrease its HBA strength. The compounds nevertheless display high potency. A second patent application the following year described closely related fused diaminopyrimidine derivatives, such as (39) and (40), with $A\beta_{42}$ IC_{50} values of 4.6 and 4 nM, respectively [45] (Figure 3.9). A follow-up patent application in 2012 detailed closely related fused diaminopyrimidine derivatives where the imidazole had been replaced by a nitrile group, such as in (41) with an $A\beta_{42}$ IC_{50} of 11 nM [46] (Figure 3.9). Earlier in the same year, the BMS group detailed work where they linked the phenolic substituent to the alkylamino moiety on the pyrimidine to give macrocycles such as (42) and (43); $A\beta_{42}$ IC_{50} 3.9 and 7.8 nM, respectively [47] (Figure 3.9). The activity appeared relatively insensitive to the nature of the macrocyclic linker, and a range of imidazole replacements were found to be acceptable including the 1,2,4-triazole. It is interesting to note that the chloro-imidazole HBA moiety in this series can be replaced by a nitrile group, for example, (42) versus (43), which is in contrast to that found by other research groups with their series, for example, Roche, Table 3.2.

2.2.6 Pfizer

To date, there is only one peer reviewed publication from the Pfizer group which follows on from some published patent applications. The early Pfizer templates are centred on benzamide derivatives as replacements for the

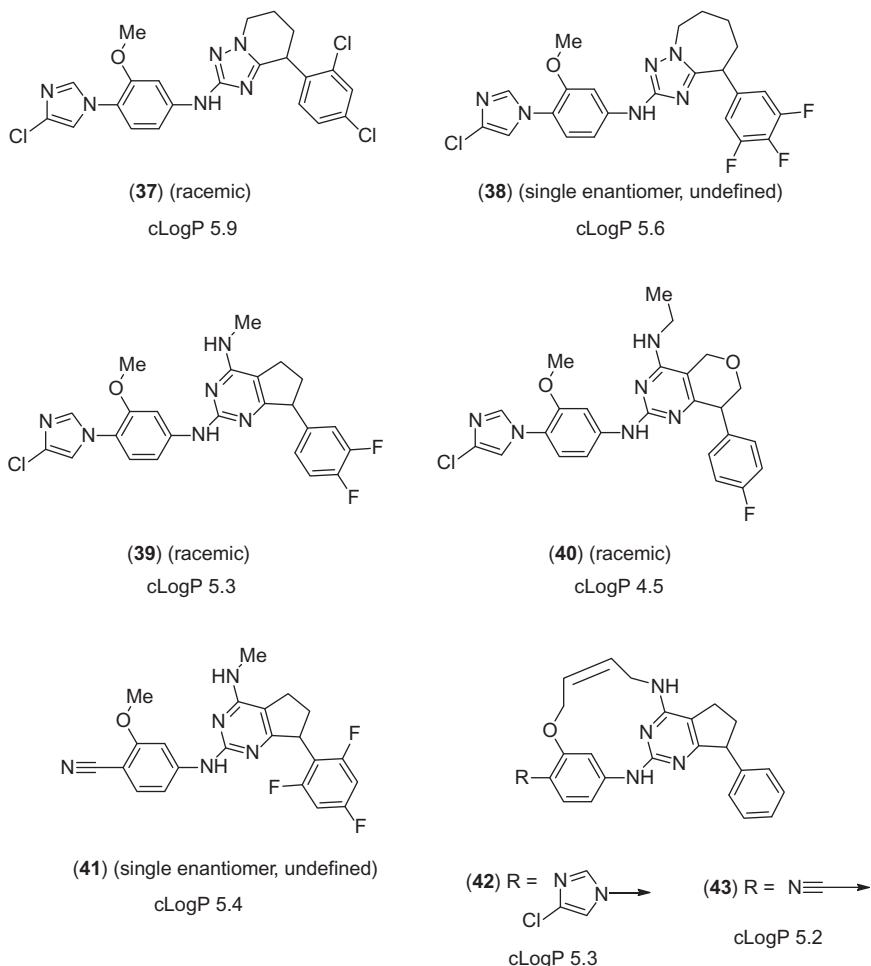


Figure 3.9 Summary of BMS compounds from the patent literature.

cinnamide moiety found in front runner compounds such as (12) (Figure 3.4). The most potent example from a 2010 patent application [48] is (44) ($A\beta_{42}$ IC_{50} = 137 nM) (Figure 3.10). The SAR in this series appears relatively flat with most examples displaying $A\beta_{42}$ IC_{50} values in the range 300–700 nM. A follow-up disclosure [49] described closely related examples where the methoxyphenyl moiety had been replaced by pyridine and pyrazine, leading to compounds such as (45) ($A\beta_{42}$ IC_{50} = 207 nM) (Figure 3.10), which incorporate the same amide group as that identified by scientists at Merck (see below).

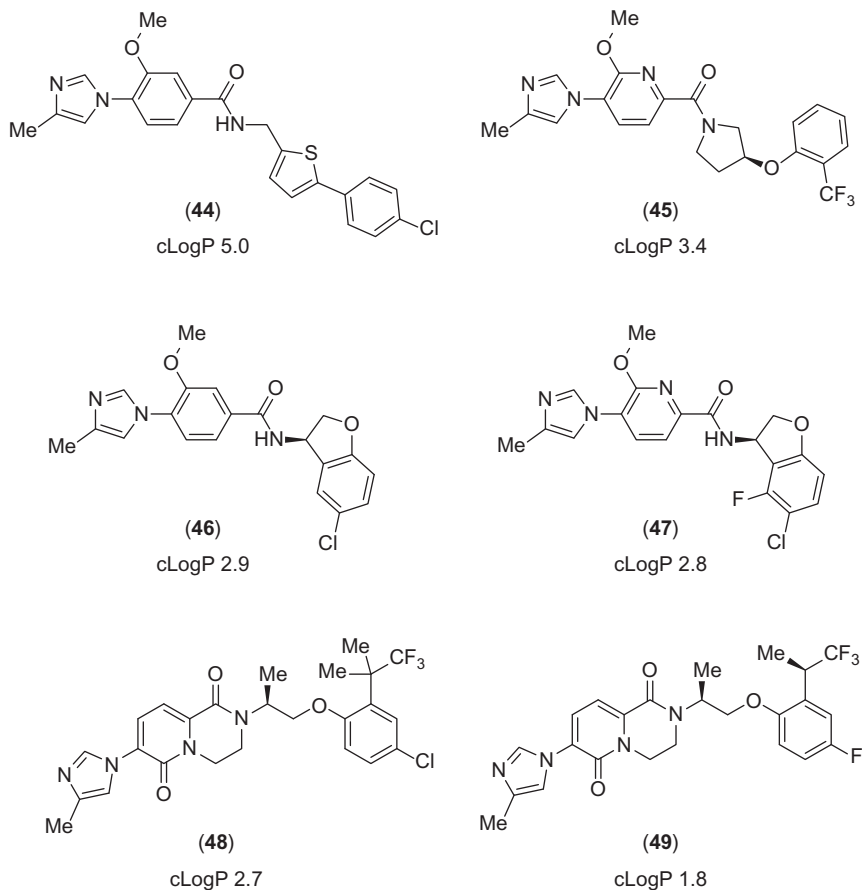


Figure 3.10 Summary of Pfizer compounds from the patent literature.

Further optimisation of this series has recently been disclosed [50]. Optimised compounds (46) and (47) (Figure 3.10) (Pfizer cLogP for both = 4.0) showed moderate *in vitro* activity ($A\beta_{42}$ IC₅₀ = 531 and 188 nM, respectively). Neither compound was a substrate for Pgp (efflux ratios of 1.6 and 1.4, respectively) and both showed moderate stability in human liver microsomes. In the rat, (46) showed good metabolic stability (Cl = 3.6 mL/min/kg) and a moderate volume of distribution (V_{dss} = 1.87 L/kg). This translated to a $t_{1/2}$ of 2.43 h and high oral bioavailability (100%). In contrast (47) showed lower metabolic stability (Cl = 31.4 mL/min/kg) but a similar V_{dss} (1.78 L/kg) which resulted in a shorter half-life of 0.64 h. The molecule also had a lower F_{po} of 51%. Efficacy was assessed in the guinea pig 4 h after a 100 mg/kg oral dose. While (46) caused a 57% reduction of brain $A\beta_{42}$ with a corresponding free brain

concentration of 1038 nM, that is, $2.1 \times IC_{50}$, (**47**) caused a 36% reduction of brain $A\beta_{42}$ with a corresponding free brain concentration of 89 nM, that is, $0.3 \times IC_{50}$, thus highlighting non-correlation between free brain concentrations and *in vivo* efficacy. Even considering the relatively short half-life of (**47**), the free brain concentrations are still likely to be similar to the *in vitro* IC_{50} at the maximal brain concentration and therefore are unlikely to explain the efficacy seen with this compound. The most recent patent application describes fused pyridone derivatives. The most pertinent examples are (**48**) ($A\beta_{42} IC_{50} = 3.54$ nM) and (**49**) ($A\beta_{42} IC_{50} < 6.64$ nM) [51] (Figure 3.10).

2.2.7 Merck

Prior to the Merck-Schering Plough merger, both legacy companies had active GSM projects and began publishing work from 2010 onwards. The legacy Merck research from the Boston site will be discussed first.

In a first paper, the group disclosed a piperazine-linked pyrimidine series which bears a close resemblance to the TorreyPines Therapeutics series (**14**) (Figure 3.4) and is exemplified by compounds (**50**) and (**51**), both of which showed high *in vitro* potency ($A\beta_{42} IC_{50} = 169$ and 34 nM, respectively) [52] (Figure 3.11). Major points of interest with this series are that the methoxyphenyl core has been replaced by a dimethyl piperazine, and the imidazole HBA moiety has been replaced by methoxyphenyl group. Cyclisation resulted in derivatives such as (**52**) ($A\beta_{42} IC_{50} = 21$ nM) (Figure 3.11) which demonstrated a 73% reduction in brain $A\beta_{42}$ in the APP-YAC Tg mouse 6 h after a 100 mg/kg oral dose. The resultant brain and plasma concentrations of 7.8 and 23 μ M, respectively, indicated high exposure. Interestingly, this series appeared to have a wide tolerance of functional groups that could be used as spacer or for HBA. For example, (**53**) (Figure 3.11) demonstrated potent *in vitro* activity with an $A\beta_{42} IC_{50}$ of 16 nM and in the APP-YAC Tg mouse gave a 69% reduction of brain $A\beta_{42}$ 6 h post 100 mg/kg dose, with corresponding brain and plasma concentrations of 7.8 and 27 μ M, respectively [53].

Subsequent work from the same group detailed efforts to remove the cinnamide from what is postulated to be E2012 (**12**) (Figure 3.4) and resulted in trans-olefin derivatives such as (**54**) ($A\beta_{42} IC_{50} = 660$ nM) [54] (Figure 3.11). Despite demonstrating acceptable rat pharmacokinetics (Cl_p 6.8 mL/min/kg, $V_{dss} = 1.8$ L/kg, $t_{1/2} = 5.8$ h, $F_{po} = 59\%$), this series was plagued by poor solubility which resulted in variable exposure at higher doses. A search for trans-olefin replacements led to the identification of 1,2,3-triazoles such as (**55**) ($A\beta_{42} IC_{50} = 400$ nM) (Figure 3.11) which also

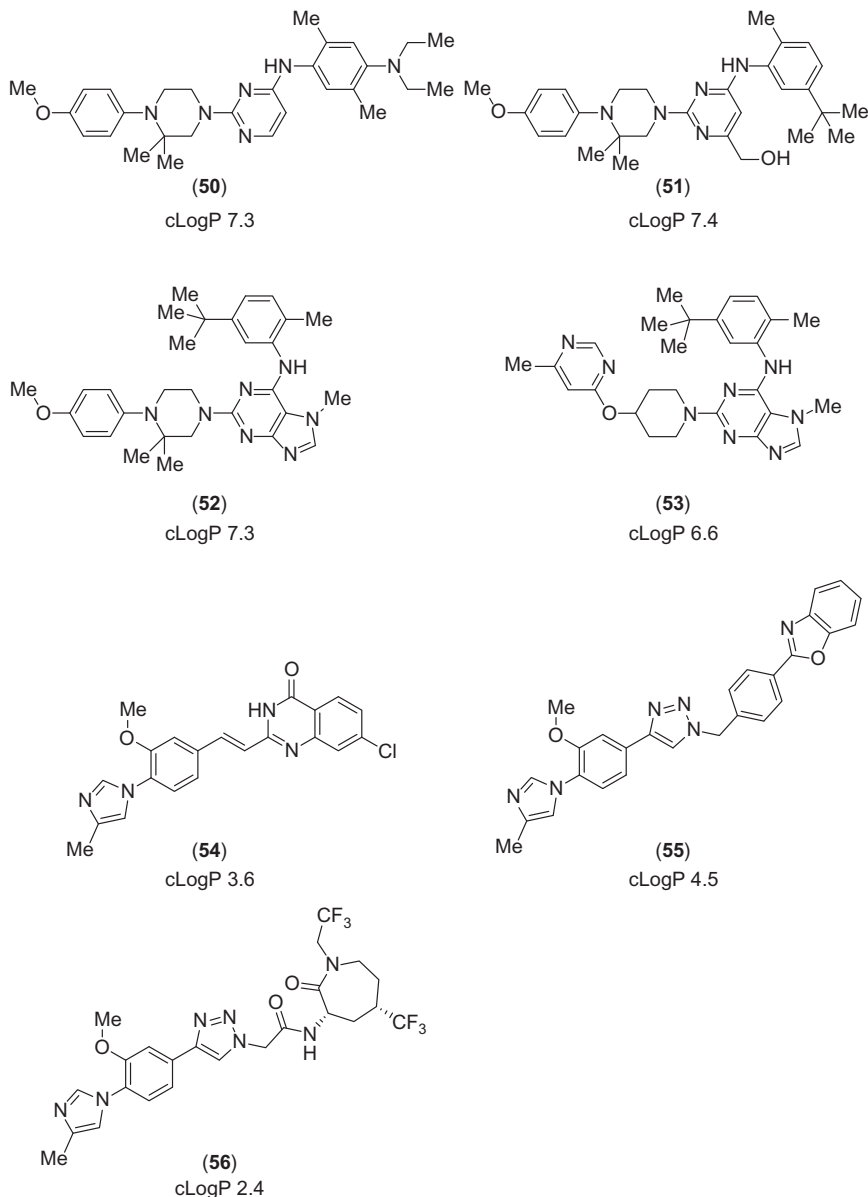


Figure 3.11 Summary of compounds from Merck Boston.

showed good pharmacokinetic parameters in the rat ($Cl_p = 13.7$ mL/min/kg, $V_{dss} = 2.8$ L/kg, $t_{1/2} = 5.4$ h, $F_{po} = 49\%$) [55]. This compound produced a 42% reduction in brain $A\beta_{42}$ levels in the rat 6 h after a 60 mg/kg oral dose, resulting in brain and plasma concentrations of 9.4 and 40 μ M, respectively.

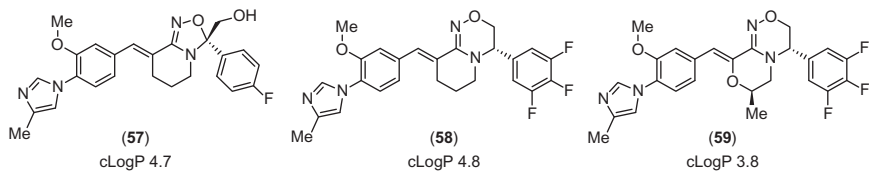


Figure 3.12 Compounds from Merck Rahway.

In the final publication on this series, azide cycloaddition chemistry was utilised to optimise the right-hand side of the 1,2,3-triazole series. This resulted in the identification of derivatives such as (56) (Figure 3.11), which showed potent *in vitro* activity ($A\beta_{42}$ IC_{50} = 20 nM) [56].

In a parallel effort, researchers at the Merck Rahway site have successfully replaced the amide moiety of (12) (Figure 3.4) by cyclic amidoximes, giving derivatives such as (57) ($A\beta_{42}$ IC_{50} = 75 nM) (Figure 3.12). Optimisation of this chemotype resulted in the identification of (58) ($A\beta_{42}$ IC_{50} = 33 nM) (Figure 3.12). When dosed to rats at 10 mg/kg, (58) reduced CSF $A\beta_{42}$ by 62% 3 h post-dose. The Br:Pl ratio was found to be 0.4, 6 h after an oral dose. Rat pharmacokinetic parameters proved promising with a low clearance of 1.4 mL/min/kg, a low V_{dss} of 0.4 L/kg and a moderate half-life of 3.5 h together with 100% oral bioavailability. Furthermore, (58) showed no QTc prolongation in the dog, despite exhibiting 76% inhibition of hERG at 10 μ M. Further optimisation resulted in the identification of (59) ($A\beta_{42}$ IC_{50} = 11 nM) (Figure 3.12) which caused a 60% reduction of $A\beta_{42}$ in rat CSF 3 h after a 20 mg/kg oral dose.

Researchers at Schering Plough had also initiated lead generation activities using the Eisai template. Early work led to the discovery of (60) ($A\beta_{42}$ IC_{50} = 85 nM) (Figure 3.13) in which the δ -lactam of (12) (Figure 3.4) has been replaced by an iminohydantoin. When dosed orally to the rat, (60) elicited a 38% reduction in CSF $A\beta_{42}$ 3 h after a 100 mg/kg dose. Despite delivering high plasma (7.1 μ M) and brain (5.9 μ M) concentrations 3 h after a 30 mg/kg dose, efficacy was weak with only a 10% reduction in CSF $A\beta_{42}$ [57]. Other efforts from the group centred on replacement of the cinnamide moiety which resulted in the identification of aminopyridazone (61) ($A\beta_{42}$ IC_{50} = 44 nM) [58] (Figure 3.13), a close analogue of aminopyridine derivatives such as (31) (Figure 3.7) from Janssen, which delivered weak efficacy in the rat following a 100 mg/kg oral dose, causing a 26% reduction in brain $A\beta_{42}$ and a 40% reduction in CSF $A\beta_{42}$. An alternative strategy used a triazole to mimic the cinnamide moiety delivering derivatives such as (62) ($A\beta_{42}$ IC_{50} = 116 nM) [59] (Figure 3.13). This compound showed no

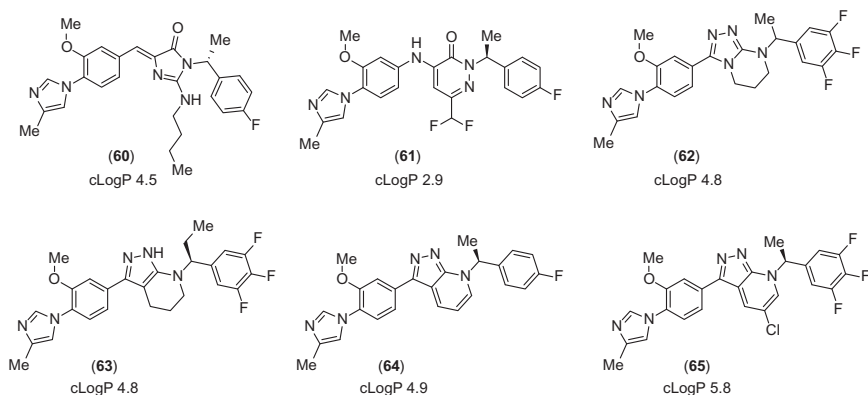


Figure 3.13 Key compounds from former Schering Plough.

efficacy in the rat at 30 mg/kg (at the 3 h time point), which might be attributed to insufficient brain concentration (0.49 μM). Further optimisation resulted in the pyrazolopiperidine derivative **(63)** ($\text{A}\beta_{42}$ IC_{50} = 122 nM) (Figure 3.13) and this compound reduced CSF $\text{A}\beta_{42}$ in the rat by 16% 3 h after a 30 mg/kg dose. No exposure data was provided for **(63)** to put the efficacy into context.

A subsequent publication detailed the aromatisation of the pyrazolopiperidine moiety to deliver the pyrazolopyridine/7-aza-indazole scaffold, exemplified by **(64)** ($\text{A}\beta_{42}$ IC_{50} = 97 nM) [60] (Figure 3.13). When dosed orally to the rat at 30 mg/kg, this compound failed to lower CSF amyloid. Bioanalysis revealed low brain concentrations (0.17 μM) in comparison to plasma concentrations (2.88 μM), which was attributed to the compound being a Pgp substrate, with an efflux ratio of 33.8. Addition of a chlorine atom to the 5-position of the 7-aza-indazole diminished Pgp efflux and led to compounds such as **(65)** ($\text{A}\beta_{42}$ IC_{50} = 107 nM) (Figure 3.13). In a single dose rat efficacy study, **(65)** reduced CSF $\text{A}\beta_{42}$ by 45% 3 h post-dose (30 mg/kg), with corresponding plasma and brain concentrations of 5.02 and 1.22 μM , respectively.

2.2.8 AstraZeneca

Researchers at AstraZeneca have described studies on fused triazole derivatives such as **(66)** ($\text{A}\beta_{42}$ IC_{50} = 25 nM in HEK cells and 50 nM in PCN cells) [32] (Figure 3.14). An investigation into imidazole replacements on this template led to the conclusion that the HBA strength correlated with potency and the 6-methyl-4-pyridazinyl group proved optimal for potency.

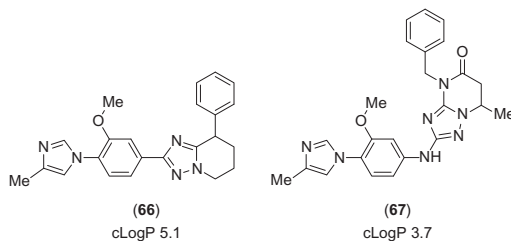


Figure 3.14 Fused triazole derivatives from AstraZeneca.

These compounds were not pursued further as fused triazole derivatives have been described by other companies; for example, (35) (Figure 3.8) from Janssen. Thus, efforts were directed to improve novelty. Insertion of an amino linker between the phenyl ring and the triazole, and concomitant replacement of the fused piperidine moiety by a fused dihydropyrimidine, resulted in (67) ($A\beta_{42}$ IC_{50} = 10 nM in HEK cells and 20 nM in PCN cells) (Figure 3.14). Solubility was improved over earlier examples, but was still low (6 μ M), while hERG activity remained an issue (IC_{50} = 3.7 μ M). Mouse developability profiling demonstrated the compound possessed good CNS penetration with a $Br_u:Pl_u$ ratio of 0.72, in addition to moderate clearance (21 mL/min/kg) and volume of distribution (0.9 L/kg), a short half-life of 0.6 h and 32% oral bioavailability. In wild-type (C57BL/6) mice, a dose of 150 μ mol/kg produced a reduction of 24% in brain $A\beta_{42}$ levels 1.5 h post-dose, whereas a dose of 50 μ mol/kg was inactive.

2.2.9 Boehringer Ingelheim

Recently, Boehringer Ingelheim has disclosed some of their efforts to identify novel GSMs containing a fused diaminopyrimidine, such as (68) ($A\beta_{42}$ IC_{50} = 90 nM) [61] (Figure 3.15), which is closely related to the template described by BMS in Figure 3.9. This template lacks the aromatic ring on the right-hand side of the molecule, which appears to be obligatory in other templates.

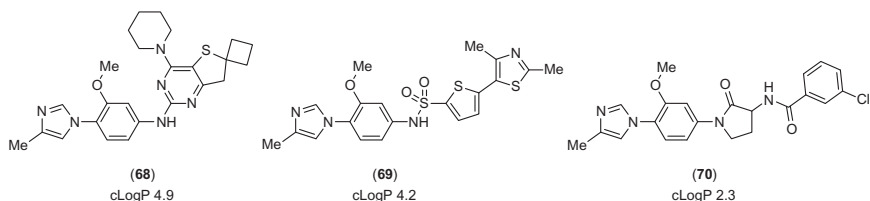


Figure 3.15 Compounds from Boehringer Ingelheim and Shionogi.

2.2.10 Shionogi

Shionogi has described a sulphonamide template, exemplified by (69) [62] with weak activity ($IC_{50}=2.21\ \mu\text{M}$) and a similar lactam template, exemplified by (70) ($IC_{50}=800\ \text{nM}$) [63], Figure 3.15.

2.2.11 Dainippon Sumitomo

The group at Dainippon Sumitomo has recently become active in the GSM area and has disclosed several chemotypes, such as (71) (Figure 3.16) in which the amino-oxadiazole acts as a cinnamide replacement [64], the amide derivative (72) [65] (Figure 3.16) which is closely related to Pfizer derivatives such as (44) and (45) (Figure 3.10) and trans-olefin (73) [66] (Figure 3.16) which is very closely related to Eisai derivative (13) (Figure 3.4).

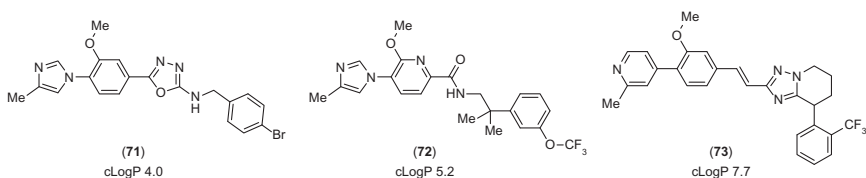


Figure 3.16 Selected chemotypes from Dainippon Sumitomo.

2.2.12 Summary

Many research groups have commented on the issues encountered by compounds with this chemotype. These include P450 inhibition (especially 2D6 and 3A4), hERG inhibition, Pgp-mediated efflux, toxicology issues, efficacy limits and poor correlations between exposure and efficacy. As with the acid series, the total concentrations associated with *in vivo* efficacy tend to be very high, whereas the free concentrations tend to be low, with respect to *in vitro* activity. Although many scientists have worked within this chemical series and considerable structural diversity has been achieved, it could be said that the pharmacophore is broadly associated with these developability issues, many of which can be attributed to the high lipophilicity of the compounds as highlighted by the calculated log *P* values provided in this review. Balancing lipophilicity and potency has proved to be a challenge [67]. Incorporation of polar groups such as hydroxyls often leads to Pgp efflux, whereas addition of nitrogen atoms may reduce potency or have a minimal effect on lipophilicity. The SAR within each compound series appears somewhat nebulous, which makes significant jumps in potency difficult to achieve.

This may be due to the allosteric nature of the target-binding site, which could be more two-dimensional than three-dimensional, or it may be a shallow-binding pocket, or simply due to the fact that by the very nature of its allosteric location it can impart only limited effects on the orthosteric substrate. Although the literature contains details of several well-characterised compounds, few seem to have progressed beyond toxicological studies into the clinic. So, it seems that optimisation of analogues from within this series will require a long-term commitment. To this end, it appears that Janssen has made the most progress and may be the first to make a breakthrough in this area [67,68].

2.3. Natural Products

Satori reported on a novel series of GSMs that was identified from a natural product screen. The active component (74) (Figure 3.17) was an extract from the black cohosh plant and displayed an unusual modulatory profile whereby it decreased $A\beta_{42}$ and $A\beta_{38}$, increased $A\beta_{39}$ and did not affect $A\beta_{37}$ or $A\beta_{40}$, measured in CHO 7PA2 cells expressing V717F mutant APP [69]. In CHO 7W cells expressing wild-type APP, the compound reduced $A\beta_{42}$ and $A\beta_{38}$, but increased $A\beta_{37}$ in addition to $A\beta_{39}$ while slightly reducing $A\beta_{40}$ levels. In H4 cells stably expressing wild-type human APP, the compound inhibited $A\beta_{42}$ production with an IC_{50} of 100 nM. *In vivo* profiling of (74) revealed that the acetate group was rapidly hydrolysed, in addition to the much slower hydrolysis of the tri-hydroxy THP. Optimisation included reduction of the

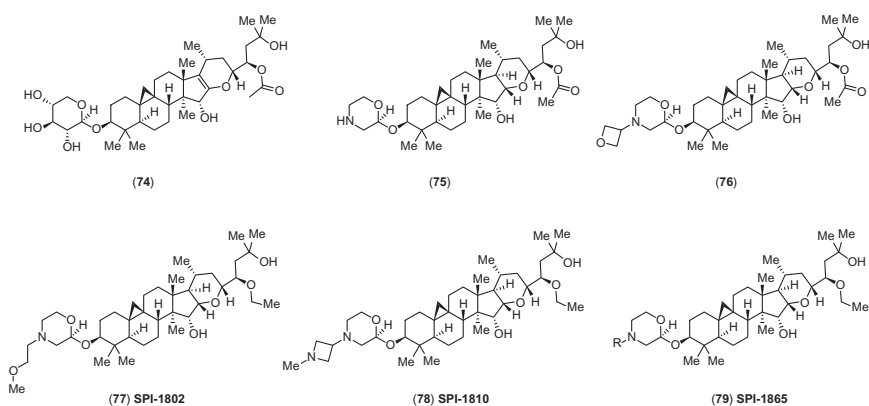


Figure 3.17 Key compounds from Satori.

enol ether and replacing the tri-hydroxy THP moiety with esters [70] and O-linked morpholine derivatives which resulted in (75) ($A\beta_{42} IC_{50} = 55$ nM) and (76) ($A\beta_{42} IC_{50} = 270$ nM) [71] (Figure 3.17). In a mouse PK study, compound (75) displayed a moderate clearance of 3.1 L/h/kg, a high distribution volume of 12.1 L/kg, a long half-life of 6.5 h and moderate oral bioavailability at 37%, in addition to good CNS penetration with a Br:Pl ratio of 1.7 at the 6 h time point. Compound (76) also displayed a moderate clearance of 3.3 L/h/kg, a moderate volume ($V_d = 0.6$ L/kg), a short half-life (0.3 h) and low oral bioavailability (11%) in addition to moderate CNS penetration with a Br:Pl ratio of 0.23 at the 6 h time point. Neither compound proved efficacious in the CD1 mouse despite reasonable exposure: (75) achieved brain concentrations of 1336 ng/g at 4 h, 1628 ng/g at 6 h and 2263 ng/g at 8 h after a 30 mg/kg dose, resulting in a Br:Pl exposure (AUC) ratio between 4 and 24 hours of 1.86. Even at a higher dose of 100 mg/kg, (76) gave much lower brain concentrations: 185 ng/g at 4 h, 453 ng/g at 6 h with the resulting Br:Pl $AUC_{(2-6h)}$ of 0.39.

Subsequent optimisation studies investigated replacement of the acetate group. The most interesting examples of this approach were found to be the ethyl derivatives (77) ($A\beta_{42} IC_{50} = 270$ nM) and (78) ($A\beta_{42} IC_{50} = 100$ nM) [72,73] (Figure 3.17). Both compounds were found to be highly bound to plasma protein: 98.9% for (77) and 99.2% for (78), as well as brain tissue; 99.9% for (77) and 99.8% for (78). *In vivo* pharmacokinetics were assessed in the mouse, where (77) displayed low clearance (0.29 L/h/kg), a low distribution volume (0.42 L/kg) and low oral bioavailability (19%) whereas (78) displayed low clearance (0.15 L/h/kg), a moderate distribution volume (5.3 L/kg) and high oral bioavailability (75%). CNS penetration was assessed in the CD1 mouse 6 h after an i.v. dose of 1 mg/kg. In this study, the plasma concentration of (77) was 35 nM (0.4 nM free) and the corresponding brain concentration was 9 nM (0.01 nM free), resulting in a Br:Pl ratio of 0.26 and a $Br_u:Pl_u$ ratio of 0.025, implying that the compound is actively effluxed. In a similar study, the plasma concentration of (78) was 107 nM (0.9 nM free) and the corresponding brain concentration was 52 nM (0.1 nM free), resulting in a Br:Pl ratio of 0.49 and a $Br_u:Pl_u$ ratio of 0.11, again implying the compound is actively effluxed. When (77) was dosed at 100 mg/kg i.p., it elicited a 46% reduction of brain $A\beta_{42}$ and a 31% reduction of brain $A\beta_{38}$ 6 h post-dose. The corresponding brain concentration was 23 μ M, resulting in a free brain concentration of 23 nM which is considerably below the *in vitro* IC_{50} . The plasma concentration was 12 μ M, that is, Pl_u 12 nM, resulting in $Br_u:Pl_u$ of 2, which is very different from the i.v. study result. In a corresponding study, (78) administered at 100 mg/kg p.o. effected

a 26% reduction of brain $A\beta_{42}$ and a 31% reduction of brain $A\beta_{38}$ 6 h post-dose. The brain concentration was 20 μM , resulting in a free brain concentration of 40 nM which is still below the *in vitro* IC_{50} . The plasma concentration was 15 μM , that is a Pl_u of 120 nM, resulting in $Br_u:Pl_u$ of 0.3, which is slightly higher than in the i.v. study. Finally, in a 5-day dosing study, (78) administered at 50 mg/kg p.o. effected a 42% reduction of brain $A\beta_{42}$ and a 38% reduction of brain $A\beta_{38}$ 8 h post-final dose. The corresponding brain concentration was 31 μM ($Br_u = 62$ nM) and the plasma concentration was 16 μM ($Pl_u = 128$ nM). Further optimisation resulted in the identification of SPI-1865 (79) [74] (Figure 3.17) (full structure not disclosed) which was selected as a development compound. In CHO-2B7 cells (stably transfected with human βAPP695), (79) reduced $A\beta_{42}$ with an IC_{50} of 106 nM. Profiling in the mouse revealed a volume of distribution of 9.2 L/kg and a Br:Pl ratio between 0.4 and 1.4, while in the rat the distribution volume was 5.8 L/kg, and the $t_{1/2}$ was extremely long at 129 h with the Br:Pl ratio between 0.5 and 1.5. In an acute dose-response study in the rat, efficacy was assessed 24 h after oral doses (due to the T_{max} of 6–8 h) of 10, 30 and 100 mg/kg which produced 21%, 37% and 50% reductions in brain $A\beta_{42}$, respectively, with corresponding brain concentrations of 2.8, 11 and 33 μM and plasma concentrations of 3.3, 8.5 and 14 μM , respectively. A 6-day dosing study in the rat was conducted at oral doses of 10, 30 and 60 mg/kg which resulted in 24%, 44% and 66% reductions of brain $A\beta_{42}$, respectively 24 h post-final dose. The brain concentrations were 4.4, 16 and 45 μM , with corresponding plasma concentrations of 8.0, 13 and 19 μM . Although exposure in the brain is somewhat higher than in the acute study, it does not appear to be as high as might be anticipated given the extremely long half-life in rat. Both acute and repeat dose studies in the rat showed similar reductions in $A\beta_{38}$ and $A\beta_{42}$. A 6-day dosing study was also conducted in Tg2576 mice, 3 months of age, with doses of 10, 30, 60 and 90 mg/kg administered once daily with efficacy assessed 24 h after the final dose. None of these dose levels gave a statistically significant reduction of either CSF or brain $A\beta_{42}$, although plasma $A\beta_{42}$ was reduced at the 60 and 90 mg/kg doses. Total brain concentrations were 0.5, 1.3, 3.9 and 6.9 μM with corresponding plasma concentrations of 1.1, 2.5, 5.4 and 6.4 μM , respectively. Thus based on rat efficacy and exposures, one might have predicted 20–30% reduction of brain amyloid in the 60 and 90 mg/kg dose groups. Although reductions in brain $A\beta_{42}$ approaching the expected levels were observed the changes were not statistically significant. High ppb (97.6%) and btb (99.9%) were postulated as a potential reason why efficacy was not observed. Although the species used for the ppb/btb assays is not noted, it is assumed that this is mouse or rat data. As it has been found that there is little variation in btb across species [75], the

btb data can be used to calculate both mouse and rat free brain concentrations from the *in vivo* efficacy studies. Hence it is unclear why similar total (and therefore free) brain concentrations result in amyloid lowering in the rat but not the Tg2576 mouse. An alternative explanation for the lack of efficacy in the Tg2576 mouse could be because it overexpresses the Swedish mutant APP which is known to be a better BACE substrate and therefore poses a higher hurdle to reduce amyloid production. In a follow-up study, the efficacy of SPI-1865 was assessed in CD1 mice at doses of 15, 30 and 50 mg/kg b.i.d. for 6 days, with efficacy measured 6 h after the final dose. Brain $A\beta_{42}$ levels were reduced at all doses, by 22%, 39% and 47%, respectively, while brain $A\beta_{38}$ levels were reduced by 30% and 28% in the 30 and 50 mg/kg groups only. The brain concentrations from this study were measured at 3.6, 8.7 and 22 μM at doses of 15, 30 and 50 mg/kg, respectively. Thus, similar levels of brain $A\beta_{42}$ reduction were observed at similar brain concentrations in the CD1 mouse and rat but not in the Tg2576 mouse. Thus, the fact that efficacy is observed in non-transgenic mice but not Tg2576 mice is consistent with the hypothesis above, that lack of efficacy in Tg2576 mice is due to the overexpression of the Swedish mutant form of APP. Calculation of the free brain concentrations from the CD1 mouse study results in values of 4, 9 and 22 nM for the dose groups 15, 30 and 50 mg/kg, respectively, all of which are considerably lower than the *in vitro* IC_{50} value of 106 nM. The calculated $Br_u:Pl_u$ ratio for the three ascending dose groups are 0.05, 0.08 and 0.12 which implies active efflux.

Unfortunately, it has recently been disclosed that the development of SPI-1865 has been halted due to the finding that it disrupted adrenal function in monkeys, an observation that is believed to be unrelated to γ -secretase modulation.

While the Satori work has established that complex natural product derivatives with multiple HBA/HBD motifs can penetrate the CNS to some extent, the pre-clinical efficacy appears somewhat limited, perhaps more so than the other series discussed herein. The fact that SPI-1865 did not prove efficacious in the Tg2576 model, despite achieving similar free and total brain concentrations that were efficacious in the wild-type mouse and rat, should raise considerable concern [74].



3. CHEMICAL BIOLOGY

A frustration for researchers working on γ -secretase over the years has been the lack of structural information and a desire to improve the understanding of the mechanism of action of GSMs. A crystal structure of a presenilin homologue PSH has recently appeared [76], but a solved crystal

structure of γ -secretase in complex with a modulator is still some way off. In recent years, there have been some elegant studies conducted to elucidate the binding site of different modulator chemotypes.

The Pfizer group in conjunction with academic collaborators has used piperidine acetic acid derivative (**80**) (Figure 3.18) to elucidate the binding site of compounds from this series [77]. Incubation with HeLa membranes containing the γ -secretase complex, followed by UV irradiation, caused loss of nitrogen with concomitant covalent bond formation with nearby proteins. Azide cycloaddition onto the acetylene group with a streptavidin containing moiety allowed capture. Western blot analysis revealed the compound bound to the N-terminal fragment (NTF) of presenilin-1. The binding could be blocked by pre-incubation with related piperidine acid GSMs. Further work with a photoaffinity-labelled orthosteric substrate revealed that compounds from the piperidine acetic acid series bind to an allosteric site and enhance the labelling of the orthosteric substrate in the S1 pocket but not the S2, S1' or S3' pockets.

Weggen *et al.* have conducted similar work, using a diazirine moiety in place of the azide, which allows use in live cells. (**81**) (AR243) (Figure 3.18),

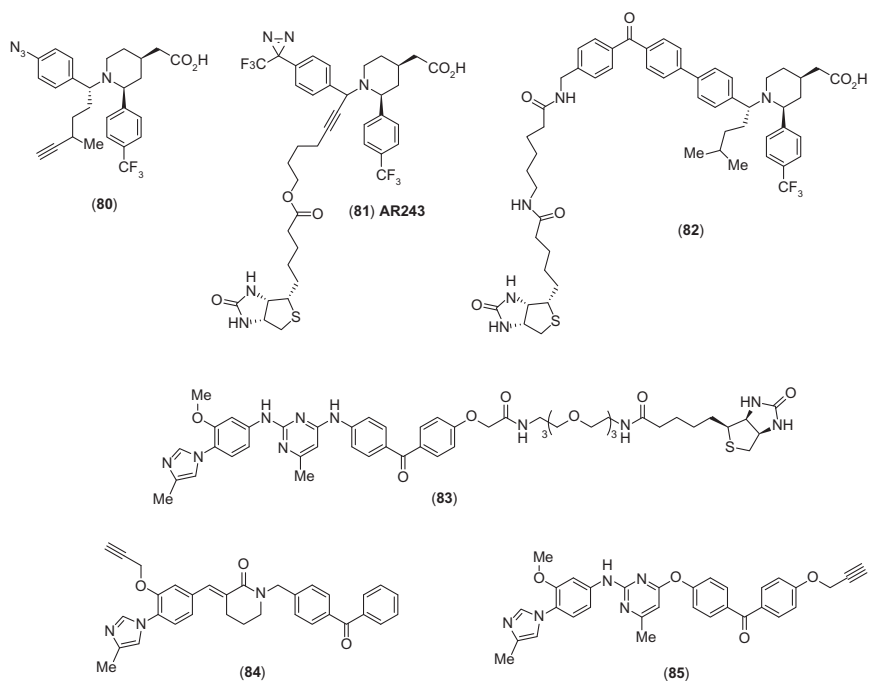


Figure 3.18 Structures of photoaffinity labelling probes.

with a biotin tag incorporated to allow affinity purification, was also found to bind to the NTF of presenilin-1 following irradiation of N2a-NPP cells which stably overexpress APP and the four γ -secretase subunits [78]. In related work, the same group found that (81) binding to presenilin-1 NTF was blocked by (4) [15,79]. A non-acid derivative from the Merck series of compounds, a close analogue of compound (50) (Figure 3.11), was also able to block the binding of (81) as effectively as the acid derivatives. Compounds (12) (Figure 3.4) and (17) (Figure 3.5) also diminished the binding of the probe to some extent; with the effect of (17) being weak, implying that there may be a partial overlap of binding sites for the two distinct modulator series.

A further recent publication [80], describes the utilisation of (82) (Figure 3.18) as a ligand, this time with a benzophenone photoactivation group. Photoaffinity labelling experiments were conducted on mouse brain microsomes which revealed (82) bound to the NTF of presenilin-1. Further studies confirmed an allosteric-binding site, and that ligands of this class modulate the conformation of the orthosteric-binding site, shifting it to an 'open form'. More detailed experiments have refined the binding site to a lipophilic region on the extracellular/luminal side of the transmembrane domain 1 (TMD1). These results counter the rationale that the free concentrations needed for *in vivo* efficacy are not applicable, as the binding site is neither on the intracellular surface nor deep within the cell membrane.

Photoaffinity labelling studies have also been conducted on compounds from the imidazole and related series, that is, those derived from the Eisai and TorreyPines Therapeutics templates (Figure 3.4). To this end, a photoaffinity probe Ro-57-BpB (83) (Figure 3.18) derived from a Roche GSM has been prepared and studied [81]. Surprisingly, (83) was found not only to label presenilin-1 NTF but also presenilin-2 NTF when HEK293 cell membranes were irradiated in the presence of 1 μ M (83). Presenilin-2 labelling was more pronounced. The binding could be blocked by Eisai compounds such as (12) (Figure 3.4), but interestingly one TorreyPines Therapeutics derivative blocked the binding while another did not. A piperidine acetic acid derivative (GSM-1), which is a close analogue of (5) (Figure 3.3), weakly diminished the labelling of presenilin-1 by (83) but more strongly diminished the labelling of presenilin-2 by (83). Again this is somewhat surprising as the studies discussed earlier have identified the NTF of presenilin-1 as the binding site for ligands such as GSM-1. A recent publication has detailed similar work using ligands E2012-Bpyne (84) and RO-57-Byne (85) [82] (Figure 3.18). Utilising HeLa cell membranes, both (84) and (85) were found to bind to presenilin-1 NTF. No binding to

presenilin-2 NTF was observed, in contrast to that observed for (83). Similar results were obtained in H4 cells overexpressing wild-type APP. The binding of (84) to presenilin-1 NTF was blocked by E2102, but not by GSM-1 from the piperidinyl acetic acid class. In complementary studies, it was shown that the binding to presenilin-1 by probe (80) could be blocked by a compound from the same series (GSM1) but not by E2012. Further studies revealed that orthosteric ligands enhance the binding of (84) to presenilin-1 NTF, which is driven by an increase in affinity in the presence of an orthosteric ligand.

In summary, the consensus is that GSMs bind to the NTF domain of presenilin-1, although there may be some binding of particular ligands to presenilin-2 NTF, and the dependency of the probe and assay systems requires verification. It seems that the binding site of GSMs from the two structural classes may be complementary or even partially overlap, although this could be due to the nature of the photoaffinity group used and the length and position of the linker employed in each probe. Additionally, some probes contain the capture group (biotin with a linker) already in place which may also affect binding. Going forward, it would be interesting to see if compounds with a different modulatory profile, for example, those from Satori and other novel structural classes, also bind to presenilin-1 NTF, and determine if this binding site overlaps or is complementary to the acid and imidazole derivatives. Needless to say, all researchers actively involved in the γ -secretase field would welcome a detailed crystal structure with each class of modulator to give a definitive understanding of how and where these ligands bind to enable further medicinal chemistry efforts.



4. OUTLOOK

A considerable amount of research has been expended on the acid series. Despite the efforts of many research groups to optimise the potency of these derivatives, limited success has been achieved. Driving potency down to below 100 nM and into single digit nanomolar potency range has proved a significant challenge. That, coupled with the high lipophilicity of these analogues, has posed a huge hurdle to the identification of the next generation of clinical candidates. Discovering compounds with good ADME properties and even CNS penetration has not been a challenge for these classes. However, these properties may be linked to the extremely high plasma protein and brain tissue binding of these derivatives and this gives rise to other issues. Additionally, there

appears to be no direct correlation with efficacious *in vivo* concentrations and *in vitro* activity data, and equally the corresponding free plasma or brain concentrations are out of step with *in vitro* values. One explanation for the discrepancy between free concentrations in *in vivo* and *in vitro* data could be because the binding site of the γ -secretase complex is on the inner side of the plasma membrane and it is possible that the intracellular and extracellular concentrations are not equal due to active influx or efflux. However, this hypothesis is not supported by the work of Iwatsubo and colleagues who have found that the binding site, at least for the acid modulators, is a hydrophobic region on the extracellular side on TMD1 of presenilin-1 [80,83] which would therefore predict that free concentrations should be reflective of those at the binding site. Binding kinetics could also play an important role, as a slow off-rate could influence this aspect. An alternative explanation would be that the total concentrations more accurately mimic the *in vitro* activity as all assays are whole cell assays which require the presence of serum albumin or equivalent. It would be expected that this would also be the case for another AD target, β -secretase (BACE) where cell assays are also used. However, in the case of BACE many groups have reported a good correlation between cellular IC_{50} values and *in vivo* free plasma/brain concentrations.

With all these facts in mind, it seems many research groups have now terminated their effort on the acid derivatives and instead shifted to the Eisai/TorreyPines Therapeutics imidazole series and related derivatives. Again, despite many years of sustained research by many companies, there has been limited success in terms of compounds entering clinical development, only Eisai, with E2012 and E2212, have done so thus far. As with the acid series, identifying compounds with good *in vivo* ADME properties is generally not an issue with these derivatives. However, there have been numerous other issues observed such as hERG inhibition, CYP450 inhibition and high plasma and brain tissue binding, all of which are linked to the high lipophilicity of the compounds from this series. Furthermore, as with the acid series, there appears to be no direct correlation between total (plasma and brain) concentrations and *in vivo* efficacy. The total concentrations achieved are far in excess of *in vitro* activity and the calculated free concentrations are almost always inferior to *in vitro* activity values. Achieving high levels of efficacy *in vivo* has also presented a considerable challenge to researchers in the GSM field, and compared to BACE inhibitors, the efficacy achieved with GSMs seems considerably weaker, although this is obviously influenced by the brain extraction reagents used. Taken

together, it appears that there remain daunting hurdles to overcome in this field. Sustained effort may bear fruit as evidenced by the progress made by the Janssen group.

5. CLINICAL STUDIES

(R)-Flurbiprofen (**1**), CHF 5074 (**2**) (Figure 3.1), EVP-0962 (**3**) (Figure 3.2), E2012 and E2212 are the only GSMs for which information in the public domain shows that they have entered clinical trials (Figure 3.19).

(R)-Flurbiprofen (**1**) was evaluated in a large Phase III trial where patients with mild AD were dosed with 800 mg b.i.d. [84]. There was no significant improvement in the cognitive decline or activities of daily living over the 18-month trial period. The failure of this trial may be attributed to its failure to reduce amyloid in humans, most likely due to its weak γ -secretase modulatory activity, ($A\beta_{42}$ IC₅₀ = 307 μ M) [85]. This hypothesis is supported by data from early clinical trials which showed the compound failed to have any effect on CSF $A\beta_{42}$ levels, although modest acute

Development status of γ -secretase modulators

Active research	Pre-clinical	Phase I	Phase II	Phase III
Amgen Astellas Biogen Idec BMS Boehringer Ingelheim Dainippon Sumitomo EnVivo Janssen/J&J Merck Pfizer Roche Shionogi Takeda	BMS	E2212 (Eisai)	EVP-0015962 (EVP-0962 (EnVivo) CHF5074 (Chiesi)	
Active Discontinued AstraZeneca Eisai GSK Torrey Pines Therapeutics	JNJ-42601572 (Janssen) JNJ-40418677 (Janssen) SPI-1865 (Satori) BIIB042 (Biogen)	E2012 (Eisai)	Flurizan (Myriad)	

Figure 3.19 Proposed current status of GSM development based on press releases and published patent applications.

reductions in plasma $A\beta_{42}$ levels were observed [86,87]. Analysis of the pre-clinical data for (*R*)-flurbiprofen reveals that it reduced formic acid extracted brain $A\beta_{42}$ in 3-month-old Tg2576 mice following oral administration for 3 days at doses of 10, 25 and 50 mg/kg, $n = 3/\text{dose}$, by 26%, 60% and 34%, respectively [88]. The lack of dose–response could be explained by the drug concentrations in plasma (83, 117 and 78 μM at 10, 25 and 50 mg/kg, respectively) which also did not show a linear increase with dose. Despite the fact that the plasma drug levels were reported to be similar to that achieved in humans at therapeutic doses (131–483 μM), the total brain concentrations in the Tg2576 mouse study were 1.5, 2.6 and 2.5 μM at 10, 25 and 50 mg/kg, respectively, which are far below the compound's *in vitro* IC_{50} . Thus, it is unclear how the compound elicits its efficacy pre-clinically, however, the lack of dose–response and the disconnect between *in vivo* brain concentrations and *in vitro* activity may provide a clue as to the failure to reduce amyloid in a clinical setting.

CHF5074 (**2**) (Figure 3.1) is another carboxylic acid agent that has advanced into clinical trials with the pre-clinical evidence indicating that the compound has weak GSM activity ($\text{IC}_{50} = 3.6 \mu\text{M}$) [89]. The clinical data to date have failed to demonstrate that this agent modulates the $A\beta_{42}$ levels in man. The compound is still progressing; however, the mode of action has been rebranded as modulation of microglial activation, based on recent clinical data, from its Phase II trial [90] where it showed effects on $\text{TNF}\alpha$ and sCD40L. There have been no reports on the effect on $A\beta_{42}$ levels in this trial. CereSpir has recently released a letter of intent to say they intend to licence worldwide development and commercialisation rights to CHF5074 (**2**) [91].

Further information, released by EnVivo Pharmaceuticals, has indicated that EVP-0962 (**3**) (Figure 3.2) achieved sufficient exposure in man to warrant advancing this molecule into Phase II clinical trials [92].

E2012 was the first imidazole derivative GSM to enter clinical trials and some data has been presented from these trials at recent conferences. Pre-clinical data for E2012 has demonstrated that the molecule reduces the production of $A\beta_{40}$ and $A\beta_{42}$ in rat primary cortical neurones ($\text{IC}_{50} = 100 \text{ nM}$) with an increase in $A\beta_{1-38}$ being measured [93]. There was no accumulation of APP-CTF and no inhibition of the production of notch intracellular domain (NICD) indicating that E2012 has the characteristics of a Notch-sparing GSM [94]. In an acute dosing study in the rat, oral administration of E2012 (10 and 30 mg/kg, oral) reduced plasma, brain and CSF levels of $A\beta_{40}$ and $A\beta_{42}$ in a dose-dependent manner by approximately 50% over

a 12 h period [93]. Data for E2012 from a single ascending dose study in human volunteers demonstrated a dose-dependent increase in drug plasma concentrations between 1 and 800 mg [95]. A dose-dependent reduction in A β_{42} levels was reported above 50 mg with a 53% reduction in plasma A β_{42} reported at the 400 mg dose [95]. Although there have been no public announcements, there are currently no clinical trials listed for this compound and it does not appear on the company pipeline at the FY2012 Financial Results Presentation on 13 May 2013 [96].

E2212 has one single ascending dose trial listed which was scheduled for completion in November 2012 [97]. There is no publicly available information on the current status of this compound and it also did not appear on the recent company pipeline presentation [96].

Several other companies appear to have progressed compounds to the pre-clinical development stage, such as Biogen Idec, GSK, Janssen and Satori. However, it seems the development of these compounds has been terminated based on either press releases or the lack of reported development or listed clinical trials. As discussed previously, BMS has recently disclosed that they have a GSM around the pre-clinical development stage, and thus appear to be one of the companies that have made recent progress.



6. CONCLUSIONS

There has been a considerable effort by scientists to identify potent and safe GSMs. A number of different pharmacophores have been explored with varying degrees of success. Several compounds have advanced into clinical trials but as yet there is no sign of a successful drug emerging from these efforts. Based on the continued publications of patents, some which have been reported in this chapter, there is still on-going activity in this field. Safety and efficacy remain the main challenges in developing drugs for this target.

Although considerable challenges remain in the GSM field, the BACE field is making good progress with compounds moving through the clinical development pipeline, several of which have demonstrated near full reductions in CSF amyloid. Thus, although the BACE field appears more likely to deliver an answer to the amyloid hypothesis in the near term, researchers who have worked in the amyloid area for a sustained period will appreciate that favour has fluctuated from γ -secretase to β -secretase and back several times. Thus, sustained effort is required, as disease modifying or disease

retarding drugs are urgently required to address the huge burden imposed by AD on individuals, carers, family and the healthcare systems.

REFERENCES

- [1] Thies W, Bleiler L. 2013 Alzheimer's disease facts and figures. *Alzheimers Dement* 2013;9(2):208–45.
- [2] Tanzi RE. The genetics of Alzheimer disease. *Cold Spring Harb Perspect Med* 2012; 2(10):a006296.
- [3] Selkoe DJ, Wolfe MS. Presenilin: running with scissors in the membrane. *Cell* 2007;131(2):215–21.
- [4] Osenkowski P, Ye W, Wang R, Wolfe MS, Selkoe DJ. Direct and potent regulation of gamma-secretase by its lipid microenvironment. *J Biol Chem* 2008;283 (33):22529–40.
- [5] Osenkowski P, Li H, Ye W, Li D, Aeschbach L, Fraering PC, et al. Cryoelectron microscopy structure of purified gamma-secretase at 12 Å resolution. *J Mol Biol* 2009;385(2):642–52.
- [6] Jonsson T, Atwal JK, Steinberg S, Snaedal J, Jonsson PV, Bjornsson S, et al. A mutation in APP protects against Alzheimer's disease and age-related cognitive decline. *Nature* 2012;488(7409):96–9.
- [7] Oehlrich D, Berthelot DJ, Gijzen HJ. Gamma-secretase modulators as potential disease modifying anti-Alzheimer's drugs. *J Med Chem* 2011;54(3):669–98.
- [8] Hopkins CR. ACS chemical neuroscience molecule spotlight on BMS-708163. *ACS Chem Neurosci* 2012;3(3):149–50.
- [9] Hopkins CR. ACS chemical neuroscience molecule spotlight on ELND006: another gamma-secretase inhibitor fails in the clinic. *ACS Chem Neurosci* 2011;2(6):279–80.
- [10] Doody RS, Raman R, Farlow M, Iwatsubo T, Vellas B, Joffe S, et al. A phase 3 trial of semagacestat for treatment of Alzheimer's disease. *N Engl J Med* 2013;369(4):341–50.
- [11] Hopkins CR. ACS chemical neuroscience molecule spotlight on Begacestat (GSI-953). *ACS Chem Neurosci* 2012;3(1):3–4.
- [12] Mullane K, Williams M. Alzheimer's therapeutics: continued clinical failures question the validity of the amyloid hypothesis-but what lies beyond? *Biochem Pharmacol* 2013;85(3):289–305.
- [13] Pettersson M, Kauffman GW, am Ende CW, Patel NC, Stiff C, Tran TP, et al. Novel gamma-secretase modulators: a review of patents from 2008 to 2010. *Expert Opin Ther Pat* 2011;21(2):205–26.
- [14] Pettersson M, Stepan AF, Kauffman GW, Johnson DS. Novel gamma-secretase modulators for the treatment of Alzheimer's disease: a review focusing on patents from 2010 to 2012. *Expert Opin Ther Pat* 2013;23:1349–66.
- [15] Bulic B, Ness J, Hahn S, Rennhack A, Jumpertz T, Weggen S. Chemical biology, molecular mechanism and clinical perspective of gamma-secretase modulators in Alzheimer's disease. *Curr Neuropharmacol* 2011;9(4):598–622.
- [16] Heneka MT, Kummer MP, Weggen S, Bulic B, Multhaup G, Munter L, et al. Molecular mechanisms and therapeutic application of NSAIDs and derived compounds in Alzheimer's disease. *Curr Alzheimer Res* 2011;8(2):115–31.
- [17] Pignatello R, Panto V, Salmaso S, Bersani S, Pistara V, Kepe V, et al. Flurbiprofen derivatives in Alzheimer's disease: synthesis, pharmacokinetic and biological assessment of lipoamino acid prodrugs. *Bioconjug Chem* 2008;19(1):349–57.
- [18] Sivilia S, Lorenzini L, Giuliani A, Gusciglio M, Fernandez M, Baldassarro VA, et al. Multi-target action of the novel anti-Alzheimer compound CHF5074: in vivo study of long term treatment in Tg2576 mice. *BMC Neurosci* 2013;14:44.

- [19] Van BB, Chen JM, Treton G, Desmidt M, Hopf C, Ramsden N, et al. Chronic treatment with a novel gamma-secretase modulator, JNJ-40418677, inhibits amyloid plaque formation in a mouse model of Alzheimer's disease. *Br J Pharmacol* 2011;163(2):375–89.
- [20] Gijzen HJ, Mercken M. Gamma-secretase modulators: can we combine potency with safety? *Int J Alzheimers Dis* 2012;2012:295207. <http://dx.doi.org/10.1155/2012/295207>, Epub@2012 Dec 17.
- [21] Rogers K, Felsenstein KM, Hrdlicka L, Tu Z, Albayya F, Lee W, et al. Modulation of γ -secretase by EVP-0015962 reduces amyloid deposition and behavioral deficits in Tg2576 mice. *Mol Neurodegener* 2012;7:61.
- [22] Blurton P, Burkamp F, Churcher I, Harrison T, Neduveilil J, inventors. Arylacetic acids and related compounds and their preparation, pharmaceutical compositions and their use for treatment of diseases associated with the deposition of β -amyloid peptides in the brain such as Alzheimer's disease. Patent WO2006008558A1; 2006.
- [23] Hall A, Elliott RL, Giblin GM, Hussain I, Musgrave J, Naylor A, et al. Piperidine-derived gamma-secretase modulators. *Bioorg Med Chem Lett* 2010;20(3):1306–11.
- [24] Hawkins J, Harrison DC, Ahmed S, Davis RP, Chapman T, Marshall I, et al. Dynamics of Abeta42 reduction in plasma, CSF and brain of rats treated with the gamma-secretase modulator, GSM-10h. *Neurodegener Dis* 2011;8(6):455–64.
- [25] Hussain I, Harrison DC, Hawkins J, Chapman T, Marshall I, Facci L, et al. TASTPM mice expressing amyloid precursor protein and presenilin-1 mutant transgenes are sensitive to gamma-secretase modulation and amyloid-beta(4)(2) lowering by GSM-10 h. *Neurodegener Dis* 2011;8(1–2):15–24.
- [26] Stanton MG, Hubbs J, Sloman D, Hamblett C, Andrade P, Angagaw M, et al. Fluorinated piperidine acetic acids as gamma-secretase modulators. *Bioorg Med Chem Lett* 2010;20(2):755–8.
- [27] Peng H, Talreja T, Xin Z, Cuervo JH, Kumaravel G, Humora MJ, et al. Discovery of BIIB042, a potent, selective, and orally bioavailable Γ^{23} -secretase modulator. *ACS Med Chem Lett* 2011;2(10):786–91.
- [28] Xin Z, Peng H, Zhang A, Talreja T, Kumaravel G, Xu L, et al. Discovery of 4-aminomethylphenylacetic acids as gamma-secretase modulators via a scaffold design approach. *Bioorg Med Chem Lett* 2011;21(24):7277–80.
- [29] Am E, Fish BA, Johnson DS, Lira R, O'Donnell CJ, Pettersson MY, et al., inventors. Aminocyclohexanes and aminotetrahydropyrans as γ -secretase modulators and their preparation and use for the treatment of neurological and psychiatric diseases. Patent WO2011092611A1; 2011.
- [30] Yamasaki S, Honjo E, Samizu K, Kuroda A, Yonezawa K, Hayashibe S, et al., inventors. Preparation of cycloalkane compounds as γ secretase modulators. Patent WO2012046771A1; 2012.
- [31] Kimura T, Kawano K, Doi E, Kitazawa N, Shin K, Miyagawa T, et al., inventors. Preparation of cinnamide, 3-benzylidenepiperidin-2-one, phenylpropynamide compounds as amyloid β production inhibitors. Patent WO2005115990A1; 2005.
- [32] Yngve U, Paulsen K, Macsari I, Sundstrom M, Santangelo E, Linde C, et al. Triazolopyrimidinones as [gamma]-secretase modulators: structure-activity relationship, modulator profile, and in vivo profiling. *Med Chem Commun* 2013;4(2):422–31.
- [33] Portelius E, Van BB, Andreasson U, Gustavsson MK, Mercken M, Zetterberg H, et al. Acute effect on the Abeta isoform pattern in CSF in response to gamma-secretase modulator and inhibitor treatment in dogs. *J Alzheimers Dis* 2010;21(3):1005–12.
- [34] Kounnas MZ, Danks AM, Cheng S, Tyree C, Ackerman E, Zhang X, et al. Modulation of gamma-secretase reduces beta-amyloid deposition in a transgenic mouse model of Alzheimer's disease. *Neuron* 2010;67(5):769–80.

- [35] Wan Z, Hall A, Jin Y, Xiang JN, Yang E, Eatherton A, et al. Pyridazine-derived gamma-secretase modulators. *Bioorg Med Chem Lett* 2011;21(13):4016–9.
- [36] Eatherton AJ, Giblin GMP, Hall A, Johnson MR, Le J, Mitchell WL, et al., inventors. Pyridazine derivatives for inhibiting β -amyloid peptide production and their preparation, pharmaceutical compositions and use in the treatment of Alzheimer's disease. Patent WO2009050227A1; 2009.
- [37] Wan Z, Hall A, Sang Y, Xiang JN, Yang E, Smith B, et al. Pyridine-derived gamma-secretase modulators. *Bioorg Med Chem Lett* 2011;21(16):4832–5.
- [38] Huang Y, Li T, Eatherton A, Mitchell WL, Rong N, Ye L, et al. Orally bioavailable and brain-penetrant pyridazine and pyridine-derived gamma-secretase modulators reduced amyloidogenic Abeta peptides in vivo. *Neuropharmacology* 2013;70:278–86. <http://dx.doi.org/10.1016/j.neuropharm.2013.02.003>, Epub@2013 Feb 26.
- [39] Lubbers T, Flohr A, Jolidon S, David-Pierson P, Jacobsen H, Ozmen L, et al. Aminothiazoles as gamma-secretase modulators. *Bioorg Med Chem Lett* 2011;21(21):6554–8.
- [40] Bischoff F, Berthelot D, De CM, Macdonald G, Minne G, Oehlich D, et al. Design and synthesis of a novel series of bicyclic heterocycles as potent gamma-secretase modulators. *J Med Chem* 2012;55(21):9089–106.
- [41] Borghys H, Tuefferd M, Van B, Clessens E, Dillen L, Cools W, et al. A canine model to evaluate efficacy and safety of γ -secretase inhibitors and modulators. *J Alzheimers Dis* 2012;28(4):809–22.
- [42] Oehlich D, Rombouts FJ, Berthelot D, Bischoff FP, De Cleyn MA, Jaroskova L, et al. Design and synthesis of bicyclic heterocycles as potent gamma-secretase modulators. *Bioorg Med Chem Lett* 2013;23(17):4794–800.
- [43] Cuss F. BMS_Cowen Healthcare Conference March 2013. 3–3–2013.
- [44] Marcin LR, Thompson LA, III, Boy KM, Guernon JM, Higgins MA, Shi J, et al., inventors. Preparation of bicyclic compounds, especially bicyclic triazoles, for the reduction of beta-amyloid protein production. Patent WO2010083141A1; 2010.
- [45] Boy KM, Guernon JM, Macor JE, Olson RE, Shi J, Thompson LA, III, et al., inventors. Preparation of fused pyrimidine compounds as modulators of β -amyloid production. Patent WO2011014535A1; 2011.
- [46] Boy KM, Guernon JM, Macor JE, Olson RE, Shi J, Thompson LA, III, et al., inventors. Preparation of bicyclic pyrimidine compounds for the reduction of β -amyloid production. Patent WO2012103297A1; 2012.
- [47] Boy KM, Guernon JM, Macor JE, Thompson LA, III, Wu YJ, Zhang Y, inventors. Preparation of macrocyclic compounds fused to benzene and pyrimidine rings for the reduction of beta-amyloid production. Patent WO2012009309A1; 2012.
- [48] Allen MP, Am E, Brodney MA, Dounay AB, Johnson DS, Pettersson MY, et al., inventors. Preparation of phenylimidazole derivatives and analogs for use as gamma-secretase modulators. Patent WO2010100606A1; 2010.
- [49] Am E, Johnson DS, O'Donnell CJ, Pettersson MY, Subramanyam C, inventors. Preparation of heteroaryl imidazoles and heteroaryl triazoles as γ -secretase modulators. Patent WO2011048525A1; 2011.
- [50] Pettersson M, Johnson DS, Subramanyam C, Bales KR, am Ende CW, Fish BA, et al. Design and synthesis of dihydrobenzofuran amides as orally bioavailable, centrally active gamma-secretase modulators. *Bioorg Med Chem Lett* 2012;22(8):2906–11.
- [51] Am E, Fish BA, Green ME, Johnson DS, Mullins PB, O'Donnell CJ, et al., inventors. Preparation of pyrido[1,2-a]pyrazine-1,6-dione derivatives as γ -secretase modulators. Patent WO2012131539A1; 2012.
- [52] Rivkin A, Ahearn SP, Chichetti SM, Kim YR, Li C, Rosenau A, et al. Piperaziny pyrimidine derivatives as potent gamma-secretase modulators. *Bioorg Med Chem Lett* 2010;20(3):1269–71.

- [53] Rivkin A, Ahearn SP, Chichetti SM, Hamblett CL, Garcia Y, Martinez M, et al. Purine derivatives as potent gamma-secretase modulators. *Bioorg Med Chem Lett* 2010;20(7):2279–82.
- [54] Fischer C, Shah S, Hughes BL, Nikov GN, Crispino JL, Middleton RE, et al. Quinazolinones as gamma-secretase modulators. *Bioorg Med Chem Lett* 2011;21(2):773–6.
- [55] Fischer C, Zultanski SL, Zhou H, Methot JL, Brown WC, Mampreian DM, et al. Triazoles as gamma-secretase modulators. *Bioorg Med Chem Lett* 2011;21(13):4083–7.
- [56] Fischer C, Zultanski SL, Zhou H, Methot JL, Shah S, Nuthall H, et al. Triazoloamides as potent gamma-secretase modulators with reduced hERG liability. *Bioorg Med Chem Lett* 2012;22(9):3140–6.
- [57] Caldwell JP, Bennett CE, McCracken TM, Mazzola RD, Bara T, Buevich A, et al. Iminoheterocycles as gamma-secretase modulators. *Bioorg Med Chem Lett* 2010;20(18):5380–4.
- [58] Huang X, Aslanian R, Zhou W, Zhu X, Qin J, Greenlee W, et al. The discovery of pyridone and pyridazone heterocycles as $\tilde{\Gamma}^3$ -secretase modulators. *ACS Med Chem Lett* 2010;1(4):184–7.
- [59] Qin J, Dhondi P, Huang X, Mandal M, Zhao Z, Pissamitski D, et al. Discovery of fused 5,6-bicyclic heterocycles as gamma-secretase modulators. *Bioorg Med Chem Lett* 2011;21(2):664–9.
- [60] Qin J, Zhou W, Huang X, Dhondi P, Palani A, Aslanian R, et al. Discovery of a potent pyrazolopyridine series of $\tilde{\Gamma}^3$ -secretase modulators. *ACS Med Chem Lett* 2011;2(6):471–6.
- [61] Gerlach K, Heine N, Hobson S, Hoenke C, Weber A, inventors. Preparation of dihydrothienopyrimidines γ -secretase modulators. Patent WO2013020992A1; 2013.
- [62] Nishitomi K, Kano K, Kato I, Sako Y, inventors. Preparation of pharmaceutical products containing heterocyclic sulfonamide compounds as γ -secretase modulators. Patent WO2010126002A1; 2010.
- [63] Kato I, Kano K, inventors. Preparation of lactam or benzenesulfonamide compounds as inhibitors for production of amyloid β protein. Patent WO2011007819A1; 2011.
- [64] Iwama S, Nakagawa H, Kato Y, inventors. Oxadiazole derivative as therapeutic agent for β -amyloid-associated neuropsychiatric disorders. Patent WO2011001931A1; 2011.
- [65] Iwama S, Kato Y, Kobayashi T, Fusano A, inventors. Preparation of 4-(1H-imidazol-1-yl)benzamide and (1H-imidazol-1-yl)pyridinecarboxamide derivatives as beta amyloid 42 production inhibitors. Patent WO2011059048A1; 2011.
- [66] Iwama S, Ikeda T, Kobayashi T, inventors. Preparation of 4-(4-pyridinyl)phenyl-substituted fused 1,2,4-triazole derivatives as inhibitors of beta-amyloid production. Patent WO2012057300A1; 2012.
- [67] Gijzen HJM, Mercken M. γ -Secretase modulators: can we combine potency with safety? *Int J Alzheimers Dis* 2012;2012: Article ID 295207.
- [68] Gijzen HJM, Bischoff FP. Secretase inhibitors and modulators as a disease-modifying approach against Alzheimer's disease. *Annu Rep Med Chem* 2012;47:55–69.
- [69] Findeis MA, Schroeder F, McKee TD, Yager D, Fraering PC, Creaser SP, et al. Discovery of a novel pharmacological and structural class of gamma secretase modulators derived from the extract of *Actaea racemosa*. *ACS Chem Neurosci* 2012;3(11):941–51.
- [70] Austin WF, Hubbs JL, Fuller NO, Creaser SP, McKee TD, Loureiro RMB, et al. SAR investigations on a novel class of gamma-secretase modulators based on a unique scaffold. *Med Chem Commun* 2013;4(3):569–74.
- [71] Fuller NO, Hubbs JL, Austin WF, Creaser SP, McKee TD, Loureiro RMB, et al. Initial optimization of a new series of γ -secretase modulators derived from a triterpene glycoside. *ACS Med Chem Lett* 2012;3(11):908–13.

- [72] Hubbs JL, Fuller NO, Austin WF, Shen R, Creaser SP, McKee TD, et al. Optimization of a natural product-based class of γ -secretase modulators. *J Med Chem* 2012;55(21):9270–82.
- [73] Tate B, McKee TD, Loureiro RM, Dumin JA, Xia W, Pojasek K, et al. Modulation of gamma-secretase for the treatment of Alzheimer's disease. *Int J Alzheimers Dis* 2012;2012:210756. <http://dx.doi.org/10.1155/2012/210756>, Epub@2012 Dec@19.
- [74] Loureiro RM, Dumin JA, McKee TD, Austin WF, Fuller NO, Hubbs JL, et al. Efficacy of SPI-1865, a novel gamma-secretase modulator, in multiple rodent models. *Alzheimers Res Ther* 2013;5(2):19.
- [75] Di L, Umland JP, Chang G, Huang Y, Lin Z, Scott DO, et al. Species independence in brain tissue binding using brain homogenates. *Drug Metab Dispos* 2011;39(7):1270–7.
- [76] Li X, Dang S, Yan C, Gong X, Wang J, Shi Y. Structure of a presenilin family intramembrane aspartate protease. *Nature* 2013;493(7430):56–61.
- [77] Crump CJ, Fish BA, Castro SV, Chau DM, Gertsik N, Ahn K, et al. Piperidine acetic acid based β -secretase modulators directly bind to presenilin-1. *ACS Chem Neurosci* 2011;2(12):705–10.
- [78] Weggen S, Beher D. Molecular consequences of amyloid precursor protein and presenilin mutations causing autosomal-dominant Alzheimer's disease. *Alzheimers Res Ther* 2012;4(2):9.
- [79] Jumpertz T, Rennhack A, Ness J, Baches S, Pietrzik CU, Bulic B, et al. Presenilin is the molecular target of acidic gamma-secretase modulators in living cells. *PLoS One* 2012;7(1):e30484.
- [80] Ohki Y, Higo T, Uemura K, Shimada N, Osawa S, Berezovska O, et al. Phenylpiperidine-type gamma-secretase modulators target the transmembrane domain 1 of presenilin 1. *EMBO J* 2011;30(23):4815–24.
- [81] Ebke A, Luebbers T, Fukumori A, Shirotani K, Haass C, Baumann K, et al. Novel gamma-secretase enzyme modulators directly target presenilin protein. *J Biol Chem* 2011;286(43):37181–6.
- [82] Pozdnyakov N, Murrey HE, Crump CJ, Pettersson M, Ballard TE, am Ende CW, et al. Gamma-secretase modulator (GSM) photoaffinity probes reveal distinct allosteric binding sites on presenilin. *J Biol Chem* 2013;288(14):9710–20.
- [83] Tomita T, Iwatsubo T. Structural biology of presenilins and signal peptide peptidases. *J Biol Chem* 2013;288:14673–80.
- [84] Green RC, Schneider LS, Amato DA, Beelen AP, Wilcock G, Swabb EA, et al. Effect of tarenfluril on cognitive decline and activities of daily living in patients with mild Alzheimer disease: a randomized controlled trial. *JAMA* 2009;302(23):2557–64.
- [85] Narlawar R, Perez Revuelta BI, Haass C, Steiner H, Schmidt B, Baumann K. Scaffold of the cyclooxygenase-2 (COX-2) inhibitor carprofen provides Alzheimer gamma-secretase modulators. *J Med Chem* 2006;49(26):7588–91.
- [86] Wilcock GK, Black SE, Hendrix SB, Zavitz KH, Swabb EA, Laughlin MA. Efficacy and safety of tarenfluril in mild to moderate Alzheimer's disease: a randomised phase II trial. *Lancet Neurol* 2008;7(6):483–93.
- [87] Galasko DR, Graff-Radford N, May S, Hendrix S, Cottrell BA, Sagi SA, et al. Safety, tolerability, pharmacokinetics, and Abeta levels after short-term administration of R-flurbiprofen in healthy elderly individuals. *Alzheimer Dis Assoc Disord* 2007;21(4):292–9.
- [88] Eriksen JL, Sagi SA, Smith TE, Weggen S, Das P, McLendon DC, et al. NSAIDs and enantiomers of flurbiprofen target gamma-secretase and lower Abeta 42 in vivo. *J Clin Invest* 2003;112(3):440–9.
- [89] Imbimbo BP, Del GE, Colavito D, D'Arrigo A, Dalle CM, Villetti G, et al. 1-(3',4'-Dichloro-2-fluoro[1,1'-biphenyl]-4-yl)-cyclopropanecarboxylic acid (CHF5074), a novel gamma-secretase modulator, reduces brain beta-amyloid pathology in a

- transgenic mouse model of Alzheimer's disease without causing peripheral toxicity. *J Pharmacol Exp Ther* 2007;323(3):822–30.
- [90] Ross J, Sharma S, Winston J, Nunez M, Bottini G, Franceschi M, et al. CHF5074 reduces biomarkers of neuroinflammation in patients with mild cognitive impairment: a 12-week, double-blind, placebo-controlled study. *Curr Alzheimer Res* 2013;10(7):742–53.
- [91] CereSpir Announcement. <http://www.cerespir.com/072613b.htm>. 1–8-2013.
- [92] En Vivo EVP0962 Press release, <http://www.envivopharma.com/news-item.php?id=44>; 2013.
- [93] Hashimoto T, Ishibashi A, Hagiwara H, Murata Y, Takenaka O, Miyagawa T. E2012: a novel gamma-secretase modulator-pharmacology part. *Alzheimers Dement* 2010;6(4):S242.
- [94] Amino H, Hagiwara H, Murata Y, Watanabe H, Sasaki T, Miyagawa T. E2012: a novel gamma-secretase modulator-mechanism of action. *Alzheimer's Dement* 2010;6(4):S541–S542.
- [95] Nagy C, Schuck E, Ishibashi A, Nakatani Y, Rege B, Logovinsky V. E2012, a novel gamma-secretase modulator, decreases plasma amyloid-beta (A β) levels in humans. *Alzheimer's Dement* 2010;6(4):S574.
- [96] Eisai Financial Update 1st May 2013. http://www.eisai.com/pdf/eir/emat/e4523_130513.pdf; 1–5-2013.
- [97] E2212 clinical trials. <http://clinicaltrials.gov/ct2/show/NCT01221259?intr=E2212&rank=1>; 2013.



Recent Progress in the Discovery and Development of N-Type Calcium Channel Modulators for the Treatment of Pain

Margaret S. Lee

Research & Translational Medicine, Zalicus Inc., Cambridge MA, USA

Contents

1. Introduction	147
2. Voltage-Gated Calcium Channels	148
2.1 Ca_v Channel Architecture	148
2.2 Ca_v Channel Physiology	152
2.3 Ca_v Channel States	154
2.4 Implications for Therapeutic Intervention	155
3. N-Type Calcium Channels	156
3.1 N-Type Biology	156
3.2 N-Type Physiology	157
3.3 Role in the Pathophysiology of Pain	158
4. N-Type Clinical Landscape and Emerging Pipeline	159
4.1 Peptide-Derived Therapeutics	159
4.2 Small Molecule N-Type Blockers	164
4.3 N-Type Calcium Channel Modulators in the Clinic	177
5. Concluding Remarks	178
References	179

Keywords: Voltage-gated calcium channel, N-type calcium channel, State-dependent, Use-dependent, Pain, ω -Conotoxin, Inactivation, $Ca_v2.2$, CACNA1B



1. INTRODUCTION

The superfamily of ion channels encompasses a diverse set of multi-subunit pore complexes capable of transporting a variety of monovalent and divalent ions, both positive and negative, across cellular membranes

in response to signals ranging from tactile, thermal, chemical to electrical. As the name suggests, the family of ion channels categorized as voltage-gated calcium channels (VGCCs) transport calcium ions into the cell in response to changes in plasma membrane voltage. The VGCC family consists of at least 10 distinct subtypes defined by genetically distinct $\alpha 1$ subunits and characterized by a spectrum of biophysical properties, tissue distribution and biological functions (see [Table 4.1](#)). The importance of VGCCs to basic physiological processes such as cardiac and neurological function has generated decades of intense interest in these proteins as targets of pharmacological intervention. The fruits of this investment are presently exemplified by L-type calcium channel blockers, a class of approved drugs useful in cardiac arrhythmias, hypertension and angina.

The targeting of VGCCs found in the central and peripheral nervous system for therapeutic intervention is also an area of intense interest and investigation, although relatively fewer approved drugs have emerged from these efforts. In particular, both N-type and T-type calcium channels play a role in neuronal hyper-excitability and the pathophysiology of hyper-excitability disorders including pain and epilepsy. The approved N-type calcium channel blocker ziconotide provides crucial human validation of the importance of this target in pain. However, with the approval of ziconotide now nearly a decade in the past, we have not yet seen additional N-type blockers entering the market. Several recent and comprehensive reviews discuss multiple individual aspects of VGCC biology, physiology and pharmacology. This review will focus on N-type calcium channels as targets for pain drugs and attempt to highlight recent advances and clinically relevant findings. Peer reviewed and patent literature for the past decade was considered with an emphasis on new findings of the past 5 years.



2. VOLTAGE-GATED CALCIUM CHANNELS

2.1. Ca_v Channel Architecture

Our understanding of the structure of VGCCs comes from endogenous channels purified from tissue membranes and from crystallization and modelling of bacterial ion channels. VGCCs are multi-subunit complexes composed of an $\alpha 1$ subunit of approximately 190 kDa responsible for the formation of the calcium transporting pore and defined by individual genes ([Table 4.1](#)). The pore forming $\alpha 1$ subunit is found in complex with a single cytoplasmic β subunit, a transmembrane γ subunit and an extracellular oriented disulphide linked $\alpha 2\delta$ dimer ([Figure 4.1](#)). The large $\alpha 1$ subunit

Table 4.1 Voltage-Gated Calcium Channel Types, Nomenclature and Relevance

Category	Type	Channel Type	$\alpha 1$ Subunit	Gene Name	Localization	Therapeutic Relevance	Pharmacology
HVA	L-type	Ca _V 1.1	$\alpha 1S$	CACNA1S	Skeletal muscle		Dihydropyridines
		Ca _V 1.2	$\alpha 1C$	CACNA1C	Cardiac muscle, endocrine cells, neurons	Cardiovascular disorders	Phenylalkamines Benzothiazepines
		Ca _V 1.3	$\alpha 1D$	CACNA1D	Endocrine cells, neurons	Parkinsons disease, cardiac arrhythmia	
		Ca _V 1.4	$\alpha 1F$	CACNA1F	Retina		
Neuronal P/Q-type	N-type	Ca _V 2.1	$\alpha 1A$	CACNA1A	Nerve terminals, dendrites	Epilepsy, migraine	ω -Agatoxin IVA ω -Conotoxin MVIIC
		Ca _V 2.2	$\alpha 1B$	CACNA1B	Nerve terminals, dendrites	Pain	ω -Conotosin GVIA, MVIIA, CVID
		Ca _V 2.3	$\alpha 1E$	CACNA1E	Cell bodies, nerve terminals, dendrites	Diabetes	SNX-482
LVA	T-type	Ca _V 3.1	$\alpha 1G$	CACNA1G	Cardiac muscle, skeletal muscle, neurons	Cardiac arrhythmia, epilepsy, hypertension, sleep disorders	Nickel Ethosuximide Zonisamide
		Ca _V 3.2	$\alpha 1H$	CACNA1H	Cardiac muscle, neurons	Pain, epilepsy	Mibefradil Kurtoxin
		Ca _V 3.3	$\alpha 1I$	CACNA1I	neurons	Sleep disorders, epilepsy	

From [1–5].

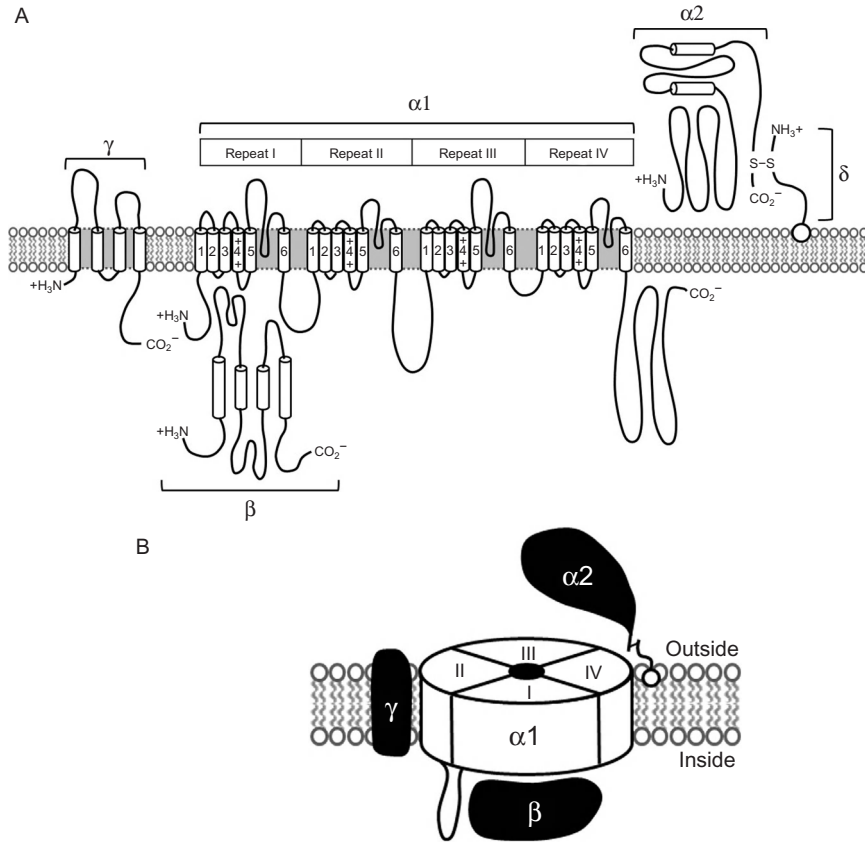


Figure 4.1 Subunit architecture of VGCCs. (A) Schematic of VGCC subunits illustrating plasma membrane topology and transmembrane spanning sequences. Sequences predicted to be α -helical are shown as cylinders. The glycosphosphatidylinositol anchor of the δ subunit is illustrated as a circle. (B) Schematic of the three-dimensional architecture of VGCCs illustrating the fourfold symmetry of the $\alpha 1$ pore forming subunit.

consists of four repeating domains each consisting of six transmembrane sequences each with an intervening membrane-embedded loop that defines the voltage sensing domain. These loops participate in the binding of regulatory proteins and contribute to pharmacological selectivity.

Models of the three-dimensional structure of Ca_V channels, built through image reconstruction techniques and similarities to crystallized bacterial ion channel subunits, give clues to the functional organization of the $\alpha 1$ subunit. These models predict fourfold symmetrical organization of the repeating transmembrane domains of the $\alpha 1$ subunit into a pore forming unit tightly bound to the scaffold-like β subunit which extends into the

cytoplasm. The transmembrane helices S5 and S6 and the intervening pore loop or P-loop of each repeated domain together form the inner lining of the pore with a pair of glutamate residues in each P-loop defining selectivity for calcium ions. Channel opening is tightly regulated by conformational changes in the voltage sensing domains of each of the four repeated domains. These so-called S4 segments move outwards into the membrane with a twisting motion in response to membrane depolarization, resulting in a conformational change that allows pore opening [6,7]. These general structural features are conserved across the Ca_V family of channels although the amino acid sequences of the S6 segments, which confer selectivity for L-type VGCC pore blocking antagonists, are found only in the Ca_V1 channels. It is generally accepted that venom peptide toxins act as pore blockers of the $\text{Ca}_V2.2 \alpha1$ subunit, although the specific structural and peptidic determinants of binding are complex and not clearly elucidated. The residues involved in peptide binding have been mapped to the external vestibule of the pore, in the S5–S6 region of the third repeat domain; however, binding interactions can be further modulated by channel subunit composition and membrane voltage. Notably, multiple splice variants of the $\text{Ca}_V2.2 \alpha1$ subunit have been identified, some with differential expression in the central and peripheral nervous system and others with differential selectivity to ω -conotoxins [8].

While expression of the $\alpha1$ subunit can be sufficient to form functional channels, expression at the plasma membrane, voltage dependence and channel gating characteristics are heavily influenced by the β subunit and to a lesser extent $\alpha2\delta$ and γ subunits. Models of channel three-dimensional architecture suggest tight interactions between channel subunits and predict the $\alpha1$, γ and δ subunits embedded in the lipid membrane and the β and $\alpha2$ subunits extending into the cytoplasm and extracellular space, respectively. The $\alpha2$ subunit is tightly linked through disulphide bonding with the δ subunit (formed through post-translational cleavage of the $\alpha2$ subunit).

The $\text{Ca}_V \beta$ subunit was first purified from skeletal muscle VGCC complexes, and subsequent molecular biology efforts resulted in the cloning and sequencing of four distinct subfamilies of $\text{Ca}_V \beta$ subunits ($\beta1$ – $\beta4$) [9] each encoded by distinct genes with multiple possible splice variants. $\text{Ca}_V \beta$ subunits bind with high affinity to the cytoplasmic linker region connecting repeat domains 1 and 2 of the Ca_V1 and $\text{Ca}_V2 \alpha1$ subunit [10–12]. Crystal structures of the $\text{Ca}_V \beta$ subunit have revealed that this ‘ α interaction domain’ or AID binds to a hydrophobic groove in the $\text{Ca}_V \beta$ subunit causing dramatic changes to the secondary structure of the AID region resulting in

the formation of rigid and continuous α helical structures that are important for the regulation of calcium channel gating [9]. The $\text{Ca}_v \beta$ subunit also plays an important role in channel surface expression, degradation and intracellular signalling pathways regulating channel function (reviewed in [13] and [9]).

The $\text{Ca}_v \alpha 2\delta$ subunit is important in both the sub-cellular trafficking and plasma membrane localization of the channel as well as in modulation of biophysical and pharmacological properties. It is formed by post-translational proteolytic cleavage into distinct $\alpha 2$ and δ peptides which remain tethered by disulphide bonds [14,15]. The δ subunit anchors the heterodimer to the plasma membrane via a glycosylphosphatidylinositol linker [16] while the $\alpha 2$ subunit extends entirely into the extracellular space [8,13,17]. There are four subtypes designated $\alpha 2\delta$ 1–4. Isoforms 1 and 2 are the targets of the gabapentinoid drugs gabapentin and pregabalin [8,18–20]. The molecular mechanism of gabapentinoid drug action after binding to the $\alpha 2\delta$ subunit is not fully understood, but it is thought to result in downregulation of $\text{Ca}_v 2.2$ sub-cellular trafficking as well as regulation of $\text{Ca}_v 2.2$ channel currents [13,20–22].

The γ subunit is relatively less well studied than other VGCC subunits, but is now understood to be defined by a family of eight genes with differential expression in skeletal muscle and brain. The protein consists of four transmembrane sequences, with intracellular N- and C-terminal domains. Three-dimensional architectural models of Ca_v channels based on cryo-electron microscopy propose tight interactions between the γ subunit and the $\alpha 1$ subunit [17]. While the effects of the γ subunit are highly dependent on the profile of other subunits in the complex, in general they result in small reductions in current, mainly caused by a hyperpolarizing shift in the voltage dependence of inactivation and/or a positive shift in the voltage dependence of activation [13]. The recent discovery that mutations in the $\gamma 2$ subunit underlie the stargazer mouse model of absence epilepsy highlights the importance of the γ subunit in regulating normal VGCC function [23].

2.2. Ca_v Channel Physiology

When defined by physiological and pharmacological calcium current characteristics, VGCCs are further subdivided into high voltage-activated (HVA) and low voltage-activated (LVA) channels, distinguished by the membrane potential at which channel opening occurs [17]. The LVA channels open at relatively lower membrane potentials (–55 to –20 mV) [24], are rapidly inactivated (1–5 ms) and recover from inactivation relatively

more slowly. Also called T-type in reference to their rapid voltage-dependent inactivation, and thus transient nature, T-type channels and the $\text{Ca}_v3 \alpha 1$ subunits associated with them are widely distributed throughout the central nervous system (CNS) and peripheral nervous system (PNS) as well as visceral innervation. Of the HVA channels, L-type or Long-acting channels of the Ca_v1 family demonstrate relatively slower voltage-dependent inactivation (1–5 s) and channel activation at relatively higher membrane potentials (+30 to +50 mV) [25–28]. These form the major Ca_v channels in cardiac, smooth and skeletal muscle and are defined pharmacologically by their sensitivity to inhibition by dihydropyridines (DHPs), phenylalkylamines and benzothiazepines [17]. Ca_v2 channels, initially described by current recordings in dorsal root ganglion (DRG) neurons, activate at intermediate membrane potentials and inactivation rates. Ca_v2 channels are pharmacologically distinct from the L-type Ca_v1 channels in their insensitivity to small molecule L-type blockers. The Ca_v2 family is now known to consist of N-, P-, Q- and R-type channels which all demonstrate intermediate physiological properties with pre-synaptic N- and P/Q-type channels being the predominant mechanism initiating neurotransmitter release. Defined by three distinct genes, this group can be further categorized pharmacologically by their exquisite selectivity to the peptide toxins found in the venom of spiders, scorpions and marine snails (summarized in [17]). In particular, N-type channels are defined by the binding and inhibition by cone snail peptide ω -conotoxin peptides [29].

The families of Ca_v channels share some common characteristics of voltage-dependent gating. All are stimulated to open in response to positive changes in membrane voltage and demonstrate voltage-dependent inactivation. As mentioned earlier, voltage-dependent channel opening or activation occurs in response to membrane depolarization, resulting in the outwards movement and rotation of $\alpha 1$ S4 segments, producing a conformational change that allows pore opening [6,7]. After channel opening, the resulting influx of calcium ions leads to further membrane depolarization, activation of additional ion channels (sodium and potassium) and the formation of the ascending phase of the action potential. In parallel, membrane depolarizations result in voltage-dependent inactivation and channel closure. This negative feedback loop (along with the voltage-dependent activation of outwards potassium currents) determines the duration of the action potential.

$\text{Ca}_v \beta$ subunits are important regulators of voltage-dependent gating. All $\text{Ca}_v \beta$ s shift the voltage dependence of channel activation to more

hyperpolarized membrane voltages by about 10–15 mV [13]. Channels without a β subunit tend to open less frequently, for a shorter duration, and require more positive activation voltages [13]. $\text{Ca}_V \beta$ (with the exception of $\text{Ca}_V \beta 2a$) subunits also shift the voltage dependence of inactivation to more hyperpolarized voltages by approximately 10–20 mV, thus in the presence of these subunits, weaker membrane depolarizations are able to inactivate VGCCs [13]. Voltage-dependent gating of Ca_V channels is also regulated by a number of intracellular factors including binding of the β/γ subunits of hetero-trimeric G-proteins to $\text{Ca}_V \alpha 1$ subunit.

2.3. Ca_V Channel States

Calcium channels reside in several different conformational states that are closely interconnected and modulated by electrical fields, associated auxiliary subunits, signalling molecules and calcium concentrations. These conformations include closed or resting, activated or open and several inactivated states [30]. The differential kinetics of voltage-dependent channel transition from one conformational state to another is an important feature of channel function and regulation. Channel activation (i.e. transition from closed to open conformation) occurs on a timescale of milliseconds, while recovery from inactivation (i.e. transition from inactivated to resting conformation) is substantially slower, occurring on a timescale of tens of milliseconds or seconds. These differential kinetics of channel state transitions, along with changes in resting membrane potential, result in differing proportions of calcium channels in any given state. Calcium channels dwell in the inactivated conformation for longer than in the open conformation and must recover from inactivation before being able to open again. Thus, if the frequency of action potentials is such that a membrane depolarization arrives before recovery from inactivation is complete, subsequent channel opening, and therefore Ca_V -dependent current, is reduced. The magnitude of the cell's resting membrane potential significantly impacts the steady-state populations of closed and inactivated channels, with more depolarized voltages resulting in a higher probability of channel inactivation. The steady-state equilibrium between resting and inactivated states therefore dictates the ability of Ca_V channels to respond to action potentials [30].

It has been reported that the intracellular loop linking repeat domains 1 and 2 play a role in voltage-dependent inactivation through an interaction with the ends of the S6 segments, effecting a physical block of the channel pore [31]. An analogous mechanism of conformational change resulting in

pore blockade is seen with sodium and potassium channels [31]. This intracellular loop is also a key determinant for binding of the cytoplasmic β subunit, so important in the regulation of voltage dependence, as well as being a binding site for modulatory G-proteins.

2.4. Implications for Therapeutic Intervention

The multiple subunit compositions, splice variants, expression patterns and conformational states of Ca_V channels result in staggering diversity in this target class. This is in addition to the fact that there are multiple intracellular signalling molecules and processes that are tightly linked to Ca_V channel function. This diversity offers opportunities for engineering molecular and functional selectivity in pharmacological agents. The notion of use-dependent inhibition of channel function is of particular interest. As the name suggests, a use-dependent inhibitor would demonstrate differential activity depending on the physiological 'use' of the channel. One manifestation of such 'use' would be found in situations where a Ca_V channel is undergoing high frequency firing, such as occurs during rapid trains of action potentials. In this situation, the impact of rapid membrane potential changes on the populations of various channel conformational states, and their associated constellation of signalling complexes, creates a distinct molecular profile of the channel population involved in this type of 'use'. This distinct profile offers an opportunity to develop agents with pharmacological selectivity for channels undergoing this type of use. A subset of use dependence is referred to as state dependence. In this case, a pharmacologic agent may have greater affinity for a particular conformational state of the channel (closed, open and inactivated) and thus be most effective when channels are predominantly found in this state. The concept of use dependence has important implications for the clinical use of Ca_V channel blockers. This is illustrated by the clinically important dihydropyridine (DHP) class of L-type calcium channel blockers widely used in treatment of angina, hypertension and cardiac arrhythmias. These drugs demonstrate voltage- and use-dependent channel block [32,33]. High-affinity DHP binding to the $\text{Ca}_V1.2$ channel has been mapped to amino acids deep within the hydrophobic transmembrane sequences of repeats 3 and 4 of the $\alpha1$ subunit, a region important in channel inactivation [31], and it is facilitated by calcium binding in the selectivity filter region [34]. Current models suggest that DHP binding prevents Ca_V channel conductance by stabilizing a non-conducting, blocked conformation of the outer pore [34]. Similarly, many anti-epileptic drugs exert their therapeutic action by modifying the inactivation properties of voltage-

gated sodium channels [35]. It may be possible, by targeting a specific state of VGCCs, to selectively target channels functioning in a pathological manner while sparing channels operating under normal physiological states [36].



3. N-TYPE CALCIUM CHANNELS

3.1. N-Type Biology

The N-type or Neuronal-type VGCCs were originally described on the basis of current recordings in dissociated DRG neurons, distinguishable from L-type currents by their voltage dependence and inactivation rate as well as insensitivity to classical L-type channel blockers [37]. Further described by the cloning and sequencing of the $\alpha 1B$ subunit and defined pharmacologically as $Ca_v2.2$ by ω -conotoxin sensitivity, the N-type channel is prominently expressed at synapses in the somatic and autonomic components of the peripheral nervous system and some synapses in the central nervous system [38–41]. In cooperation with P/Q-type channels ($Ca_v2.1$ $\alpha 1A$) calcium entry through N-type channels is responsible for triggering neurotransmitter release through exocytosis from pre-synaptic vesicles [42,43]. In the somatic nervous system, N-type channels are concentrated in the pre-synaptic nerve terminals in lamina I and II of the dorsal horn of the spinal cord and are prominently overexpressed in response to injury that induces chronic neuropathic pain [41,44]. In the perivascular nerve network, N-type channels are expressed in the synapses of vascular smooth muscle, equivalently in vein and artery. Under high frequency stimulus of post-ganglionic perivascular nerves, release of the co-transmitters norepinephrine and ATP from artery smooth muscle cells is modulated by N-type channels and P/Q-type channels, respectively, thereby playing a role in fine tuning of vascular tone by the autonomic nervous system [45]. Indeed early experiments with ω -conotoxin GVIA, a potent peptide inhibitor of N-type calcium channels (see below) in rat mesenteric artery neurons, demonstrated a role for N-type channels in the frequency-dependent contraction of artery smooth muscle cells [46].

Investigation of N-type channels in heterologous expression systems and in native sympathetic and hippocampal neurons suggests that alternative splicing in the S3–S4 repeat linkers of $Ca_v2.2$ results in modulation of channel gating kinetics and not steady-state voltage dependence [47]. These effects appear to be regulated by differential association of auxiliary Ca_v β subunits with important binding sites in this region. Expression of the Ca_v β subunit increases channel conductance by at least 10-fold in

heterologous expression systems [48]. The $\text{Ca}_v\beta$ subtype plays a critical role in modulating the voltage dependence and inactivation properties of the N-type channel.

3.2. N-Type Physiology

As is true of all Ca_v2 channels, the N-type channel opens in response to moderate levels of membrane depolarization, opening at higher potentials than T-types but lower than L-type channels. N-type channels tend to show slower kinetics of activation than T-types but return from open to closed states with relatively fast kinetics and at less negative voltages as membranes repolarize. This biophysical profile is well suited to channel conductance occurring only after achievement of action potential thresholds and where channels can rapidly reset in response to membrane repolarizations. Additionally, the kinetics of inactivation and recovery from inactivation of N-type channels are relatively slower than those of T-types, with inactivation being favoured at higher frequency depolarizations [49]. Inactivation of N-type channels would appear to preferentially occur via the closed channel state where the channel moves directly from the closed to the inactivated state under conditions of sub-threshold depolarizations [50]. The biophysical and kinetic properties of N-type channel inactivation and recovery suggest that under tonic conditions, that is, low frequency action potentials with adequate time for full membrane repolarization, N-type channels are relatively resistant to inactivation. In contrast, under conditions such as high frequency action potential firing, where repetitive membrane depolarizations result in increased transition between open and closed states and reduced repolarization potentials, access to the inactivated state would increase resulting in accumulation in an inactivated state [49]. By this model, some degree of accumulation in the inactivated state would occur in response to any action potential train, but the high frequency action trains characteristic of damaged neurons would favour a greatly increased inactivated population. Given that pathological pain is characterized by spontaneous and persistent activation of primary afferent neurons [29], and that neurons of the somatic peripheral nervous system can signal at frequencies of up to 100 Hz during transmission of painful signals, this accumulation could have profound implications to the selective targeting of analgesic drugs [36]. Targeting the inactivated channel state may afford an opportunity to selectively modulate pathological pain signalling while sparing normal, low frequency autonomic functions of central and peripheral control [36].

3.3. Role in the Pathophysiology of Pain

A pivotal role for N-type channels in the pathophysiology of pain has been demonstrated by numerous lines of pre-clinical and clinical evidence. Mice lacking the N-type $\text{Ca}_v2.2$ $\alpha1\text{B}$ subunit demonstrate reduced pain responses and modified anxiolytic and reward behaviours, but are otherwise normal [51–53] with the exception of reduced baroreflex function and elevated heart rate and blood pressure [54]. This is in contrast to the phenotype associated with P/Q-type $\text{Ca}_v2.1$ $\alpha1\text{A}$ subunit knockout which, in addition to reduced pain responses, demonstrates severe ataxia, absence seizures and early death, suggesting additional important functions outside pain signal transmission and sympathetic nerve function [55]. These results highlight the importance of N-type channels to functional pain signal transmission, as well as emphasizing the importance of selectivity over the P/Q-type channel in the development of pain therapeutics. The expression of N-type channels at crucial pre-synaptic terminals also supports a critical role in synaptic transmission and neurotransmitter release. Numerous pharmacological experiments with the exquisitely selective peptide toxins from the venoms of marine snails, spiders and scorpions provide further support for the role of N-type channels in pain. This body of work has demonstrated anti-nociceptive effects of specific conotoxins with known selectivity for N-type channel pore block [29]. Perhaps, the strongest evidence validating the N-type calcium channel in the pathophysiology of human pain is the ability of the currently marketed drug ziconotide, a synthetic conotoxin peptide indicated to treat severe chronic cancer or AIDS pain, to afford, in some cases, complete or near complete relief in patients whose pain was found to be unmanageable even by the intrathecal administration of morphine [56–58]. Ziconotide block by occlusion of the channel pore does not discriminate between different frequencies of action potential firing and thus, unfortunately, demonstrates no apparent selectivity for the inactivated state of the channel. This lack of selectivity for high frequency firing states of the N-type channel is widely believed to be responsible for the narrow therapeutic window associated with ω -conotoxin peptides which show profound effects on tonic N-type channel function in the autonomic nervous system, particularly the perivascular nerves. These results further emphasize the need for more selective, use-dependent N-type calcium channel blockers with an improved therapeutic window.



4. N-TYPE CLINICAL LANDSCAPE AND EMERGING PIPELINE

4.1. Peptide-Derived Therapeutics

4.1.1 N-Type Blockade by Venom Toxins

The venoms of predatory marine snails and terrestrial arthropods such as spiders and scorpions contain a diverse array of peptide toxins, many with highly potent binding to mammalian voltage-gated ion channels. In particular, the venom of the marine snails in the family *Conidae* contains many different small, cysteine-rich, disulphide-bridged peptides, with diverse pharmacology against voltage-gated ion channels. The diversity, pharmacology, structure–activity relationships and therapeutic potential of these so-called conotoxins have been recently and comprehensively reviewed [8,59–61]. Perhaps, the most well studied of these are the ω -conotoxins (Figure 4.2) which are single- to double-digit nanomolar inhibitors of VGCCs and have demonstrated effects in a wide variety of neuropathic and inflammatory pain models (reviewed in [29]). Our understanding of the pharmacology of ω -conotoxins is derived largely from studies of ω -conotoxins GVIA, MVIIA and CVID, isolated from *Conus geographus*, *C. magus* and *C. catus*, respectively, which are generally considered to function as irreversible $\alpha 1$ subunit pore blockers, and are now appreciated to be among some of the most selective known inhibitors of N-type channels [60,63–65]. The ω -conotoxin binding site has been mapped to the external vestibule of the channel in the S5–S6 linker region of the $\alpha 1$ subunit repeat domain 3 [66,67] and reciprocal residues critical for ω -conotoxin activity in this respect have also been mapped [68,69]. While the specific amino acid residues responsible for conferring selectivity of particular ω -conotoxins to different Ca_v2 channels are still under investigation, it appears that the homogeneity of peptide loops 2 and 4 within the conotoxin secondary structure is an important determinant of differential selectivity between the Ca_v2 channel subtypes [70]. It is also clear that the presence of $\alpha 2\delta$ and β subunits as well as the membrane potential can have profound effects on the affinity and reversibility of binding of ω -conotoxins to $\text{Ca}_v \alpha 1$ subunits, thus further increasing the diversity of pharmacological effects among this class of peptides [71–74]. Compared to the cone snail, relatively fewer peptide blockers with specificity for N-type channels have been identified

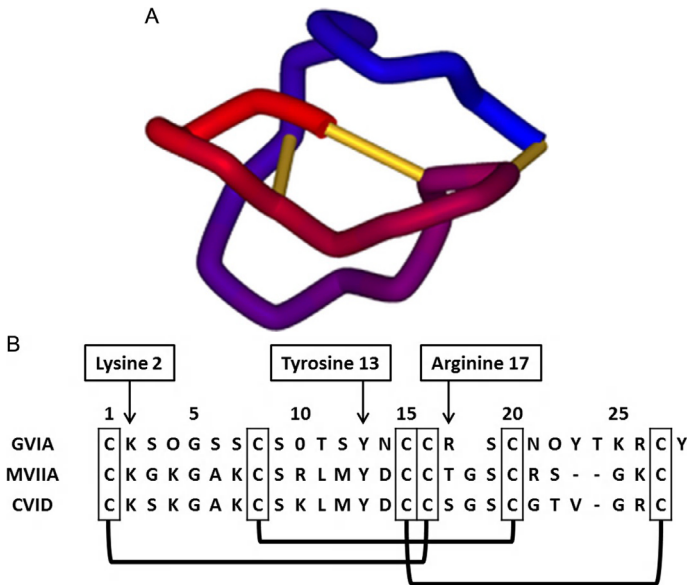


Figure 4.2 ω -Conotoxin peptide and three-dimensional structures. (A) Three-dimensional structure of ω -conotoxin MVIIA showing a compact folded structure linked by three disulphide bonds between cysteine residues [62]. (B) Peptide sequence of ω -conotoxins GVIA, MVIIA and CVID. Critical cysteine residues are boxed and bold lines indicate disulphide linkages. Residues important for N-type channel binding are indicated.

from the venoms of terrestrial arthropods [8,75]. Recently, certain peptide toxins from the Chinese bird spider *Orthinoctonus huwena* (huwentoxins), funnel web spider *Agelenopsis aperta* (agatoxins) and the South American armed spider *Phoneutria nigriventer* have been described as selective inhibitors of N-type calcium channel currents and some share common structural motifs with ω -conotoxins, although continued research will be required to further understand their level of selectivity as compared to ω -conotoxins [8,76,77].

4.1.2 Peptide-Derived Therapeutics

The only FDA approved ω -conotoxin is a synthetic version of MVIIA, also known as SNX-111, ziconotide and Prialt, supplied as a solution for intrathecal infusion. This peptide demonstrates picomolar binding affinity

to N-type calcium channels in rat brain membranes or synaptosomes and single- to double-digit nanomolar potency in electrophysiological studies of the function of both native and recombinant N-type channels (reviewed in [78]). Ziconotide displays greater than 1000-fold selectivity over other Ca_v2 channels and has demonstrated efficacy in a number of non-clinical pain models [29,78]. Ziconotide was approved in the United States in 2004 and in Europe in 2005 and is indicated for the management of severe chronic pain in patients for whom intrathecal therapy is warranted and who are intolerant or refractory to other treatments such as systemic analgesics, adjunctive therapies or intrathecal morphine. The clinical efficacy of ziconotide was established in three randomized, double-blind placebo-controlled trials (reviewed in [78]) without any evidence of the development of tolerance [79] or the risk of withdrawal symptoms. While randomized controlled trials of ziconotide only evaluated the drug's efficacy as a monotherapy, non-clinical and open label clinical studies with ziconotide in combination with other analgesic drugs have generated evidence supporting the potential for additive or synergistic effects [80,81]. Despite ziconotide's advantages over intrathecal opioids, its use has been hampered by a high incidence of CNS side effects. The most commonly reported adverse events include dizziness, nausea, confusional state and nystagmus; severe psychiatric symptoms and neurological impairment have also been observed. In particular, events of acute psychiatric disturbances such as hallucinations, paranoid reactions and some types of psychosis have been reported [82]. Importantly, the use of ziconotide is limited to intrathecal administration due to severe effects on blood pressure, heart rate and the baroreceptor-heart rate reflex after systemic administration [83,84] probably resulting from blockade of N-type calcium channel function in the sympathetic neurons responsible for haemodynamic control [78,85–87].

Leuconotide, a synthetic version of ω -conotoxin CVID (also known as AM336 and CNSB004) has been evaluated in human clinical trials [78,88]. It is reported to be more effective than ziconotide in non-clinical pain models and demonstrates fewer cardiovascular side effects [83,89]. Recent reports suggest that intravenous administration of leuconotide can cause significant reversal of hyperalgesia in a rat model of diabetic neuropathy with a wider therapeutic window than ziconotide and can enhance the effects of other opioid and non-opioid analgesics when used in combination [90,91]. These effects may be due in part to the enhanced ability of leuconotide to discriminate between Ca_v2 subtypes, demonstrating similar

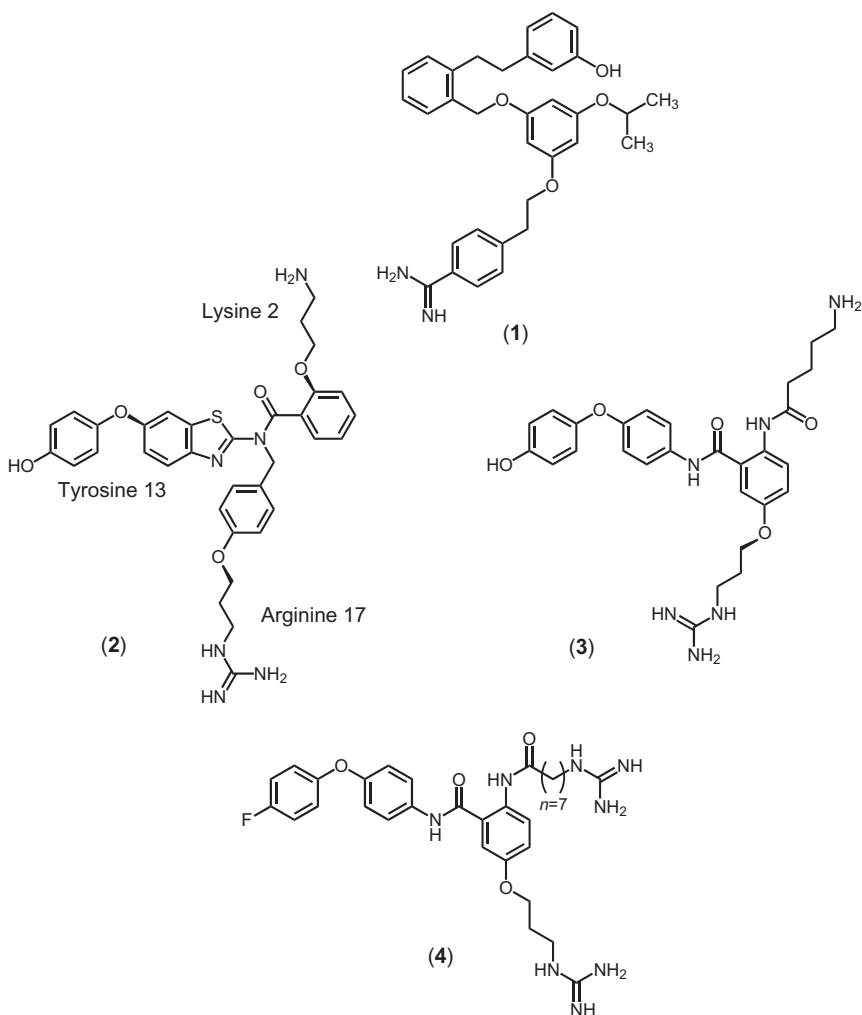
potency at N-type channels as ω -conotoxin MVIIA but with 100-fold greater selectivity over P/Q-type VGCCs [65]. Relevare Pharmaceuticals (formerly CNSBio) reports that a placebo-controlled Phase IIa clinical trial of leuconotide in cancer patients with intractable severe pain is ready to start in the near future [92].

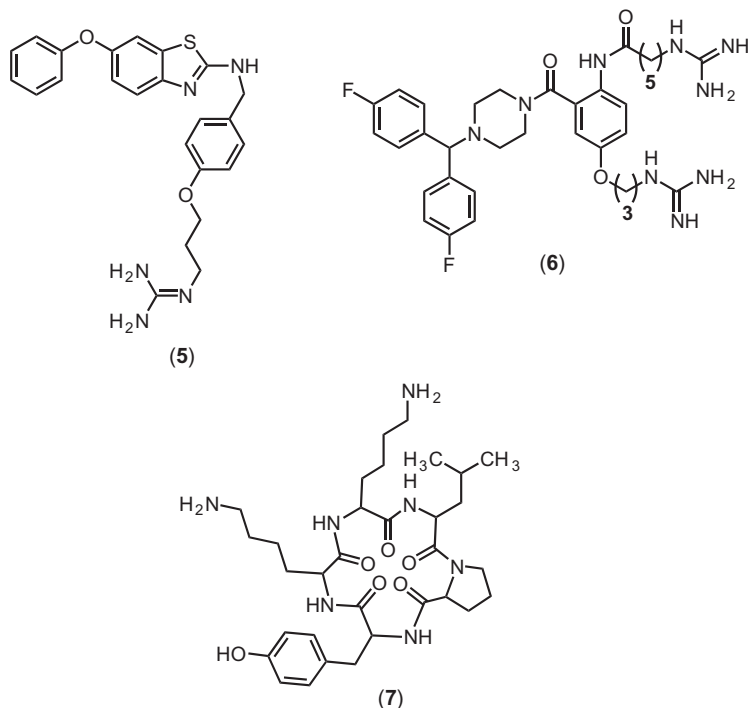
Other venom peptide toxins of therapeutic importance include huwentoxins isolated from species of the Chinese bird spider. Huwentoxin-I and -X both demonstrate selectivity for N-type channels over other VGCCs as well as voltage-gated sodium or potassium channels [76,77]. Structure predictions for huwentoxin-X suggest that this peptide adopts the same cysteine knot motif characteristic of ω -conotoxins [76]. Inventors from Xiamen Bioway Biotech have published patents describing therapeutic preparations of huwentoxin-I [93]. Also described are methods and compositions for blocking calcium channels with Ph α -1B (ω -ctenitoxin-Pn4a), a toxin isolated from the spider *P. nigriventer* [93–96]. Additionally, novel ω -conotoxins continue to be discovered and characterized, providing increasing opportunities to understand the therapeutic potential of venom peptide toxins [97].

4.1.3 Peptide Mimetics

The therapeutic validation of peptide blockers of N-type VGCCs in pain has encouraged several approaches to rationally design organic small molecules that mimic the binding properties of peptide toxins (reviewed in [98]). Alkylphenyl ether-based analogues of MVIIA that incorporate the side chains of MVIIA Arg10, Leu11 and Tyr13 into a central aromatic core have been reported (1) [99–101]. Using *in silico* approaches to overlay bond vectors of key residues in ω -conotoxin GVIA, residues Lys2, Tyr13 and Arg17 were mimicked with benzothiazole (2) and anthranilamide (3) scaffolds [102–104] demonstrating low single digit micromolar affinity in displacement of radio-labelled ω -conotoxin GVIA from rat brain membranes and selectivity for the N-type channel over Ca_v2.1 [104]. Further modification of the anthranilamide scaffold by the substitution of a fluorine atom at the 4-position of tyrosine and guanidines at both Lys and Arg positions resulted in the displacement of ω -conotoxin GVIA binding at similar potencies (4) [104]. Truncation at the Lys2 moiety in (2) produced a mimetic for Tyr13 and Arg17 having similar potency but substantially reduced molecular weight (5) [105]. Hybrid approaches combining the anthranilamide and a

diphenylmethylpiperazine commonly found in small molecule blockers of N-type channels also displayed low micromolar potency (6) [106]. A virtual screening approach to identify cyclic pentapeptides mimicking crucial residues of CVID has also been reported to demonstrate selectivity for N-type channels (7) [107]. This body of work represents important advances in the understanding of the critical components of activity and selectivity in peptide mimetics of N-type calcium channels, but all demonstrate substantially less functional and molecular affinity than ω -conotoxins.





4.2. Small Molecule N-Type Blockers

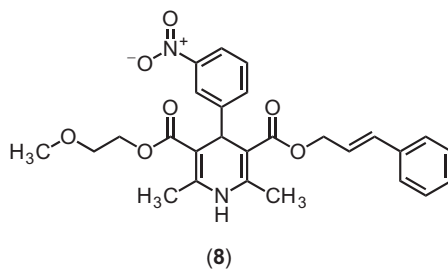
The synthesis and structure–activity relationships (SAR) of small molecule blockers of N-type calcium channels have been extensively reviewed elsewhere [88,108,109]. This section will focus on more recent advances (2009 to present) in the discovery and development of small molecule N-type calcium channel blockers. Peer reviewed literature will be emphasized, while recent patent disclosures of note will also be covered.

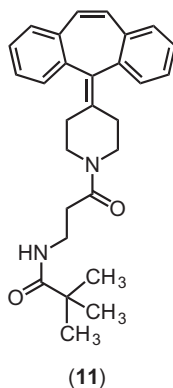
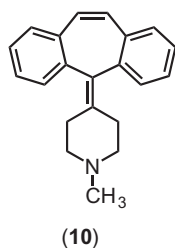
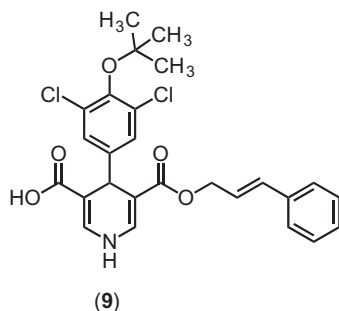
4.2.1 Non-Selective Calcium Channel Blockers as a Starting Point

Some early efforts to design selective N-type calcium channel blockers began with non-selective or dual selective VGCC blockers. An important example of this approach is the work from researchers at Ajinomoto who started from the privileged pharmacophore associated with the DHP drug cilnidipine (8), a dual L/N-type calcium channel blocker used widely in

the treatment of hypertension in Asia. After the discovery that cilnidipine had N-type calcium channel blocking activity [110], SAR screening and structural optimization of the cilnidipine scaffold led to a number of derivatives which retained N-type activity with improved selectivity over L-type channels, some of which demonstrated activity in the rat formalin model of pain [88,111,112]. Expanding on these efforts in recent years, the introduction of hydrogen atoms at the 2 and 6 positions of the 1,4-DHP structure resulted in further improved potency and selectivity [113]. One of the most potent and selective of these derivatives is (+)-4-(3,5-dichloro-4-methoxyphenyl)-1,4-DHP-3,5-dicarboxylic acid 3-cinnamyl ester (**9**) which demonstrated sub-micromolar inhibition of N-type channels with more than 60-fold selectivity over L-type channels. Furthermore, this molecule demonstrated robust inhibition of phase 2 pain responses in the rat formalin model, similar to that observed with gabapentin. Interestingly, the (–) enantiomer of (**9**) demonstrated equipotent activity at N-type channels but with a somewhat lower selectivity over L-type channels.

A second example comes from the non-selective, diphenylmethylpiperazine-containing calcium channel blockers flunarizine and lomerizine, both of which demonstrate sub-micromolar potency at the N-type channel but with little selectivity over L-types [114]. Several independent early chemistry efforts to produce N-type blockers resulted in molecules containing similar pharmacophores [88,111]. Building on this observation, Yamamoto and colleagues surmised that cyproheptadine (**10**), an approved anti-allergic drug that contains this pharmacophore, would have N-type calcium channel blocking activity [111]. Derivatization and optimization of cyproheptadine resulted in the discovery of an N-pivaloyl- β -alanyl derivative (**11**) with a 3.2 μM IC_{50} against the N-type channel, analgesic activity in the rat formalin model and improved selectivity for N-type over L-type as well as over 5-HT_{2A} and H₁ receptors.





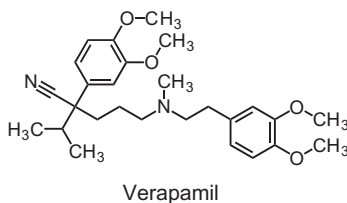
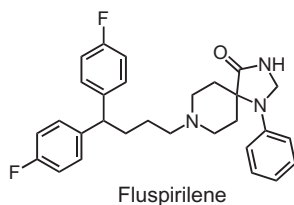
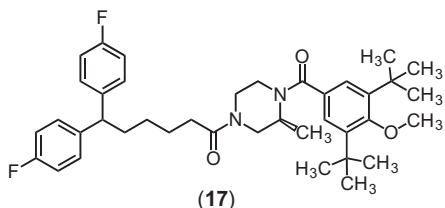
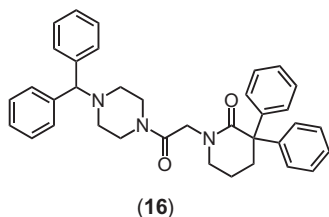
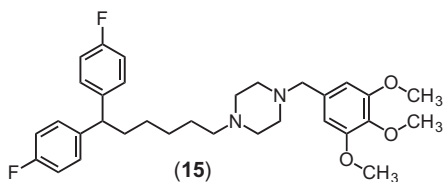
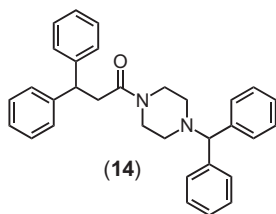
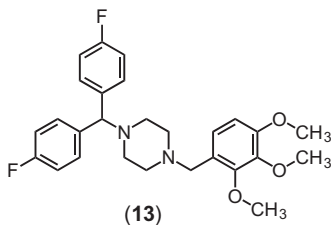
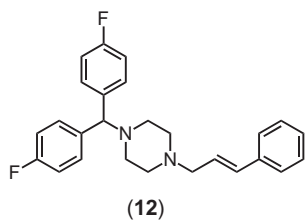
4.2.2 Piperazine-Based Structures

SAR studies around the flunarizine (12) and lomerizine (13) diphenylmethylpiperazine backbones resulted in a series of N-type calcium channel blockers with affinities below 200 nM and with 25- to 111-fold selectivity over L-type channels [114]. This work led to NP118809 (14) (now known as Z160) and NP078585 (15) both of which show strong analgesic activity in the rat formalin model and suitable pharmacokinetic characteristics for further development. The most potent and selective compound in this series, Z160, gives an IC_{50} of 110 nM against the N-type calcium channel, 111-fold selectivity over L-type channels and 25-fold selectivity over P/Q-type channels. Z160 demonstrates substantially greater selectivity (67-fold) over the hERG potassium channel than NP078585 (<10-fold), as well as a lack of a significant interaction against 112 additional safety pharmacology targets [114]. Later work demonstrates that Z160 mediates a hyperpolarizing shift in the midpoint of the steady-state inactivation curve for N-type channels consistent with a mechanism involving modulation of the inactivated state. Z160 also produces

frequency-dependent block of N-type channels. Further non-clinical evaluation of Z160 shows robust efficacy after oral dosing in multiple animal models of neuropathic pain with comparable efficacy to morphine, gabapentin and ω -conotoxin [115,116]. NP078585 is now known to possess mixed N/T-type channel activity and has demonstrated significant analgesic activity in a non-clinical model of visceral pain [117]. Similar approaches have been applied to the other non-selective calcium channel blockers fluspirilene and verapamil (reviewed in [88]). Taken together, these efforts have resulted in a number of series with potent activity against N-type channels, selectivity over L-type channels and efficacy in non-clinical models of pain.

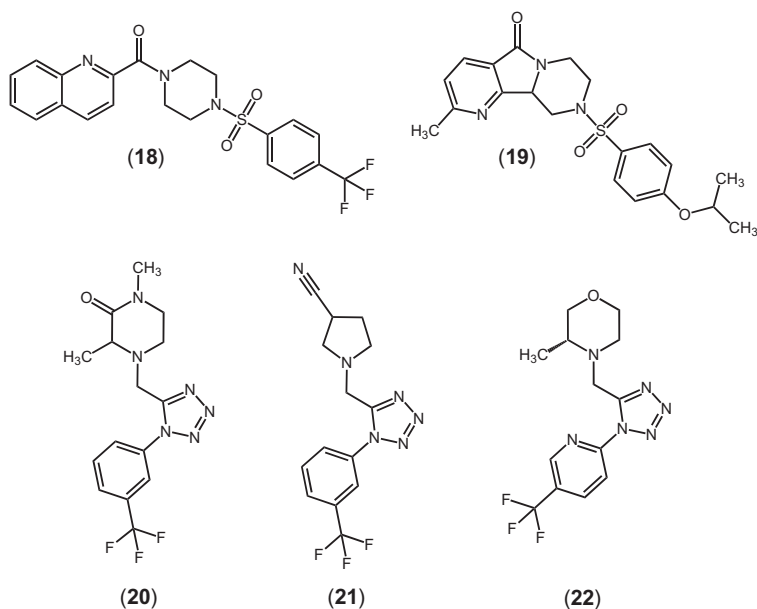
It should be noted that, to date, the only molecule from early efforts to optimize the diphenylmethyl piperazine backbone which has been reported to achieve development into the clinic is Z160. Indeed further SAR studies and optimization around the benzhydryl moiety of the piperazine core of Z160 [118] did not identify molecules with greater potency or selectivity. Modification of NP078585 to produce (**17**), including replacement of R1 and R3 groups on the benzyl region with tert-butyl groups, S-methyl substitution off the piperazine ring adjacent to the benzoyl linker and substitution of amine linkages on either side of the piperazine core, resulted in the most potent (40 nM IC₅₀) and selective (3600-fold vs. L-type) compounds with the greatest selectivity over the hERG channel (>100-fold) [119].

Following high-throughput screening efforts, researchers from Abbott surmised that a diphenyl lactam moiety may act as a bioisosteric replacement for the diphenylmethylpiperazine group that had been established as an important determinant of calcium channel binding affinity. On the basis of this hypothesis, a number of benzydryl piperazine analogues containing the diphenyl lactam were prepared, some of which demonstrated both good N-type calcium channel activity and efficacy in a capsaicin model of secondary hyperalgesia [120]. One molecule derived from this series, A-1048400 (**16**), was further characterized in a number of electrophysiological and non-clinical efficacy models [120]. These studies revealed that A-1048400 possesses sub-micromolar activity at N-type calcium channels with approximately fivefold greater potency for the inactivated state of the channel. This molecule also demonstrated state-dependent activity for both T- and P/Q-type calcium channels with potencies of ~ 1 μ M. In electrophysiological assays, A-1048400 demonstrated state-dependent block of L-type calcium channels as well, with block nearly equipotent to that at N-type channels. Interestingly, the pharmacological selectivity of this molecule on both rat aorta tissue relaxation and on rat haemodynamic measure was considerably greater; at least 14-fold compared to doses effective in reducing nociceptive, inflammatory and neuropathic pain.



A number of notable piperazine containing structures have recently been disclosed from researchers at GlaxoSmithKline (GSK) and Convergence Pharmaceuticals which spun out of GSK in October 2010 following the acquisition of clinical stage assets. Building around a 4-sulfonyl-1-piperizinyl-carbonyl-quinoline scaffold, a number of molecules with trifluoromethylphenyl substitutions of the sulfonyl group, some with trifluoromethoxy linkages, were found to demonstrate low micromolar blockade of N-type channels. In this disclosure, the inventors evaluated the potency of compounds under both tonic and inactivated state conditions and demonstrated several molecules with selectivity for the inactivated state

[121,122]. Of these, (18) demonstrated a potency of 1.6 μM for 30% inhibition of the inactivated channel state (IC_{30}) with 15-fold selectivity over the IC_{50} for the resting state of the channel. This molecule also blocked the inactivated state of the T-type channel with an IC_{30} of 4 μM for the inactivated state and with sixfold selectivity over the resting state, making them equipotent at closed channels. This scaffold could support derivatization and substitution on the quinolone side chain without significant loss of potency or state dependence. Replacement of the trifluoromethylphenyl side chain with a benzonitrile was also effective. In a subsequent disclosure, a piperazine containing heterocyclic fused rings (19) demonstrated substantially greater selectivity for the inactivated state (50-fold), with similar potency to (18) [123]. Single-digit micromolar potency at the inactivated channel was preserved after replacement of the sulfonyl linker with a tetrazole as in (20), described in [124]. While (20) does not possess differential selectivity over the resting state, other compounds in this series did demonstrate selectivity. Compounds (21) and (22) are reported to inhibit the inactivated state by 30% at less than or equal to 3.2 μM with 3- to 10-fold selectivity over the resting state. It appears that in the context of the tetrazole linker the piperazine core, which is a predominant feature of the progression of this class, can be replaced altogether with diverse functional groups.



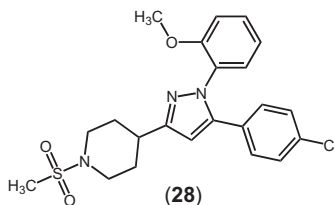
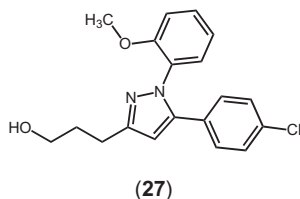
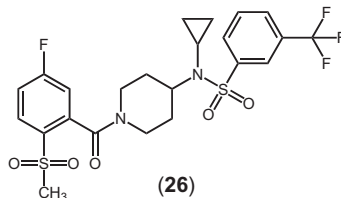
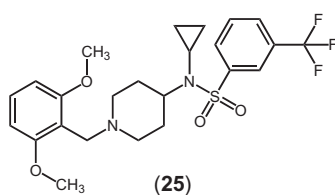
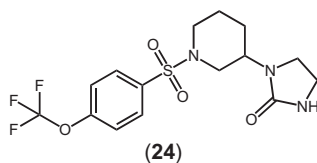
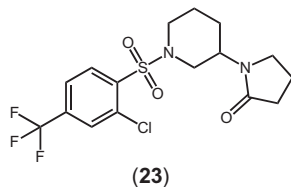
4.2.3 Piperidine-Containing Structures

Building from the trifluoromethylbenzylsulfonyl side of the molecule, researchers at GSK disclosed derivatives replacing the piperazine with a piperidine aryl sulfone, with the best potency and selectivity demonstrated with 2-pyrrolidinone and 2-imidazolidinone groups (**23**) and (**24**) [125]. The most potent and selective of this series (**23**) demonstrated an IC_{30} of 1 μ M at the inactivated channel with 32-fold selectivity over the resting state. Others in this series were reported to have IC_{30} values ranging from 4 to 8 μ M and 8- to 20-fold selectivity over the resting state. Interestingly, the degree of selectivity in this series may be influenced by chirality as it was reported that a faster running enantiomer of (**24**) demonstrated half the selectivity with equivalent potency to the chiral mixture.

Shao and colleagues identified an aminopiperidine sulfonamide screening hit (**25**) with an IC_{50} of 120 nM at the N-type inactivated state and 40-fold selectivity over the resting state but insufficient selectivity with respect to safety pharmacology targets [126]. Modification of the sulfonamide alkyl substituent to a cyclopropyl derivative resulted in a twofold increase in potency. SAR optimization resulted in (**26**) where the basic amide is replaced with an amine, and substitution of the benzamide with a polar methylsulfone group at the 2-position and a fluoro group at the 5-position, preserve sub-micromolar potency at the N-type channel while broadening the selectivity against hERG and L-type channels. Characterization of (**26**) *in vitro* and *in vivo* demonstrated a profile consistent with potent state-dependent N-type channel block and dose-dependent analgesic efficacy in neuropathic and inflammatory pain models. The analgesic efficacy of (**26**) was dependent on target expression as the molecule failed to reverse hyperalgesia in $Ca_v2.2$ -deficient mice. The lack of haemodynamic effects after intravenous administration in anesthetized dogs confirmed selectivity over cardiovascular safety targets. Further development of (**26**) revealed some significant metabolic liabilities including the accumulation of an active metabolite and these limited its clinical utility. Several related compounds were disclosed by the same group in the patent literature [127–129].

Subasinghe and colleagues describe the SAR optimization of a pyrazolyl-piperidine hit (**27**) from a high-throughput screen for N-type calcium channel inhibitors [130]. N-substitution of the piperidine moiety with a methanesulfonyl group gave improved metabolic stability while maintaining potency and frequency-dependent block (**28**). Further SAR evaluation with a focus on maintaining metabolic stability and understanding the importance

of substitutions and replacements at the 2-methoxy-phenyl residue and the 4-chloro-phenyl rings, revealed a series of novel molecules with high *in vitro* potency and good metabolic stability. Further evaluation of (28) in animal models of inflammatory and neuropathic pain demonstrated significant reversal of thermal hypersensitivity and cold allodynia, respectively, at a dose of 30 mg/kg i.p. which also resulted in a peak plasma level of 8 μ M.



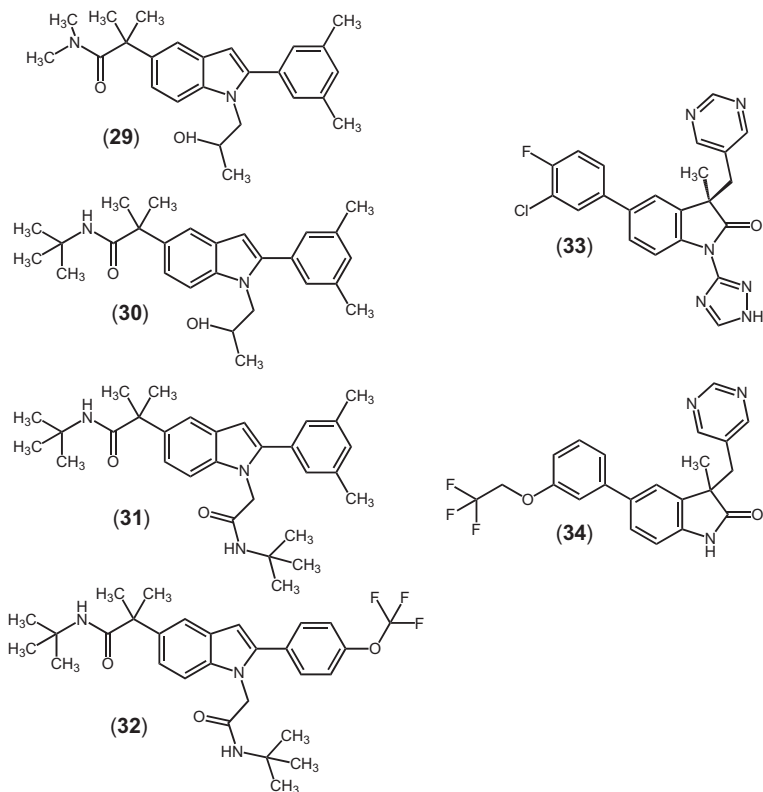
4.2.4 Indoles and Oxindoles

A number of publications and patent disclosures describe a series of indoles and oxindole state-dependent N-type channel blockers [130–135]. Derived from a high-throughput screening hit, a simplified indole scaffold (29) was investigated for SAR. Optimization at the C5 position of the indole resulted in a lipophilic *t*-butyl amide (30) that maintained N-type activity [134]. A *t*-butyl acetamide at the N1 position of the indole gave significantly improved potency at N-type calcium channels but only modest selectivity over the L-type channel, as well as a metabolic liability associated with the 3,5-dimethyl phenyl substituent (31). Further optimization for metabolic and pharmacokinetic properties resulted in (32) which contains a trifluoromethoxyphenyl substitution at the C2 position of the indole.

Further characterization of (32) revealed dose-dependent efficacy in rat inflammatory and neuropathic pain models at concentrations well separated from those that produce motor defects. This aryl indole analogue caused dose-dependent haemodynamic effects in dog cardiovascular safety pharmacology models, further underscoring the importance of selectivity over the L-type channel.

Other series containing a modified oxindole core structure have been disclosed in the patent literature. Duffy *et al.* describe a number of oxindoles withazole and pyrazine containing side chain substitutions at the N1 position, and fluorobenzyl and trifluoromethoxyphenyl side chain substitutions at the C5 position are also reported [132]. These derivatives contain further substitutions at the C3 position of the oxindole, notably the di-substituted 3-methylpyrimidine. This series, discovered by researchers at Merck, is exemplified by the *N*-triazole oxindole TROX-1, (33) which contains a 3-chloro-4-fluoro-phenyl substitution at C5 and a 1,2,4-triazole group at N1. From another series described in [131], it appears that oxindoles with the methylpyrimidine-5-ylmethyl group at position C3 are able to support removal of the side chain at position N1 while retaining substantial potency at the N-type channel (34) [131].

Further non-clinical evaluation of TROX-1 has been reported. Using recombinantly expressed channels, Abbadie and colleagues [135] reported an IC_{50} of 250 nM under N-type channel inactivating conditions with approximately 100-fold selectivity compared to channel resting conditions. Similarly, potencies at the endogenous N-type channel from isolated DRG neurons are reported as 400 nM under inactivating conditions and 2.6 μ M under resting state conditions. TROX-1 also demonstrates selectivity over other ion channel targets including the L-type channel, as well as in a binding and functional evaluation of 166 additional targets. Demonstrating favourable oral bioavailability, dose proportional pharmacokinetics and CNS exposure, TROX-1 also effectively inhibits pain responses in several inflammatory models of pain. Furthermore, a detailed therapeutic window investigation provides evidence for an approximately 20-fold differential between efficacy and CNS side effects on the basis of plasma exposure and an approximately 38-fold differential for cardiovascular safety pharmacology. More detailed electrophysiological evaluation of TROX-1 molecular and functional selectivity demonstrate voltage- and use-dependent inhibition of N-type channels and significant functional selectivity for $Ca_v2.2$ and $Ca_v2.3$ currents over $Ca_v2.1$ currents under closed state but not inactivating conditions [133].

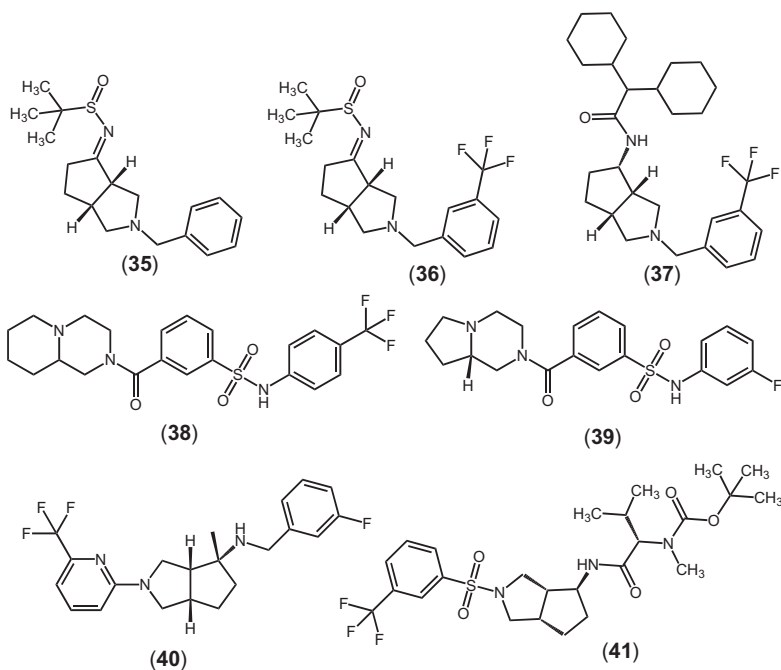


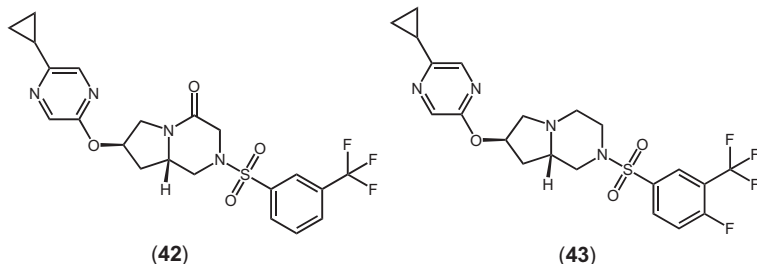
4.2.5 Other Approaches

An interesting chiral aminocyclopentapyrrolidine series was recently reported by Beebe and coworkers from Abbott [136]. This series is exemplified by a cyclopentapyrrole core bearing a 2-methylpropanesulfinamide at the 4-position and an *N*-benzyl substituent at the 2-position. (35). Replacement of the *N*-benzyl with a 3-trifluoromethylbenzyl substituent, as exemplified in (36), resulted in a fivefold increase in potency at N-type channels. Substitution at the amide with lipophilic groups, such as the bis-cyclohexyl acetamide in (37), resulted in sub-micromolar potencies at the N-type channel. Chiral separation of the *S,S,R*-enantiomer of (37) revealed a fourfold difference in potency compared with the *R,R,S*-enantiomer and resulted in the most potent and selective molecule reported in the series. Evaluation of the activity of (37) revealed substantial potency for the inactivated state of the channel with an IC_{50} of 41 nM under inactivating conditions and close to 10-fold selectivity for the inactivated state. As is the case with many

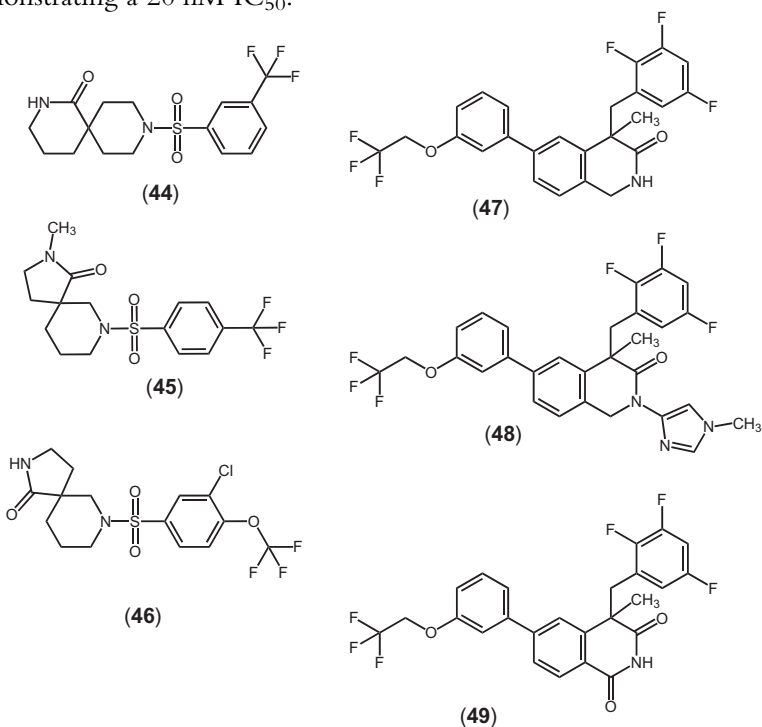
N-type calcium channel blockers, the lipophilic bis-cyclohexyl moiety imparts poor physicochemical properties to these derivatives, which have low aqueous solubility and high plasma protein binding, leading to poor oral bioavailability. In non-clinical models of inflammatory pain, (37) significantly and dose dependently reduced pain behaviours in the carrageenan and formalin models when administered at a dose of 30 mg/kg i.p. with an approximately 15-fold therapeutic window over cardiovascular safety or motor side effect levels.

Related molecules are disclosed in the recent patent literature. Benzotrifluoro (38) and benzfluoro (39) benzenesulfonamide substitutions at the N1 position of a pyrrolo or pyrido-pyrazine core are described by researchers at Abbott in [137]. In subsequent patents from the same group, 4-amino (40) and 4-oxy (41) substitutions of the cyclopentapyrrolidine ring are described, many of which contain trifluoromethyl or trifluoromethoxyphenyl, pyridine or pyrimidine substitutions at N1 [138] and [139]. In another patent from AbbVie, 7-oxy-5-cyclopropylpyrazine substitutions on the pyrrolpiperidine core, which maintain a sulfonamide-linked trifluoromethylbenzyl moiety, for example (42) and (43), show sub-micromolar potency at the N-type channel, and in the case of (43) demonstrate a substantial effect in the chronic constriction injury model of neuropathic pain [140].



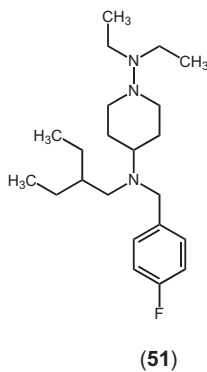
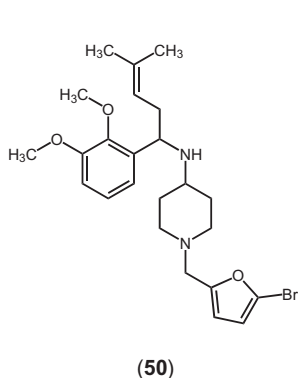


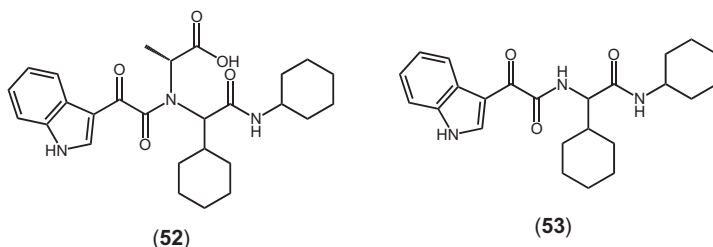
Another recent disclosure by researchers at Convergence describes spirocyclic derivatives with IC_{30} s for the N-type inactivated state in the low micromolar range with at least 10-fold selectivity over the resting channel state [141,142]. Both 5- and 6-membered rings support this potency profile, illustrated by (44) and (45) with either trifluoromethoxy or trifluoromethyl-phenyl-sulfonyl substituents, which can also allow chloro or bromo substitutions, for example (46). Dihydroisoquinolinone (47) and isoquinolinedione (48) compounds have also been disclosed [143]. These compounds are reported to block the N-type channel at approximately 250 nM, with 1,3-dione-containing compound (49) reportedly demonstrating a 20 nM IC_{50} .



The Beijing Institute of Pharmacology and Toxicology has reported analgesic N-type calcium channel blockers. ZC88 (**50**), originally described by Meng and colleagues [144], demonstrated dose-dependent antinociceptive effects and potentiation of morphine analgesia in non-clinical models of pain. However, later work on this molecule has demonstrated a significant hERG liability [145]. The same group reported the discovery of C101 (**51**) through optimization of the 4-aminopiperidine template [146]. Further characterization of C101 revealed an IC_{50} of 2.2 μ M for inhibition of the N-type channel and a modest but significant effect on the voltage dependence of steady-state inactivation at this concentration. At concentrations up to 50-fold greater than the IC_{50} for N-type channels, C101 showed no effect on L-, P/Q- and R-type channel currents or on sodium, potassium or hERG channels.

Utilizing an orthogonal approach to inhibition of the N-type channel, researchers from Lectus disclosed compounds able to inhibit the interaction between the $Ca_V \alpha 1$ subunit and the regulatory $Ca_V \beta 3$ subunit, thereby modulating the activity of N-type channels through functional effects on channel expression and gating [147]. Two molecules from this series (**52**), (**53**) were reported to have IC_{50} s below 500 nM in a cell-free assay, disrupting association of the $Ca_V \alpha 1$ interacting domain and β subunit binding. The presence of some structural features common to more traditional N-type channel blockers makes it tempting to speculate that their effects could be in part due to effects on the $Ca_V \alpha 1/Ca_V \beta$ interactions. Other approaches include the development of a 2D-QSAR model that may be useful in the further design and optimization of N-type calcium channel blockers [148].





4.3. N-Type Calcium Channel Modulators in the Clinic

4.3.1 Z160

To date, only two small molecule blockers of N-type calcium channels have been reported to have advanced into human clinical evaluation. Early studies to evaluate Z160 [14] in humans have been hampered by the molecule's poor aqueous solubility and consequent limited bioavailability in initial formulations [108,109]. The application of amorphous dispersion technology to the formulation of Z160 has been used to successfully improve its oral bioavailability (Zalicus personal communication). An amorphous dispersion formulation of Z160 is currently being evaluated in two randomized placebo-controlled Phase II studies in neuropathic pain. A Phase II efficacy trial of Z160 in lumbosacral radiculopathy was initiated in August 2012 and is being conducted at 23 study locations in the United States. Using a parallel group design in approximately 140 subjects, this randomized double-blind study is evaluating 375 mg of Z160 versus placebo administered twice daily for 6 weeks in patients suffering from neuropathic pain due to lumbosacral radiculopathy as determined by the StEP assessment. The primary endpoint is change from baseline to week 6 in weekly average pain score based on the pain intensity numeric rating scale (PI-NRS) and a number of safety and efficacy secondary endpoints are planned [149]. A study of the efficacy and safety of Z160 in subjects with post-herpetic neuralgia was initiated in December 2012. Using a similar parallel group study design and primary endpoint, this study is being conducted in 53 study locations in the United States. The study will evaluate 375 mg of Z160 versus placebo administered twice daily for 6 weeks in patients suffering from neuropathic pain due to post-herpetic neuralgia [150]. Both Z160 Phase II trials have completed enrollment and top line data is expected in the fourth quarter of 2013.

4.3.2 CNV2197944

Convergence Pharmaceuticals Ltd. spun out of Glaxo SmithKline plc in October 2010 after GSK decided to discontinue discovery and development in pain [151]. Convergence has advanced two ion channel blockers into Phase II evaluation in neuropathic pain indications. The structure of the Convergence N-type calcium channel blocker, CNV2197944, has not been publicly disclosed although it is probably described in the patent literature referenced herein. A Phase II study of the efficacy and safety of CNV2197944 versus placebo in patients with post-herpetic neuralgia was initiated in April 2013 to evaluate repeat oral dosing of CNV2197944 75 mg three times daily in approximately 90 subjects [152]. This study is being conducted in Europe and South Africa and top line results are expected in the first half of 2014. A second Phase II study of the efficacy and safety of CNV2197944 versus placebo in patients with diabetic peripheral neuropathy was initiated in July 2013 to investigate the effect of repeat oral dosing of 75 mg three times per day [153]. The study is being conducted in Eastern Europe and will enroll an estimated 165 patients with top line data also expected in 2014. Both studies utilize a randomized crossover design with 3 weeks of treatment separated by a 2-week washout period and a primary outcome measure of change from baseline in a PI-NRS at the end of 3 weeks of treatment.



5. CONCLUDING REMARKS

This is an exciting time for researchers and drug developers working on N-type calcium channel modulators for the treatment of pain. Within months of the publication of this review, we will learn the results of four randomized Phase II trials evaluating two distinct small molecule modulators of the N-type calcium channel in three different neuropathic pain indications. Furthermore, both these molecules, CNV944 and Z160, are reported to demonstrate use-dependent activity, with greater potency towards the inactivated channel state, and thus are on the leading edge of evaluating this key pharmacological feature for its relevance in safely and effectively treating pain in humans. If either of these molecules demonstrates activity in humans, this will surely spur an increased focus on the discovery and development of novel peptide and small molecule N-type channel modulators. Indeed, as this review summarizes, there are a number of new and interesting compounds and peptides described in the scientific and patent literature that seem poised for further development and ultimately evaluation in human

pain indications. Given the substantial unmet medical need for new treatments for chronic pain, this body of work offers a great deal of optimism for those whose goal it is to alleviate human such suffering.

REFERENCES

- [1] Triggler DJ. Calcium channel antagonists: clinical uses—past, present and future. *Biochem Pharmacol* 2007;74(1):1–9.
- [2] Mohan CG, Gandhi T. Therapeutic potential of voltage gated calcium channels. *Mini Rev Med Chem* 2008;8(12):1285–90.
- [3] Bingham JP, Mitsunaga E, Bergeron ZL. Drugs from slugs—past, present and future perspectives of omega-conotoxin research. *Chem Biol Interact* 2010;183(1):1–18.
- [4] Vink S, Alewood PF. Targeting voltage-gated calcium channels: developments in peptide and small-molecule inhibitors for the treatment of neuropathic pain. *Br J Pharmacol* 2012;167(5):970–89.
- [5] Swayne LA, Bourinet E. Voltage-gated calcium channels in chronic pain: emerging role of alternative splicing. *Pflugers Arch* 2008;456(3):459–66.
- [6] Loots Es, Isacoff EY. Molecular coupling of S4 to a K(+) channel's slow inactivation gate. *J Gen Physiol* 2000;116(5):623–36.
- [7] Bezanilla F. Voltage sensor movements. *J Gen Physiol* 2002;120(4):465–73.
- [8] Sousa SR, Vetter I, Lewis RJ. Venom peptides as a rich source of cav2.2 channel blockers. *Toxins (Basel)* 2013;5(2):286–314.
- [9] Buraei Z, Yang J. Structure and function of the beta subunit of voltage-gated Ca(2)(+) channels. *Biochim Biophys Acta* 2013;1828(7):1530–40.
- [10] Pragnell M, De Waard M, Mori Y, Tanabe T, Snutch TP, Campbell KP. Calcium channel beta-subunit binds to a conserved motif in the I-II cytoplasmic linker of the alpha 1-subunit. *Nature* 1994;368(6466):67–70.
- [11] De Waard M, Witcher DR, Pragnell M, Liu H, Campbell KP. Properties of the alpha 1-beta anchoring site in voltage-dependent Ca²⁺ channels. *J Biol Chem* 1995;270(20):12056–64.
- [12] Witcher DR, De Waard M, Liu H, Pragnell M, Campbell KP. Association of native Ca²⁺ channel beta subunits with the alpha 1 subunit interaction domain. *J Biol Chem* 1995;270(30):18088–93.
- [13] Buraei Z, Yang J. The β subunit of voltage-gated Ca²⁺ channels. *Physiol Rev* 2010;90(4):1461–506.
- [14] Klugbauer N, Lacinova L, Marais E, Hobom M, Hofmann F. Molecular diversity of the calcium channel alpha2delta subunit. *J Neurosci* 1999;19(2):684–91.
- [15] Qin N, Yagel S, Momplaisir ML, Codd EE, D'Andrea MR. Molecular cloning and characterization of the human voltage-gated calcium channel alpha(2)delta-4 subunit. *Mol Pharmacol* 2002;62(3):485–96.
- [16] Davies A, Kadurin I, Alvarez-Laviada A, Douglas L, Nieto-Rostro M, Bauer CS, et al. The alpha2delta subunits of voltage-gated calcium channels form GPI-anchored proteins, a posttranslational modification essential for function. *Proc Natl Acad Sci U S A* 2010;107(4):1654–9.
- [17] Catterall WA. Voltage-gated calcium channels. *Cold Spring Harb Perspect Biol* 2011;3(8):a003947.
- [18] Luo ZD, Calcutt NA, Higuera ES, Valder CR, Song YH, Svensson CI, et al. Injury type-specific calcium channel alpha 2 delta-1 subunit up-regulation in rat neuropathic pain models correlates with antiallodynic effects of gabapentin. *J Pharmacol Exp Ther* 2002;303(3):1199–205.

- [19] Finnerup NB, Sindrup SH, Jensen TS. Chronic neuropathic pain: mechanisms, drug targets and measurement. *Fundam Clin Pharmacol* 2007;21(2):129–36.
- [20] Hendrich J, Van Minh AT, Hebllich F, Nieto-Rostro M, Watschinger K, Striessnig J, et al. Pharmacological disruption of calcium channel trafficking by the alpha2delta ligand gabapentin. *Proc Natl Acad Sci U S A* 2008;105(9):3628–33.
- [21] Davies A, Hendrich J, Van Minh AT, Wratten J, Douglas L, Dolphin AC. Functional biology of the alpha(2)delta subunits of voltage-gated calcium channels. *Trends Pharmacol Sci* 2007;28(5):220–8.
- [22] Dolphin AC. Calcium channel $\alpha 2\delta$ subunits in epilepsy and as targets for antiepileptic drugs. In: Noebels JL, Avoli M, Rogawski M, Olsen R, Delgado-Escueta A, editors. Jasper's basic mechanisms epilepsies. Bethesda, MD: Oxford University Press; 2012.
- [23] Letts VA, Felix R, Biddlecome GH, Arikath J, Mahaffey CL, Valenzuela A, et al. The mouse stargazer gene encodes a neuronal Ca²⁺-channel gamma subunit. *Nat Genet* 1998;19(4):340–7.
- [24] Minor Jr DL, Findeisen F. Progress in the structural understanding of voltage-gated calcium channel (CaV) function and modulation. *Channels (Austin)* 2010;4(6):459–74.
- [25] Calin-Jageman I, Lee A. Ca(v)1 L-type Ca²⁺ channel signaling complexes in neurons. *J Neurochem* 2008;105(3):573–83.
- [26] Catterall WA, Few AP. Calcium channel regulation and presynaptic plasticity. *Neuron* 2008;59(6):882–901.
- [27] Catterall WA, Perez-Reyes E, Snutch TP, Striessnig J. International Union of Pharmacology. XLVIII. Nomenclature and structure–function relationships of voltage-gated calcium channels. *Pharmacol Rev* 2005;57(4):411–25.
- [28] Tedford HW, Zamponi GW. Direct G protein modulation of Cav2 calcium channels. *Pharmacol Rev* 2006;58(4):837–62.
- [29] Tringham E, Snutch TP. Voltage-gated N-type and T-type calcium channels and excitability disorders. In: Gribkoff VK, Kaczmarek LK, editors. Structure, function and modulation of neuronal voltage-gated ion channels. Hoboken, NJ: John Wiley & Sons, Inc.; 2008.
- [30] Hering S, Berjukow S, Sokolov S, Marksteiner R, Weiss RG, Kraus R, et al. Molecular determinants of inactivation in voltage-gated Ca²⁺ channels. *J Physiol* 2000;528(Pt 2):237–49.
- [31] Stotz SC, Jarvis SE, Zamponi GW. Functional roles of cytoplasmic loops and pore lining transmembrane helices in the voltage-dependent inactivation of HVA calcium channels. *J Physiol* 2004;554(Pt 2):263–73.
- [32] Lacinova L, Klugbauer N, Hofmann F. State- and isoform-dependent interaction of isradipine with the alpha1C L-type calcium channel. *Pflugers Arch* 2000;440(1):50–60.
- [33] Bean BP. Nitrendipine block of cardiac calcium channels: high-affinity binding to the inactivated state. *Proc Natl Acad Sci U S A* 1984;81(20):6388–92.
- [34] Peterson BZ, Catterall WA. Allosteric interactions required for high-affinity binding of dihydropyridine antagonists to Ca(V)1.1 channels are modulated by calcium in the pore. *Mol Pharmacol* 2006;70(2):667–75.
- [35] Niespodziany I, Leclere N, Vandenplas C, Foerch P, Wolff C. Comparative study of lacosamide and classical sodium channel blocking antiepileptic drugs on sodium channel slow inactivation. *J Neurosci Res* 2013;91(3):436–43.
- [36] Winquist RJ, Pan JQ, Gribkoff VK. Use-dependent blockade of Cav2.2 voltage-gated calcium channels for neuropathic pain. *Biochem Pharmacol* 2005;70(4):489–99.
- [37] Nowycky MC, Fox AP, Tsien RW. Three types of neuronal calcium channel with different calcium agonist sensitivity. *Nature* 1985;316(6027):440–3.
- [38] Olivera BM, Miljanich GP, Ramachandran J, Adams ME. Calcium channel diversity and neurotransmitter release: the omega-conotoxins and omega-agatoxins. *Annu Rev Biochem* 1994;63:823–67.

- [39] Poncer JC, McKinney RA, Gahwiler BH, Thompson SM. Either N- or P-type calcium channels mediate GABA release at distinct hippocampal inhibitory synapses. *Neuron* 1997;18(3):463–72.
- [40] Ali AB, Nelson C. Distinct Ca²⁺ channels mediate transmitter release at excitatory synapses displaying different dynamic properties in rat neocortex. *Cereb Cortex* 2006;16(3):386–93.
- [41] Li W, Thaler C, Brehm P. Calcium channels in *Xenopus* spinal neurons differ in somas and presynaptic terminals. *J Neurophysiol* 2001;86(1):269–79.
- [42] Stanley EF. Single calcium channels and acetylcholine release at a presynaptic nerve terminal. *Neuron* 1993;11(6):1007–11.
- [43] Sheng J, He L, Zheng H, Xue L, Luo F, Shin W, et al. Calcium-channel number critically influences synaptic strength and plasticity at the active zone. *Nat Neurosci* 2012;15(7):998–1006.
- [44] Cizkova D, Marsala J, Lukacova N, Marsala M, Jergova S, Orendacova J, et al. Localization of N-type Ca²⁺ channels in the rat spinal cord following chronic constrictive nerve injury. *Exp Brain Res* 2002;147(4):456–63.
- [45] Smyth LM, Yamboliev IA, Mutafova-Yambolieva VN. N-type and P/Q-type calcium channels regulate differentially the release of noradrenaline, ATP and beta-NAD in blood vessels. *Neuropharmacology* 2009;56(2):368–78.
- [46] Pruneau D, Angus JA. Omega-conotoxin GVIA is a potent inhibitor of sympathetic neurogenic responses in rat small mesenteric arteries. *Br J Pharmacol* 1990;100(1):180–4.
- [47] Lin Y, McDonough SI, Lipscombe D. Alternative splicing in the voltage-sensing region of N-Type CaV2.2 channels modulates channel kinetics. *J Neurophysiol* 2004;92(5):2820–30.
- [48] Dolphin AC. Beta subunits of voltage-gated calcium channels. *J Bioenerg Biomembr* 2003;35(6):599–620.
- [49] Patil PG, Brody DL, Yue DT. Preferential closed-state inactivation of neuronal calcium channels. *Neuron* 1998;20(5):1027–38.
- [50] Jones LP, DeMaria CD, Yue DT. N-type calcium channel inactivation probed by gating-current analysis. *Biophys J* 1999;76(5):2530–52.
- [51] Kim C, Jun K, Lee T, Kim SS, McEnery MW, Chin H, et al. Altered nociceptive response in mice deficient in the alpha(1B) subunit of the voltage-dependent calcium channel. *Mol Cell Neurosci* 2001;18(2):235–45.
- [52] Saegusa H, Kurihara T, Zong S, Kazuno A, Matsuda Y, Nonaka T, et al. Suppression of inflammatory and neuropathic pain symptoms in mice lacking the N-type Ca²⁺ channel. *EMBO J* 2001;20(10):2349–56.
- [53] Saegusa H, Matsuda Y, Tanabe T. Effects of ablation of N- and R-type Ca(2+) channels on pain transmission. *Neurosci Res* 2002;43(1):1–7.
- [54] Ino M, Yoshinaga T, Wakamori M, Miyamoto N, Takahashi E, Sonoda J, et al. Functional disorders of the sympathetic nervous system in mice lacking the alpha 1B subunit (Cav 2.2) of N-type calcium channels. *Proc Natl Acad Sci U S A* 2001;98(9):5323–8.
- [55] Pietrobon D. Function and dysfunction of synaptic calcium channels: insights from mouse models. *Curr Opin Neurobiol* 2005;15(3):257–65.
- [56] Brose WG, Gutlove DP, Luther RR, Bowersox SS, McGuire D. Use of intrathecal SNX-111, a novel, N-type, voltage-sensitive, calcium channel blocker, in the management of intractable brachial plexus avulsion pain. *Clin J Pain* 1997;13(3):256–9.
- [57] Staats PS, Yearwood T, Charapata SG, Presley RW, Wallace MS, Byas-Smith M, et al. Intrathecal ziconotide in the treatment of refractory pain in patients with cancer or AIDS: a randomized controlled trial. *JAMA* 2004;291(1):63–70.
- [58] Wallace MS. Ziconotide: a new nonopioid intrathecal analgesic for the treatment of chronic pain. *Expert Rev Neurother* 2006;6(10):1423–8.

- [59] Adams DJ, Berecki G. Mechanisms of conotoxin inhibition of N-type (Ca_v2.2) calcium channels. *Biochim Biophys Acta* 2013;1828(7):1619–28.
- [60] Adams DJ, Callaghan B, Berecki G. Analgesic conotoxins: block and G protein-coupled receptor modulation of N-type (Ca_v2.2) calcium channels. *Br J Pharmacol* 2012;166(2):486–500.
- [61] Lewis RJ, Dutertre S, Vetter I, Christie MJ. Conus venom peptide pharmacology. *Pharmacol Rev* 2012;64(2):259–98.
- [62] Atkinson RA, Kieffer B, Dejaegere A, Sirockin F, Lefevre JF. Structural and dynamic characterization of omega-conotoxin MVIIA: the binding loop exhibits slow conformational exchange. *Biochemistry* 2000;39(14):3908–19.
- [63] Adams ME, Myers RA, Imperial JS, Olivera BM. Toxotyping rat brain calcium channels with omega-toxins from spider and cone snail venoms. *Biochemistry* 1993;32(47):12566–70.
- [64] Dunlap K, Luebke JI, Turner TJ. Identification of calcium channels that control neurosecretion. *Science* 1994;266(5186):828–31.
- [65] Lewis RJ, Nielsen KJ, Craik DJ, Loughnan ML, Adams DA, Sharpe IA, et al. Novel omega-conotoxins from *Conus catus* discriminate among neuronal calcium channel subtypes. *J Biol Chem* 2000;275(45):35335–44.
- [66] Ellinor PT, Zhang JF, Horne WA, Tsien RW. Structural determinants of the blockade of N-type calcium channels by a peptide neurotoxin. *Nature* 1994;372(6503):272–5.
- [67] Payandeh J, Scheuer T, Zheng N, Catterall WA. The crystal structure of a voltage-gated sodium channel. *Nature* 2011;475(7356):353–8.
- [68] Kim JI, Takahashi M, Ogura A, Kohno T, Kudo Y, Sato K. Hydroxyl group of Tyr13 is essential for the activity of omega-conotoxin GVIA, a peptide toxin for N-type calcium channel. *J Biol Chem* 1994;269(39):23876–8.
- [69] Lew MJ, Flinn JP, Pallaghy PK, Murphy R, Whorlow SL, Wright CE, et al. Structure-function relationships of omega-conotoxin GVIA. Synthesis, structure, calcium channel binding, and functional assay of alanine-substituted analogues. *J Biol Chem* 1997;272(18):12014–23.
- [70] Nielsen KJ, Adams D, Thomas L, Bond T, Alewood PF, Craik DJ, et al. Structure-activity relationships of omega-conotoxins MVIIA, MVIIC and 14 loop splice hybrids at N and P/Q-type calcium channels. *J Mol Biol* 1999;289(5):1405–21.
- [71] Berecki G, Motin L, Haythornthwaite A, Vink S, Bansal P, Drinkwater R, et al. Analgesic (omega)-conotoxins CVIE and CVIF selectively and voltage-dependently block recombinant and native N-type calcium channels. *Mol Pharmacol* 2010;77(2):139–48.
- [72] Mould J, Yasuda T, Schroeder CI, Beedle AM, Doering CJ, Zamponi GW, et al. The alpha2delta auxiliary subunit reduces affinity of omega-conotoxins for recombinant N-type (Cav2.2) calcium channels. *J Biol Chem* 2004;279(33):34705–14.
- [73] Motin L, Yasuda T, Schroeder CI, Lewis RJ, Adams DJ. Omega-conotoxin CVIB differentially inhibits native and recombinant N- and P/Q-type calcium channels. *Eur J Neurosci* 2007;25(2):435–44.
- [74] Motin L, Adams DJ. omega-Conotoxin inhibition of excitatory synaptic transmission evoked by dorsal root stimulation in rat superficial dorsal horn. *Neuropharmacology* 2008;55(5):860–4.
- [75] Herzig V, Wood DL, Newell F, Chaumeil PA, Kaas Q, Binford GJ, et al. ArachnoServer 2.0, an updated online resource for spider toxin sequences and structures. *Nucleic Acids Res* 2011;39(Database issue):D653–D657.
- [76] Liu Z, Dai J, Dai L, Deng M, Hu Z, Hu W, et al. Function and solution structure of Huwentoxin-X, a specific blocker of N-type calcium channels, from the Chinese bird spider *Ornithoctonus huwena*. *J Biol Chem* 2006;281(13):8628–35.

- [77] Peng K, Chen XD, Liang SP. The effect of Huwentoxin-I on Ca(2+) channels in differentiated NG108-15 cells, a patch-clamp study. *Toxicol* 2001;39(4):491-8.
- [78] McGivern JG. Ziconotide: a review of its pharmacology and use in the treatment of pain. *Neuropsychiatr Dis Treat* 2007;3(1):69-85.
- [79] Webster LR, Fisher R, Charapata S, Wallace MS. Long-term intrathecal ziconotide for chronic pain: an open-label study. *J Pain Symptom Manage* 2009;37(3):363-72.
- [80] Wallace MS, Kosek PS, Staats P, Fisher R, Schultz DM, Leong M. Phase II, open-label, multicenter study of combined intrathecal morphine and ziconotide: addition of ziconotide in patients receiving intrathecal morphine for severe chronic pain. *Pain Med* 2008;9(3):271-81.
- [81] Wallace MS, Rauck RL, Deer T. Ziconotide combination intrathecal therapy: rationale and evidence. *Clin J Pain* 2010;26(7):635-44.
- [82] Prialt. Package insert.
- [83] Wright CE, Robertson AD, Whorlow SL, Angus JA. Cardiovascular and autonomic effects of omega-conotoxins MVIIA and CVID in conscious rabbits and isolated tissue assays. *Br J Pharmacol* 2000;131(7):1325-36.
- [84] McGuire D, Bowersox S, Fellmann JD, Luther RR. Sympatholysis after neuron-specific, N-type, voltage-sensitive calcium channel blockade: first demonstration of N-channel function in humans. *J Cardiovasc Pharmacol* 1997;30(3):400-3.
- [85] McGivern JG. Targeting N-type and T-type calcium channels for the treatment of pain. *Drug Discov Today* 2006;11(5-6):245-53.
- [86] Penn RD, Paice JA. Adverse effects associated with the intrathecal administration of ziconotide. *Pain* 2000;85(1-2):291-6.
- [87] Takahara A, Koganei H, Takeda T, Iwata S. Antisymphathetic and hemodynamic property of a dual L/N-type Ca(2+) channel blocker cilnidipine in rats. *Eur J Pharmacol* 2002;434(1-2):43-7.
- [88] Yamamoto T, Takahara A. Recent updates of N-type calcium channel blockers with therapeutic potential for neuropathic pain and stroke. *Curr Top Med Chem* 2009;9(4):377-95.
- [89] Smith MT, Cabot PJ, Ross FB, Robertson AD, Lewis RJ. The novel N-type calcium channel blocker, AM336, produces potent dose-dependent antinociception after intrathecal dosing in rats and inhibits substance P release in rat spinal cord slices. *Pain* 2002;96(1-2):119-27.
- [90] Kolosov A, Aurini L, Williams ED, Cooke I, Goodchild CS. Intravenous injection of leconotide, an omega conotoxin: synergistic antihyperalgesic effects with morphine in a rat model of bone cancer pain. *Pain Med* 2011;12(6):923-41.
- [91] Kolosov A, Goodchild CS, Cooke I. CNSB004 (Leconotide) causes antihyperalgesia without side effects when given intravenously: a comparison with ziconotide in a rat model of diabetic neuropathic pain. *Pain Med* 2010;11(2):262-73.
- [92] Pharmaceuticals R. <http://www.relevarepharmacom/>, accessed September 2013.
- [93] Gomes M, Maximo Prado M, Prado VF. PHA1B toxin, cDNA of PHA1B toxin gene, pharmaceutical composition containing PHA1B toxin, process and product. US Patent Application 2010; US20100168009.
- [94] Souza AH, Ferreira J, Cordeiro Mdo N, Vieira LB, De Castro CJ, Trevisan G, et al. Analgesic effect in rodents of native and recombinant Ph alpha 1beta toxin, a high-voltage-activated calcium channel blocker isolated from armed spider venom. *Pain* 2008;140(1):115-26.
- [95] de Souza AH, Lima MC, Drewes CC, da Silva JF, Torres KC, Pereira EM, et al. Antiallodynic effect and side effects of Phalpha1beta, a neurotoxin from the spider *Phoneutria nigriventer*: comparison with omega-conotoxin MVIIA and morphine. *Toxicol* 2011;58(8):626-33.

- [96] de Souza AH, Castro Jr CJ, Rigo FK, de Oliveira SM, Gomez RS, Diniz DM, et al. An evaluation of the antinociceptive effects of Phalpa1beta, a neurotoxin from the spider *Phoneutria nigriventer*, and omega-conotoxin MVIIA, a cone snail *Conus magus* toxin, in rat model of inflammatory and neuropathic pain. *Cell Mol Neurobiol* 2013;33(1):59–67.
- [97] Essack M, Bajic VB, Archer JA. Conotoxins that confer therapeutic possibilities. *Mar Drugs* 2012;10(6):1244–65.
- [98] Brady RM, Baell JB, Norton RS. Strategies for the development of conotoxins as new therapeutic leads. *Mar Drugs* 2013;11(7):2293–313.
- [99] Menzler S, Bikker JA, Suman-Chauhan N, Horwell DC. Design and biological evaluation of non-peptide analogues of omega-conotoxin MVIIA. *Bioorg Med Chem Lett* 2000;10(4):345–7.
- [100] Guo Z-X, Cammidge A, Horwell DC. Dendroid peptide structural mimetics of ω -conotoxin MVIIA based on a 2(1H)-quinolinone core. *Tetrahedron* 2000;56: 5169–75.
- [101] Menzler S, Bikker JA, Horwell DC. Synthesis of a non-peptide analogue of omega-conotoxin MVIIA. *Tetrahedron Lett* 1998;39:7619–22.
- [102] Baell JB, Forsyth SA, Gable RW, Norton RS, Mulder RJ. Design and synthesis of type-III mimetics of omega-conotoxin GVIA. *J Comput Aided Mol Des* 2001;15 (12):1119–36.
- [103] Baell JB, Duggan PJ, Forsyth SA, Lewis RJ, Lok YP, Schroeder CI. Synthesis and biological evaluation of nonpeptide mimetics of omega-conotoxin GVIA. *Bioorg Med Chem* 2004;12(15):4025–37.
- [104] Baell JB, Duggan PJ, Forsyth SA, Lewis RJ, Lok YP, Schroeder C, et al. Synthesis and biological evaluation of anthranilamide-based non-peptide mimetics of ω -conotoxin GVIA. *Tetrahedron* 2006;62:7284–92.
- [105] Duggan PJ, Lewis RJ, Phei Lok Y, Lumsden NG, Tuck KL, Yang A. Low molecular weight non-peptide mimics of omega-conotoxin GVIA. *Bioorg Med Chem Lett* 2009;19(10):2763–5.
- [106] Tranberg CE, Yang A, Vetter I, McArthur JR, Baell JB, Lewis RJ, et al. omega-Conotoxin GVIA mimetics that bind and inhibit neuronal Ca(v)2.2 ion channels. *Mar Drugs* 2012;10(10):2349–68.
- [107] Schroeder CI, Smythe ML, Lewis RJ. Development of small molecules that mimic the binding of omega-conotoxins at the N-type voltage-gated calcium channel. *Mol Divers* 2004;8(2):127–34.
- [108] Bear B, Asgian J, Termin A, Zimmermann N. Small molecules targeting sodium and calcium channels for neuropathic pain. *Curr Opin Drug Discov Dev* 2009;12 (4):543–61.
- [109] Pexton T, Moeller-Bertram T, Schilling JM, Wallace MS. Targeting voltage-gated calcium channels for the treatment of neuropathic pain: a review of drug development. *Expert Opin Invest Drugs* 2011;20(9):1277–84.
- [110] Takahara A, Fujita S, Moki K, Ono Y, Koganei H, Iwayama S, et al. Neuronal Ca2+ channel blocking action of an antihypertensive drug, cilnidipine, in IMR-32 human neuroblastoma cells. *Hypertens Res* 2003;26(9):743–7.
- [111] Yamamoto T, Niwa S, Iwayama S, Koganei H, Fujita S, Takeda T, et al. Discovery, structure-activity relationship study, and oral analgesic efficacy of cyproheptadine derivatives possessing N-type calcium channel inhibitory activity. *Bioorg Med Chem* 2006;14(15):5333–9.
- [112] Yamamoto T, Niwa S, Ohno S, Tokumasu M, Masuzawa Y, Nakanishi C, et al. The structure-activity relationship study on 2-, 5-, and 6-position of the water soluble 1,4-dihydropyridine derivatives blocking N-type calcium channels. *Bioorg Med Chem Lett* 2008;18(17):4813–6.

- [113] Yamamoto T, Niwa S, Tokumasu M, Onishi T, Ohno S, Hagihara M, et al. Discovery and evaluation of selective N-type calcium channel blockers: 6-unsubstituted-1,4-dihydropyridine-5-carboxylic acid derivatives. *Bioorg Med Chem Lett* 2012;22(11):3639–42.
- [114] Zamponi GW, Feng ZP, Zhang L, Pajouhesh H, Ding Y, Belardetti F, et al. Scaffold-based design and synthesis of potent N-type calcium channel blockers. *Bioorg Med Chem Lett* 2009;19(22):6467–72.
- [115] Lee MS, Snutch TP. Z160: a potent and state-dependent, small molecule blocker of N-type calcium channels effective in nonclinical models of neuropathic pain. *Pain* 2013;14(4):S71.
- [116] Lee MS, Snutch TP. Z160: a potent, state-dependent, N-type calcium channel blocker effective in animal models of neuropathic pain. In: 4th International congress on neuropathic pain; 2013, PS1.
- [117] Marger F, Gelot A, Alloui A, Matricon J, Ferrer JF, Barrere C, et al. T-type calcium channels contribute to colonic hypersensitivity in a rat model of irritable bowel syndrome. *Proc Natl Acad Sci U S A* 2011;108(27):11268–73.
- [118] Pajouhesh H, Feng ZP, Ding Y, Zhang L, Morrison JL, Belardetti F, et al. Structure-activity relationships of diphenylpiperazine N-type calcium channel inhibitors. *Bioorg Med Chem Lett* 2010;20(4):1378–83.
- [119] Pajouhesh H, Feng ZP, Zhang L, Jiang X, Hendricson A, Dong H, et al. Structure-activity relationships of trimethoxybenzyl piperazine N-type calcium channel inhibitors. *Bioorg Med Chem Lett* 2012;22(12):4153–8.
- [120] Doherty GA, Bhatia P, Vortherms TA, Marsh KC, Wetter JM, Mack H, et al. Discovery of diphenyl lactam derivatives as N-type calcium channel blockers. *Bioorg Med Chem Lett* 2012;22(4):1716–8.
- [121] Heer JP, Cridland AP, Norton D. Piperazine derivatives for blocking Cav2.2 calcium channels. International PCT. Patent WO2011086377; 2011.
- [122] Heer JP, Cridland AP, Norton D. Piperazine derivatives for blocking Cav2.2 calcium channels. US Patent Application. Patent WO20130072499; 2013.
- [123] Norton D, Andreotti D, Ward SE, Profeta R, Spada S, Price HS. Piperazine derivatives as Cav2.2 calcium channel blockers. International PCT. Patent WO2012098400; 2012.
- [124] Beswick PJ, Gleave RJ, Hachisu S, Vile S, Bertheleme N, Ward SE. Tetrazole compounds as calcium channel blockers. International PCT. Patent WO2012004604; 2012.
- [125] Beswick PJ, Gleave RJ. 3-substituted 1-arylsulfonylpiperidine derivatives for the treatment of pain. international PCT. Patent WO2010091721; 2010.
- [126] Shao PP, Ye F, Chakravarty PK, Varughese DJ, Herrington JB, Dai G, et al. Aminopiperidine sulfonamide Cav2.2 channel inhibitors for the treatment of chronic pain. *J Med Chem* 2012;55(22):9847–55.
- [127] Chakravarty PK, Duffy JL, Shao PP. Substituted aryl sulfone derivatives as calcium channel blockers. International PCT. Patent WO2010036589; 2010.
- [128] Chakravarty PK, Shao PP. Substituted aryl sulfone derivatives as calcium channel blockers. International PCT. Patent WO2010036596; 2010.
- [129] Chakravarty PK, Ding Y, Duffy JL, Pajouhesh H, Shao PP, Tyagarajan S, et al. Substituted aryl sulfone derivatives as calcium channel blockers. US Patent 2012; US8304434.
- [130] Subasinghe NL, Wall MJ, Winters MP, Qin N, Lubin ML, Finley MF, et al. A novel series of pyrazolylpiperidine N-type calcium channel blockers. *Bioorg Med Chem Lett* 2012;22(12):4080–3.
- [131] Duffy JL, Hoyt SB, London C, Stevenson CP. N-substituted oxindoline derivatives as calcium channel blockers. International PCT. Patent WO2009045381; 2009.

- [132] Duffy JL, Hoyt SB, London C. N-substituted oxindoline derivatives as calcium channel blockers. International PCT. Patent WO2009045386; 2009.
- [133] Swensen AM, Herrington J, Bugianesi RM, Dai G, Haedo RJ, Ratliff KS, et al. Characterization of the substituted N-triazole oxindole TROX-1, a small-molecule, state-dependent inhibitor of Ca(V)₂ calcium channels. *Mol Pharmacol* 2012;81(3):488–97.
- [134] Tyagarajan S, Chakravarty PK, Park M, Zhou B, Herrington JB, Ratliff K, et al. A potent and selective indole N-type calcium channel (Ca_v2.2) blocker for the treatment of pain. *Bioorg Med Chem Lett* 2011;21(2):869–73.
- [135] Abbadie C, McManus OB, Sun SY, Bugianesi RM, Dai G, Haedo RJ, et al. Analgesic effects of a substituted N-triazole oxindole (TROX-1), a state-dependent, voltage-gated calcium channel 2 blocker. *J Pharmacol Exp Ther* 2010;334(2):545–55.
- [136] Beebe X, Darczak D, Henry RF, Vortherms T, Janis R, Namovic M, et al. Synthesis and SAR of 4-aminocyclopentapyrrolidines as N-type Ca₂(+) channel blockers with analgesic activity. *Bioorg Med Chem* 2012;20(13):4128–39.
- [137] Zhang Q, Sterwart AO, Xia Z. Novel benzenesulfonamides as calcium channel blockers. International PCT. Patent WO2010083264; 2010.
- [138] Searle XB, Yeung MC, Schrimpf MR. Substituted octahydrocyclopenta[c]pyrroles as calcium channel modulators. International PCT. Patent WO2011149993; 2011.
- [139] Searle XB, Yeung MC, Didomenico S, Stewart AO, Darczak D, Schrimpf MR, et al. Novel substituted octahydrocyclopenta[c]pyrrol-4-amines as calcium channel blockers. International PCT. Patent WO2011149995; 2011.
- [140] Li T, Patel S, Perner RJ, Randolph JT, Schrimpf MR, Woller KR, et al. Substituted octahydropyrrolo[1,2-A]pyrazine sulfonamides as calcium channel blockers. International PCT. Patent WO2013049174; 2013.
- [141] Gleave RJ, Hachisu S, Page LW, Beswick PJ. Spirocyclic derivatives with affinity for calcium channels. International PCT. Patent WO2011141728; 2011.
- [142] Gleave RJ, Hachisu S, Page LW. Novel compounds. International PCT. Patent WO2011141729; 2011.
- [143] Duffy JL, Hoyt SB, London C, Stevenson CP, Ullman AM. Substituted dihydroisoquinolinone and isoquinolinone derivatives as calcium channel blockers. International PCT. Patent WO2010017048; 2010.
- [144] Meng G, Wu N, Zhang C, Su RB, Lu XQ, Liu Y, et al. Analgesic activity of ZC88, a novel N-type voltage-dependent calcium channel blocker, and its modulation of morphine analgesia, tolerance and dependence. *Eur J Pharmacol* 2008;586(1–3):130–8.
- [145] Wei X, Sun H, Yan H, Zhang C, Zhang S, Liu X, et al. ZC88, a novel 4-amino piperidine analog, inhibits the growth of neuroblastoma cells through blocking hERG potassium channel. *Cancer Biol Ther* 2013;14(5):450–7.
- [146] Zhang S, Su R, Zhang C, Liu X, Li J, Zheng J. C101, a novel 4-amino-piperidine derivative selectively blocks N-type calcium channels. *Eur J Pharmacol* 2008;587(1–3):42–7.
- [147] Boffey RJ, Burckhardt S, Cansfield JE, Khan NM, Lawton G, Tickle D, et al. Calcium ion channel modulators and uses thereof. International PCT. Patent WO2009019508; 2009.
- [148] Mungalpara J, Pandey A, Jain V, Mohan CG. Molecular modelling and QSAR analysis of some structurally diverse N-type calcium channel blockers. *J Mol Model* 2010;16(4):629–44.
- [149] Zalicus. NCT01655849. www.clinicaltrials.gov; 2012.
- [150] Zalicus. NCT01757873. www.clinicaltrials.gov; 2012.
- [151] Hansen S. Convergence: toning down pain. *BioCentury* 2010;October 18, 2010.
- [152] Convergence. NCT01848730. www.clinicaltrials.gov; 2013.
- [153] Convergence. NCT01893125. www.clinicaltrials.gov; 2013.

SUBJECT INDEX

Note: Page numbers followed by “f” indicate figures, and “t” indicate tables.

A

- Adenosine triphosphate (ATP), 65–66, 67, 70–71
- Affectis Pharmaceuticals, 48–49
- Alzheimer’s disease (AD), 48–49, 68, 101–102
- Amyloid precursor proteins (APP), 102

B

- β_2 -adrenergic receptor (β_2 AR), 32
- Ballesteros–Weinstein nomenclature, 33
- Biogen Idec derivatives, 109–110
- Biophysical MappingTM, 51–52
- Boehringer Ingelheim, 127
- β -secretase (BACE), 135–137

C

- Carrageenan-induced paw oedema model, 52–53
- Central nervous system (CNS)
 - animal models, 88–92
 - ATP, 67
 - neurodegenerative disorders, 68–69
 - neurogenesis and axonal sprouting, 66
 - neuropsychiatric disorders, 67–68
 - pain, 69–70
- Chiesi derivatives, 104–105
- Chronic constriction injury (CCI) model, 88
- Complete Freund’s adjuvant (CFA) model, 38–39
- Corticotropin releasing factor (CRF1), 3
- Cyclotides, 52–53

E

- EnVivo derivatives, 106–107
- Epilepsy, 68
- Experimental autoimmune encephalomyelitis (EAE), 69

G

- γ -aminobutyric acid (GABA), 31
- Glucagon-like peptide receptor (GLP-1), 3

G protein coupled receptors (GPCRs)

- agonist bound structures
 - adenosine A_{2A} receptor, 37–38
 - 5-HT_{1B} and 5-HT_{2B}, 38–39
 - intracellular signalling pathways, 35–36
 - ligand binding site, 36
 - neurotensin receptor, 38
 - SBDD, 35–36
 - ternary complex model, 36
 - thermostabilised structures, 36–37
- biased agonism, 39–40
- crystal structures, 4t
- drug discovery, 40–41
- protein–ligand x-ray structures
 - amino acid residues, 33
 - antibody fragments, 32
 - Ballesteros–Weinstein number, 33
 - β_2 AR, 32
 - crystallisation, 31
 - crystallographic ligands, 33–35
 - LCP crystallisation/*in meso* crystallisation, 32–33
 - PDB, 33
 - stabilised receptors, 32
 - thermostabilisation, 32
 - T4L fusion approach, 32
- SBDD AND FBDD
 - adenosine receptors, 46–52
 - beta adrenergic receptors, 42–45
 - CRF₁ receptor, 53
 - CXCR4 chemokine receptor, 52–53
 - histamine receptor, 45–46
 - lead compounds, 41–42
 - medicinal chemistry, 41–42
 - receptor selectivity, 42
- structural architecture
 - adhesion receptors, 3
 - aminergic receptors, 3
 - calcium sensing receptor, 31
 - chemokine receptors, 3
 - frizzled (FZD) receptors, 31
 - GABA_B receptor, 31

G protein coupled receptors (GPCRs)

(Continued)

- glucagon receptor, 3
- glutamate receptor family, 31
- neuropeptide receptors, 3
- olfactory receptors, 3
- Secretin family (15 members) and Adhesion family (33 members), 3
- smoothed receptor, 31
- 7TM, 3

Growth hormone releasing hormone receptor (GHRH), 41

 γ -Secretase modulators (GSM)

- Alzheimer's disease, 101–102
- amyloid precursor proteins, 102
- BACE inhibitors, 135–137
- Biogen Idec derivatives, 109–110
- biology, 102–104
- chemical biology
 - NTF, 134–135
 - photoaffinity labelling probes, 133, 133f
 - western blot analysis, 133

Chiesi derivatives, 104–105

clinical studies, 137–139

EnVivo derivatives, 106–107

GSK derivatives, 108

imidazoles and analogues

- AstraZeneca group, 126–127
- BMS group, 120
- Boehringer Ingelheim, 127
- Dainippon Sumitomo group, 128
- GSK heterocyclic derivatives, 113–115
- Janssen research group, 116–120
- Merck research group, 123–126
- Pfizer group, 120–123
- Roche derivatives, 116
- Shionogi group, 128
- TorreyPines therapeutics, 111–113

Janssen derivatives, 105–106

Merck derivatives, 109

Myriad derivatives, 104–105

natural products, 129–132

Pfizer/Astellas derivatives, 110

GSK derivatives, 108

H

Highthroughput screening (HTS), 40–41

Huntington's disease, 68

Huwentoxins, 162

I

Intracellular loop (ICL3), 32

J

Janssen derivatives, 105–106

Janssen Pharmaceuticals, 86–87

L

Leuconotide, 161–162

Lipidic cubic phase (LCP), 32–33

Lipopolysaccharides (LPS), 67–68

M

Merck derivatives, 109

Merck-Schering Plough merger, 123–126

Monoiodoacetate (MIA) model, 90

Multiple sclerosis (MS), 68

Myriad derivatives, 104–105

N

N-terminal fragment (NTF) of presenilin-1, 133

N-terminal fragment (NTF) of presenilin-2, 134–135

N-Type calcium channel modulators

biology, 156–157

in clinical evaluation

CNV2197944, 178

Z160, 177

pain, pathophysiology of, 158

peptide-derived therapeutics

huwentoxins, 162

leuconotide, 161–162

mimetics, 162–164

by venom toxins, 159–160

 ω -conotoxin, 160–161

ziconotide, 160–161

physiology, 157

small molecule blockers

chiral aminocyclopentapyrrolidine series, 173–174

dihydroisoquinolinone and

soquinolinedione compounds, 175

indoles and oxindoles, 171–173

non-selective calcium channel

blockers, 164–166

orthogonal approach, 176–177

piperazine-based structures, 166–169

piperidine-containing structures,
170–171
spirocyclic derivatives, 175

P

Parathyroid hormone receptor (PTH1), 3
Parkinson's disease, 48–49, 51–52
Pfizer/Astellas derivatives, 110
Protein Database code (PDB), 33
Proteochemometric (PCM) modelling,
47–48

P2X7 antagonists

AstraZeneca's adamantanes (5), 72
benzoylbenzoyl ATP, 72–73
clinical trials
AstraZeneca's AZD9056, 71
Conba Pharmaceuticals, 71–72
IL-1 β release, 70–71
methotrexate, 71
neuropathic and inflammatory pain,
70–71

CNS

animal models, 88–92
ATP, 67
neurodegenerative disorders, 68–69
neurogenesis and axonal sprouting, 66
neuropsychiatric disorders, 67–68
pain, 69–70

heteroaromatic-fused core antagonists,
81–87

monocyclic hetero and carbocyclic
antagonists

Actelion, 80
amide carbonyl group, 77
CFA model, 74–75
3,4-dihydropyridin-2-ones, 78–79
dihydropyridones, 79
GSK1482160, 75–76
memory disorders, 80
methyl pyrazoles, 74–75
Nissan Chemical, 80
piperazinones, 77
pyrazole and oxazole-based antagonists,
73–74
pyroglutamic acid amide, 75
Roche patent applications, 78–79

sulfone, 76
TDI, 74–75

Pfizer's phenyl-6-azauracil amides (4), 72
radioligand binding assays, 72–73
Pyrazoloquinazolines, 49–50

R

Rheumatoid arthritis (RA), 32

S

Schering Corporation, 86
Seven membrane spanning
a-helices (7TM), 3
Structure–activity relationships (SAR), 164
Surface plasmon resonance (SPR) screening,
44–45

T

Target-immobilised NMR screening
(TINS), 48–49
Time-dependent inhibition (TDI), 38–39
T4 lysozyme (T4L), 32
TorreyPines therapeutics, 111–113
Transmembrane domain (TMD), 3

V

Venom toxins, 159–160
Venus fly trap, 31
Voltage-gated calcium channels (VGCCs).
See also N-Type calcium channel
modulators
architecture
Ca $_v$ α 2 δ subunits, 152
Ca $_v$ β subunits, 151–152
 γ subunits, 152
S5 and S6 segments, 150–151
 α 1 subunits, 148–150
 α 2 subunits, 151
three-dimensional structure, 150–151
channel states, 154–155
physiology, 152–154
therapeutic intervention, 155–156

Z

Ziconotide, 160–161

CUMULATIVE INDEX OF AUTHORS FOR VOLUMES 1–53

The volume number, (year of publication) and page number are given in that order.

- Aboul-Ela, F., 39 (2002) 73
Adam, J., 44 (2006) 209
Adams, J.L., 38 (2001) 1
Adams, S.S., 5 (1967) 59
Afshar, M., 39 (2002) 73
Agrawal, K.C., 15 (1978) 321
Ahmed, M., 48 (2009) 163
Albert, J.S., 48 (2009) 133
Albrecht, W.J., 18 (1981) 135
Albrecht-Küpper, B., 47 (2009) 163
Allain, H., 34 (1997) 1
Allen, M.J., 44 (2006) 335
Allen, N.A., 32 (1995) 157
Allender, C.J., 36 (1999) 235
Altmann, K.-H., 42 (2004) 171
Andrews, P.R., 23 (1986) 91
Ankersen, M., 39 (2002) 173
Ankier, S.I., 23 (1986) 121
Appendino, G., 44 (2006) 145
Arrang, J.-M., 38 (2001) 279
Armour, D., 43 (2005) 239
Aubart, K., 44 (2006) 109
- Badger, A.M., 38 (2001) 1
Bailey, E., 11 (1975) 193
Ballesta, J.P.G., 23 (1986) 219
Bamford, M., 47 (2009) 75
Banner, K.H., 47 (2009) 37
Banting, L., 26 (1989) 253; 33 (1996) 147
Barbier, A.J., 44 (2006) 181
Barker, G., 9 (1973) 65
Barnes, J.M., 4 (1965) 18
Barnett, M.I., 28 (1991) 175
Bartolomé, J.M., 49 (2010) 37
Batt, D.G., 29 (1992) 1
Beaumont, D., 18 (1981) 45
Beckett, A.H., 2 (1962) 43; 4 (1965) 171
Beckman, M.J., 35 (1998) 1
Beddell, C.R., 17 (1980) 1
Beedham, C., 24 (1987) 85
Beeley, L.J., 37 (2000) 1
Beher, D., 41 (2003) 99
Beisler, J.A., 19 (1975) 247
Bell, J.A., 29 (1992) 239
Belliard, S., 34 (1997) 1
- Benfey, B.G., 12 (1975) 293
Bentué-Ferrer, D., 34 (1997) 1
Bernstein, P.R., 31 (1994) 59
Besra, G.S., 45 (2007) 169
Bhattacharya, A., 53 (2014) 65
Bhowruth, V., 45 (2007) 169
Binnie, A., 37 (2000) 83
Bischoff, E., 41 (2003) 249
Biswas, K., 46 (2008) 173
Black, M.E., 11 (1975) 67
Blandina, P., 22 (1985) 267
Bond, P.A., 11 (1975) 193
Bonta, I.L., 17 (1980) 185
Booth, A.G., 26 (1989) 323
Boreham, P.F.I., 13 (1976) 159
Böls, M., 44 (2006) 65
Bowman, W.C., 2 (1962) 88
Bradner, W.T., 24 (1987) 129
Bragt, P.C., 17 (1980) 185
Brain, K.R., 36 (1999) 235
Branch, S.K., 26 (1989) 355
Braquet, P., 27 (1990) 325
Brezina, M., 12 (1975) 247
Brooks, B.A., 11 (1975) 193
Brown, J.R., 15 (1978) 125
Brunelleschi, S., 22 (1985) 267
Bruni, A., 19 (1982) 111
Buckingham, J.C., 15 (1978) 165
Budelsky, A.L., 50 (2010) 51
Bulman, R.A., 20 (1983) 225
Burgey, C.S., 47 (2009) 1
- Calderón, F., 52 (2012) 97
Camaioni, E., 42 (2004) 125
Carman-Krzan, M., 23 (1986) 41
Carruthers, N.I., 44 (2006) 181
Cassells, A.C., 20 (1983) 119
Casy, A.F., 2 (1962) 43; 4 (1965) 171; 7 (1970) 229; 11 (1975) 1; 26 (1989) 355
Casy, G., 34 (1997) 203
Caton, M.P.L., 8 (1971) 217; 15 (1978) 357
Cecil, A., 48 (2009) 81, 50 (2010) 107
Chambers, M.S., 37 (2000) 45
Chang, J., 22 (1985) 293
Chappel, C.I., 3 (1963) 89

- Chatterjee, S., 28 (1991) 1
 Chawla, A.S., 17 (1980) 151; 22 (1985) 243
 Chen, C., 45 (2007) 111
 Chen, J.J., 46 (2008) 173, 50 (2010) 51
 Chen, K.X., 48 (2010) 1
 Cheng, C.C., 6 (1969) 67; 7 (1970) 285; 8 (1971) 61; 13 (1976) 303; 19 (1982) 269; 20 (1983) 83; 25 (1988) 35
 Cherry, M., 44 (2006) 1
 Chrovian, C.C., 53 (2014) 65
 Chuang, T.T., 48 (2009) 163
 Chung, C-W., 51 (2012) 1
 Clark, R.D., 23 (1986) 1
 Clitherow, J.W., 41 (2003) 129
 Cobb, R., 5 (1967) 59
 Cochrane, D.E., 27 (1990) 143
 Congreve, M., 53 (2014) 1
 Corbett, J.W., 40 (2002) 63
 Costantino, G., 42 (2004) 125
 Coulton, S., 31 (1994) 297; 33 (1996) 99
 Cowley, P.M., 44 (2006) 209
 Cox, B., 37 (2000) 83
 Crossland, J., 5 (1967) 251
 Crowshaw, K., 15 (1978) 357
 Cushman, D.W., 17 (1980) 41
 Cuthbert, A.W., 14 (1977) 1
- Dabrowiak, J.C., 24 (1987) 129
 Daly, M.J., 20 (1983) 337
 D'Arcy, P.F., 1 (1961) 220
 Daves, G.D., 13 (1976) 303; 22 (1985) 1
 Davies, G.E., 2 (1962) 176
 Davies, R.V., 32 (1995) 115
 De Clercq, E., 23 (1986) 187
 De Gregorio, M., 21 (1984) 111
 De Luca, H.F., 35 (1998) 1
 De, A., 18 (1981) 117
 Deaton, D.N., 42 (2004) 245
 Demeter, D.A., 36 (1999) 169
 Denyer, J.C., 37 (2000) 83
 Derouensé, C., 34 (1997) 1
 Dias, J.M., 53 (2014) 1
 Dimitrakoudi, M., 11 (1975) 193
 Donnelly, M.C., 37 (2000) 83
 Dover, L.G., 45 (2007) 169
 Draffan, G.H., 12 (1975) 1
 Drewe, J.A., 33 (1996) 233
 Drysdale, M.J., 39 (2002) 73
 Dubinsky, B., 36 (1999) 169
 Duckworth, D.M., 37 (2000) 1
 Duffield, J.R., 28 (1991) 175
 Durant, G.J., 7 (1970) 124
 Dvorak, C.A., 44 (2006) 181
- Eccleston, J.F., 43 (2005) 19
 Edwards, D.I., 18 (1981) 87
 Edwards, P.D., 31 (1994) 59
 Eglen, R.M., 43 (2005) 105
 Eldred, C.D., 36 (1999) 29
 Ellis, G.P., 6 (1969) 266; 9 (1973) 65; 10 (1974) 245
 Ertl, P., 49 (2010) 113
 Evans, B., 37 (2000) 83
 Evans, J.M., 31 (1994) 409
- Falch, E., 22 (1985) 67
 Fantozzi, R., 22 (1985) 267
 Feigenbaum, J.J., 24 (1987) 159
 Ferguson, D.M., 40 (2002) 107
 Feuer, G., 10 (1974) 85
 Finberg, J.P.M., 21 (1984) 137
 Fletcher, S.R., 37 (2000) 45
 Flörsheimer, A., 42 (2004) 171
 Floyd, C.D., 36 (1999) 91
 Franc-ois, I., 31 (1994) 297
 Frank, H., 27 (1990) 1
 Freeman, S., 34 (1997) 111
 Fride, E., 35 (1998) 199
- Gale, J.B., 30 (1993) 1
 Gamo, F-J., 52 (2012) 97
 Ganellin, C.R., 38 (2001) 279
 Garbarg, M., 38 (2001) 279
 Garratt, C.J., 17 (1980) 105
 Gedeck, P., 49 (2010) 113
 Geney, R., 52 (2012) 153
 Gerspacher, M., 43 (2005) 49
 Gill, E.W., 4 (1965) 39
 Gillespie, P., 45 (2007) 1
 Ginsburg, M., 1 (1961) 132
 Glennon, R.A., 42 (2004) 55
 Goldberg, D.M., 13 (1976) 1
 Goodnow, Jr. R.A., 45 (2007) 1
 Gould, J., 24 (1987) 1
 Graczyk, P.P., 39 (2002) 1
 Graham, J.D.P., 2 (1962) 132
 Green, A.L., 7 (1970) 124
 Green, D.V.S., 37 (2000) 83; 41 (2003) 61
 Greenhill, J.V., 27 (1990) 51; 30 (1993) 206
 Griffin, R.J., 31 (1994) 121
 Griffiths, D., 24 (1987) 1
 Griffiths, K., 26 (1989) 299
 Groenewegen, W.A., 29 (1992) 217
 Groundwater, P.W., 33 (1996) 233
 Guile, S.D., 38 (2001) 115

- Gunda, E.T., 12 (1975) 395; 14 (1977) 181
Gyllys, J.A., 27 (1990) 297
- Hacksell, U., 22 (1985) 1
Haefner, B., 43 (2005) 137
Hall, A.D., 28 (1991) 41; 53 (2014) 101
Hall, S.B., 28 (1991) 175
Hallidin, C., 38 (2001) 189
Halliday, D., 15 (1978) 1
Hammond, S.M., 14 (1977) 105; 16 (1979) 223
Hamor, T.A., 20 (1983) 157
Haning, H., 41 (2003) 249
Hanson, P.J., 28 (1991) 201
Hanus, L., 35 (1998) 199
Hargreaves, R.B., 31 (1994) 369
Harris, J.B., 21 (1984) 63
Harrison, R., 50 (2010) 107
Harrison, T., 41 (2003) 99
Hartley, A.J., 10 (1974) 1
Hartog, J., 15 (1978) 261
Heacock, R.A., 9 (1973) 275;
11 (1975) 91
Heard, C.M., 36 (1999) 235
Heinisch, G., 27 (1990) 1; 29 (1992) 141
Heller, H., 1 (1961) 132
Henke, B.R., 42 (2004) 1
Heptinstall, S., 29 (1992) 217
Herling, A.W., 31 (1994) 233
Hider, R.C., 28 (1991) 41
Hill, S.J., 24 (1987) 30
Hill, T., 48 (2009) 81, 50 (2010) 107
Hillen, F.C., 15 (1978) 261
Hino, K., 27 (1990) 123
Hjeds, H., 22 (1985) 67
Holdgate, G.A., 38 (2001) 309
Hooper, M., 20 (1983) 1
Hopwood, D., 13 (1976) 271
Horne, G., 50 (2010) 133
Hosford, D., 27 (1990) 325
Hu, B., 41 (2003) 167
Hubbard, R.E., 17 (1980) 105
Hudkins, R.L., 40 (2002) 23
Hughes, A.D., 51 (2012) 71
Hughes, R.E., 14 (1977) 285
Hugo, W.B., 31 (1994) 349
Hulin, B., 31 (1994) 1
Humber, L.G., 24 (1987) 299
Hunt, E., 33 (1996) 99
Hutchinson, J.P., 43 (2005) 19
- Ijzerman, A.P., 38 (2001) 61
Imam, S.H., 21 (1984) 169
Ince, F., 38 (2001) 115
- Ingall, A.H., 38 (2001) 115
Ireland, S.J., 29 (1992) 239
- Jacques, L.B., 5 (1967) 139
James, K.C., 10 (1974) 203
Jameson, D.M., 43 (2005) 19
Jászberényi, J.C., 12 (1975) 395; 14 (1977) 181
Jenner, F.D., 11 (1975) 193
Jennings, L.L., 41 (2003) 167
Jewers, K., 9 (1973) 1
Jindal, D.P., 28 (1991) 233
Jones, B.C., 41 (2003) 1; 47 (2009) 239
Jones, D.W., 10 (1974) 159
Jones, L.H., 52 (2012) 45
Jorvig, E., 40 (2002) 107
Judd, A., 11 (1975) 193
Judkins, B.D., 36 (1999) 29
- Kadow, J.F., 32 (1995) 289
Kapoor, V.K., 16 (1979) 35; 17 (1980) 151; 22
(1985) 243; 43 (2005) 189
Kawato, Y., 34 (1997) 69
Kelly, M.J., 25 (1988) 249
Kemp, M.I., 49 (2010) 81
Kendall, H.E., 24 (1987) 249
Kennett, G.A., 46 (2008) 281
Kennis, L.E.J., 33 (1996) 185
Kew, J.N.C., 46 (2008) 131
Khan, M.A., 9 (1973) 117
Kiefel, M.J., 36 (1999) 1
Kilpatrick, G.J., 29 (1992) 239
Kinson, N.D., 38, (2001) 115
King, F.D., 41 (2003) 129
Kirst, H.A., 30 (1993) 57; 31
(1994) 265
Kitteringham, G.R., 6 (1969) 1
Kiyoi, T., 44 (2006) 209
Knight, D.W., 29 (1992) 217
Körner, M., 46 (2008) 205
Kobayashi, Y., 9 (1973) 133
Koch, H.P., 22 (1985) 165
Kopelent-Frank, H., 29 (1992) 141
Kort, M.E., 51 (2012) 57
Kramer, C., 49 (2010) 113
Kramer, M.J., 18 (1981) 1
Krause, B.R., 39 (2002) 121
KrogsgaardLarsen, P., 22 (1985) 67
Kulkarni, S.K., 37 (2000) 135
Kumar, K., 43 (2005) 189
Kumar, M., 28 (1991) 233
Kumar, S., 38 (2001) 1; 42 (2004) 245
Kwong, A.D., 39 (2002) 215
Kym, P.R., 51 (2012) 57

- Lambert, P.A., 15 (1978) 87
 Launchbury, A.P., 7 (1970) 1
 Law, H.D., 4 (1965) 86
 Lawen, A., 33 (1996) 53
 Lawson, A.M., 12 (1975) 1
 Leblanc, C., 36 (1999) 91
 Lee, C.R., 11 (1975) 193
 Lee, J.C., 38 (2001) 1
 Lee, M.S., 53 (2014) 147
 Lenton, E.A., 11 (1975) 193
 Lentzen, G., 39 (2002) 73
 Letavic, M.A., 44 (2006) 181; 53 (2014) 65
 Levin, R.H., 18 (1981) 135
 Lewis, A.J., 19 (1982) 1; 22 (1985) 293
 Lewis, D.A., 28 (1991) 201
 Lewis, J.A., 37 (2000) 83
 Li, Y., 43 (2005) 1
 Lien, E.L., 24 (1987) 209
 Lightfoot, A.P., 46 (2008) 131
 Ligneau, X., 38 (2001) 279
 Lin, T.-S., 32 (1995) 1
 Liu, M.-C., 32 (1995) 1
 Livermore, D.G.H., 44 (2006) 335
 Llinas-Brunet, M., 44 (2006) 65
 Lloyd, E.J., 23 (1986) 91
 Lockhart, I.M., 15 (1978) 1
 Lord, J.M., 24 (1987) 1
 Lowe, I.A., 17 (1980) 1
 Lucas, R.A., 3 (1963) 146
 Lue, P., 30 (1993) 206
 Luscombe, D.K., 24 (1987) 249

 MacDonald, G.J., 49 (2010) 37
 Mackay, D., 5 (1967) 199
 Main, B.G., 22 (1985) 121
 Malhotra, R.K., 17 (1980) 151
 Malmström, R.E., 42 (2004) 207
 Manchanda, A.H., 9 (1973) 1
 Mander, T.H., 37 (2000) 83
 Mannaioni, P.F., 22 (1985) 267
 Maroney, A.C., 40 (2002) 23
 Marshall, F.H., 53 (2014) 1
 Martin, I.L., 20 (1983) 157
 Martin, J.A., 32 (1995) 239
 Masini, F., 22 (1985) 267
 Matassova, N., 39 (2002) 73
 Matsumoto, J., 27 (1990) 123
 Matthews, R.S., 10 (1974) 159
 Maudsley, D.V., 9 (1973) 133
 May, P.M., 20 (1983) 225
 McCague, R., 34 (1997) 203
 McFadyen, I., 40 (2002) 107
 McKerrecher, D., 52 (2012) 1

 McLelland, M.A., 27 (1990) 51
 McNamara, A., 51 (2012) 71
 McNeil, S., 11 (1975) 193
 Mechoulam, R., 24 (1987) 159; 35 (1998) 199
 Meggens, A.A.H.P., 33 (1996) 185
 Megges, R., 30 (1993) 135
 Meghani, P., 38 (2001) 115
 Menet, C.J., 52 (2012) 153
 Merritt, A.T., 37 (2000) 83
 Metzger, T., 40 (2002) 107
 Michel, A.D., 23 (1986) 1
 Middlemiss, D.N., 41 (2003) 129
 Middleton, D.S., 47 (2009) 239
 Miura, K., 5 (1967) 320
 Moncada, S., 21 (1984) 237
 Monck, N.J.T., 46 (2008) 281
 Monkovic, I., 27 (1990) 297
 Montgomery, J.A., 7 (1970) 69
 Moody, G.J., 14 (1977) 51
 Mordaunt, J.E., 44 (2006) 335
 Morris, A., 8 (1971) 39; 12 (1975) 333
 Morrison, A.J., 44 (2006) 209
 Mort, C.J.W., 44 (2006) 209
 Mortimore, M.P., 38 (2001) 115
 Munawar, M.A., 33 (1996) 233
 Murchie, A.I.H., 39 (2002) 73
 Murphy, F., 2 (1962) 1; 16 (1979) 1
 Musallan, H.A., 28 (1991) 1
 Musser, J.H., 22 (1985) 293

 Natoff, I.L., 8 (1971) 1
 Neidle, S., 16 (1979) 151
 Nell, P.G., 47 (2009) 163
 Nicholls, P.J., 26 (1989) 253
 Niewöhner, U., 41 (2003) 249
 Njoroge, F.G., 49 (2010) 1
 Nodiff, E.A., 28 (1991) 1
 Nordlind, K., 27 (1990) 189
 Nortey, S.O., 36 (1999) 169

 O'Hare, M., 24 (1987) 1
 O'Reilly, T., 42 (2004) 171
 Ondetti, M.A., 17 (1980) 41
 Ottenheim, H.C.J., 23 (1986) 219
 Oxford, A.W., 29 (1992) 239

 Paget, G.E., 4 (1965) 18
 Palatini, P., 19 (1982) 111
 Palazzo, G., 21 (1984) 111
 Palfreyman, M.N., 33 (1996) 1
 Palmer, D.C., 25 (1988) 85
 Palmer, M.J., 47 (2009) 203
 Parkes, M.W., 1 (1961) 72

- Parnham, M.J., 17 (1980) 185
Parratt, J.R., 6 (1969) 11
Patel, A., 30 (1993) 327
Patel, T.R., 53 (2014) 101
Paul, D., 16 (1979) 35; 17 (1980) 151
Pearce, F.L., 19 (1982) 59
Peart, W.S., 7 (1970) 215
Pellicciari, R., 42 (2004) 125
Perni, R.B., 39 (2002) 215
Petrow, V., 8 (1971) 171
Picard, J.A., 39 (2002) 121
Pike, V.W., 38 (2001) 189
Pinder, R.M., 8 (1971) 231; 9 (1973) 191
Poda, G., 40 (2002) 107
Ponnudurai, T.B., 17 (1980) 105
Potter, B.V.L., 46 (2008) 29
Powell, W.S., 9 (1973) 275
Power, E.G.M., 34 (1997) 149
Press, N.J., 47 (2009) 37
Price, B.J., 20 (1983) 337
Price, D.A., 52 (2012) 45
Prior, B., 24 (1987) 1
Procopiou, P.A., 33 (1996) 331
Purohit, M.G., 20 (1983) 1

Ram, S., 25 (1988) 233
Rampe, D., 43 (2005) 1
Reader, J., 44 (2006) 1
Rech, J.C., 53 (2014) 65
Reckendorf, H.K., 5 (1967) 320
Reddy, D.S., 37 (2000) 135
Redshaw, S., 32 (1995) 239
Rees, D.C., 29 (1992) 109
Reitz, A.B., 36 (1999) 169
Repke, K.R.H., 30 (1993) 135
Richards, W.G., 11 (1975) 67
Richardson, P.T., 24 (1987) 1
Roberts, L.M., 24 (1987) 1
Rodgers, J.D., 40 (2002) 63
Roe, A.M., 7 (1970) 124
Rogers, H., 48 (2009) 81, 50 (2010) 107
Rose, H.M., 9 (1973) 1
Rosen, T., 27 (1990) 235
Rosenberg, S.H., 32 (1995) 37
Ross, K.C., 34 (1997) 111
Roth, B., 7 (1970) 285; 8 (1971) 61;
19 (1982) 269
Roth, B.D., 40 (2002) 1
Rowley, M., 46 (2008) 1
Russell, A.D., 6 (1969) 135; 8 (1971) 39;
13 (1976) 271; 31 (1994) 349; 35
(1998) 133
Ruthven, C.R.J., 6 (1969) 200
Sadler, P.J., 12 (1975) 159
Salvatore, C.A., 47 (2009) 1
Sampson, G.A., 11 (1975) 193
Sandler, M., 6 (1969) 200
Sanger, G.J., 48 (2009) 31
Saporito, M.S., 40 (2002) 23
Sarges, R., 18 (1981) 191
Sartorelli, A.C., 15 (1978) 321; 32 (1995) 1
Saunders, J., 41 (2003) 195
Schiller, P.W., 28 (1991) 301
Schmidhammer, H., 35 (1998) 83
Schön, R., 30 (1993) 135
Schunack, W., 38 (2001) 279
Schwartz, J.-C., 38 (2001) 279
Schwartz, M.A., 29 (1992) 271
Scott, M.K., 36 (1999) 169
Sewell, R.D.E., 14 (1977) 249;
30 (1993) 327
Shank, R.P., 36 (1999) 169
Shaw, M.A., 26 (1989) 253
Sheard, P., 21 (1984) 1
Shepherd, D.M., 5 (1967) 199
Shuttleworth, S., 48 (2009) 81, 50
(2010) 107
Silva, F., 48 (2009) 81, 50 (2010) 107
Silver, P.J., 22 (1985) 293
Silvestrini, B., 21 (1984) 111
Singh, H., 16 (1979) 35; 17 (1980) 151;
22 (1985) 243; 28 (1991) 233
Skidmore, J., 46 (2008) 131
Skotnicki, J.S., 25 (1988) 85
Slater, J.D.H., 1 (1961) 187
Sliskovic, D.R., 39 (2002) 121
Smith, G.F., 48 (2009) 1, 50 (2010) 1
Smith, H.J., 26 (1989) 253; 30 (1993) 327
Smith, R.C., 12 (1975) 105
Smith, W.G., 1 (1961) 1; 10 (1974) 11
Solomons, K.R.H., 33 (1996) 233
Sorenson, J.R.J., 15 (1978) 211;
26 (1989) 437
Souness, J.E., 33 (1996) 1
Southan, C., 37 (2000) 1
Spencer, P.S.J., 4 (1965) 1; 14 (1977) 249
Spinks, A., 3 (1963) 261
Stähle, L., 25 (1988) 291
Stark, H., 38 (2001) 279
Steiner, K.E., 24 (1987) 209
Steinfeld, T., 51 (2012) 71
Stenlake, J.B., 3 (1963) 1; 16 (1979) 257
Stevens, M.F.G., 13 (1976) 205
Stewart, G.A., 3 (1963) 187
Studer, R.O., 5 (1963) 1
Su, X., 46 (2008) 29

- Subramanian, G., 40 (2002) 107
 Sullivan, M.E., 29 (1992) 65
 Suschitzky, J.L., 21 (1984) 1
 Swain, C.J., 35 (1998) 57
 Swallow, D.L., 8 (1971) 119
 Sykes, R.B., 12 (1975) 333
 Szallasi, A., 44 (2006) 145
- Talley, J.J., 36 (1999) 201
 Taylor, E.C., 25 (1988) 85
 Taylor, E.P., 1 (1961) 220
 Taylor, S.G., 31 (1994) 409
 Tegnér, C., 3 (1963) 332
 Terasawa, H., 34 (1997) 69
 Thomas, G.J., 32 (1995) 239
 Thomas, I.L., 10 (1974) 245
 Thomas, J.D.R., 14 (1977) 51
 Thompson, E.A., 11 (1975) 193
 Thompson, M., 37 (2000) 177
 Thurairatnam, S., 51 (2012) 97
 Tibes, U., 46 (2008) 205
 Tilley, J.W., 18 (1981) 1
 Timmerman, H., 38 (2001) 61
 Tomassi, C., 48 (2009) 81, 50 (2010) 107
 Townsend, P., 48 (2009) 81, 50 (2010) 107
 Traber, R., 25 (1988) 1
 Tucker, H., 22 (1985) 121
 Tyers, M.B., 29 (1992) 239
- Upton, N., 37 (2000) 177
- Valler, M.J., 37 (2000) 83
 Van de Waterbeemd, H., 41 (2003) 1
 Van den Broek, L.A.G.M., 23 (1986) 219
 Van Dijk, J., 15 (1978) 261
 Van Muijlwijk-Koezen, J.E., 38 (2001) 61
 Van Rompaey, L., 52 (2012) 153
 Van Wart, H.E., 29 (1992) 271
 Vaz, R.J., 43 (2005) 1
 Vicker, N., 46 (2008) 29
 Vincent, J.E., 17 (1980) 185
 Volke, J., 12 (1975) 247
 Von Itzstein, M., 36 (1999) 1
 Von Seeman, C., 3 (1963) 89
 Von Wartburg, A., 25 (1988) 1
 Vyas, D.M., 32 (1995) 289
- Waigh, R.D., 18 (1981) 45
 Wajsbort, J., 21 (1984) 137
 Walker, R.T., 23 (1986) 187
 Walls, L.P., 3 (1963) 52
 Walz, D.T., 19 (1982) 1
- Ward, W.H.J., 38 (2001) 309
 Waring, M.J., 52 (2012) 1
 Waring, W.S., 3 (1963) 261
 Wartmann, M., 42 (2004) 171
 Watson, N.S., 33 (1996) 331
 Watson, S.P., 37 (2000) 83
 Wedler, F.C., 30 (1993) 89
 Weidmann, K., 31 (1994) 233
 Weiland, J., 30 (1993) 135
 West, G.B., 4 (1965) 1
 Westaway, S.M., 48 (2009) 31
 White, P.W., 44 (2006) 65
 Whiting, R.L., 23 (1986) 1
 Whittaker, M., 36 (1999) 91
 Whittle, B.J.R., 21 (1984) 237
 Wiedling, S., 3 (1963) 332
 Wiedeman, P.E., 45 (2007) 63
 Wien, R., 1 (1961) 34
 Williams, T.M., 47 (2009) 1
 Wikström, H., 29 (1992) 185
 Wikström, H.V., 38 (2001) 189
 Wilkinson, S., 17 (1980) 1
 Williams, D., 44 (2006) 1
 Williams, D.R., 28 (1991) 175
 Williams, J., 41 (2003) 195
 Williams, J.C., 31 (1994) 59
 Williams, K.W., 12 (1975) 105
 Williams-Smith, D.L., 12 (1975) 191
 Wilson, C., 31 (1994) 369
 Wilson, D.M., 52 (2012) 97
 Wilson, F.X., 50 (2010) 133
 Wilson, H.K., 14 (1977) 285
 Witte, E.C., 11 (1975) 119
 Witty, D., 48 (2009) 163
 Wold, S., 25 (1989) 291
 Wood, A., 43 (2005) 239
 Wood, E.J., 26 (1989) 323
 Wright, I.G., 13 (1976) 159
 Wyard, S.J., 12 (1975) 191
 Wyman, P.A., 41 (2003) 129
- Yadav, M.R., 28 (1991) 233
 Yates, D.B., 32 (1995) 115
 Youdim, K., 47 (2009) 239
 Youdim, M.B.H., 21 (1984) 137
 Young, P.A., 3 (1963) 187
 Young, R.N., 38 (2001) 249
- Zalacain, M., 44 (2006) 109
 Zee-Cheng, R.K.Y., 20 (1983) 83
 Zon, G., 19 (1982) 205
 Zylicz, Z., 23 (1986) 219

CUMULATIVE INDEX OF SUBJECTS FOR VOLUMES 1–53

The volume number, (year of publication) and page number are given in that order.

- ACAT inhibitors, 39 (2002) 121
- Adamantane,
 amino derivatives, 18 (1981) 1
- Adenosine A₁ receptor ligands, 47 (2009) 163
- Adenosine A₃ receptor ligands, 38 (2001) 61
- Adenosine triphosphate, 16 (1979) 223
- Adenylate cyclase, 12 (1975) 293
- Adipose tissue, 17 (1980) 105
- Adrenergic agonists, β_3 -, 41 (2003) 167
 multivalent dual pharmacology MABA, 51 (2012) 71
- Adrenergic blockers, α -, 23 (1986) 1 β -, 22 (1985) 121
- α_2 -Adrenoceptors, antagonists, 23 (1986) 1
- Adrenochrome derivatives, 9 (1973) 275
- Adriamycin, 15 (1978) 125; 21 (1984) 169
- AIDS, drugs for, 31 (1994) 121
- Aldehyde thiosemicarbazones as antitumour agents, 15 (1978) 321; 32 (1995) 1
- Aldehydes as biocides, 34 (1997) 149
- Aldose reductase inhibitors, 24 (1987) 299
- Allergy, chemotherapy of, 21 (1984) 1; 22 (1985) 293
- Alzheimer's disease, chemotherapy of, 34 (1997) 1; 36 (1999) 201
 M1 agonists in, 43 (2005) 113
- Amidines and guanidines, 30 (1993) 203
- Aminoadamantane derivatives, 18 (1981) 1
- Aminopterin as antitumour agents, 25 (1988) 85
- 8-Aminoquinolines as antimalarial drugs, 28 (1991) 1; 43 (2005) 220
- Analgesic drugs, 2 (1962) 43; 4 (1965) 171; 7 (1970) 229; 14 (1977) 249
- Anaphylactic reactions, 2 (1962) 176
- Angiotensin, 17 (1980) 41; 32 (1995) 37
- Anthraquinones, antineoplastic, 20 (1983) 83
- Antiallergic drugs, 21 (1984) 1; 22 (1985) 293; 27 (1990) 34
- Antiapoptotic agents, 39 (2002) 1
- Antiarrhythmic drugs, 29 (1992) 65
- Antiarthritic agents, 15 (1978) 211; 19 (1982) 1; 36 (1999) 201
- Anti-atherosclerotic agents, 39 (2002) 121
- Antibacterial agents, 6 (1969) 135; 12 (1975) 333; 19 (1982) 269; 27 (1990) 235; 30 (1993) 203; 31 (1994) 349; 34 (1997) resistance to, 32 (1995) 157; 35 (1998) 133
- Antibiotics, antitumour, 19 (1982) 247; 23 (1986) 219
 carbapenem, 33 (1996) 99
 β -lactam, 12 (1975) 395; 14 (1977) 181; 31 (1994) 297; 33 (1996) 99
 macrolide, 30 (1993) 57; 32 (1995) 157
 mechanisms of resistance, 35 (1998) 133
 polyene, 14 (1977) 105; 32 (1995) 157
 resistance to, 31 (1994) 297; 32 (1995) 157; 35 (1998) 133
- Anticancer agents — *see* Antibiotics, Antitumour agents
- Anticonvulsant drugs, 3 (1963) 261; 37 (2000) 177
- Antidepressant drugs, 15 (1978) 261; 23 (1986) 121
- Antidiabetic agents, 41 (2003) 167; 42 (2004) 1
- Antiemetic action of 5-HT₃ antagonists, 27 (1990) 297; 29 (1992) 239
- Antiemetic drugs, 27 (1990) 297; 29 (1992) 239
- Antiepileptic drugs, 37 (2000) 177
- Antifilarial benzimidazoles, 25 (1988) 233
- Antifolates as anticancer agents, 25 (1988) 85; 26 (1989) 1
- Antifungal agents, 1 (1961) 220
- Antihyperlipidemic agents, 11 (1975) 119
- Anti-inflammatory action of cyclooxygenase-2 (COX-2) inhibitors, 36 (1999) 201
 of thalidomide, 22 (1985) 165
 of 5-lipoxygenase inhibitors, 29 (1992) 1
 of p38 MAP kinase inhibitors, 38 (2001) 1
- Anti-inflammatory agents, 5 (1967) 59; 36 (1999) 201; 38 (2001) 1; 39 (2002) 1
- Antimalarial agents, 43 (2005) 189
- Antimalarial 8-aminoquinolines, 28 (1991) 1
- Antimalarial drug discovery, 52 (2012) 97
- Antimicrobial agents for sterilization, 34 (1997) 149
- Antineoplastic agents, a new approach, 25 (1988) 35
 anthraquinones as, 20 (1983) 83
- Anti-osteoporosis drugs, 42 (2004) 245
- Antipsychotic drugs, 33 (1996) 185
- Ami-rheumatic drugs, 17 (1980) 185; 19 (1982) 1; 36 (1999) 201
- Antisecretory agents, 37 (2000) 45

- Antithrombotic agents, 36 (1999) 29
- Antitumour agents, 9 (1973) 1; 19 (1982) 247; 20 (1983) 83; 23 (1986) 219; 24 (1987) 1, 129; 25 (1988) 35, 85; 26 (1989) 253, 299; 30 (1993) 1; 32 (1995) 1, 289; 34 (1997) 69; 42 (2004) 171
- Antitussive drugs, 3 (1963) 89
- Anti-ulcer drugs, of plant origin, 28 (1991) 201
 ranitidine, 20 (1983) 67
 synthetic, 30 (1993) 203
- Antiviral agents, 8 (1971) 119; 23 (1986) 187; 36 (1999) 1; 39 (2002) 215
- Anxiety neurokinin receptors in, 43 (2005) 53
- Anxiolytic agents, CCK-B antagonists as, 37 (2000) 45
- Anxiolytic agents, pyrido[1,2-*a*]benzimidazoles as, 36 (1999) 169
- Aromatase inhibition and breast cancer, 26 (1989) 253; 33 (1996) 147
- Arthritis neurokinin receptors in, 43 (2005) 53
- Aspartic proteinase inhibitors, 32 (1995) 37, 239
- Asthma, drugs for, 21 (1984) 1; 31 (1994) 369, 409; 33 (1996) 1; 38 (2001) 249
 neurokinin receptors in, 43 (2005) 53
- Atorvastatin, hypolipidemic agent, 40 (2002) 1
- ATPase inhibitors, gastric, H⁺ /K⁺-31 (1994) 233
- Atypical antipsychotics, 49 (2010) 37
- Azides, 31 (1994) 121
- Bacteria, mechanisms of resistance to antibiotics and biocides, 35 (1998) 133
- Bacterial and mammalian collagenases: their inhibition, 29 (1992) 271
- Benzamide glucokinase activators, 52 (2012) 1
- 1-Benzazepines, medicinal chemistry of, 27 (1990) 123
- Benzimidazole carbamates, antifilarial, 25 (1988) 233
- Benzothiazole derivatives, 18 (1981) 117
- Benzodiazepines, 20 (1983) 157; 36 (1999) 169
- Benzo[*b*]pyranol derivatives, 37 (2000) 177
- β-secretase inhibitors, 48 (2009)
- Biocides, aldehydes, 34 (1997) 149
 mechanisms of resistance, 35 (1998) 133
- Boceprevir, 49 (2010) 1
- Bradykinin B1 receptor antagonists, 46 (2008) 173
- British Pharmacopoeia Commission, 6 (1969) 1
- Bromodomain-containing proteins (BCPs), 51 (2012) 1
- Bronchodilator and anti-allergic therapy, 22 (1985) 293
- Calcitonin gene-related peptide receptor antagonists, 47 (2009) 1
- Calcium and histamine secretion from mast cells, 19 (1982) 59
- Calcium channel blocking drugs, 24 (1987) 249
- Camptothecin and its analogues, 34 (1997) 69
- Cancer, aromatase inhibition and breast, 26 (1989) 253
 azides and, 31 (1994) 121
 camptothecin derivatives, 34 (1997) 69
 endocrine treatment of prostate, 26 (1989) 299
 retinoids in chemotherapy, 30 (1993) 1
- Cannabinoid drugs, 24 (1987) 159; 35 (1998) 199; 44 (2006) 207
- Carbapenem antibiotics, 33 (1996) 99
- Carcinogenicity of polycyclic hydrocarbons, 10 (1974) 159
- Cardiotonic steroids, 30 (1993) 135
- Cardiovascular system, effect of azides, 31 (1994) 121
 effect of endothelin, 31 (1994) 369
 4-quinolones as antihypertensives, 32 (1995) 115
 renin inhibitors as antihypertensive agents, 32 (1995) 37
- Caspase inhibitors, 39 (2002) 1
- Catecholamines, 6 (1969) 200
- Cathepsin K inhibitors, 42 (2004) 245
- CCK-B antagonists, 37 (2000) 45
- CCR5 Receptor antagonists, 43 (2005) 239
- Cell membrane transfer, 14 (1977) 1
- Central nervous system (CNS)
 drugs, transmitters and peptides, 23 (1986) 91
 P2X7 antagonists, 53 (2014) 65
- Centrally acting dopamine D₂ receptor agonists, 29 (1992) 185
- CEP-1347/KT-7515, inhibitor of the stress activated protein kinase signalling pathway (JNK/SAPK), 40 (2002) 23
- Chartreusin, 19 (1982) 247
- Chelating agents, 20 (1983) 225
 tripositive elements as, 28 (1991) 41
- Chemotherapy of herpes virus, 23 (1985) 67
- Chemotopography of digitalis recognition matrix, 30 (1993) 135
- Chiral synthesis, 34 (1997)
- Cholesterol-lowering agents, 33 (1996) 331; 40 (2002) 1
- Cholinergic receptors, 16 (1976) 257
- Chromatography, 12 (1975) 1, 105
- Chromone carboxylic acids, 9 (1973) 65

- Clinical enzymology, 13 (1976) 1
- Collagenases, synthetic inhibitors, 29 (1992) 271
- Column chromatography, 12 (1975) 105
- Combinatorial chemistry, 36 (1999) 91
- Computers in biomedical education, 26 (1989) 323
- Medlars information retrieval, 10 (1974) 1
- Copper complexes, 15 (1978) 211; 26 (1989) 437
- Coronary circulation, 6 (1969) 11
- Corticotropin releasing factor receptor antagonists, 41 (2003) 195
- Coumarins, metabolism and biological actions, 10 (1974) 85
- Cyclic AMP, 12 (1975) 293
- Cyclooxygenase-2 (COX-2) inhibitors, 36 (1999) 201
- Cyclophosphamide analogues, 19 (1982) 205
- Cyclosporins as immunosuppressants, 25 (1988) 1; 33 (1996) 53
- Cytochrome P450 metabolism and inhibitors, 47 (2009) 239
- Data analysis in biomedical research, 25 (1988) 291
- Depression neurokinin receptors in, 43 (2005) 53
- Designing drugs, to avoid toxicity, 50 (2010) 1
- Diaminopyrimidines, 19 (1982) 269
- Digitalis recognition matrix, 30 (1993) 135
- Dipeptidyl peptidase IV inhibitors, 45 (2007) 63
- Diuretic drugs, 1 (1961) 132
- DNA-binding drugs, 16 (1979) 151
- Dopamine D₂ receptor agonists, 29 (1992) 185
- Doxorubicin, 15 (1978) 125; 21 (1984) 169
- Drug-receptor interactions, 4 (1965) 39
- Drugs, transmitters and peptides, 23 (1986) 91
- Elastase, inhibition, 31 (1994) 59
- Electron spin resonance, 12 (1975) 191
- Electrophysiological (Class III) agents for arrhythmia, 29 (1992) 65
- Emesis neurokinin receptors in, 43 (2005) 53
- Enantiomers, synthesis of, 34 (1997) 203
- Endorphins, 17 (1980) 1
- Endothelin inhibition, 31 (1994) 369
- Endothelin receptor antagonists, 47 (2009) 203
- Enkephalin-degrading enzymes, 30 (1993) 327
- Enkephalins, 17 (1980) 1
- Enzymes, inhibitors of, 16 (1979) 223; 26 (1989) 253; 29 (1992) 271; 30 (1993) 327; 31 (1994) 59, 297; 32 (1995) 37, 239; 33 (1996) 1; 36 (1999) 1, 201; 38 (2001) 1; 39 (2002) 1, 121, 215; 40 (2002) 1, 23, 63; 41 (2003) 99, 249; 42 (2004) 125, 245
- Enzymology, clinical use of, 10 (1976) 1
- in pharmacology and toxicology, 10 (1974) 11
- Epothilones A and B and derivatives as anticancer agents, 42 (2004) 171
- Erythromycin and its derivatives, 30 (1993) 57; 31 (1994) 265
- Feverfew, medicinal chemistry of the herb, 29 (1992) 217
- Fibrinogen antagonists, as antithrombotic agents, 36 (1999) 29
- Flavonoids, physiological and nutritional aspects, 14 (1977) 285
- Fluorescence-based assays, 43 (2005) 19
- Fluoroquinolone antibacterial agents, 27 (1990) 235
- mechanism of resistance to, 32 (1995) 157
- Folic acid and analogues, 25 (1988) 85; 26 (1989) 1
- Formaldehyde, biocidal action, 34 (1997) 149
- Free energy, biological action and linear, 10 (1974) 205
- GABA, heterocyclic analogues, 22 (1985) 67
- GABAA receptor ligands, 36 (1999) 169
- γ -secretase modulators, 53 (2014) 101
- Gas-liquid chromatography and mass spectrometry, 12 (1975) 1
- Gastric H⁺/K⁺ - ATPase inhibitors, 31 (1994) 233
- Genomics, impact on drug discovery, 37 (2000) 1
- Glucagon-like peptide receptor agonists, 52 (2012) 45
- Glutaraldehyde, biological uses, 13 (1976) 271
- as sterilizing agent, 34 (1997) 149
- Gold, immunopharmacology of, 19 (1982) 1
- G protein-coupled receptors (GPCRs), 53 (2014) 1
- Growth hormone secretagogues 39 (2002) 173
- Guanidines, 7 (1970) 124; 30 (1993) 203
- Haematopoietic prostaglandin D synthase (H-PGDS) inhibitors, 51 (2012) 97
- Halogenoalkylamines, 2 (1962) 132
- Heparin and heparinoids, 5 (1967) 139
- Hepatitis C virus NS3-4 protease, inhibitors of, 39 (2002) 215
- Hepatitis C virus NS3/NS4A protease inhibitors, 44 (2006) 65; 49 (2010) 1
- Herpes virus, chemotherapy, 23 (1985) 67

- Heterocyclic analogues of GABA, 22 (1985) 67
Heterocyclic carboxaldehyde thiosemicarbazones, 16 (1979) 35; 32 (1995) 1
Heterosteroids, 16 (1979) 35; 28 (1991) 233
H⁺ /K⁺ ATPase inhibitors, 47 (2009) 75
High-throughput screening techniques, 37 (2000) 83; 43 (2005) 43
Histamine, H₃ ligands, 38 (2001) 279; 44 (2006) 181
Hit identification, 45 (2007) 1
H₂-antagonists, 20 (1983) 337
 receptors, 24 (1987) 30; 38 (2001) 279
 release, 22 (1985) 26
 secretion, calcium and, 19 (1982) 59
5-HT₆ receptor ligands, 48 (2009) 5
5-HT_{1A} receptors, radioligands for *in vivo* studies, 38 (2001) 189
5-HT_{2C} ligands, 46 (2008) 281
Histidine decarboxylases, 5 (1967) 199
Histone deacetylase inhibitors, 46 (2008) 205
HIV CCR5 antagonists in, 43 (2005) 239
 proteinase inhibitors, 32 (1995) 239
HIV integrase inhibitors, 46 (2008) 1
HMG-CoA reductase inhibitors, 40 (2002) 1
Human Ether-a-go-go (HERG), 43 (2005) 1
Hydrocarbons, carcinogenicity of, 10 (1974) 159
11β-Hydroxysteroid dehydrogenase inhibitors, 46 (2008) 29
Hypersensitivity reactions, 4 (1965) 1
Hypocholesterolemic agents, 39 (2002) 121; 40 (2002) 1
Hypoglycaemic drugs, 1 (1961) 187; 18 (1981) 191; 24 (1987) 209; 30 (1993) 203; 31 (1994) 1
Hypolipidemic agents, 40 (2002) 1
Hypotensive agents, 1 (1961) 34; 30 (1993) 203; 31 (1994) 409; 32 (1995) 37, 115

Iminosugars, therapeutic applications of, 50 (2010) 133
Immunopharmacology of gold, 19 (1982) 1
Immunosuppressant cyclosporins, 25 (1988) 1
India, medicinal research in, 22 (1985) 243
Influenza virus sialidase, inhibitors of, 36 (1999) 1
Information retrieval, 10 (1974) 1
Inotropic steroids, design of, 30 (1993) 135
Insulin, obesity and, 17 (1980) 105
Ion-selective membrane electrodes, 14 (1977) 51
Ion transfer, 14 (1977) 1
Irinotecan, anticancer agent, 34 (1997) 68
Isothermal titration calorimetry, in drug design, 38 (2001) 309

Isotopes, in drug metabolism, 9 (1973) 133
 stable, 15 (1978) 1

JAK inhibitors, selective, 52 (2012) 153

Kappa opioid non-peptide ligands, 29 (1992) 109; 35 (1998) 83
Kinetics of receptor binding, 48 (2009) 1

Lactam antibiotics, 12 (1975) 395; 14 (1977) 181
β-Lactamase inhibitors, 31 (1994) 297
Lead identification, 45 (2007) 1
Leprosy, chemotherapy, 20 (1983) 1
Leukocyte elastase inhibition, 31 (1994) 59
Leukotriene D₄ antagonists, 38 (2001) 249
Ligand-receptor binding, 23 (1986) 41
Linear free energy, 10 (1974) 205
Lipid-lowering agents, 40 (2002) 1
5-Lipoxygenase inhibitors and their anti-inflammatory activities, 29 (1992) 1
Literature of medicinal chemistry, 6 (1969) 266
Lithium, medicinal use of, 11 (1975) 193
Local anaesthetics, 3 (1963) 332
Lonidamine and related compounds, 21 (1984) 111

Macrolide antibiotics, 30 (1993) 57; 31 (1994) 265
Malaria, drugs for, 8 (1971) 231; 19 (1982) 269; 28 (1991) 1; 43 (2005) 189
Manganese, biological significance, 30 (1993) 89
Manufacture of enantiomers of drugs, 34 (1997) 203
Mass spectrometry and glc, 12 (1975) 1
Mast cells, calcium and histamine secretion, 19 (1982) 59
 cholinergic histamine release, 22 (1985) 267
 peptide regulation of, 27 (1990) 143
Medicinal chemistry
 GLP agonists, 52 (2012) 45
 literature of, 6 (1969) 266
Medlars computer information retrieval, 10 (1974) 1
Melanocortin receptor 4 ligands, 45 (2007) 111
Membrane receptors, 23 (1986) 41
Membranes, 14 (1977) 1; 15 (1978) 87; 16 (1979) 223
Mercury (II) chloride, biological effects, 27 (1990) 189
Methotrexate analogues as anticancer drugs, 25 (1988) 85; 26 (1989) 1 26
Microcomputers in biomedical education, 26 (1989) 323

- Migraine neurokinin receptors in, 43 (2005) 53
Molecular modelling of opioid receptor-ligand complexes, 40 (2002) 107
Molecularly imprinted polymers, preparation and use of, 36 (1999) 235
Molybdenum hydroxylases, 24 (1987) 85
Monoamine oxidase inhibitors, 21 (1984) 137
Montelukast and related leukotriene D4 antagonists, 38 (2001) 249
Motilin receptor, 48 (2009) 2
Multivalent dual pharmacology MABA, 51 (2012) 71
Multivariate data analysis and experimental design, 25 (1988) 291
Muscarinic Receptors, 43 (2005) 105
 multivalent dual pharmacology MABA, 51 (2012) 71
Neuraminidase inhibitors, 36 (1999) 1
Neurokinin receptor antagonists, 35 (1998) 57; 43 (2005) 49
Neuromuscular blockade, 2 (1962) 88; 3 (1963) 1; 16 (1979) 257
Neuropeptide Y receptor ligands, 42 (2004) 207
Neurosteroids, as psychotropic drugs, 37 (2000) 135
Next decade [the 1970's], drugs for, 7 (1970) 215
NFkB, 43 (2005) 137
Nickel(II) chloride and sulfate, biological effects, 27 (1990) 189
 $\alpha 7$ Nicotinic acetylcholine receptor agonists, 46 (2008) 131
Nicotinic cholinergic receptor ligands, a4b2, 42 (2004) 55
Nitriles, synthesis of, 10 (1974) 245
Nitrofurans, 5 (1967) 320
Nitroimidazoles, cytotoxicity of, 18 (1981) 87
NMR spectroscopy, 12 (1975) 159
 high-field, 26 (1989) 355
Non-steroidal anti-inflammatory drugs, 5 (1967) 59; 36 (1999) 201
Non-tricyclic antidepressants, 15 (1978) 39
NS3-NS4 HCV protease inhibitor, 49 (2010) 1
N-type calcium channel modulators, treatment of pain, 53 (2014) 147
C-Nucleosides, 13 (1976) 303; 22 (1985) 1
Nutrition, total parenteral, 28 (1991) 175
Obesity and insulin, 17 (1980) 105
Ondansetron and related 5-HT₃ antagonists, 29 (1992) 239
Opioid peptides, 17 (1980) 1
 receptor antagonists, 35 (1998) 83
 receptor-specific analogues, 28 (1991) 301
 receptor-ligand complexes, modelling of, 40 (2002) 107
Oral absorption and bioavailability, prediction of, 41 (2003) 1
Organophosphorus pesticides, pharmacology of, 8 (1971) 1
Oxopyranoazines and oxopyranoazoles, 9 (1973) 117
Oxytocin antagonists, 44 (2006) 331
Poly(ADP-ribose)polymerase (PARP) inhibitors, 42 (2004) 125
P2 Purinoreceptor ligands, 38 (2001) 115
p38 MAP kinase inhibitors, 38 (2001) 1
Paclitaxel, anticancer agent, 32 (1995) 289
Pain neurokinin receptors in, 43 (2005) 53, 55
Parasitic infections, 13 (1976) 159; 30 (1993) 203
Parasympathomimetics, 11 (1975) 1
Parenteral nutrition, 28 (1991) 175
Parkinsonism, pharmacotherapy of, 9 (1973) 191; 21 (1984) 137
Patenting of drugs, 2 (1962) 1; 16 (1979) 1
Peptides, antibiotics, 5 (1967) 1
 enzymic, 31 (1994) 59
 hypoglycaemic, 31 (1994) 1
 mast cell regulators, 27 (1990) 143
 opioid, 17 (1980) 1
Peptide deformylase inhibitors, 44 (2006) 109
Peroxisome proliferator-activated receptor gamma (PPAR γ) ligands, 42 (2004) 1
Pharmacology of Alzheimer's disease, 34 (1997) 1
Pharmacology of Vitamin E, 25 (1988) 249
Phosphates and phosphonates as prodrugs, 34 (1997) 111
Phosphodiesterase type 4 (PDE4) inhibitors, 33 (1996) 1; 47 (2009) 37
Phosphodiesterase type 5 (PDE5) inhibitors, 41 (2003) 249
Phosphoinositide-3-kinase inhibitors, 48 (2009) 3
Phospholipids, 19 (1982) 111
Photodecomposition of drugs, 27 (1990) 51
Physicochemistry in drug design, 48 (2009) 1
Plasmodium, 43 (2005) 190
Plasmodium falciparum dihydrofolate reductase (PfDHFR), 43 (2005) 226
Platelet-aggregating factor, antagonists, 27 (1990) 325
Platinum antitumour agents, 24 (1987) 129

- Platelet aggregation, inhibitors of, 36 (1999) 29
- Polarography, 12 (1975) 247
- Polycyclic hydrocarbons, 10 (1974) 159
- Polyene antibiotics, 14 (1977) 105
- Polypeptide antibiotics, 5 (1967) 1
- Polypeptides, 4 (1965) 86
from snake venom, 21 (1984) 63
- Positron emission tomography (PET), 38 (2001) 189
- Prodrugs based on phosphates and phosphonates, 34 (1997) 111
- Property-based design, benzamide glucokinase activators, 52 (2012) 1
- Prostacyclins, 21 (1984) 237
- Prostaglandin D2 receptor CRTH2 antagonists, 50 (2010) 51
- Prostaglandins, 8 (1971) 317; 15 (1978) 357
- Proteinases, inhibitors of, 31 (1994) 59; 32 (1995) 37, 239
- Proteasome inhibitors, 43 (2005) 155
- Pseudomonas aeruginosa*, resistance of, 12 (1975) 333; 32 (1995) 157
- Psychotomimetics, 11 (1975) 91
- Psychotropic drugs, 5 (1967) 251; 37 (2000) 135
- Purines, 7 (1970) 69
- P2X7 antagonists, CNS disorders, 53 (2014) 65
- Pyridazines, pharmacological actions of, 27 (1990) 1; 29 (1992) 141
- Pyrimidines, 6 (1969) 67; 7 (1970) 285; 8 (1971) 61; 19 (1982) 269
- Quantum chemistry, 11 (1975) 67
- Quinolines, 8-amino-, as antimalarial agents, 28 (1991) 1
- 4-Quinolones as antibacterial agents, 27 (1990) 235
as potential cardiovascular agents, 32 (1995) 115
- QT interval, 43 (2005) 4
- Radioligand-receptor binding, 23 (1986) 417
- Raltegravir, 46 (2008) 1
- Ranitidine and H₂-antagonists, 20 (1983) 337
- Rauwolfia* alkaloids, 3 (1963) 146
- Recent drugs, 7 (1970) 1
- Receptors, adenosine, 38 (2001) 61
adrenergic, 22 (1985) 121; 23 (1986) 1; 41 (2003) 167
cholecystokinin, 37 (2000) 45
corticotropin releasing factor, 41 (2003) 195
fibrinogen, 36 (1999) 29
histamine, 24 (1987) 29; 38 (2001) 279
neurokinin, 35 (1998) 57
neuropeptide Y, 42 (2004) 207
nicotinic cholinergic, 42 (2004) 55
opioid, 35 (1998) 83
peroxisome proliferator-activated receptor gamma (PPAR_γ), 42 (2004) 1
purino, 38 (2001) 115
Retin inhibitors, 32 (1995) 37
- Reverse transcriptase inhibitors of HIV-1, 40 (2002) 63
Serotonin, 41 (2003) 129
Ricin, 24 (1987) 1
- RNA as a drug target, 39 (2002) 73
Rule of five, 48 (2009) 1
- Schizophrenia Neurokinin receptors in, 43 (2005) 53
M1 agonists in, 43 (2005) 113, 117
M2 antagonists in, 43 (2005) 121
M4 antagonists in, 43 (2005) 129
- Screening tests, 1 (1961) 1
- β-secretase inhibitors, 48 (2009) 4
- Secretase inhibitors, g-, 41 (2003) 99
Serine protease inhibitors, 31 (1994) 59
- Selective JAK inhibitors, 52 (2012) 153
- Serotonin 2c ligands, 46 (2008) 281
- Serotonin 5-HT_{1A} radioligands, 38 (2001) 189
- Serotonin (5-HT)-terminal autoreceptor antagonists, 41 (2003) 129
- Single photon emission tomography (SPET), 38 (2001) 189
- Small molecule therapeutics targeting Th17 cell function for, 50 (2010) 107
- Snake venoms, neuroactive, 21 (1984) 63
- Sodium channel blockers, 49 (2010) 81
- Sodium cromoglycate analogues, 21 (1984) 1
- Sparsomycin, 23 (1986) 219
- Spectroscopy in biology, 12 (1975) 159, 191; 26 (1989) 355
- Statistics in biological screening, 3 (1963) 187; 25 (1988) 291
- Sterilization with aldehydes, 34 (1997) 149
- Steroids, hetero-, 16 (1979) 35; 28 (1991) 233
design of inotropic, 30 (1993) 135
- Stress activated protein kinase inhibitors, 40 (2002) 23
- Structure-activity relationships (SARs), 49 (2010) 113
- Structure-based drug design, G protein-coupled receptors, 53 (2014) 1
- Structure-based lead generation, 44 (2006) 1
- Synthesis of enantiomers of drugs, 34 (1997) 203

- Tachykinins, 43 (2005) 50
- Tetrahydroisoquinolines, β -adrenomimetic activity, 18 (1981) 45
- Tetrazoles, 17 (1980) 151
- Thalidomide as anti-inflammatory agent, 22 (1985) 165
- Thermodynamics of receptor binding, 48 (2009) 1
- Thiosemicarbazones, biological action, 15 (1978) 321; 32 (1995) 1
- Thromboxanes, 15 (1978) 357
- Tilorone and related compounds, 18 (1981) 135
- Time resolved energy transfer (TRET), 43 (2005) 40
- Toxic actions, mechanisms of, 4 (1965) 18
- Tranquillizers, 1 (1961) 72
- 1,2,3-Triazines, medicinal chemistry of, 13 (1976) 205
- Tripositive elements, chelation of, 28 (1991) 41
- TRPV1 antagonists, 51 (2012) 57
- vanilloid receptors, 44 (2006) 145
- Trypanosomiasis, 3 (1963) 52
- Tuberculosis chemotherapy, 45 (2007) 169
- Ubiquitinylation, 43 (2005) 153
- Vanilloid receptors, TRPV1 antagonists, 44 (2006) 145
- Venoms, neuroactive snake, 21 (1984) 63
- Virtual screening of virtual libraries, 41 (2003) 61
- Virus diseases of plants, 20 (1983) 119
- Viruses, chemotherapy of, 8 (1971) 119; 23 (1986) 187; 32 (1995) 239; 36 (1999) 1; 39 (2002) 215
- Vitamin D₃ and its medical uses, 35 (1998) 1
- Vitamin E, pharmacology of, 25 (1988) 249